CHEMICAL REVIEWS

pubs.acs.org/CR

Review

Colloidal Synthesis of Metal Nanocrystals: From Asymmetrical Growth to Symmetry Breaking

Quynh N. Nguyen,[§] Chenxiao Wang,[§] Yuxin Shang,[§] Annemieke Janssen,[§] and Younan Xia*

Cite This: *Chem. Rev.* 2023, 123, 3693−3760

Read Online

ACCESS | Metrics & More | Article Recommendations

ABSTRACT: Nanocrystals offer a unique platform for tailoring the physicochemical properties of solid materials to enhance their performances in various applications. While most work on controlling their shapes revolves around symmetrical growth, the introduction of asymmetrical growth and thus symmetry breaking has also emerged as a powerful route to enrich metal nanocrystals with new shapes and complex morphologies as well as unprecedented properties and functionalities. The success of this route critically relies on our ability to lift the confinement on symmetry by the underlying unit cell of the crystal structure and/or the initial seed in a systematic manner. This Review aims to provide an account of recent progress in understanding and controlling asymmetrical growth and symmetry breaking in a colloidal synthesis of noble-metal nanocrystals. With a touch on both the nucleation and growth steps, we discuss a number of methods capable of generating seeds with diverse symmetry while achieving asymmetrical growth for mono-, bi-, and multimetallic systems. We then showcase a variety of symmetry-broken nanocrystals that have been reported, together with insights into their growth mechanisms. We also highlight their properties and applications and conclude with perspectives on future directions in developing this class of nanomaterials. It is hoped that the concepts and existing challenges outlined in this Review will drive further research into understanding and controlling the symmetry breaking process.

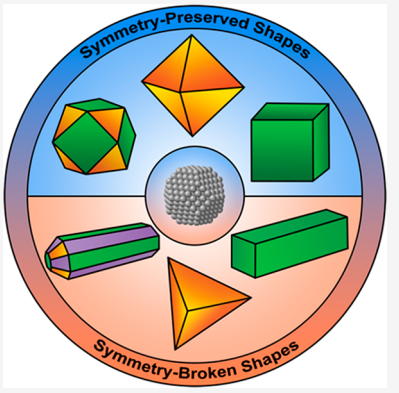

CONTENTS

Special Issue: Anisotropic Nanomaterials

Received: July 5, 2022
Published: December 22, 2022

https://doi.org/10.1021/acs.chemrev.2c00468
Chem. Rev. 2023, 123, 3693−3760

1. INTRODUCTION

Nanoscience and nanotechnology, the investigation of peculiar properties at the nanoscale and the exploration of nanomaterials for various applications, represent two of the most exciting advances in modern science. Constituting a major class of nanomaterials, metal nanocrystals can be broadly defined as metallic structures or particles possessing a crystalline lattice and at least one dimension in the range of 1−100 nm.[1] Their long history can be traced back to the fourth century when glass artifacts such as the Lycurgus Cup were crafted to present beautiful colors through the incorporation of Au and/or Ag dust.[2−4] The first scientific report on metal nanocrystals was published by Michael Faraday in 1857 when he prepared and studied several original samples of Au colloids: stable suspensions of Au nanocrystals.[5] Faraday's pioneering work on "metals in a finely-divided state" laid the foundation for a research field commonly referred to as "colloid science", one of the forerunners of nanoscience and nanotechnology.[6] Thanks to the advancements in both experimental tools and theoretical methods, our understanding of the invisible nanoscale world has progressed at an ever-increasing speed. Starting as a scientific curiosity, research on nanocrystals has spanned from the development of methods for engineering their properties in a controllable manner to the exploration of new applications superior to their bulk counterparts. Today, metal nanocrystals represent one of the most viable and exciting research areas due to their major impacts on fundamental sciences and practical applications in the context of plasmonics,[7−9] photonics,[10−12] electronics,[13−15] sensing,[16,17] catalysis,[18−20] and biomedicine.[21−23]

About 25 years ago, a paradigm shift occurred in metal nanocrystal research as a result of the realization that the properties and applications of nanocrystals could be greatly augmented by posing a tight control over their elemental composition,[24,25] size,[26−28] shape,[29−31] morphology,[32−34] and internal structure.[35,36] Most significantly, novel features that cannot be achieved in their bulk counterparts have emerged, including localized surface plasmon resonance (LSPR),[37] local field enhancement,[38] and superparamagnetism,[39] as well as the presence of high-index facets abundant in low-coordination atoms.[31] Notably, most of these properties are strongly dependent on the geometric shape or symmetry of a nanocrystal, which determines not only the arrangement of atoms on the surface[40−43] but also how the polarization of conduction electrons occurs and how the surface charges are distributed on the surface.[16,44,45] A prototypical example can be found in Ag nanocrystals, a multifunctional nanomaterial with extensive use in plasmonic, optoelectronic, and catalytic applications. By simply tuning the size of Ag nanoparticles with a polycrystalline structure and a poorly defined, quasi-spherical shape in the range of 40−90 nm, the ultraviolet−visible (UV−vis) extinction spectra displayed a resonance peak tunable from 410−500 nm.[46,47] When switching to Ag cubic nanocrystals with a similar size (e.g., 90 nm), the spectra exhibited multiple resonance peaks, with the most intense one red-shifting to almost 600 nm due to the presence of sharp features on the surface.[46,48] In this case, the shape of metal nanocrystals offers a more effective knob than the size for tailoring their LSPR properties. When serving as catalysts, Ag nanocubes encased by {100} facets have been found to be more selective toward ethylene epoxidation relative to the conventional Ag nanoparticles with a quasi-spherical shape owing to the favorable transformation of the surface oxametallacycle intermediate to ethylene epoxide on Ag(100) surface.[49,50] Similar correlations between other catalytic properties and the geometric shape have also been demonstrated for nanocrystals made of metals such as Au, Pt, Pd, and Rh.[18,51−56] All these examples manifest the promise of shape control in augmenting the performance and thereby accomplishing cost-effective use of precious metals notoriously known for their extremely low abundances in Earth's crust.

The hallmark of shape-controlled nanocrystals naturally leads to the next question in the quest for functional nanomaterials: how to engineer the shape of metal nanocrystals in a predictable and precise manner without losing control over other parameters? Different from how bulk metals are manufactured as macroscopic objects, a bottom-up approach is typically pursued to "assemble" the atomic building blocks into nanocrystals with a specific shape. Among numerous methods available for the assembly process, colloidal synthesis in a solution phase has proven to be the most versatile yet robust and reproducible route to metal nanocrystals with the quality and quantity needed for evaluating their properties and exploring their applications.[1] During such a synthesis, metal atoms, the building blocks, are produced in the initial stage via chemical reduction or decomposition of a precursor through the use of a reducing agent or thermal activation (Figure 1).[1,57,58] Once the concentration of the atoms reaches the threshold for homogeneous nucleation, nuclei with a fluctuating structure will be formed, followed by their evolution into seeds with fixed and well-defined internal structures.[59,60] Based on their internal structures, the seeds can be broadly classified into four major types, including those

https://doi.org/10.1021/acs.chemrev.2c00468
Chem. Rev. 2023, 123, 3693−3760

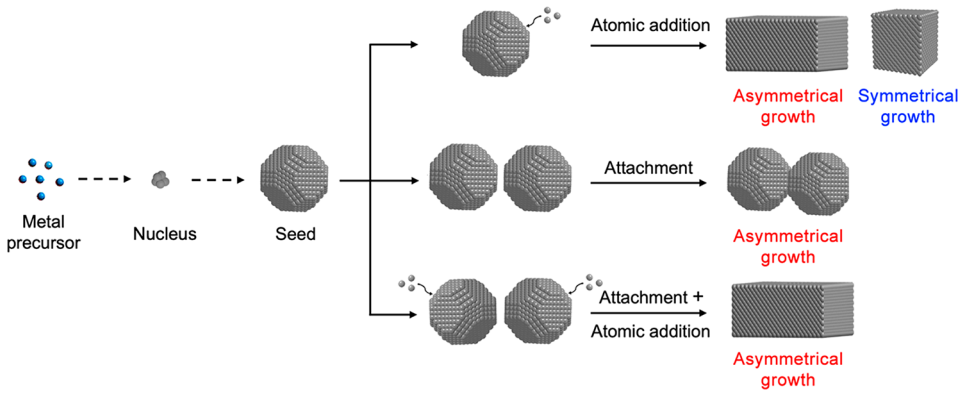

Figure 1. Schematic showing the formation of nuclei fluctuating in structure via homogeneous nucleation, followed by their evolution into seeds with a specific internal structure (together with the involvement of symmetry breaking), and then growth of the seeds into nanocrystals through either atomic addition (with the possible involvement of either asymmetrical or symmetrical growth), particle attachment (mostly, asymmetrical growth), or both.

featuring a single-crystal, singly-twinned, multiply-twinned, or stacking-fault-lined structure. The as-formed seeds subsequently grow into nanocrystals with enlarged dimensions and distinct shapes through atomic addition and/or particle attachment.[1,61−64] It turns out that the shape taken by a nanocrystal has a strong correlation with its symmetry, a characteristic that is intrinsically encoded in both the nucleation and growth steps. The shape taken by a metal nanocrystal usually inherits the symmetry of the initial seeds, which is, in turn, governed by the crystal structure adopted by the bulk metal.[65,66] To a certain extent, the confinement imposed by the inherent symmetry of a crystal structure has to be lifted in the course of nucleation and/or growth in order to obtain nanocrystals with exotic shapes. During the growth process, symmetry breaking can occur as a result of asymmetrical growth in terms of size enlargement, facet development, and/or structure evolution. In this case, one or more symmetry elements can be removed from their precursors (i.e., the unit cell and/or the seed from which the nanocrystal grows), resulting in symmetry-broken nanocrystals.[67,69] In essence, the nanocrystal is expected to follow a pattern of asymmetrical growth that is manifested by different rates along symmetry-related crystal axes.[67,68] In contrast, the transfer of symmetry from the unit cell into a seed and then a nanocrystal can be regarded as symmetry preservation, which is often accompanied by symmetrical growth.[66,69] In this Review, we avoid using terms such as "an/isotropic growth" or "an/isotropic shape" habitually exploited in the literature when referring to an un/even growth pattern that leads to a product with broken/preserved symmetry. Instead, we introduce and then stick to "a/symmetrical growth" and product with "broken/preserved symmetry". Defined as a direction-dependent feature, "anisotropy" can arise from elemental, geometric, morphological, structural, functional, and chemical properties of a nanoparticle, as well as its formation process. In theory, it is only possible to achieve "isotropic growth" for an amorphous or noncrystalline material (e.g., silica). Any system/process involving a crystalline material, like in the case of a nanocrystal, should always have a certain degree of anisotropy in terms of shape, morphology, or growth pattern because of the underlying crystalline structure. In a sense, all metal nanocrystals should be considered to have anisotropy in terms of atomic arrangement or shape, regardless of the growth pattern. As such, "asymmetrical growth" and the accompanying result of "symmetry breaking" are more appropriate when describing this subcategory of growth patterns for metal nanocrystals. The product of such a process should be referred to as a "symmetry-broken" rather than "anisotropic" nanostructure.

Depending on the interplay between thermodynamic and kinetic parameters as defined by the experimental conditions, two growth pathways (atomic addition and particle attachment) can take place individually or simultaneously, dictating the growth patterns (symmetrical vs asymmetrical) of the seeds and thus the symmetry and shape of the resultant nanocrystals (Figure 1).[68,70−72] For the former route that involves the continuous deposition of newly formed atoms onto the growing seeds, it can follow either symmetrical or asymmetrical growth to preserve or break the symmetry of the seeds, generating products with shapes similar to or different from those of the seeds.[51,66,73−76] Alternatively, the seeds can undergo asymmetrical growth through an attachment mechanism, giving rise to products with a lower order of symmetry than the constituent particles.[77−81] When atomic addition accompanies particle attachment, the seeds also undergo asymmetrical growth to evolve into larger nanocrystals with lower symmetry.[82,83]

Despite being a ubiquitous phenomenon in the colloidal synthesis of metal nanocrystals, the fundamental science underlying the mechanistic details of asymmetrical growth and symmetry breaking remains elusive and needs further investigation. One of the major motivations for studying the mechanistic details is the diversity and complexity that can be brought into a colloidal system, including the production of nanocrystals with novel shapes or morphologies, as well as new properties and applications. Like how low symmetry is necessary to accommodate or promote complex behaviors of natural systems, the metal nanocrystals derived from asymmetrical growth often exhibit enriched, enhanced, and sometimes superb properties that are challenging to achieve by simply controlling the size of the symmetrical counterparts. Taking the aforementioned Ag nanocrystals as an example, increasing their size does cause the LSPR peak to red-shift, albeit only to 600 nm even when their edge length is increased to 100 nm.[46,47] However, when Ag nanocrystals are elongated along one direction into bars or rods, the LSPR peaks will split into two modes, with the longitudinal mode capable of red-shifting from the visible to the near-infrared range (650−900 nm), where soft tissues show remarkable transparency for

https://doi.org/10.1021/acs.chemrev.2c00468
Chem. Rev. 2023, 123, 3693−3760

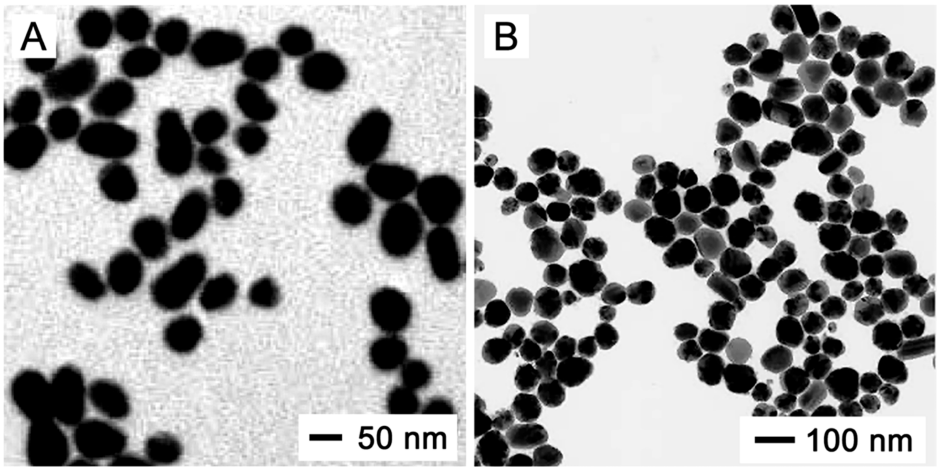

Figure 2. Transmission electron microscopy (TEM) images of two old examples of (A) Au and (B) Ag nanocrystals obtained using the citrate reduction and silver mirror reaction, respectively. In principle, each sample can be viewed as a mix of different products under stochastic symmetry breaking, in addition to the involvement of assorted seeds and diverse growth conditions. (A) Reproduced with permission from ref 93. Copyright 2007 American Chemical Society. (B) Reproduced with permission from ref 94. Copyright 2002 Royal Society of Chemistry.

optical imaging and photothermal treatment.[16,84] Another interesting example is bimetallic Janus nanocrystals with reduced symmetry relative to their monometallic counterparts or those with core−satellite, -frame, and -shell structures. The heterogeneous interface associated with the side-by-side elemental distribution provides a unique mechanism for charge transfer, offering a means to maneuver the electronic structures and thus bestowing Janus nanocrystals with new catalytic and photocatalytic capabilities.[85−88] Furthermore, as a potential alternative to the indium−tin oxide (ITO) technology, polymer films containing Ag or Cu nanowires exhibit high optical transparency, excellent electrical conductivity, and good mechanical flexibility to allow for the fabrication of touchscreen panels, flexible displays, and solar cells.[89−92] Taken together, introducing asymmetrical growth and thus symmetry breaking at the nanoscale offers a versatile handle for not only diversifying the shape of metal nanocrystals but also accessing additional properties and new functionality, enabling the exploration of complex nanocrystals for a vast array of applications.

Inspired by the prospects of symmetry-broken nanocrystals, tremendous efforts have been devoted to exploring effective routes for synthesizing this class of nanomaterials. However, finding a universal knob to systematically activate asymmetrical growth and break the symmetry is not a trivial task. As a matter of fact, the lack of control over these processes contributed to the source of polydispersity or irregularity that plagued essentially all colloidal nanocrystals reported before 2000. Most old samples produced using traditional methods, like those involving citrate reduction or silver mirror reaction, contained a mix of nanocrystals involving different patterns of asymmetrical growth (Figure 2).[93,94] The root of such polydispersity can be attributed to the different types of seeds involved and the diverse growth conditions, as well as the stochastic nature of symmetry breaking. Constrained by the high symmetry of the crystal structure, there is no inherent driving force to induce and maintain asymmetrical growth in a specific pattern. For example, a truncated octahedral seed made of a face-centered cubic (*fcc*) metal is characterized by an O_h point group while possessing multiple equivalent crystal axes or facets where the surface atoms have the same spatial arrangement and coordination number. The high order of symmetry of the truncated octahedral seed favors the growth in a symmetrical pattern, giving rise to shapes that retain the symmetry of an *fcc* metal, such as a cube or an octahedron depending on the relative growth rates along the <100> and <111> directions.[72,95] If the symmetry of the seed is broken stochastically, polydispersed samples will result. Only in a well-controlled manner will it be feasible and even predictable to obtain metal nanocrystals with unusual shapes and novel functionalities while maintaining high quality and uniformity. The possibility of this research direction, however, could not be explored until the early 2000s when metal nanocrystals with well-defined attributes became available and could be employed as seeds for further growth.[96−99]

Thanks to the efforts of many research groups around the world, the past two decades have witnessed spectacular advances in the development of shape-controlled syntheses of colloidal metal nanocrystals. In particular, a vast collection of metal nanocrystals with different or lower symmetry relative to the unit cell has been prepared with a high degree of precision through either one-pot synthesis or seed-mediated growth. Notable examples include tetrahedra, bars, and octagonal rods/wires with a single-crystal structure, beams with a singly-twinned structure, and pentagonal rods/wires with a multiply-twinned structure (Figure 3).[1,18,68,100] The key determinant for the successful synthesis of metal nanocrystals with reduced symmetry remains to be a tight control over both nucleation and growth, which ensures the formation of one type of seed while maintaining an exclusive growth pattern for the generation of products uniform in both size and shape. Now it is an exciting time to utilize the nanocrystals emanating from asymmetrical growth as a new platform to probe the structure−property relationship while developing methods for the rational synthesis of nanomaterials with desired functionality for various applications.

This Review aims to offer a representative snapshot of recent progress in understanding and controlling both asymmetrical growth and symmetry breaking during a colloidal synthesis of metal nanocrystals. We begin with a brief introduction to the concept of symmetry in the context of nucleation, including the structural features of an *fcc* metal and the classification of

https://doi.org/10.1021/acs.chemrev.2c00468
Chem. Rev. 2023, 123, 3693−3760

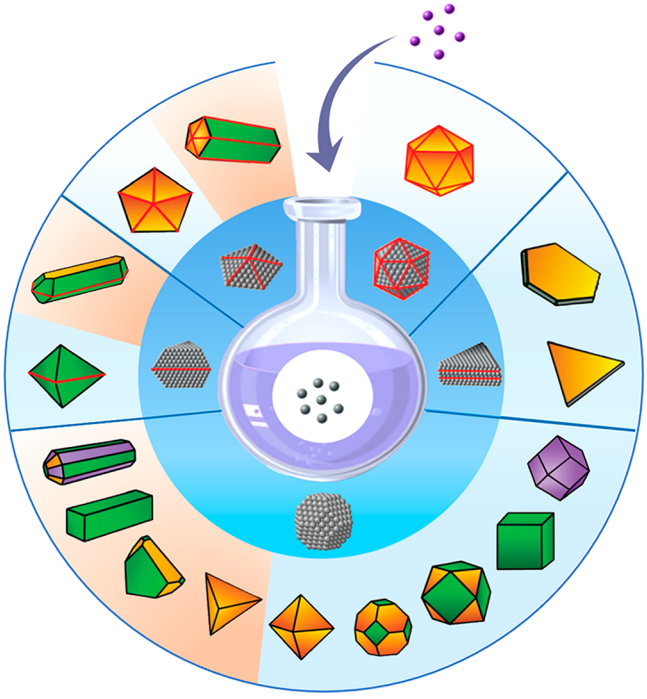

Figure 3. Schematic illustrating the concept of symmetry breaking in a colloidal synthesis of nanocrystals made of an *fcc* metal. The metal atoms (in the center) are formed via the reduction or decomposition of a precursor (on the top), followed by their aggregation into nuclei, evolution into different types of seeds with distinct internal structures and in diverse symmetry groups (in the middle ring), and then the growth into nanocrystals with various shapes (in the outer ring). The red lines mark the twin defects or stacking faults, while the green, purple, and yellow colors correspond to the {100}, {110}, and {111} facets, respectively. The light orange color of the outermost ring indicates that the final nanocrystals have reduced symmetry relative to that of the initially formed seeds. Adapted with permission from ref 100. Copyright 2021 American Chemical Society.

seeds based on their symmetry relative to the underlying unit cell. We then discuss the phenomenon of symmetry breaking in the growth process, with an emphasis on the synthetic methods capable of promoting asymmetrical growth for mono-, bi-, and multimetallic systems. Built upon the concepts and methodologies introduced in the preceding sections, we then showcase a diverse array of symmetry-broken metal nanocrystals that have been successfully synthesized, together with insights into their growth mechanisms. We also highlight various properties and applications endowed by the symmetry-broken nanocrystals. In the end, we summarize the state of the art while offering perspectives on the challenges, opportunities, and future directions in developing nanocrystals with reduced symmetry. Although our discussion centers on nanocrystals made of *fcc* metals, the concepts, methods, and mechanisms should be extendible to metals with different crystal structures and even to other types of solid materials, including semiconductors and their hybrids with metals. We hope the readers will gain a broad range of necessary knowledge on the fundamentals of asymmetrical growth and symmetry breaking and, more importantly, find the inspiration to further advance this fast-evolving multidisciplinary field of nanomaterial research.

2. NUCLEATION: FORMATION OF NUCLEI AND THEN SEEDS

In the context of colloidal synthesis, nucleation, the emergence of a new thermodynamic phase in the reaction system, is considered the very first step responsible for inducing the transition from atomic/molecular precursors to nanocrystals. In the simplest picture, nucleation can be divided into three major steps: (i) generation of atomic species, also referred to as monomers, from the reduction or decomposition of a precursor, (ii) creation of nuclei through aggregation of the atoms or stepwise addition and reduction, and (iii) evolution of the nuclei into seeds with a fixed internal structure.[1] In this section, we focus on the symmetry breaking phenomenon during the nucleation step and its impacts on the symmetry and internal structures taken by seeds made of an *fcc* metal, in addition to a brief discussion of the shapes favored by the seeds under thermodynamically and kinetically controlled conditions, respectively.

2.1. Face-Centered Cubic Metal

In theory, a nanosized crystal should adopt the same crystal structure as its bulk counterpart. As such, the concept of symmetry with regard to the nucleation step in a colloidal synthesis of metal nanocrystals should originate from the crystalline nature of metallic elements, by which atoms are arranged into a crystalline lattice. Many metals, especially noble metals, are crystallized in the *fcc* structure under atmospheric pressure. The unit cell of an *fcc* metal embraces a number of symmetry elements, including three 4-fold (C_4) rotational axes through the faces, four 3-fold (C_3) rotational axes through the corners, and six 2-fold (C_2) rotational axes, in addition to nine mirror planes (σ) and one center of inversion (i) at the center of the unit cell. The symmetry of the unit cell belongs to the O_h point group due to the presence of mirror planes (σ_h) perpendicular to the principal C_4 axes of rotation.[101,102] The high symmetry point group of an *fcc* metal accounts for the highly symmetric shapes (e.g., cube, cuboctahedron, or octahedron) that are often adopted by Au, Ag, Pt, Pd, and Rh nanocrystals.

2.2. Formation of Nuclei

Under homogeneous nucleation without the introduction of preformed seeds, all nanocrystal syntheses begin with the aggregation or assembly of metal atoms into small clusters, commonly referred to as nuclei. The nuclei may not have a specific symmetry because of fluctuations in the number and/or ordering of the atoms.[59,60] Their small sizes, coupled with the dearth of characterization tools, pose a technical challenge in unveiling the exact structural characteristics, not to mention their explicit roles and dynamic nature in the initial stage of nanocrystal synthesis. More efforts to capture, identify, and monitor such minuscule structures would help deconvolute the exact pathways in which they evolve from a metal precursor, providing a guideline to correlate synthetic parameters with the nuclei and eventual internal structures of the seeds.

To this end, various hypotheses pertaining to the formation and structure of nuclei have been proposed, with most of them related to the explicit route that the precursors are transformed into clusters (direct vs indirect), stacking fault energy of the metal, and reaction kinetics.[1,103−106] For example, it was suggested that the metal nuclei favor random hexagonal close packing instead of *fcc* when the precursor is reduced or decomposed at an extremely slow rate.[1,62,107] This trend is

https://doi.org/10.1021/acs.chemrev.2c00468
Chem. Rev. 2023, 123, 3693−3760

more pronounced for metals with a relatively low stacking fault energy or twin boundary energy, such as Cu, Ag, and Au.[65,108−111] Considering the debatable uncertainty about the evolution of nuclei, limitation on imaging quality, and potential impacts of the electron beam on the atomic structure, the following discussion focuses on two most plausible routes to the formation of nuclei, including (i) stepwise addition and reduction to generate clusters with gradually increasing sizes and (ii) aggregation of atoms and/or clusters.

2.2.1. Stepwise Addition and Reduction. In retrospect, the most ambiguous aspect of homogeneous nucleation is the actual pathway that a salt precursor undertakes before transforming to nuclei: whether the precursor is reduced into zerovalent atoms first, followed by their aggregation into nuclei, or the precursor directly evolves into nuclei prior to reduction. Computational studies based on first-principles molecular dynamics simulations have shed some light on this mystery and suggested that nucleation could be achieved by forming clusters or nuclei from the partially reduced precursors.[1,103] In this case, the precursor compounds can be directly converted into nuclei and added to other precursor-based nuclei or growing nanocrystals without going through the zerovalent state. When simulating the nucleation step involved in a synthesis of Pt nanocrystals, it was proposed that a Pt(II)−Pt(I) dimer stabilized with Cl^- ions could be generated directly from two dissolved $PtCl_2(H_2O)_2$ complexes, which were the hydrolysis product of $PtCl_4^{2-}$ precursor, through the injection of one electron.[112,113] The Pt(I)−Pt(II) dimer could be subsequently converted to a Pt(I)−Pt(I) dimer through the addition of another electron and the loss of Cl^- ions. Interestingly, a third reduction step could also occur, where both previously formed Pt(II)−Pt(I) and Pt(I)−Pt(I) dimers would react with another $PtCl_2(H_2O)_2$ complex to form a Pt(I)−Pt(II)−Pt(I) or Pt(I)−Pt(II)−Pt(II) trimer. The formation of these partially reduced precursors (dimers and trimers) was expected to be the early intermediate steps toward the emergence of larger clusters or nuclei. The preferred reduction via electron transfer from the reducing agent to these dimeric and trimeric clusters could be ascribed to their higher electron affinities than the starting precursor because of orbital delocalization. This plausible mechanism excludes the direct reduction of the monomeric precursor to atoms before being added to the growing clusters to form larger nuclei.

Simulations of the reaction between a $PtCl_2(H_2O)_2$ complex and growing clusters also demonstrated that the growth of nuclei progressed via the continuous addition of unreduced Pt(II) complexes to partially reduced Pt complexes or small clusters (Figure 4).[114] The structural fluxionality of the clusters and the redistribution of ligands on the surface during each stepwise addition and reduction cycle suggested the possible occurrence of symmetry breaking in the early stage of nucleation. With the continuous addition of unreduced Pt(II) complexes and the detachment of ligands from the surface, the clusters grow in an accelerated manner because of a process known as autocatalysis.[115−118] This reduction mechanism was found to be only favorable under slow reduction kinetics, such as when a mild reducing agent and a low concentration of precursor are involved. Under these conditions, the precursor tends not to be completely reduced to atomic species before being added to the surface of a growing cluster. Since it was also not necessary for the cluster (or a nanocrystal) to be fully reduced to the zerovalent state, its surface might be terminated

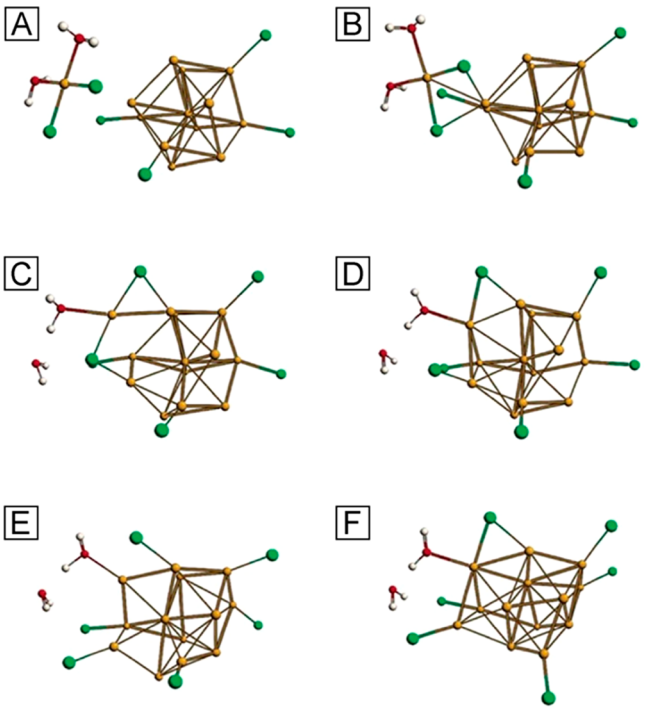

Figure 4. Snapshots from a first-principles molecular dynamics simulation, showing the reaction between a $PtCl_2(H_2O)_2$ complex and a $Pt_{12}Cl_4$ cluster. Pt: yellow. Cl: green. O: red. H: white. Simulation time: (A) 0, (B) 0.6, (C) 1.3, (D) 2.0, (E) 3.2, and (F) 5.0 ps, respectively. Adapted with permission from ref 114. Copyright 2003 American Chemical Society.

in positively charged metal ions coordinated to ligands or solvated by solvent molecules. This unique structure at the interface might be connected to the capping effect of some ionic additives such as Cl^-, Br^-, and citrate, as well as polymeric species commonly used in a colloidal synthesis of metal nanocrystals.[1,119] While the mechanistic hypothesis was found to be energetically acceptable, the predictions would be more realistic and valuable if additional physical details could be integrated into the simulations, such as other types of solvents, surfactants, and impurities commonly involved in a synthesis. Thanks to recent advances in time-resolved characterization techniques, a more detailed picture has also been obtained for the formation of nuclei from the partially reduced precursors or clusters through the integration of a continuous flow reactor with in situ X-ray absorption fine structure spectroscopy.[104] For the synthesis of Au nanocrystals, partial reduction of $AuCl_4^-$ indeed occurred in the early stage of nucleation, followed by the formation of intermediates such as $Cl_3^-Au-AuCl_3^-$ dimers and then larger Au_nCl_{n+x} clusters, rather than Au_n^0 clusters, under a mild reaction condition.

2.2.2. Aggregation of Atoms and/or Clusters. As an alternative route, atoms are formed through chemical reduction, followed by their collision and aggregation into agglomerates with a fluctuating structure due to the thermal energy. This classical theory on homogeneous nucleation is based upon the LaMer model, which was formulated in the 1950s to account for the synthesis of sulfur colloids with a uniform size distribution.[120] When extended to the colloidal synthesis of metal nanocrystals, this simple model offers qualitative insights into the production of samples with minimal size variations. When the precursor is reduced or

https://doi.org/10.1021/acs.chemrev.2c00468
Chem. Rev. 2023, 123, 3693−3760

decomposed, the concentration of metal atoms in the reaction solution will increase steadily as a function of time. Once the concentration of metal atoms exceeds the minimum value for nucleation, homogeneous nucleation (or self-nucleation) will transpire, in which the atoms spontaneously aggregate to form small clusters. When the synthesis is conducted in air and accompanied by the halide ions added into the solution or from the precursor complex, the possible involvement of oxidative etching (discussed later in section 2.4) can oxidize the atoms/clusters back to the ionic species.[121,122] As a result, the atoms or clusters comprised of both atoms and ions are expected to undergo constant aggregation or attachment in tandem with the oxidative etching process. Such an aggregation cycle can be repeated multiple times until the clusters have a large enough size to become stable. When their size reaches a critical threshold, these clusters will evolve into well-defined nuclei.[123] These larger clusters or nuclei with the densest packing of atoms are expected to adopt symmetry similar to those that typify the stable and observable seeds emerging in the later stage.[124−128] As the synthesis proceeds, the rapid consumption of atoms in the solution will cause their concentration to drop quickly. If the concentration drops below the minimum level for nucleation, homogeneous nucleation will cease. Again, most claims on the morphology of the nuclei are supported by very limited experimental evidence due to the instrumental limitation in imaging such minuscule structures in a highly dynamic liquid environment. The elementary steps of nucleation should continue to be scrutinized through a combination of computational simulations and experimental studies, especially when techniques with real-time visualization capability become more commercially available.

2.3. Formation of Seeds

The birth of a seed is marked by the moment a nucleus grows past a critical size and structural fluctuation becomes too energetically costly, locking the internal structure of the nucleus into a well-defined one.[1] As such, seeds can be defined as species with a nonfluxional internal structure (or crystallinity) but poorly defined shape (or morphology) in the initial stage of a synthesis. At the atomic level, the size, shape/morphology, and surface composition of a seed are supposed to constantly evolve during the course of a synthesis as a result of atomic deposition and diffusion, size enlargement, facet development, and shape transformation. For simplicity, the seeds discussed herein will be confined to assemblies of atoms with a distinct shape (or symmetry) and a fixed crystallinity, regardless of their size and surface composition. They are essentially "growing nanocrystals," meaning that the nanocrystals obtained at any time point can be considered as "seeds" for growth in the following steps. Although these building blocks could take different sizes in reality, surface diffusion might become an issue when the size of a seed becomes too large. Therefore, whether generated in situ through homogeneous nucleation or presynthesized for the seed-mediated growth, the seeds in our discussion are limited to those with reasonable sizes and the capability to support further growth. In general, seeds can be categorized into four major types based on their internal structures or the number of planar defects introduced into the crystal lattice in the early stage of a synthesis, including single-crystal (with no planar defect), singly-twinned (with one twin plane), multiply-twinned (with more than one planar defects), and stacking-fault-lined seeds.[65]

Assuming that the internal structure of a seed is fixed, another feature that can be deduced for a more precise description is symmetry, which is related to its overall shape. Restricted by the *fcc* structure adopted by all noble metals except Ru, the shape or symmetry of a seed should inherit the high symmetry of O_h point group featured by the unit cell.[68,69] In the ideal case where the irregularities on the atomic level (e.g., vacancies and atomic steps commonly found on the surface) are neglected, each type of seed can be assumed to exhibit a specific symmetry: O_h for truncated octahedron, D_{5h} for decahedron, I_h for icosahedron, and D_{3h} for thin plate. In principle, a seed can have symmetry different from that of the underlying unit cell. The symmetry of a seed is preserved when its shape inherits the O_h point group of the unit cell. In contrast, the symmetry of a seed is broken when it adopts different symmetry from that of the unit cell.

2.3.1. Seeds with the Same Symmetry as the Unit Cell. Intuitively, only single-crystal seeds can take the same symmetry as the underlying unit cell. As an intermediate generated in the initial stage of a synthesis, single-crystal seeds are defined by only one single-crystal domain with a continuous stacking order devoid of planar defects. Starting with a two-dimensional (2-D) polar plot of the specific surface free energy (γ_i) of an *fcc* crystal as derived from the Wulff construction (Figure 5A), it is feasible to predict the

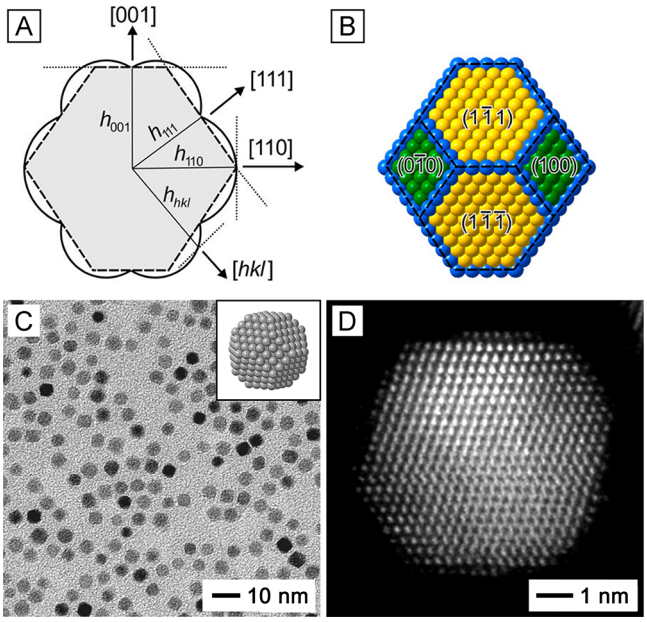

Figure 5. Single-crystal seeds featuring the same symmetry as the unit cell of an *fcc* metal. (A) A 2-D section of a polar plot of the specific surface free energies of an *fcc* metal oriented along [1$\bar{1}$0] as derived from the Wulff theorem. The inner envelope denoted by dashed lines corresponds to the equilibrium shape of a single-crystal seed. (B) A 3-D atomic model corresponding to the shape shown in panel A. (C) TEM and (D) HAADF-STEM images of truncated octahedra, a common shape taken by the single-crystal seeds made of an *fcc* metal. The inset in panel C shows the corresponding atomic model of a truncated octahedron. (A, B) Reproduced with permission from ref 72. Copyright 2015 American Chemical Society. (C, D) Reproduced with permission from ref 133. Copyright 2015 American Chemical Society.

https://doi.org/10.1021/acs.chemrev.2c00468
Chem. Rev. 2023, 123, 3693−3760

equilibrium shape or symmetry of a single-crystal seed in vacuum by correlating the polyhedral shape inside the polar plot to a three-dimensional (3-D) structure.[72,129,130] Based on the broken bond approximation for an *fcc* metal, the specific surface energy of {111} facets is lower than that of {100} facets, that is, $\gamma_{(111)} < \gamma_{(100)}$.[131,132] Hence, the {111} facets are expected to take a relatively larger proportion than the {100} facets on the surface of a nanocrystal to minimize the total surface free energy. As a result, the equilibrium shape of a single-crystal seed made of an *fcc* metal should be a truncated octahedron enclosed by eight {111} and six {100} facets (Figure 5B).[72] It should be noted that the thermodynamically favored shape of a single-crystal seed made of an *fcc* metal is often referred to as a cuboctahedron in the literature. In essence, a cuboctahedron is a special case of a truncated octahedron with a similar quasi-spherical profile but higher degree of truncation to the midpoint of the edges, giving rise to six triangular (rather than hexagonal) and four square faces. In reality, the single-crystal seed likely adopts a shape in the truncated octahedron−cuboctahedron continuum depending on the actual environment involved. For consistency and conciseness, the single-crystal seeds formed in the initial stage of a synthesis are considered to take a truncated octahedral shape in this Review.

As a thermodynamically favored product, the formation of single-crystal seeds with a truncated octahedral shape is expected to dominate a system truly under thermodynamic control and without the influence of a facet-selective capping agent (Figure 5C).[133] Such a seed also prevails over other types of seeds when the reduction rate is relatively fast due to the use of a strong reducing agent, fast injection, or a relatively high temperature because atoms tend to follow the defect-free packing pattern of the *fcc* structure under these kinetic conditions.[1,65] To experimentally confirm the existence of single-crystal, truncated octahedral seeds, high-angle annular dark-field scanning transmission electron microscopy (HAADF-STEM) image could be taken to resolve the atomic structure (Figure 5D).[133] In practice, single-crystal seeds whose shapes substantially deviated from the Wulff shape could be obtained through the addition of surface capping agents that selectively bind to a specific type of facets to alter the anisotropy of surface energy or through a kinetically controlled environment.[72,119] Some common shapes of single-crystal seeds that hold the O_h symmetry of the underlying unit cell include cube, cuboctahedron, octahedron, truncated octahedron, and rhombic dodecahedron.

2.3.2. Seeds with Symmetry Different from the Unit Cell. Not all seeds are born with a perfect crystal structure as many of them can contain one or more planar defects (i.e., twin defect or stacking fault), which disrupts the ideal ABCABC stacking sequence along the <111> direction of the *fcc* structure. A twin defect emerges when the lattices on opposite sides of a plane, termed twin boundary (denoted |A|), mirror each other. In this case, the stacking sequence is switched to ABC|A|CBA.[134] Noble metals are well-known for their tendency to produce twin defects during crystallization because of the relatively small penalty in energy when such a planar defect is introduced into the single-crystal structure.[18] In addition to the twin defect, another class of planar defect emerges through the insertion or deletion of a hexagonally packed layer, corresponding to an extrinsic or intrinsic stacking fault, respectively.[135] In an *fcc* structure, if |B| represents the inserted plane and || the missing plane, an extrinsic fault can be presented as ABC|B|ABC whereas an intrinsic fault is denoted AB||ABC. In general, the stacking fault energy correlates positively with the twin-boundary energy because a stacking fault can be considered as a pair of parallel twin boundaries, making its energy approximately twice that of the twin-boundary energy.[136] Intuitively, a thermodynamically favored product should exhibit almost crystallographic perfection and symmetry identical to the underlying unit cell. As a result, the inclusion of planar defects in the seeds suggests the occurrence of symmetry breaking during the latter stage of nucleation, resulting in seeds featuring symmetry (and thus shapes) deviating from the built-in O_h symmetry of the underlying unit cell.

2.3.2.1. Singly-Twinned Seeds. The structure of a singly-twinned seed can be regarded as two truncated single-crystal pyramids symmetrically placed base-to-base and conjoined by one twin plane positioned in between (Figure 6A,B).[137] The formation of singly-twinned seeds follows the same thermodynamic rule as the single-crystal species, by which the most stable structure is the one having the lowest possible energy. As a result, the surface of singly-twinned seeds is typically enclosed by a mixture of {100} and {111} facets, unlike other internally defected seeds (i.e., decahedra, icosahedra, and plates) that tend to favor the expression of {111} facets only.[65] The outline of a singly-twinned seed is mostly similar to that of a right bipyramid with small truncations at the corners. As a special case of the bipyramidal system, this prototype is covered by six equivalent right-isosceles triangular side faces bounded by {100} facets and is bisected by a twin plane or a set of parallel planar defects running through the equilateral triangle base.[137−141] Singly-twinned seeds with a bipyramidal shape are characterized by D_{3h} symmetry due to the presence of two C_3 rotational axes, three perpendicular C_2 axes, and one σ_h mirror plane. Other bipyramidal structures that resemble right bipyramids and have been synthesized include {111}-terminated bitetrahedra[141,142] and {110}-encased bipyramids.[143] It should be pointed out that these shapes have only been observed in a few instances and are often deduced from the images of the final nanocrystals. As such, further analysis of the seeds should be performed to confirm if the singly-twinned seeds formed in the initial stage adopt similar shapes as the products.

2.3.2.2. Multiply-Twinned Seeds. When more than one twin defect is present, the seed is said to have a multiply-twinned structure. In contrast to single-crystal and singly-twinned species, the inclusion of multiple twin defects results in strain energies that drastically increase with particle size, making multiply-twinned seeds only stable at relatively small sizes.[125] The two most commonly observed multiply-twinned seeds have decahedral and icosahedral shapes, respectively. Despite sharing a lot of structural similarities, such as the exposure of {111} facets on the surface and the presence of 5-fold twinning and tensile strain on the side faces, these two types of multiply-twinned seeds can be easily distinguished based on the number of twin boundaries.[144,145]

An assembly of five single-crystal, tetrahedral subunits interconnected by 10 twin boundaries gives rise to a decahedral seed whose surface is terminated in 10 {111} facets (Figure 6C,D).[57,146] Since the angle between adjacent {111} facets along [110] projection is 70.53°, a deficiency or geometric gap of 7.35° inevitably remains in the construction of an ideal decahedron.[147] This gap is eventually filled by slightly expanding the lattice of each tetrahedral subunit,

https://doi.org/10.1021/acs.chemrev.2c00468
Chem. Rev. 2023, 123, 3693−3760

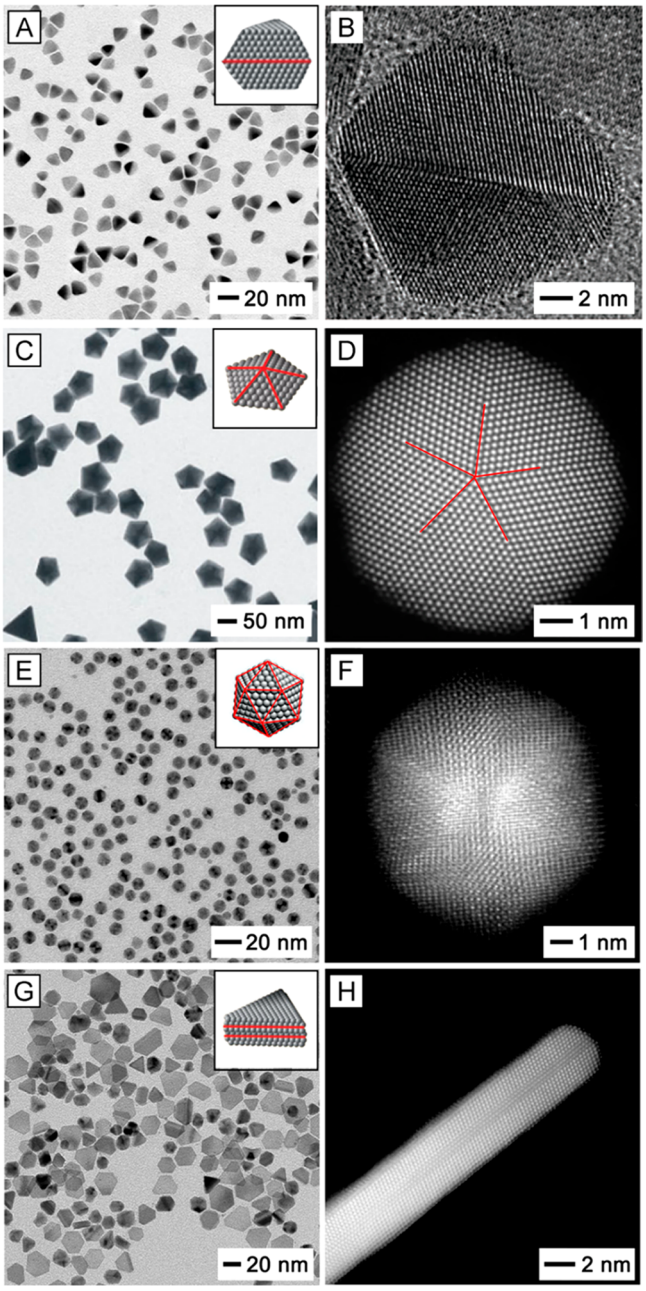

Figure 6. Seeds with symmetry different from the unit cell of an *fcc* metal. (A) TEM and (B) high-resolution TEM (HRTEM) images of singly-twinned right bipyramids, with the corresponding atomic model shown in the inset of panel A. (C) TEM and (D) HAADF-STEM images of decahedra with a penta-twinned structure and the corresponding atomic model shown in the inset of panel B. (E) TEM and (F) HAADF-STEM images of icosahedra with a multiply-twinned structure. The inset in panel E shows the corresponding atomic model of an icosahedron. (G) TEM and (H) HAADF-STEM images of triangular nanoplates with a stacking-fault-lined structure and the corresponding atomic model shown in the inset of panel G. The hexagonal nanoplates are present as byproducts in panel G. (A, B) Adapted with permission from ref 137. Copyright 2013 American Chemical Society. (C) Reproduced from ref 57. Copyright 2006 Wiley-VCH. (D) Reproduced with permission from ref 146. Copyright 2012 American Chemical Society. (E−H) Reproduced with permission from ref 133. Copyright 2015 American Chemical Society.

causing a tensile strain across the side faces. Given that the heterogeneous distribution of tensile strain increases with the lateral dimension, it is energetically unfavorable for atoms to grow laterally from a decahedral seed.[65,144] As such, atomic deposition along the axial direction is more favorable, making decahedral seeds ideal for the synthesis of nanocrystals such as penta-twinned nanorods/nanowires. Another structural peculiarity of decahedral seeds is the presence of two different types of edges: one corresponding to the five single-crystal edges along the pentagonal cross-section and the other associated with the 10 twinned edges along twin boundaries typically referred to as ridges.[144] With a unique C_5 rotational axis, decahedral seeds belong to the D_{5h} point group, which is lower in symmetry order than the underlying unit cell.

Compared to the decahedral counterpart, an icosahedral seed is much more complex, as it is comprised of 20 single-crystal, apex- and facet-sharing tetrahedral subunits. The subunits are assembled through 30 twin boundaries, giving rise to a pseudospherical profile encased by 20 {111} facets (Figure 6E,F).[133,145] Due to the unique packing of the tetrahedral subunits, an icosahedron belongs to the I_h point group characterized by C_2, C_3, and C_5 rotational axes and the highest symmetry order of 120.[148] As such, icosahedral seeds have higher symmetry order than the underlying unit cell, an exception to the effect of planar defects in reducing the symmetry of the product. Similar to the structure of decahedra with noncrystallographic symmetry, a gap of 1.54 steradians would be left behind, causing a tensile strain on the atoms of each tetrahedral subunit, as well as the side faces.[149,150]

2.3.2.3. Stacking-Fault-Lined Seeds. Often categorized as a 2-D nanostructure, stacking-fault-lined seeds possess one or more planar defects parallel to their basal faces. Depending on the metal and the synthetic protocol, the planar defect incorporated into the structure could be either a twin plane or a stacking fault. Because of the 6-fold symmetry of an *fcc* metal, the stacking-fault-lined seeds often take a triangular or hexagonal plate-like shape with the two basal planes terminated in {111} facets (Figure 6G).[133] The stacking fault parallel to the basal planes of such a nanoplate can be directly resolved under HAADF-STEM images (Figure 6H)[133] or indirectly deduced from the presence of the forbidden 1/3(422) reflection in the electron diffraction pattern recorded along the [111] zone axis.[109] Geometrically, stacking-fault-lined seeds in the form of triangular nanoplates belong to the D_{3h} point group, which is far lower in symmetry order than the unit cell of an *fcc* metal due to the loss of all symmetry operations except for the primary C_3 rotational axis perpendicular to the basal planes.[68] Commonly found as byproducts in the synthesis of triangular nanoplates, seeds containing stacking faults can also adopt a regular hexagonal plate-like shape with equivalent side lengths. These hexagonal plates still carry C_3 rather than C_6 symmetry due to the alternating {111} and {100} facets on the side faces.[151] In terms of synthesis, the formation of stacking-fault-lined seeds is not thermodynamically favored in any size range because they have a relatively higher surface energy than other structures with the same volume (e.g., quasi-spherical or Wulff shape).[152] As such, robust syntheses of stacking-fault-lined seeds require tightly controlled kinetic conditions,[153−155] coupled with other processes such as Ostwald ripening[156] or oxidative etching[157] to help decelerate the reduction kinetics.

https://doi.org/10.1021/acs.chemrev.2c00468
Chem. Rev. 2023, 123, 3693−3760

2.4. Formation of Seeds with Diverse Symmetry: Thermodynamics vs Kinetics

The internal structure and symmetry taken by a seed during the nucleation stage are dictated by the interplay between thermodynamic and kinetic factors, which are ultimately defined by a set of experimental parameters.[100,158,159] In a system mainly driven by thermodynamics, the most favorable seed should exhibit a global minimum in total Gibbs free energy, where all the energetic contributions (e.g., surface, bulk, defects, and strain) are collectively minimized.[131] By comparing the overall free energy of various structures, a phase diagram was constructed as functions of particle size and temperature, showing that single-crystal, truncated octahedral seeds are favored at relatively large sizes while multiply-twinned seeds are more stable at small sizes as the strain energy increases with particle size (Figure 7A).[152] Due to the distinct characteristics of each metal, the size (or crossover points) from one type of seed to another can vary among different metals.[125,160] In essence, if a seed is allowed to reach the equilibrium state, its shape and thus symmetry should be solely determined by thermodynamics. While the thermodynamic argument provides an insightful explanation for the most favored symmetry taken by the seeds at a given size, accumulating evidence indicates that experimental results often deviate from theoretical predictions. Under certain conditions with a significantly high surface diffusion barrier, some seeds would settle into a local minimum in terms of Gibbs free energy instead of reaching the global minimum, generating a less stable but kinetically favored product.[72,159] In this regard, a more viable strategy to maneuver the internal structure and thus symmetry of the seeds, especially those unfavored by thermodynamics, should be established from a kinetic perspective.

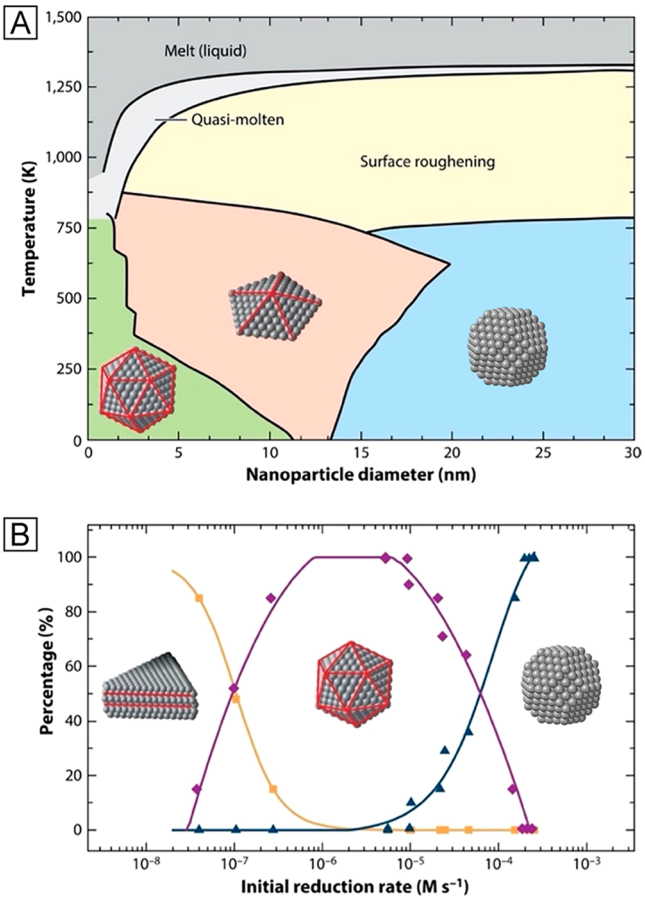

Figure 7. Thermodynamic and kinetic approaches to controlling the internal structure and thus the shape or symmetry taken by the seed. (A) Particle size−temperature phase diagram computed for Au nanoparticles. (B) Plot displaying the relative fractions of Pd nanocrystals as a function of the initial reduction rate, showing the formation of plates with stacking faults (orange line), multiply-twinned icosahedra (purple line), and single-crystal truncated octahedra (blue line) at different initial reduction rates. (A) Adapted with permission from ref 152. Copyright 2009 American Chemical Society. (B) Reproduced with permission from ref 133. Copyright 2015 American Chemical Society.

With regard to the kinetic control strategy, the reduction rate of the metal precursor in the nucleation stage of a synthesis has been found to play a crucial role in dictating the internal structure and thus symmetry of the seeds.[100,133] In general, the reduction kinetics involved in a colloidal synthesis of metal nanocrystals can be described using the Finke-Watzky model that contains two pseudoelementary steps:

$$A \rightarrow B \quad (1)$$

$$A + B^{*} \rightarrow 2B \quad (2)$$

where A, B, and B* represent the precursor molecule, metal atom, and active site on the seed, respectively.[118,161] While the first reaction corresponds to the relatively slow reduction of the precursor in solution, the second step involves faster reduction on the surface of existing seeds, referred to as solution and surface reduction, respectively (see more detailed discussion in section 3.1.2).[62,162,163] The rate of the first step primarily affects the internal structure and thus symmetry of the seeds generated during the nucleation stage, while the second step prevails in the following growth step.[163−166] Due to the collision and electron transfer between the precursor molecule and reductant, the rate of reaction 1 is expected to follow a second-order rate law, which is directly proportional to the concentrations of both reagents.[167] For most synthetic protocols, the amount of reducing agent is in great excess to ensure that its concentration remains relatively constant throughout the reaction.[58] Under this assumption, the rate law can be simplified into a pseudo-first-order reaction: reaction rate $(r) = k[A] = -d[A]/dt$, where [A] is the concentration of the metal precursor.[118] By leveraging common techniques such as inductively coupled plasma mass spectrometry (ICP-MS) or UV−vis spectroscopy, the concentration of the precursor can be tracked as a function of reaction time. The data are then fitted using the Finke-Watzky model to derive the kinetic parameters of the reduction, including the rate constant (k) and the activation energy (E_a), as well as the initial reduction rate (r_0, that is, r at $t = 0$).[158,163]

With the help of this mathematical model, a recent study on the polyol synthesis of Pd nanocrystals established a quantitative correlation between the initial reduction rate and the internal structure or symmetry of the resultant seeds.[133] It was shown that truncated octahedra, icosahedra, and plates could be generated by adjusting the initial reduction rate of the polyol synthesis through variations to the type of polyol and/or reaction temperature (Figure 7B). Specifically, when reducing $PdCl_4^{2-}$ by ethylene glycol (EG) at 140 °C, the fast initial reduction rate ($r_0 \approx 10^{-4}$ M s^{-1}) arising from the strong reducing power of EG and the elevated reaction temperature promoted the formation of single-crystal seeds, generating

https://doi.org/10.1021/acs.chemrev.2c00468
Chem. Rev. 2023, 123, 3693−3760

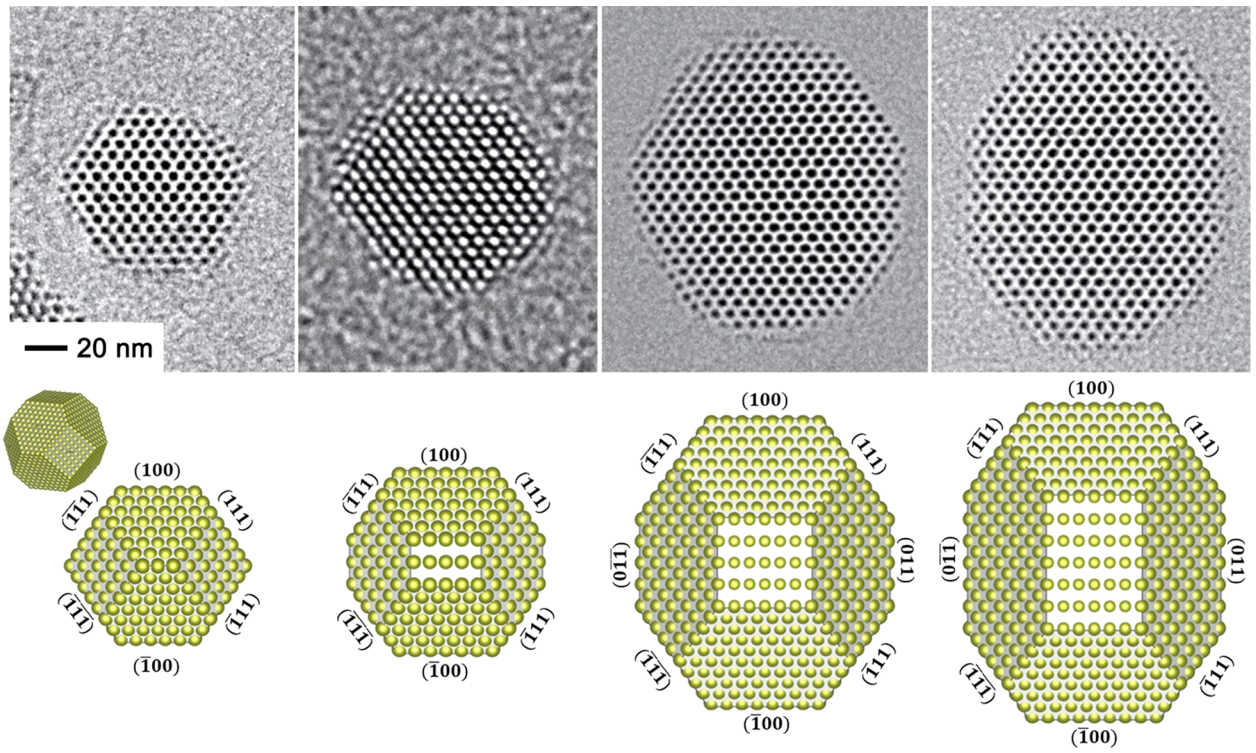

Figure 8. Phase-contrast HRTEM images (top) and the corresponding schematic models (bottom) of Au nanocrystals involved in the symmetry breaking of truncated octahedral seeds, oriented in the [011] direction. Reproduced with permission from ref 67. Copyright 2017 American Chemical Society.

truncated octahedra as the product. In contrast, the substitution of EG with diethylene glycol (DEG), which has a weaker reducing power, led to a moderate initial rate ($r_0 \approx 10^{-6}$ M s^{-1}) for the generation of multiply-twinned seeds, which subsequently grew to icosahedra. Moreover, plates with a stacking fault-lined structure were obtained when $PdCl_4^{2-}$ was reduced by DEG at a low temperature of 75 °C due to the substantially decelerated reduction rate ($r_0 \approx 10^{-8}$ M s^{-1}). Taken together, as the initial reduction rate decreased, the seeds formed in the early stage would switch from single-crystal to multiply-twinned and finally stacking-fault-lined structure.[133] In practice, the initial reduction rate can be experimentally adjusted by choosing metal precursors and reductants with appropriate reactivity, introducing additives to alter the speciation of the precursor, regulating the reducing power of the reductant, and choosing a proper reaction temperature.[154,155,168−170] The methodology has also been successfully applied to synthesize seeds made of other noble metals and even bimetallic systems with two precursors present in the solution.[166,171−174] Although the exact value of the initial reduction rate responsible for the formation of each type of seed may differ among different metal systems, it is expected to follow the same trend observed for Pd. This quantitative correlation between the initial reduction rate and the internal structure of the seeds offers an effective means to achieve a specific type of seeds with desired symmetry and thus the shape of nanocrystals developed from them.

Aside from thermodynamic and kinetic controls, oxidative etching is another method to alter the seed population for the production of seeds featuring a specific type of internal structure. As a process intrinsic to all metals, oxidative etching involves a redox reaction in the presence of an etchant consisting of an oxidant for the metal and a coordination ligand for the corresponding metal ions, such as the O_2 from air and halide ions released from the salt precursor or other additives (see detailed discussion in section 3.2.3), respectively.[121,122] It is typically initiated from the twin boundaries or other defect zones owing to their higher surface energies than the single-crystal domains.[175] The oxidative etchant can also be judicially selected to ensure the survival of single-crystal and/or singly-twinned seeds instead of multiply-twinned seeds from the sample preparation.[121,122] For example, the type and number of twin defects in the seeds, which are correlated with their symmetry, can be regulated by tuning the strength of the etchant through the use of different ligands at various concentrations.[137,140] Using the polyol synthesis of Ag nanocrystals as an example, replacing Cl^- with Br^- ions, which would lead to the formation of a less powerful etchant, removed the multiply-twinned seeds while leaving behind the singly-twinned seeds for their further growth into right bipyramids.[140] Other strategies for mitigating the oxidative etching to generate single-crystal seeds include (i) bubbling the solutions with an inert gas to remove O_2 prior to the reaction,[153,176] (ii) adding a capping agent capable of preventing O_2 adsorption, such as citric acid or citrate ion,[177−179] or (iii) scavenging O_2 in the reaction mixture with another redox pair, such as Fe(III)/Fe(II) or Cu(II)/Cu(I).[33,153] For most noble metals, it is feasible to synthesize all the different types of seeds mentioned in section 2.3 as reasonably pure samples by controlling the experimental conditions. A collection of protocols for generating monometallic nanocrystals that can serve as seeds for further growth has been extensively covered in recent reviews.[18,66]

https://doi.org/10.1021/acs.chemrev.2c00468
Chem. Rev. 2023, 123, 3693−3760

2.5. Symmetry Breaking

In principle, symmetry breaking during nucleation is a crucial step that determines not only the internal structure, morphology, and surface energy landscape of the seed but also the nascent symmetry of the growing nanocrystals. During the transition from nucleation to growth, the symmetry of a seed or growing nanocrystal is supposed to constantly evolve to accommodate the newly deposited atoms, as well as their diffusion across the surface. When the concentration of metal atoms drops below the minimum level for homogeneous due to their incorporation into the seeds, no additional nucleation event should occur, signifying the turning point at which succeeding growth will override the initial nucleation.[1,180] Instead of assembling to form more nuclei and seeds, the just-formed atoms from the reduction or decomposition of the remaining precursor will now participate solely in the development of facets by choosing which site on the surface of a seed it will land. Upon deposition onto a high-energy site under the premise of minimizing the total surface energy, the adatom can migrate to other regions on the surface if they are equipped with a sufficient kinetic energy, stochastically breaking the symmetry of the seed as the synthesis is continued.[181] Once symmetry breaking is initiated, the asymmetrical growth pattern can be well retained if the surface diffusion of adatoms is kept relatively slow.

The dynamic nature of the symmetry of a seed around the symmetry breaking point has been unveiled by observing the changes to the atomic structures of truncated octahedral seeds at the embryonic stage of Au nanorod growth (Figure 8).[67,182,183] At the beginning of the synthesis, the preformed seeds gradually grew at the same rate along all symmetry-equivalent directions while maintaining their truncated octahedral morphology. Upon reaching a critical size of approximately 4 nm, small truncated facets started to form nonuniformly at the intersection of {111} facets to remove high-energy atoms at the edges. The truncations formed asynchronously and marked the onset of symmetry breaking for the original seed structure. The emerged {011}-type facets have a more open atomic structure than the pre-existing {111} and {100} facets. In the presence of Ag^+ ions, the new facets could be stabilized through passivation with a layer of Ag adatoms, resulting in faster growth rates in other directions. As a result, the initial truncations were preserved by becoming the elongated "side facets" of the nascent nanorod. Collectively, the formation of new high-index facets was a geometrical driver for the initial symmetry breaking of the embryonic seeds in the synthesis of Au nanorods.[67] It should be noted that this analysis was carried out using an ex situ protocol,[183] where the TEM images at sequential time points could have potentially been taken from different particles. Although this sampling method has served as an invaluable means for mechanistic studies, the conclusion drawn from the data may include oversimplified assumptions that are not representative of every particle in the entire sample. An in situ atomic-scale observation, ideally on the same particle, would unequivocally infer the structural changes that lead to symmetry breaking and thus asymmetrical nanocrystals.

3. GROWTH: FROM SEEDS TO NANOCRYSTALS

After nucleation, the as-formed seeds are supposed to grow into nanocrystals with different sizes and shapes while involving preservation or breaking of symmetry.[68,69,184] Since there are many reviews about the growth and shape control of symmetry-preserved nanocrystals,[1,119,185] this section mainly discusses the synthetic methods capable of promoting asymmetrical growth and generating symmetry-broken products. To provide a simplified and straightforward discussion, the seeds formed during the nucleation step or presynthesized for the seed-mediated growth are assumed to have a specific shape and internal structure and thus well-defined symmetry. We only consider the ideal situations in which any surface inhomogeneity caused by defects (e.g., vacancies and steps) and variation in surface coverage by the capping agents on the surface of the seeds are neglected, unless otherwise mentioned.[62,103,119] As such, all symmetry-related crystal axes are assumed to be equivalent in terms of their potential for growth during the formation of final nanocrystals.

Particle attachment and atomic addition are the two main pathways for nanocrystal growth, as discussed in sections 3.1.1 and 3.1.2, respectively.[1,66,79,186] For attachment growth, nucleation results in distinct seeds, referred to as nanocrystallites, which then arrange and fuse together to generate a final product (Figure 1).[79] The products often feature a polycrystalline structure and involve symmetry breaking, with wavy rods and wires as common examples.[187,188] In contrast, growth through atomic addition involves atom-by-atom deposition on a seed.[65] This growth pathway can result in products with either preserved or broken symmetry (Figure 1).[68] It should be noted that both particle attachment and atomic addition can be involved throughout different time points of a synthesis, depending on the experimental conditions. Thus, in both sections 3 and 4, while the focus is primarily on atomic addition, the syntheses and products might involve either or both pathways.

3.1. Symmetrical vs Asymmetrical Growth

Plants are a good example to illustrate the concept of asymmetrical vs symmetrical growth. As a real-life example of asymmetrical growth, the branches of a flowering plant tend to grow outward arbitrarily in various directions, not necessarily at equal rates. When flowers start to bud, the petals grow outward evenly and symmetrically to form flowers with high symmetry, an example of symmetrical growth. Similarly, the principles of asymmetrical and symmetrical growth also apply to the case of nanocrystals, but at a significantly smaller length scale.

The surface of a nanocrystal seed often displays multiple symmetry-related crystal axes, as determined by its inherent shape and faceting.[1,18,67] During subsequent growth, the growth rates along these symmetry-related axes can be the same or different, as mentioned in the introduction. During symmetrical growth, all the symmetry-related axes and thus the corresponding corners, facets, or edges will grow at the same rate, typically giving rise to symmetry-preserved products.[68,69,189,190] Asymmetrical growth, in contrast, occurs when the growth rates along the symmetry-related axes differ from each other, resulting in one or more facets, edges, or corners growing at a faster or slower rate than the rest.[68,191,192] In this way, asymmetrical growth will commonly produce nanocrystals with broken symmetry relative to that of the seed, such as when a nanocube evolves into a nanobar, or a singly-twinned seed grows into an asymmetric bipyramid.[177,193] However, depending on the type of seeds involved (e.g., when a decahedral seed grows into a monometallic penta-twinned nanorod), asymmetrical growth may also result in symmetry-

https://doi.org/10.1021/acs.chemrev.2c00468
Chem. Rev. 2023, 123, 3693−3760

preserved products in some cases.[68,194] Therefore, while a comparison of symmetrical and asymmetrical growth can be useful as a quick assessment of the involvement of symmetry breaking, each system needs to be evaluated individually based on its unique parameters.

Alternatively, many articles define the preferential deposition on one type of facet over another as "anisotropic growth".[195,196] Under this definition, when a truncated octahedral seed covered by both {111} and {100} facets grows evenly but exclusively on all the eight {111} facets to give a cubic nanocrystal as the final product, it is considered anisotropic growth, as the {100} facets do not grow at the same rate as the {111} facets.[196] However, in our discussion, this example would be classified as symmetrical growth since all the {111} facets are symmetry-related and grow at the same rate. Under our definition, asymmetrical growth would only occur if the symmetry-related crystal axes (in this case, normal to the {111} facets) do not grow equally, such as in the formation of a pencil-like nanostructure from a truncated octahedral seed where four {111} facets grow faster than the rest {111} and {100} facets. Thus, the reader should be attentive to our definition of asymmetrical growth to distinguish the current notion from those used in other publications. Overall, asymmetrical growth and the accompanying symmetry breaking event are often seen in attachment growth, while atomic addition can result in both symmetrical and asymmetrical growth.[79] Some mechanistic details of these two methods are discussed in the following two subsections.

3.1.1. Growth via Attachment. Attachment naturally leads to asymmetrical growth and thus the formation of a symmetry-broken product. Only a brief overview of this growth process is given here, as the scope of this Review is on symmetry breaking involving atomic addition. Readers can find a number of recent reviews on attachment growth.[79,197,198]

Attachment growth, or more precisely, oriented attachment, is a unique pathway in which different nanoscale components, rather than atoms, serve as the building blocks.[63,197,199] In a typical process, the building blocks, also known as nanocrystallites or seeds, are formed during the initial stages of a synthesis, followed by their rotation into a coaligned crystallographic orientation upon interaction, then attachment, and finally coalescence to generate a new structure (Figure 9A). The new structure is larger in size than the building blocks, together with the involvement of symmetry breaking. Common shapes include rods/wires, branched structures, and other asymmetrical morphologies.[77,82,83,200,201] Additionally, attachment growth can result in nanostructures possessing a large number of stacking faults, twin planes, and other types of defects.[78,80,202] Their unusual morphology coupled with the incorporation of multiple defects can imbue these nanostructures with unique properties and enhanced applicability in plasmonics and electrocatalysis.[203−205]

From a thermodynamic point of view, oriented attachment is driven by the energy reduction when the faces of a pair of nanocrystallites attach and merge.[79,197,206] The alignment and thereby elimination of facets high in energy will force the system to achieve the minimum total surface free energy and therefore a thermodynamically stable state.[64] In practice, the preferred facet for attachment can vary depending on the capping agent, solvent, and constituent metals, among others.[207−210] In most cases, facets that are not adequately covered by the capping agent will be favored for oriented attachment.[207] During attachment growth, the nanocrystallites

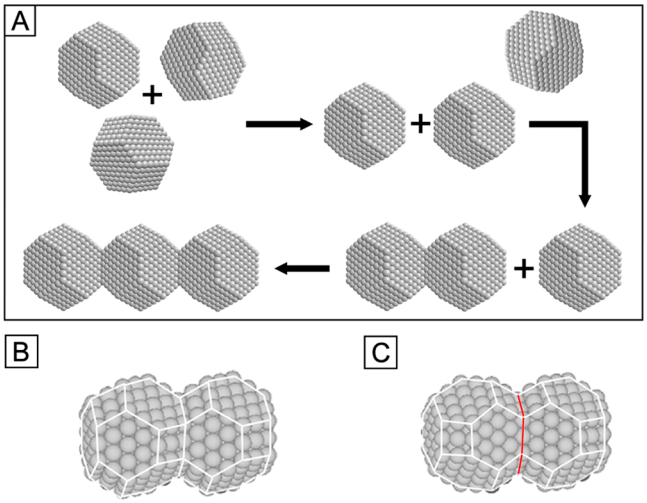

Figure 9. (A) Schematic showing the general steps of oriented attachment, in which nanoscale building blocks align with each other, attach, and finally coalesce to form a new structure. (B, C) Schematics showing the attachment of nanoscale building blocks with (B) perfect matching in orientation to give a single-crystal structure and (C) mirror-related matching to yield a twinned structure. (B, C) Reproduced with permission from ref 211. Copyright 2007 Wiley-VCH.

can rotate in space to align their crystallographic planes in either a common orientation or mirror-related symmetry prior to coalescence.[211] Several studies also suggested that surface species could affect the particle−particle interaction and thus attachment efficacy. For example, a recent experimental study involving liquid-cell TEM demonstrated that the overlap of surface citrate ligands might guide the rotation of two adjacent Au nanocrystallites from a random to a directional mode, until the same crystallographic orientation was shared by both particles.[212]

Depending on the orientation of the building blocks during attachment, the final product can have a single-crystal or defect-lined structure.[79,211] Specifically, when the crystallographic planes of the nanocrystallites are perfectly aligned during the attachment, a single-crystal structure will be generated after eliminating the interface and smoothing the surface (Figure 9B). Even with a small misorientation between the building blocks, the final product can still be single crystal due to the reorientation of the particles upon contact and diffusion of the constituent atoms.[209] On the contrary, a twin plane will be generated at the coalesced interface and incorporated into the final structure if the nanocrystallites merge through the same crystallographic planes that are arranged in a mirror image of each other (Figure 9C).[60,211] When two entirely different crystal planes are attached together, the resulting disruption in the original atomic stacking can cause the formation of stacking faults in the final structure.[79] In the case where the attached facets are not perfectly flat, dislocations will be created in the nanostructure due to the resulting misalignment and distortion of the interface. Although these structural defects could be removed through lattice relaxation to lower the total surface energy, they are usually preserved in the final structures, providing evidence for the attachment growth mechanism. In comparison with the conventional growth pathway involving atomic addition, oriented attachment offers a more powerful route to nanostructures abundant in defects.[79] In return, the unique

https://doi.org/10.1021/acs.chemrev.2c00468
Chem. Rev. 2023, 123, 3693−3760

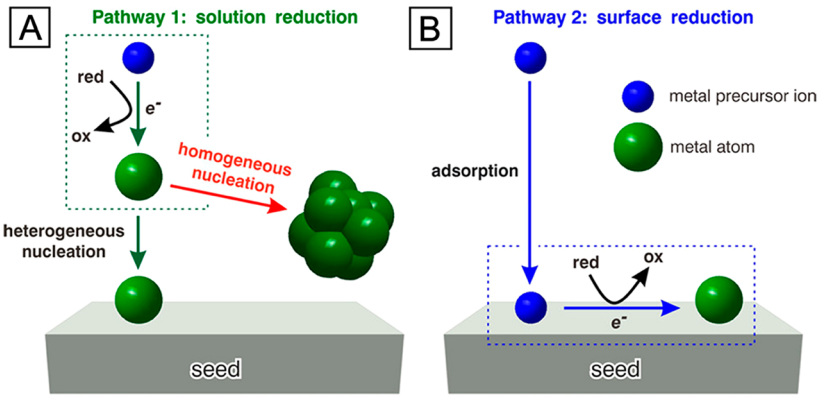

Figure 10. Schematic showing the two possible reduction pathways for nanocrystal growth, which occur (A) in the reaction solution phase and (B) on the surface of a nanocrystal, respectively. Reproduced with permission from ref 163. Copyright 2016 American Chemical Society.

assortment of defects can augment the properties of these nanostructures toward various catalytic reactions.

Oriented attachment is useful in inducing symmetry breaking due to the inherent nature of the method. By combining various nanocrystallites, oriented attachment instantaneously reduces the symmetry of the system.[12,213,214] Notable products of oriented attachment include nanorods and nanowires, either single-crystal or polycrystalline to present no or multiple defects.[187,211,215−217] Alternatively, cube-like aggregates, nanobars, nanosheets, and nanorice have also been reported.[218] Altogether, oriented attachment is an important pathway to obtaining unusual nanostructures with broken symmetry.

3.1.2. Growth via Atomic Addition. An alternative route to account for the growth of nanocrystals involves the continuous deposition of atoms on the initial seeds.[71] This route is particularly relevant to seed-mediated growth, in which a metal precursor is added to a solution containing seeds, a reducing agent, and other additives. The precursor solution is typically added in one shot or titrated dropwise into the reaction solution with the assistance of a syringe pump.[72,219] As the precursor is reduced, the newly formed atoms are continuously deposited onto the seed to sustain its growth into the final product. In this case, the shape is usually controlled with the help of a capping agent, which selectively adsorbs onto and stabilizes a specific type of facet to reduce its growth rate. Other shape-control methods include manipulation of the injection rate (section 3.2.2) and activation of oxidative etching (section 3.2.3), among others.[119,122,163,219]

In principle, the metal precursor can be reduced in the solution phase and on the particle surface, respectively (Figure 10).[158,163] The pathway depends on the reduction kinetics of the precursor and the presence of seeds, which can either be generated in situ through nucleation or presynthesized and introduced into the reaction solution. In the absence of seeds, solution reduction dominates in the initial stage as the precursor is first reduced to metal atoms, which then aggregate into larger clusters.[163] This clustering process, also known as homogeneous nucleation, eventually results in the formation of seeds. Solution reduction tends to be adopted under fast reduction kinetics, corresponding to high precursor concentration, high temperature, and strong reducing agent. Once seeds have been formed via homogeneous nucleation, the subsequently formed metal atoms tend to be deposited onto the surface of the seeds. Known as heterogeneous nucleation, this process results in atom-by-atom growth of the seeds. With seeds in the solution, additional homogeneous nucleation, referred to as secondary nucleation, can still occur to generate a second population of seeds. In general, the undesired secondary nucleation is detrimental to the uniformity of the products.[163,220] Because of a lower activation energy barrier and the associated autocatalytic mechanism, heterogeneous nucleation tends to occur more readily than homogeneous nucleation.[163] Therefore, when seeds are present, one must slow down the reduction kinetics by lowering the reaction temperature, injecting the precursor at a slower pace, and/or switching to a weak reductant in order to ensure the preferential occurrence of heterogeneous nucleation while suppressing secondary nucleation.

As an alternative route, surface reduction only occurs in the presence of preformed seeds or growing nanocrystals.[158,163] During surface reduction, the metal ions adsorb onto the surface of the seed, followed by their reduction to atoms. This reduction pathway exclusively leads to heterogeneous nucleation, resulting in products uniform in both size and shape. The lower energy barrier to surface reduction also suggests its more important role than solution reduction in the case involving slow reduction kinetics. Since homogeneous nucleation is inherently suppressed by surface reduction, no secondary population of seeds should be observed. Taken together, surface reduction and heterogeneous nucleation are preferred when a strong control over the uniformity of nanocrystals is desired.

When atomic addition prevails in the growth stage, it is possible to govern the growth pattern of seeds to induce asymmetrical growth and thus symmetry breaking.[68,72,181] Each seed has a unique shape or morphology, with its own composition of faces, edges, and vertices.[65] These features (e.g., faces) on a seed can be symmetry-related or symmetry-different depending on their atomic structures. For instance, the two axial vertices on a decahedral seed are symmetry-related with each other, as well as the five equatorial vertices. However, the axial and equatorial vertices have different atomic structures and are thus different in symmetry. In another example, the eight {111} facets on a truncated octahedral seed are symmetry-related to each other, while the {111} facets are symmetry-different to the {100} facets on the same seed. During the growth stage, the newly generated atoms can selectively grow from one or more of the symmetry-related, equivalent sites on the seed. In general, asymmetrical growth or symmetry breaking can be induced by controlling the growth rates along the symmetry-related axes.

https://doi.org/10.1021/acs.chemrev.2c00468
Chem. Rev. 2023, 123, 3693−3760

In the presence of well-defined seeds, growth can occur in a symmetrical or asymmetrical pattern.[221] For symmetrical growth, all the symmetry-related sites grow at the same rate. As illustrated in Figure 11, incoming atoms are deposited on all

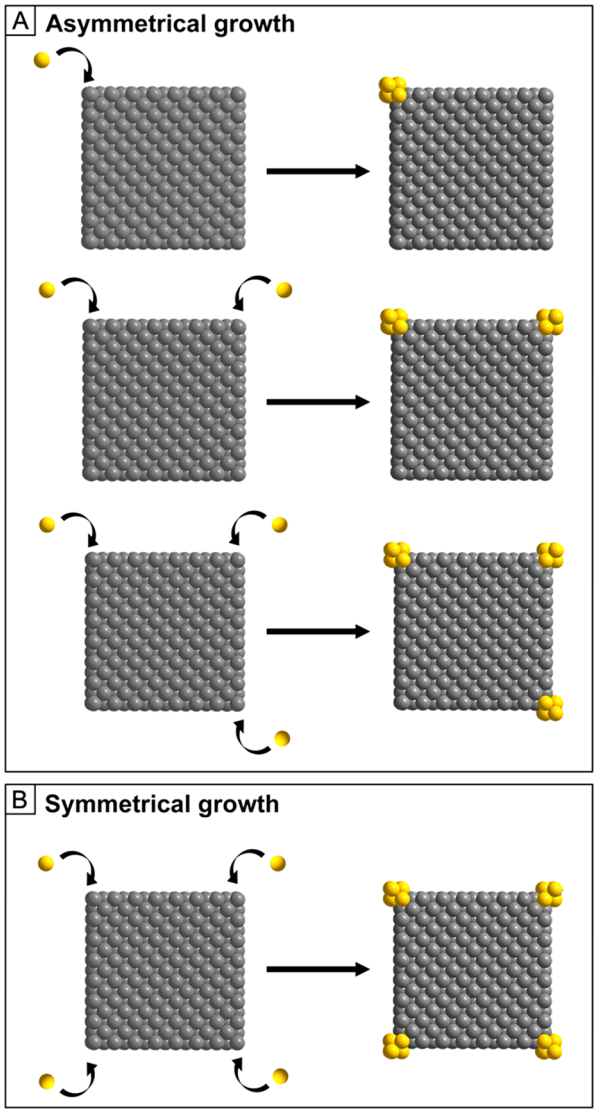

Figure 11. Schematic showing different scenarios of (A) asymmetrical and (B) symmetrical growth in the case of a 2-D model nanocrystal, in which the four corners are considered equivalent to each other and thus symmetry-related. In general, asymmetrical growth will lead to symmetry-broken products.

the symmetry-related sites (in this case, corners) without preference. Thus, symmetrical growth will lead to nanocrystals that preserve the symmetry of the seed, even if the overall shape has changed, such as when cubes or multipods are grown from a truncated octahedral seed.[222] In contrast, the symmetry-related sites will expand at different rates during asymmetrical growth, which is illustrated in Figure 13 for preferential growth from one, two, or three of the four symmetry-related corners. Under appropriate conditions (depending on the symmetry of the seed and experimental conditions), asymmetrical growth can activate the symmetry breaking event, such as when new atoms are only added to one of the faces, resulting in products such as nanobars and nanowires.[223−225]Table 1 shows a list of possible products derived from the most common seeds through symmetrical or asymmetrical growth on symmetry-related sites. For instance, in the case of a singly-twinned seed, deposition can occur symmetrically on both basal planes, leading to a bipyramidal particle. If asymmetrical growth takes place with deposition on only one of the two symmetry-related basal planes, the final particle would be an asymmetric bipyramid with reduced symmetry relative to the seed. Readers should note that this table is a partial collection of theoretical products instead of an exhaustive list of all possible outcomes, and not all of the listed nanocrystals been reported in the literature. The purpose of this table is to demonstrate the broad range of possible products resulting from symmetrical and asymmetrical growth and potentially inspire future research into some of the unreported structures.

It should be emphasized that surface diffusion plays an important role in maintaining the pattern of symmetry breaking initiated by asymmetrical growth through atomic addition.[226] As illustrated in Figure 12, adequate or inadequate diffusion of the adatoms can strongly affect the symmetry of the nanocrystals. Especially under asymmetrical growth due to a limited supply of atoms, diffusion plays a profound role in dictating the morphology of the final products.[76] Under adequate diffusion, which can arise from elevation in reaction temperature, the adatoms will be equipped with sufficient kinetic energy to migrate to other sites before additional atoms are deposited onto the surface, leading to conformal growth over the entire surface.[226] Depending on the morphology of the seed, this situation might or might not result in symmetry breaking. Under a sufficiently fast diffusion rate, the symmetry will be maintained even with the asymmetrical deposition of the newly formed atoms since they can spread evenly across the surface of the particle. In contrast, if the diffusion is limited, for instance, due to the involvement of a low reaction temperature, the adatoms will not be able to diffuse from their original sites of deposition, resulting in island growth and thus symmetry breaking for the nanocrystal.[65,226] Again, in the case of a nanobar, although deposition on just one corner would break its symmetry, fast diffusion can compensate for asymmetrical deposition to a certain extent, allowing the seed to maintain its original symmetry. In general, a combination of asymmetrical deposition and slow diffusion is instrumental to breaking the symmetry of the nanocrystal.

The impact of diffusion is related to not only the reaction temperature but also the presence of a capping agent.[119] Capping agents affect nanocrystal shape by binding selectively to certain types of facets, slowing their growth and thereby ensuring their expression on the final product. The presence of a capping agent will restrict the extent and the number of sites that the adatoms can diffuse to, which in turn control the shape evolution of the nanocrystal.[226] This concept is illustrated in Figure 12, where the final morphology of a nanocrystal is affected by both the diffusion and capping agent, with a {100} capping agent leading to a nanocrystal with a bar-like shape under adequate diffusion, while diffusion combined with a {111} capping agent induces a pencil-like morphology. Capping agents often have a more pronounced effect when used under conditions promoting surface diffusion, since the whole surface of the nanocrystal can be affected rather than selected facets.[119] However, even with inadequate diffusion, capping agents can dictate the location of island growth on the surface of a seed. For this reason, when designing a synthesis of nanocrystals, the interplay of deposition, diffusion, and capping

https://doi.org/10.1021/acs.chemrev.2c00468
Chem. Rev. 2023, 123, 3693−3760

Table 1. Summary of Symmetry-Related Sites Commonly Involved in the Growth of Different Types of Seeds and the Products Resulting from Symmetrical and Asymmetrical Growth, Respectively

Number of equivalent sites	Seed	Site type	Products of symmetrical growth	Products of asymmetrical growth
2		Axial vertices	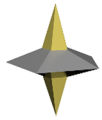	
2		Top and bottom faces		
2	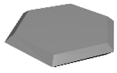	Top and bottom halves		
3		Equatorial vertices	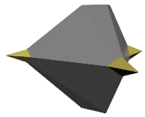	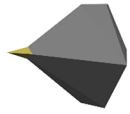
5		Equatorial vertices		
5		Equatorial edges		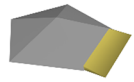
6	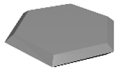	Side faces		
6		{100} faces		
6	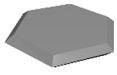	Equatorial vertices		

https://doi.org/10.1021/acs.chemrev.2c00468
Chem. Rev. 2023, 123, 3693−3760

Table 1. continued

Number of equivalent sites	Seed	Site type	Products of symmetrical growth	Products of asymmetrical growth
6	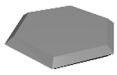	Equatorial edges		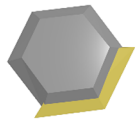
6	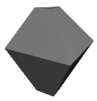	Equatorial edges	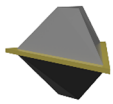	
6	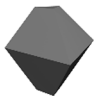	Side faces	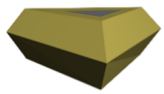	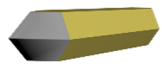
8		{111} faces		
10		Axial edges	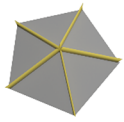	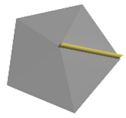
10		Side faces		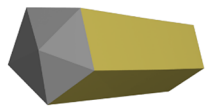
12		Vertices	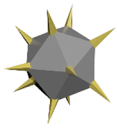	
20		Side faces		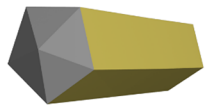

https://doi.org/10.1021/acs.chemrev.2c00468
Chem. Rev. 2023, 123, 3693−3760

Table 1. continued

Number of equivalent sites	Seed	Site type	Products of symmetrical growth	Products of asymmetrical growth
24		Vertices	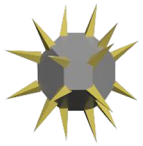	
30		Edges	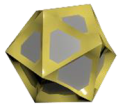	
36		Edges	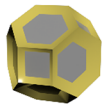	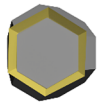

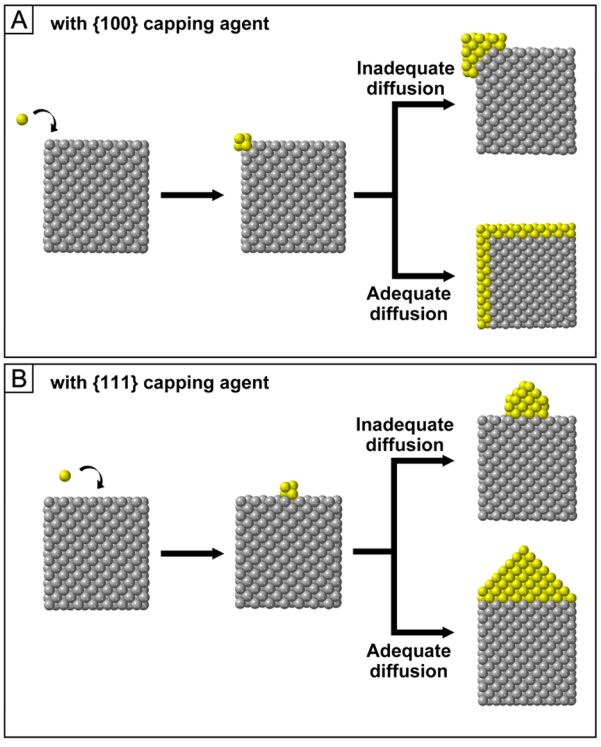

Figure 12. Schematic showing the importance of diffusion in enabling symmetry preservation or breaking in the presence of a capping agent specific toward (A) {100} and (B) {111} facets, respectively.

agent needs to be optimized to achieve symmetry breaking or preservation.

While the aforementioned concepts theoretically apply to all nanocrystal syntheses and symmetry breaking events, it can be challenging to evaluate their individual roles in the experimental work. In the following sections, various experimental methods for promoting symmetry breaking are discussed, where an understanding of the above concepts will be helpful in elucidating the mechanistic details.

3.2. Asymmetrical Growth in a Monometallic System

As discussed in sections 2.2 and 2.5, many of the mechanistic details involved in nucleation remain to be discovered, and more research regarding this topic continues to be published.[105,108,133,227−230] Nucleation is known to be an extremely sensitive, even fickle, process, where any changes to the experimental conditions, reactants, and contaminants can yield completely unexpected outcomes. Consequently, the nanocrystals obtained using a one-pot method can vary widely with subtle changes to the reaction conditions.[220] In contrast, seed-mediated growth, in which preformed seeds are allowed to grow into larger nanocrystals, is much better understood. The influences of injection rate, precursor concentration, shape and size of the seed, and other reaction parameters have all been tuned and investigated to elucidate mechanistic details about seed-mediated growth.[65,231,232] A deep understanding of the roles played by each parameter allows for the rational design of a seed-mediated synthesis for controlling the shape and size of the nanocrystals. Application of this knowledge has resulted in the discovery of numerous methods to accomplish asymmetrical growth and symmetry breaking in the setting of seed-mediated growth.[68] In the following sections, we discuss the different methods capable of inducing symmetry breaking in various systems.

First, symmetry breaking in a monometallic system is discussed, including descriptions of methods such as asymmetrical passivation of the surface, limited supply of precursor, oxidative etching, influence of an interface, and soft templating, among others.[68,69,189,233] Many of these strategies draw on overlapping concepts, and whenever relevant, we point out these similarities. Additionally, when considering the case studies described in section 4, more than one strategy might be involved in inducing symmetry breaking. Although the following synthetic strategies are intended to cover most

https://doi.org/10.1021/acs.chemrev.2c00468
Chem. Rev. 2023, 123, 3693−3760

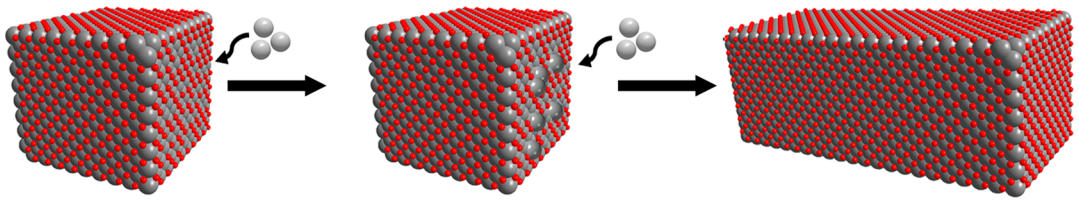

Figure 13. Schematic showing symmetry breaking through asymmetrical passivation of the seed surface. Growth tends to occur from the facet with the least coverage of the capping agent, leading to asymmetrical growth.

systems, they may not encompass some of the less common strategies found in the literature.

In a monometallic system, the seed and the final nanocrystal are made of the same metal. Consequently, their symmetry cannot be broken by changing the elemental distribution of the nanocrystal.[68,69,189,233] Moreover, it is often not possible to resolve symmetry breaking based on the growth sequence on specific facets. For instance, when a monometallic nanorod is generated from a decahedral seed, it is almost impossible to determine whether the growth occurred on one or both sides of the seed using common characterization methods.[234] Theoretically, if deposition took place on only one side of the seed, asymmetrical growth and symmetry breaking would be involved, but it is generally not feasible to experimentally prove such a growth mode without the use of in situ techniques or isotope labeling.[227] Consequently, we must assume that the seed grew through equal deposition on the symmetry-related crystal axes and symmetry was preserved. Thus, the following discussion of symmetry breaking only refers to the difference in symmetry relative to their seeds, rather than from the angle of asymmetrical growth. In contrast, the next section touches on bi- and multimetallic systems, with a focus on elemental distribution and lattice mismatch.[24] The schematics depicting the different growth strategies are all drawn using a cubic seed for clarity and consistency. However, the concepts and strategies should be applicable to all different types of seeds, regardless of composition, shape, and size. The strategies will be illustrated with explicit examples in section 4.

3.2.1. Asymmetrical Passivation of the Surface. Research throughout the past several decades has repeatedly shown that one of the most effective ways to control the shape of nanocrystals is through the use of capping agents, which are also referred to as shape-directing agents, facet-directing agents, or surfactants.[119,184,235] Capping agents can be ions, small molecules, coordination ligands, polymers, or surfactants capable of binding to the surface of a nanocrystal.[71,191,236−238] The capping agent tends to bind relatively strongly to a specific type of facet but not necessarily to all of the symmetry-equivalent facets, and this can affect the final shape of the nanocrystal by modifying thermodynamic and kinetic aspects. Thermodynamically, the presence of a capping agent will change the surface energies of different crystal facets, with those more strongly bound by the capping agent having a greater decrease in surface energy. Therefore, the thermodynamically favorable shape will change to facilitate the expression of these facets on the surface. For example, by mediating the polyol synthesis of Ag nanocrystals with poly(vinyl pyrrolidone) (PVP), the strong binding of PVP to Ag(100) can reverse the order of surface energies for (100) and (111), giving Ag nanocubes as the product.[235] Kinetically, the capping agent prevents growth by serving as a physical barrier against deposition while simultaneously restricting the diffusion of the deposited atoms on the capped facet.[239] As such, deposition on the capped facets is limited whereas the corresponding growth will occur preferentially on the uncapped facets.[119] The facets covered by a capping agent will not grow as quickly and eventually become dominant on the surface of the particle. Common examples include the use of Br^- ions as capping agents for the Pd{100} facets to produce cubic nanocrystals, while the {111} facets can be capped by citrate for the synthesis of octahedral nanocrystals.[240,241] Capping agents are invaluable in directing the shape evolution of nanocrystals during their growth. Nevertheless, it is worth noting that there are only a limited number of reports on the binding energy and adsorption/desorption dynamics of capping agents due to the difficulty of such a measurement.[120] Computational studies suggested that the efficacy of surface binding is dependent on both the structural conformations and chemical functional groups of the ligand.[235,242] For example, when analyzing the binding configurations of polymer ligands such as PVP to Ag surfaces, both van der Waals (vdW) attraction through the carbon backbone and covalent bonding through oxygen atoms should be taken into consideration, with the overall binding of PVP to Ag(100) stronger than that to Ag(111).[243] Additional efforts in simulating real experimental conditions are required to achieve a good understanding of the interaction between a metal surface and a ligand.

When a capping agent is used to synthesize the seeds, the coverage of the capping agent should be evenly distributed across all the capped facets. Under certain conditions, however, the distribution might become uneven, leading to one or multiple facets containing the capping agent at a lower coverage density.[183,244−247] As such, the seed experiences asymmetrical passivation on the surface, where the facets with the lowest coverage density are more favorable for atomic deposition.[119,184,248] When atoms start to deposit on the least-capped site, the resulting islands will become a preferred site for further growth due to the lack of capping agent, a large number of under-coordinated atoms, and a high surface energy.[65,249] Thus, the islands on the poorly capped facets will grow most quickly, whereas the facets fully covered by the capping agent will be growing minimally or not at all. The resulting asymmetrical growth on symmetry-equivalent facets will induce symmetry breaking.[68] Figure 13 shows this concept through the growth of a cubic seed bearing unevenly passivated side faces into a nanobar. The symmetry is broken because deposition only occurs on one of the six {100} facets with the lowest coverage of the capping agent. In principle, more than one symmetry-related facet can have in capping agent in low coverage density, leading to the formation of rectangular plates, multipods, or T-shaped particles depending on the specific arrangement of the poorly passivated facets.

As mentioned above, asymmetrical passivation occurs when a capping agent does not adsorb evenly on the surface of a nanocrystal. This situation can be attributed to the low concentration of capping agent (some sites might not be fully

https://doi.org/10.1021/acs.chemrev.2c00468
Chem. Rev. 2023, 123, 3693−3760

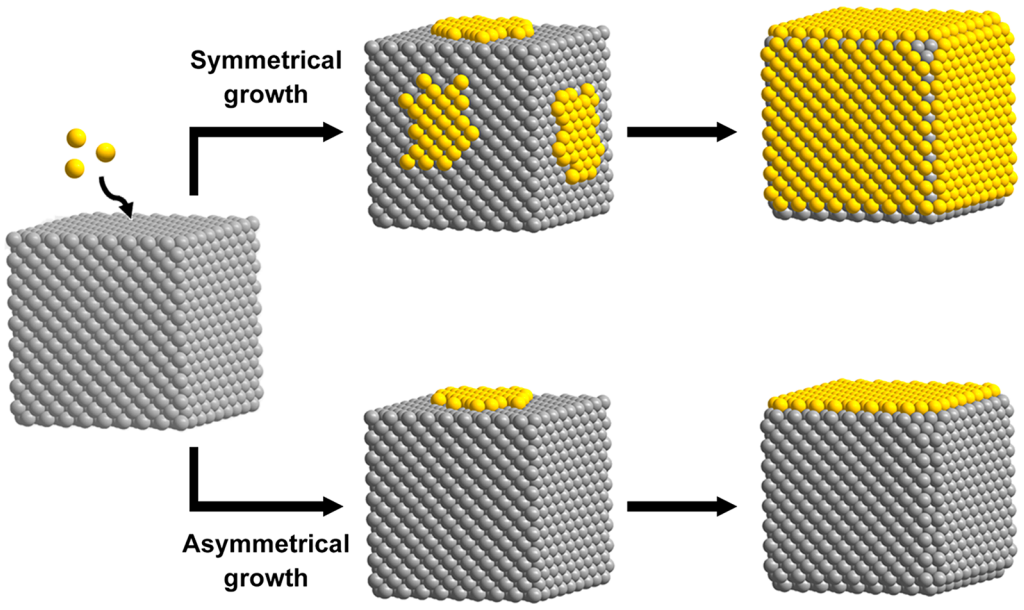

Figure 14. Schematic showing how the level of atom supply affects symmetry breaking: an adequate supply tends to result in symmetrical growth, whereas a limited or inadequate supply would lead to asymmetrical growth.

covered if there is an insufficient amount of capping agent in the reaction system), partial blocking of the facet (such as when the capping agent does not bind strongly to the nanocrystal), or inherent properties of the capping agent.[244] In practice, the capping agents can be asymmetrically deposited by design, such as in a hydrophilic−hydrophobic system.[249,250] When seeds are coated with a hydrophobic capping agent and added into a system containing a secondary hydrophilic capping agent, some of the bound hydrophobic capping agent will be replaced by the hydrophilic one.[250] The uneven passivation inevitably results in phase separation, as the hydrophobic and hydrophilic capping agents tend to migrate to different sides of the seed. During the subsequent growth process, the deposition will occur preferentially on only one side of the seed, depending on the solvent involved, coverage density, metal precursor, and other reaction conditions. This hydrophilic−hydrophobic system has some overlap with the strategy discussed in section 3.2.4 (influence of an interface), but in this case, the final growth step does not necessarily occur at an interface.

In some publications, the growth of SiO_2 or other materials to physically block only one side of a seed (usually through the aforementioned hydrophilic−hydrophobic method) to induce symmetry breaking is also referred to as asymmetrical passivation of the surface.[251] However, in this Review, the unevenly deposited SiO_2 is considered a physical barrier and will be discussed in section 3.2.6. Regardless, this method is a good example of how multiple techniques with overlapping mechanisms can be leveraged to achieve symmetry breaking in nanocrystal growth.

3.2.2. Limited Supply of Precursor or Atom. A simple and versatile method for achieving asymmetrical growth involves the limited supply of precursor/atom during the growth step.[68] In a seed-mediated synthesis, all the symmetry-equivalent facets on the surface of a seed should have the same potential for growth. With enough precursor and thus newly generated atoms, the deposition should occur on all the equivalent sites, leading to symmetrical growth.[76] However, at a limited supply of the precursor, the deposition will take place on some of the equivalent sites only. The selectivity with regard to atomic deposition is a result of the nucleation process at the beginning of a seed-mediated synthesis. When the available precursor starts to reduce, it can undergo heterogeneous nucleation on any one of the symmetry-equivalent facets, thereby activating that site.[76,252] The just-deposited atoms will have a higher surface energy, as they are undercoordinated and/or less passivated by the capping agent. Thus, additional growth will preferentially continue at the same high-energy, activated site. When there is sufficient precursor at the start of growth, nucleation will occur evenly on all the symmetry-related sites, activating all of them for symmetrical growth.[253] However, when the supply of precursor becomes limited, there will be insufficient atoms to nucleate on all symmetry-equivalent facets, so only a fraction of the symmetry-related sites will be activated, and only these selected sites will continue to grow with additional deposition.[73] The deposition on limited sites in turn results in asymmetrical growth and symmetry breaking.[76,254] In Figure 14, this technique is demonstrated using a cubic seed. When the precursor supply is limited, only one of the side faces is activated for deposition and the preferential growth on this facet eventually results in a nanobar. In contrast, at an adequate supply of atoms, all side faces of the cubic seed undergo deposition, and the seed will grow symmetrically into an enlarged cube. In principle, when the supply of precursor is tuned, two, three, four, or five side faces of the cubic seed can participate in growth to give a variety of symmetry-broken products.[76]

Limiting the supply of precursor to induce asymmetrical growth is a powerful method that can be easily controlled and modified. There exist many different methods capable of controlling the supply of atoms.[68] A common way is to manipulate the reduction rate of the metal precursor by, for example, changing the type of precursor, reducing agent, reaction temperature, and injection rate, among others.[58,69,163,181] For instance, using the metal precursor with a more strongly bound ligand or switching to a weaker reducing agent can slow down the reduction kinetics, thereby

https://doi.org/10.1021/acs.chemrev.2c00468
Chem. Rev. 2023, 123, 3693−3760

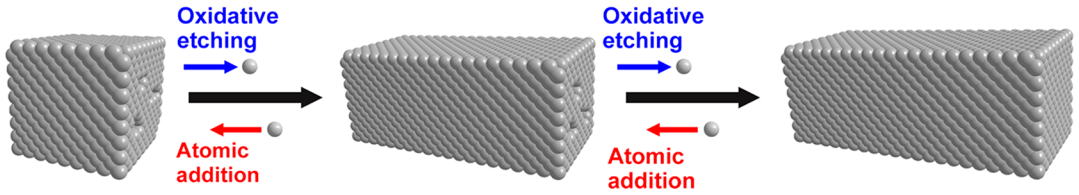

Figure 15. Schematic showing the effect of site-selective oxidative etching and thus activation of atomic addition on asymmetrical growth of nanocrystals.

lowering the supply of atoms and inducing asymmetrical growth.[68,69] Lowering the reaction temperature also results in a slower deposition rate (V_{dep}) while simultaneously compromising the diffusion rate (V_{diff}) of the adatoms.[181,226] At a higher reaction temperature, diffusion will be accelerated. Even if the reduction rate and atomic deposition are slow and restricted to one site, fast diffusion can cause the adatoms to distribute evenly across the surface of the seed, leading to symmetrical growth (see section 3.1.2). In general, the use of a sufficiently low temperature to prevent the fast diffusion of adatoms is necessary to induce and maintain asymmetrical growth.

The easiest way to control the supply of atoms for symmetry breaking is through the dropwise titration of the precursor using a syringe pump.[219] The syringe pump allows one to add the precursor solution at specific, programmable rates, keeping the precursor concentration stable throughout a synthesis. At a sufficiently slow injection rate, the concentration of precursor in the reaction vessel at any given point will remain low, and the resultant slow V_{dep} will induce asymmetrical growth from only one site.[181] When the injection rate is increased, the resulting increase in concentration and V_{dep} will enable growth on multiple symmetry-related sites. Eventually, at a fast injection rate, the high precursor concentration will cause fast deposition on all symmetry-related sites. Thus, the use of a syringe pump allows for a fine control of the growth pattern involving one or multiple sites. Such a control makes limiting the supply of atoms more versatile and robust than other methods for inducing asymmetrical growth.

3.2.3. Activation by Oxidative Etching. Oxidative etching is a process commonly observed in our daily life. A simple example can be found in the localized corrosion of steel by water and oxygen from air. When steel is exposed to the atmospheric environment for a certain period of time, the corrosion can be triggered exclusively from a spot on the surface before spreading, during which iron is removed from the steel surface through oxidation and then dissolved into the surrounding solution in the form of ferrous ions. As a hallmark of corrosion, it does not occur uniformly on the entire surface, naturally causing symmetry breaking to the affected object. Similarly, oxidative etching of nanocrystals is a localized process and can be used to induce asymmetrical growth.[121]

Oxidative etching is universally involved in nanocrystal synthesis.[122] As discussed in section 2.4, etching can be used to remove twinned seeds during nucleation, leading to single-crystal particles in high purity.[121,122] Etchants can also act as capping agents to control the shape evolution of nanocrystals.[177] Oxidative etching has been further employed to fabricate nanoframes or nanocages by etching away the core in bimetallic nanocrystals.[255] Finally, oxidative etching can induce asymmetrical growth and symmetry breaking.[68] In oxidative etching, an oxidant and a coordination ligand pair up to enable a redox reaction with the atoms on the surface of a nanocrystal. Commonly, this involves halides or nitrate, alongside the oxygen from air.[177,191,192] During etching, some surface atoms are oxidized back to ions, which coordinate with the ligand and are thus removed from the surface. Just like corrosion, oxidative etching tends to start from one site, rather than evenly across all equivalent sites.[68] As one site starts to undergo etching and atoms dissolve away, this site will become more active toward continued etching.[177] This activation occurs because the site in question has higher surface energy due to the presence of undercoordinated atoms and likely a lower density of the bound capping agent due to the disruption of the surface by etching. Additionally, the activation toward etching ensures that this site becomes preferred for deposition in the following step. When the reaction conditions shift to become more favorable for growth rather than etching, the precursor ions (either added into the synthesis or resulting from etching) start to redeposit onto the high-energy sites where etching just occurred.[192] Thus, the etched site will grow faster than any other symmetry-related sites, leading to symmetry breaking. Of course, symmetry breaking will only occur if atomic deposition overrides oxidative etching during a synthesis. If etching continually prevails over deposition, eventually the whole particle will be etched away.

Figure 15 illustrates the asymmetrical growth of a cubic nanocrystal into a nanobar through the mediation of oxidative etching.[177] At first, etching occurs on one of the six side faces, and the resulting roughened side face makes a perfect site for continued etching or atomic addition. As the synthesis proceeds, atomic addition is more rapid than oxidative etching on the etched site, leading to growth along one direction of the cube. Eventually, as atomic addition continues at a faster rate than etching, a nanobar with sharp edges and corners is obtained as the final product. It is important to realize that oxidative etching can also affect the reaction kinetics of the system. Essentially, as the etching oxidizes the metal atoms back into their precursor state after the initial deposition, this will slow down the reduction kinetics. Thus, oxidative etching and limiting the supply of precursor seem to overlap when applied to achieve asymmetrical growth.

3.2.4. Assistance of an Interface. Intuitively, one of the first ideas to induce asymmetrical growth might be simply blocking the growth on certain symmetry-related sites. In that case, only the exposed or undisturbed sites would have the opportunity to grow. Experimentally, certain sites can be blocked through the aid of an interface, usually a solid−liquid or liquid−liquid interface.[256] By trapping the seeds at the relevant interface, the symmetry and accessibility of the seed are immediately changed, as growth can only occur from one side of the interface.[257] Sometimes, this interface involves a solid, as in the case of vapor−liquid−solid or solution-liquid−solid method commonly used to grow semiconductor nanorods.[258,259] In this method, the metal seeds are

https://doi.org/10.1021/acs.chemrev.2c00468
Chem. Rev. 2023, 123, 3693−3760

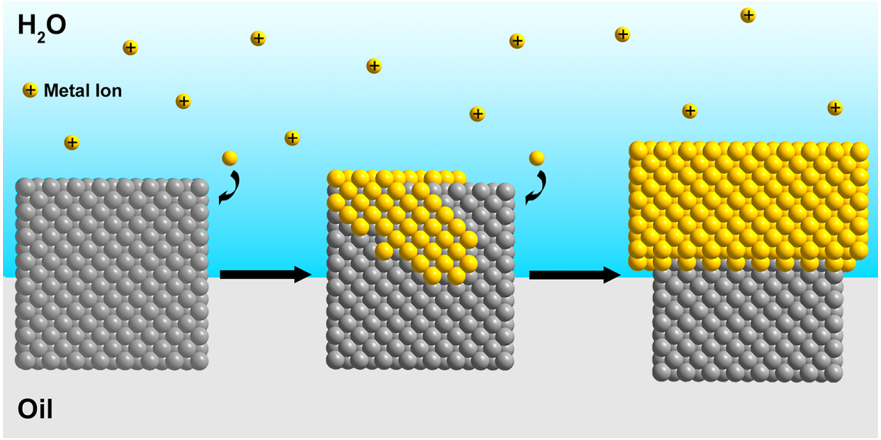

Figure 16. Schematic showing symmetry breaking during the growth of nanocrystals that are trapped at an oil–water interface. In this case, the supply of precursor compound or atoms is limited only to the water side of the interface.

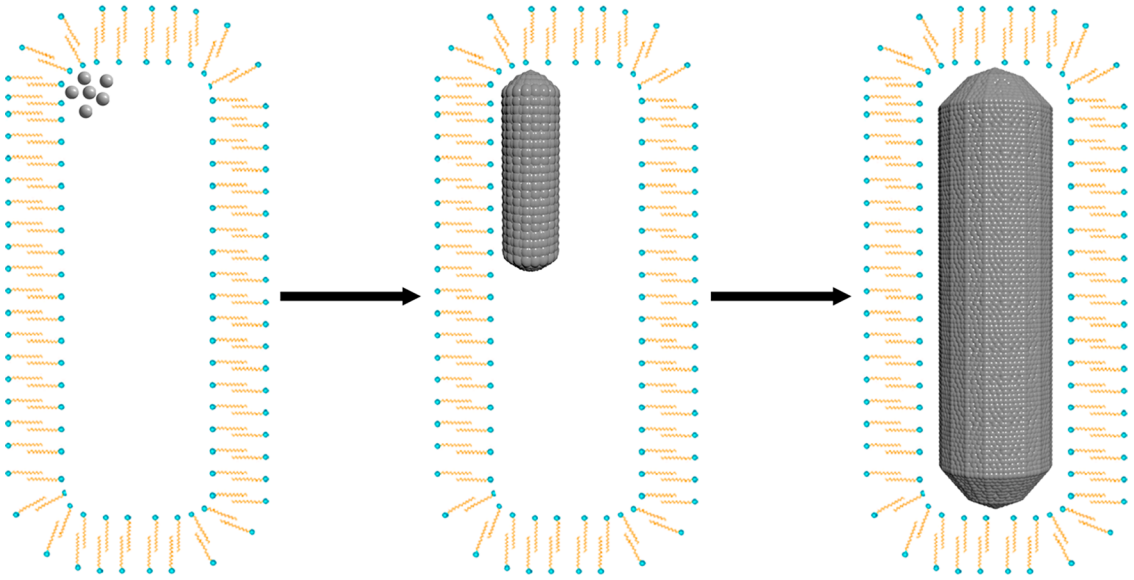

Figure 17. Schematic showing asymmetrical growth during the formation of a nanocrystal within the confinement of a soft template such as a rod-shaped micelle. Adapted with permission from ref 267. Copyright 2008 American Chemical Society.

immobilized on a solid substrate, after which the semiconductor precursor is supplied in a vapor or liquid form to grow the nanocrystals only from the sides exposed to the precursor. Such growth will lead to the formation of nanorods, nanowires, and other symmetry-broken nanostructures.

A more common method to break the symmetry of noble-metal nanocrystals is to introduce a liquid–liquid interface.[260−262] The liquid–liquid interface can be conveniently formed in a system involving oil and aqueous phases by taking advantage of the hydrophobic interaction. To trap the seeds at this interface, they first need to be functionalized with an appropriate capping agent.[260] This functionalization often involves a hydrophobic capping agent so the resulting hydrophobic interaction will ensure that the seeds are trapped at the interface to minimize the interfacial energy. Once the seeds are arranged at the interface, a precursor that is only soluble in one of the two phases will be introduced (Figure 16).[262] The precursor will be restricted to one side of the interface, and as it is reduced, the growth will occur exclusively from the accessible sites on the seed. The continued deposition will form a partial shell over the seed, generating a nanocrystal with a Janus structure. The final shape of the partial shell can also be affected by introducing additional capping agents, controlling the reduction kinetics, and more.[184,189] In this way, the assistance of an interface can be combined with other methods to fine-tune the final morphology of the nanocrystals. Additionally, the resulting nanocrystals can be modified postsynthesis to further alter their shape. Etching away the seed, depositing another shell over the whole nanocrystal, or introducing a second round of functionalization through the assistance of an interface will lead to the formation of nanocrystals with complex morphologies.[122,263,264] While this method is comparatively similar to the uneven passivation of the surface or the physical blocking of the surface described in sections 3.2.1 and 3.2.6, the trapping of the seeds at the interface during the growth step helps set it apart as a unique method.

As a hallmark of leveraging an interface to induce asymmetrical growth, this method can be adapted to improve the throughput and yield of the synthesis by switching to a flow-droplet system.[262] In such a system, reactor droplets are created from a fluid that is immiscible with the solvent used as

https://doi.org/10.1021/acs.chemrev.2c00468
Chem. Rev. 2023, 123, 3693−3760

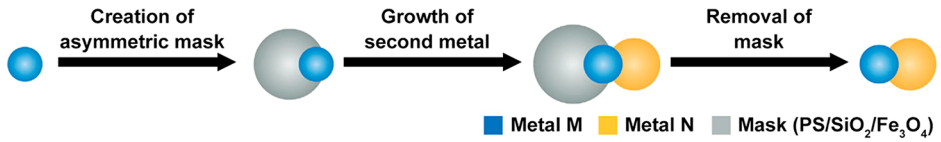

Figure 18. Schematic showing the synthesis of dimerized particles through the use of a physical mask to block the nucleation and growth from part of the surface. Reproduced with permission from ref 86. Copyright 2021 Wiley-VCH.

the carrier fluid, similar to the biphasic system described above. Thus, the seeds functionalized with a hydrophobic capping agent will be trapped at the interface of the droplets and carrier fluid. When a precursor only soluble in the droplets is introduced, the nanocrystals will grow asymmetrically only from the side accessible by the precursor, causing the symmetry to break. Such a flow-droplet system offers a greater opportunity to scale up the production of nanocrystals compared to batch reactors.

3.2.5. Direction or Confinement by a Template. When considering asymmetrical growth on a macro scale, it is easy to control the shape through the use of a mold or template, such as those used during ceramic slip casting. Some early studies essentially tried to extend this concept to the nanoscale for the creation of nanorods and nanowires through the deposition of a metal in mesoporous silica templates or anodic aluminum oxide templates.[265,266] While using such hard templates gives rod-like structures, controlling their size, shape, and quantity tends to be limited. Alternatively, a soft-templating approach can be used to confine nanocrystal growth to a surfactant-based "mold." Usually, micelles made of surfactants such as cetyltrimethylammonium bromide (CTAB) can act as the template to restrict nanocrystal growth from certain directions (Figure 17).[267] Soft templating can occur in either a single or biphasic system.

In an aqueous system, the hydrophobic tails of surfactant molecules attract each other and assemble into a specific orientation to minimize the area-to-volume ratio and avoid contact with water, while the hydrophilic heads tend to repulse each other to maximize the area-to-volume ratio. The optimal curvature of the water/surfactant interface is thus determined by the properties of the hydrophobic tail and the hydrophilic head.[268] Specifically, the amphiphilic nature of CTAB molecules forces them to self-assemble into rod-like micelles rather than globular shapes when used at sufficiently high concentrations and especially when salts, such as KBr and $NaNO_3$, are added.[269,270] The bilayers of CTAB can act as a physical barrier to confine the metal precursor to the template. Additionally, many metal ions, such as Au^{3+} or Ag^{+}, will adsorb on the CTAB layer through ionic interactions, again keeping the growth confined to the template.[271] Therefore, by physically restricting their growth, the resultant nanocrystals will automatically be shaped by the micelles. Importantly, the dual roles of CTAB as a capping agent and a surfactant can control the particle shape in a conventional manner.

Since the shape of the micelle helps determine the final shape of the particle, the choice of surfactant is essential.[267] Unfortunately, the shape of the micelle is strongly affected by the impurities contained in the surfactant, making soft-templated growth less reproducible and highly sensitive to the chemicals.[267] For instance, depending on the supplier of CTAB, the as-obtained micelles can have different aspect ratios or might even become spherical. Additionally, the CTAB may affect nanocrystal growth beyond the templating effect, such as when the long-chain ammonium ions also stabilize specific facets on the nanocrystal.[271] In another example, the Br^{-} ions can coordinate with the metal precursor to affect its reduction rate while acting as an additional capping agent. Taken together, many factors are involved in soft-templated growth, and their individual effects can be difficult to detangle.

The templated growth can occur in a similar manner in a biphasic system, albeit the metal precursor is only soluble in one of the two phases.[265] In this case, droplets of an organic solvent are formed in an aqueous environment through stirring, and CTAB will arrange at the interface of the aqueous and organic phases to minimize the interfacial energy. During this process, the CTAB forms an inverse-micellar network to shield the aqueous solution of the metal precursor from the organic phase. The metal precursor will be reduced while being confined to this inverse-micellar network, and nanowires that match the shape of the network will eventually be generated. This soft-templating method has much in common with the influence of an interface, as both methods use a biphasic system. Again, it is possible to use more than one synthetic method to promote asymmetrical growth due to their inevitable overlap.

3.2.6. Other Methods. Of course, the vast number of methods for inducing asymmetrical growth makes it impossible to discuss all of them. Instead, we decided to focus on the most common strategies in the preceding sections. Here we give a quick overview of one additional method to illustrate how other, less common techniques can influence the growth pattern.

As described in sections 3.2.1 and 3.2.5, both uneven passivation of the surface and the influence of an interface can cause asymmetrical growth by preventing atomic deposition on specific sites on a seed.[184] In those sections, we mainly focused on nanocrystals with ionic or molecular capping agents, or ones trapped at a macroscopic interface. Alternatively, a much smaller interface could be formed by attaching a secondary nanostructure to a seed (Figure 18).[86] By introducing an asymmetric mask, usually made of polystyrene or SiO_2, selectively to one side of a nanocrystal, that side will be blocked, while the other sites on the nanocrystal remain available for atomic deposition and growth.[272−274] When the mask is removed after deposition, the final nanostructure evolves into a dimer or Janus particle. Despite the subtle differences, this method is essentially a combination of two involving the assistance of an interface and selective passivation of the surface, although it is sometimes presented as a distinct method.

3.3. Asymmetrical Growth in a Bi- or Multi-Metallic System

Certainly, symmetry breaking is not limited to the monometallic system as bi- or multimetallic nanocrystals can also undergo such a transition during the growth process. In general, all the methods discussed previously in the monometallic section are also applicable to the bimetallic system, in which case the seed is made of one metal while a different metal is deposited during the symmetry breaking

https://doi.org/10.1021/acs.chemrev.2c00468
Chem. Rev. 2023, 123, 3693−3760

step.[24,73,253,254,260,275,276] The growth can also be repeated to create tri- and multimetallic systems.[24] Furthermore, when more than one metal is involved, additional options for symmetry breaking will transpire. In this section, we focus on the methods developed exclusively for a bi- or multimetallic system, albeit they can also be combined with the previously discussed techniques.

3.3.1. Symmetry Reduction Arising from Elemental Distribution. By design, both bi- and multimetallic systems involve elemental distributions. When discussing symmetry breaking in a monometallic system, we stated that, in some cases, it is almost impossible to know on which facets growth occurs.[69,189,227,233,234] For a bimetallic system, in contrast, we can resolve the issue of symmetry breaking vs preservation based on the elemental distribution in/on the nanocrystal.[24,86]

For instance, when a decahedral seed grows into a penta-twinned nanorod, the seed can be made of a different metal from that used for growth. If growth occurs evenly from both sides of the decahedral seed, symmetry (both in terms of shape and elemental distribution) will be preserved. If growth occurs from one side only, or unevenly from both sides, the symmetry will be broken due to the change in elemental distribution.[253] This phenomenon is in direct contrast to that of the monometallic system, where the growth of a decahedral seed into a nanorod does not involve symmetry breaking, as previously discussed.[68] Similarly, as illustrated in Figure 19, a second metal can be deposited on one or both sides of a growing nanobar. The symmetry of the nanobar will be preserved when the deposition occurs evenly on both sides, whereas changes to elemental distribution will cause symmetry breaking. In this way, the bimetallic system offers a unique platform to break the symmetry of a nanocrystal.

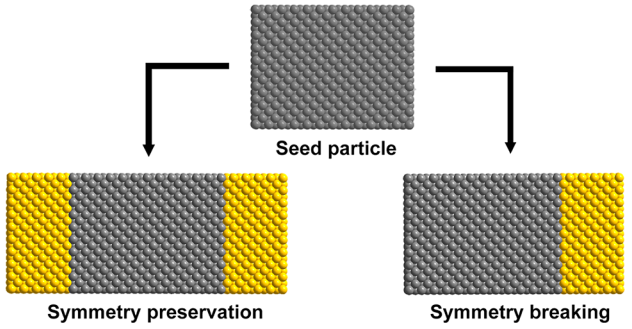

Figure 19. Schematic showing the importance of elemental distribution in preserving or breaking the symmetry of bimetallic nanocrystals. When the second metal is symmetrically deposited on a seed, it will result in symmetry preservation. If the second metal is deposited asymmetrically on the seed, it will result in symmetry breaking.

3.3.2. Asymmetrical Growth Caused by Lattice Mismatch. When two or more metals are involved, the inevitable lattice mismatch between the different metals can play an important role in inducing asymmetrical growth.[68,69,189,233,277] Depending on the metals involved, the lattice mismatch can either be negligible or significant.[65,278,279] In the case of minor lattice mismatch (<4%), the two metals can form an interface with minimal lattice strain, resulting in conformal layer-by-layer overgrowth over the entire surface. If the lattice mismatch surpasses 4%, the resulting significant lattice strain can affect the growth mode.[280] At a greater lattice mismatch, the atoms situated at the interface will experience tensile or compressive strains, resulting in an overall higher energy for the system (Figure 20A).[65,281,282] One way to relieve this strain is to shift from a layer-by-layer to an island growth mode as the distance from the interface increases, with the islands relaxing to the native lattice parameters.[65] Subsequently, additional deposition will preferentially occur at these islands to avoid any additional lattice mismatch and strain.[68]

Of course, the lattice mismatch can also affect the morphology of the resultant nanocrystals. This process is illustrated in Figure 20B, where a metal with a larger lattice parameter grows on a seed with a smaller lattice parameter. As the second metal is deposited, the growth first continues in a layer-by-layer fashion (Frank-van der Merwe mode), even when there is strain at the interface. However, as the deposited layer increases in thickness, the growth shifts to a mixed layer-plus-island (Stranski-Krastonov mode) and then island mode (Volmer−Weber mode) so as to relax the in-built strain and lower the overall energy of the system. During this process, the reduction in strain energy accommodated by the formation of islands with different lattice parameters is generally greater than the concomitantly increased surface energy, making it thermodynamically favorable. As a result, the continued deposition preferably occurs on the lattice-matched islands to avoid strain and minimize the total surface energy.[283] Thus, by limiting deposition only to the islands, the resulting asymmetrical growth will induce an unusual, symmetry-broken structure. Obviously, the greater the mismatch in lattice parameter, the higher the strain at the interface and the more likely the symmetry of the resulting particles will be affected.[68]

In this system, the rate of surface diffusion relative to that of deposition also plays a critical role in determining the growth mode.[226,284] With fast diffusion, epitaxial deposition of the second metal will be promoted. Thus, the strain and lattice mismatch will affect the growth mode as described above.[68] If the rate of deposition is faster than the rate of diffusion, the final morphology of the nanocrystal will instead be affected by inadequate diffusion (Figure 14). In this case, symmetry breaking likely results from asymmetrical growth rather than from lattice mismatch and strain relaxation. This method is also closely tied to symmetry breaking through the limited supply of atoms. Since both methods are heavily affected by the rates of diffusion and deposition, differentiating the roles of precursor supply and lattice mismatch during symmetry breaking in a bimetallic system can sometimes be challenging.

3.3.3. Other Methods. Just as for the monometallic system, there are many less-reported methods of symmetry breaking in bi- and multimetallic systems. One such method is symmetry breaking resulting from the generation of twin defects.[68] This method can be classified as a submethod of the influence of lattice mismatch because twin defects tend to be generated when there is an unusually large lattice mismatch between the seed and the deposited metal.

It is unusual for nanocrystals to develop additional twin structures during the growth step. In a conventional nanocrystal synthesis, the twin structure tends to be set during the nucleation step and remains unchanged throughout growth.[108,285] However, in some specific cases of seed-mediated growth, the final particle can develop a different twin structure from the seed.[286−290] This change in the internal structure is thermodynamically unfavorable, so asymmetrical growth will only occur when there is a large lattice mismatch between the seed metal and the deposited metal and/or when

https://doi.org/10.1021/acs.chemrev.2c00468
Chem. Rev. 2023, 123, 3693−3760

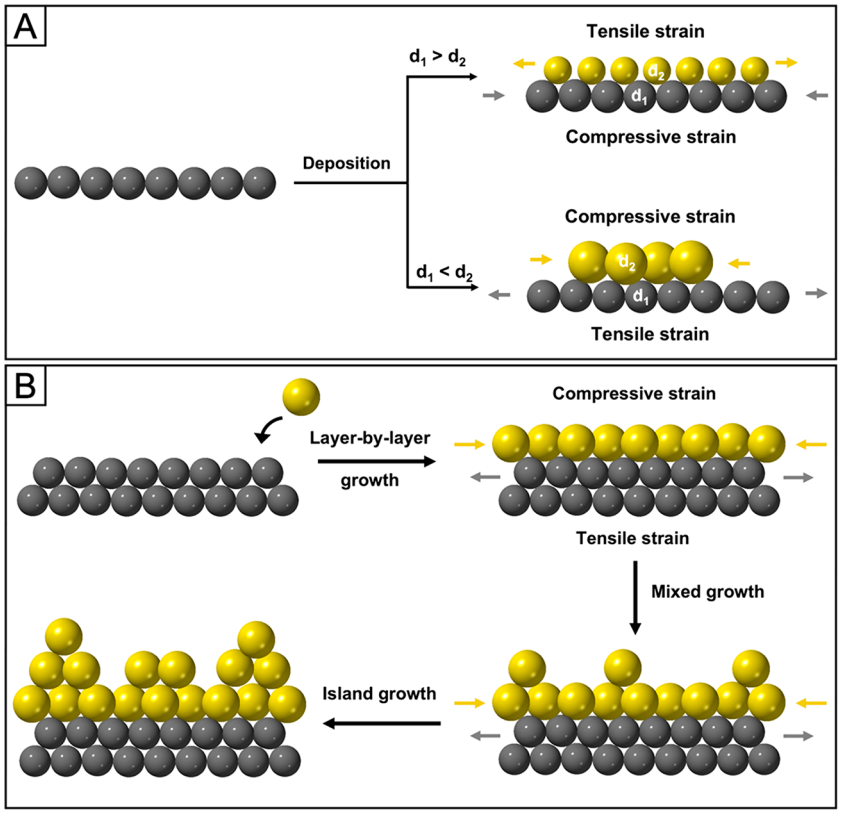

Figure 20. Schematic showing (A) different types of strain resulting from lattice mismatch in terms of atomic diameter (d) and (B) symmetry breaking at the interface of two metals with a large lattice mismatch that will result in strain at the interface.

a strongly binding ligand is involved.[68] To break symmetry in this way, the use of a multiply-twinned seed is favorable but not absolutely essential.

Most commonly, seeds with a predetermined twin structure are used to generate additional twin defects because the existing twin boundaries can be used as templates for the formation of additional twin defects.[286−288,290] For example, icosahedra can be grown from decahedral seeds and *vice versa*.[287,288] However, several studies that used single-crystal seeds to obtain penta-twinned rods have also been reported.[289] In both cases, the large lattice mismatch between the seed and the deposited metal would cause the buildup of strain, as previously discussed. Twin boundaries and other stacking defects were then formed to relieve the strain, resulting in asymmetrical growth.[68] In these cases, twin boundaries are formed early in the deposition, after which growth continues preferentially on the lattice-matched regions to form the final symmetry-broken nanocrystals. However, while mechanistically fascinating, the difficulty in controlling the generation of twin defects in a rational and reproducible way makes this method less practical compared to most of the aforementioned methods. Still, it can be seen how the generation of twin defects is closely related to, but distinct from, the use of lattice mismatch to induce symmetry breaking. This similarity raises the question of how many other submethods of symmetry breaking remain to be discovered, both for the multi- and monometallic categories.

4. CASE STUDIES

Built upon the general discussion in sections 2 and 3, this section focuses on the actual examples involving those concepts and strategies. Thanks to the great work from so many research groups, there exists an extensive library of symmetry-broken metal nanocrystals prepared using different methods. By selecting some notable examples, we highlight the synthetic approach used and the mechanism proposed in each case study. To better organize the patterns of asymmetrical growth, this section is further divided into subsections according to the shape of the original nanocrystals (i.e., the seeds). While Figure 3 and Table 1 encompass all possible products, including those theoretically feasible but not yet synthesized, this section focuses on those that have been accomplished experimentally, together with a reasonable understanding of the mechanisms. It should be pointed out that the exact mechanisms or pathways responsible for the formation of some nanocrystals are still under debate because of the multifaceted roles played by the same chemical species in the reaction system. In addition, it is not uncommon to encounter nanocrystals with complex structures arising from a combination of different mechanisms.

4.1. Asymmetrical Growth Involving Single-Crystal Seeds

As discussed in section 2.3.1, the equilibrium shape derived from Wulff construction for all the noble metals except Ru corresponds to a truncated octahedron with its surface enclosed by both {100} and {111} facets (Figure 5A).[1,72,129,130,133] It exhibits the same symmetry (O_h) as the underlying unit cell.[68,69] During colloidal synthesis, the most common growth pathway involves the formation of truncated octahedral seeds, followed by their evolution into final products with different shapes (e.g., cuboctahedra, cubes, octahedra, and rhombic dodecahedra) depending on the experimental conditions.[65] These symmetric products can

https://doi.org/10.1021/acs.chemrev.2c00468
Chem. Rev. 2023, 123, 3693−3760

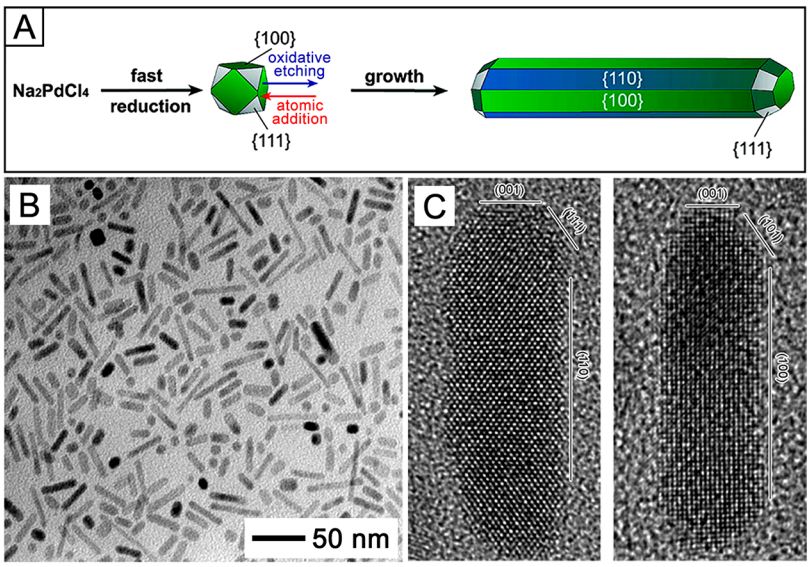

Figure 21. (A) Schematic showing the proposed mechanistic details responsible for the formation of Pd octagonal nanorods. (B, C) Typical TEM and HRTEM images of the Pd nanorods, respectively. Reproduced with permission from ref 177. Copyright 2007 American Chemical Society.

serve as seeds themselves and further evolve into symmetry-broken products such as tetrahedra, rectangular bars, and octagonal rods, creating a large family of nanocrystals possessing diversified geometrical point groups. Additionally, twin defects and stacking faults can occasionally be developed with the assistance of some external driving forces, albeit the actual mechanisms remain to be resolved.

4.1.1. Truncated Octahedral Seeds. Truncated octahedral seeds (see Figure 5B for a 3-D atomic model) are enclosed by eight {111} facets and six {100} facets symmetrically distributed on the surface. They appear pseudospherical under a transmission electron microscope when they are relatively small (typically, below 5 nm). To create truncated octahedral seeds, it is of critical importance to have a sufficiently fast initial reduction rate for the precursor in order to suppress the formation of twinned structures.[133,169] In the subsequent growth process, the identical {111} or {100} facets on a truncated octahedral seed tend to grow at roughly the same rate, leading to the formation of products with a cubic or octahedral shape. In both cases, the O_h symmetry of the seed is preserved. The most straightforward method to deviate from this symmetrical growth pathway is to selectively retard or promote the growth on some of the {111} or {100} facets, inducing asymmetrical growth. Alternatively, twin defects or stacking faults can be developed when a second metal or external stimulation (e.g., light irradiation, ligand binding) is involved, naturally changing the periodicity of the single-crystal structure and thus reducing the symmetry.

4.1.1.1. Formation of Octagonal Rods. As a class of technically important one-dimensional (1-D) nanostructures, single-crystal octagonal nanorods (especially, Au nanorods) have attracted extensive research efforts in terms of protocol development and mechanistic investigation, and great success has been achieved on both fronts.[70,291,292] In one study, oxidative etching was utilized to obtain Pd octagonal nanorods (Figure 21A).[177] The synthesis involved the fast reduction of Na_2PdCl_4 by EG in the presence of KBr, PVP, and water under ambient atmosphere. In this case, Pd truncated octahedral seeds of ca. 2 nm in size were first formed, with Br^- ions chemisorbed on the six {100} facets. The Br^- ions blocked the newly formed Pd atoms from being deposited onto these side faces and thus inhibited their growth. However, when oxidative etching was initiated by the O_2 dissolved in the reaction solution with the assistance of Br^- ions, some of the Pd atoms were oxidized and removed from one of the {100} facets. This process roughened the corresponding side face, desorbing the Br^- ions from it while creating an active site for atomic addition and preferential growth from this side face. As more Pd atoms were deposited onto this side face, the truncated octahedral seed was gradually elongated, and {110} facets began to form accordingly, resulting in a nanorod with an octagonal cross-section and D_{4h} symmetry (Figure 21B,C).

Although the oxidative etching strategy is generic and can be extended to other metals such as Au and Pt,[177] the uniformity of nanorods produced using this approach is typically plagued by a lack of control over the starting point of the etching process. The resulting polydispersity of the products will become a major issue when the desired property is highly dependent on structural features such as aspect ratio. For example, the plasmonic properties of Au nanorods offer exciting potential for theranostic applications, which must be precisely controlled by varying the aspect ratio.[293,294] To this end, protocols have been developed to obtain Au nanorods with uniform, controllable aspect ratios by adding $AgNO_3$ as a shape regulator.[22,245,295] However, the mechanism involved in such a synthesis is rather unique and still under debate. Undoubtedly, the symmetry breaking involved in the synthesis of Au octagonal nanorods is perhaps one of the most intensely studied topics in nanocrystal synthesis. A review article published in 2017 presented a systematic discussion on the multifaceted roles played by Ag^+ ions in enabling the onset of symmetry breaking and controlling the aspect ratio of the nanorods.[67] It was suggested that when the size of the preformed truncated octahedral seeds of Au reached ca. 4 nm during seed-mediated growth, truncated surfaces with {110}-type atomic configuration began to appear at the intersection of {111} facets to remove high-energy edge atoms, as indicated by HRTEM imaging (Figure 22A).[183] On these nascent surfaces, preferential underpotential deposition (UPD) and stabilizations of submonolayers of Ag adatoms would be

https://doi.org/10.1021/acs.chemrev.2c00468
Chem. Rev. 2023, 123, 3693−3760

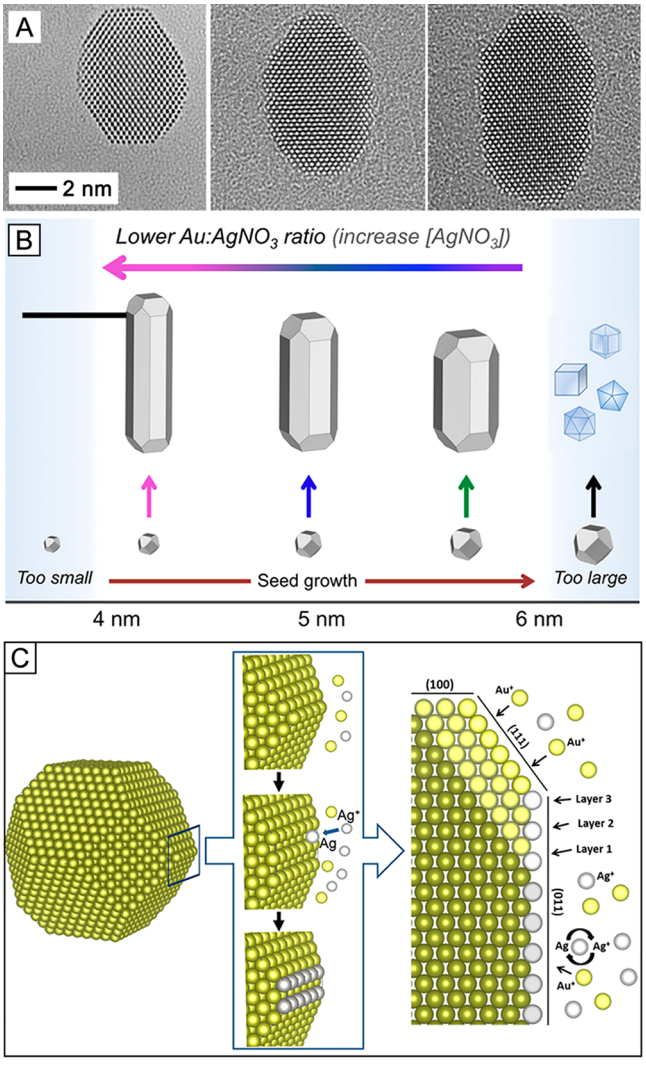

Figure 22. (A) TEM images showing the asymmetrical growth of Au nanoparticles in the presence of Ag^+. (B) Schematic showing the critical size range for the formation of nanorods, which is controlled by the concentration ratio of $HAuCl_4$ to $AgNO_3$. (C) Schematic showing the formation of a truncated surface and its stabilization by Ag UPD. (A) Adapted with permission from ref 183. Copyright 2015 American Chemical Society. (B) Reproduced with permission from ref 182. Copyright 2017 American Chemical Society. (C) Reproduced with permission from ref 67. Copyright 2017 American Chemical Society.

triggered when the $[AgNO_3]$ to $[HAuCl_4]$ ratio was high enough to create an adequate electrical potential. A higher relative concentration of Ag^+ ions, and thus an increased electrochemical potential of the electrons in the redox system, would enable the UPD of Ag on particles with a smaller size and a lower proportion of {110} facets (Figure 22B).[182] The emergence and stabilization of these rough, Ag-capped facets marked a sudden and permanent reduction in symmetry relative to the original truncated octahedral seeds. The starting point of symmetry breaking to the seed is also discussed in section 2.5. Furthermore, a higher concentration of Ag^+ ions limited the redeposition of Au onto the side faces through galvanic replacement between Ag atoms and Au(I), constraining the lateral expansion of Au nanorods and resulting in final products with greater aspect ratios (Figure 22C). Taken together, the dynamic interplay between Ag^+ ions and surface Au atoms, combined with well-defined seeds, provides a facile experimental control over both the shape and size of the final products.

4.1.1.2. Formation of Multiply-Twinned Structures. Growth from truncated octahedral seeds can produce not only single-crystal structures with symmetry-broken shapes such as octagonal nanorods but also twinned products.[286,290] For example, during the growth of Cu from pseudospherical Au seeds, the strain arising from a large (12%) lattice mismatch between the two metals led to the formation of penta-twined bipyramids in the initial stage of growth, which further evolved into pentagonal nanorods, each with a single-crystal Au particle embedded in it (Figure 23A).[286] In this case, the large lattice mismatch was proposed as a critical factor in promoting the development of twinned structures. If the Au seeds were eliminated from the reaction or replaced with Pd cubes (to give a smaller lattice mismatch with Cu), the products would be dominated by Cu or Pd@Cu nanocubes instead due to the lack of driving force arising from a substantial strain. While this argument seems reasonable, it should be pointed out that single-crystal Au@Cu nanocubes have also been obtained when single-crystal Au nanospheres were used as the seeds for Cu deposition (see section 4.1.4.2). This discrepancy emphasizes the critical importance of ensuring that the seeds indeed have a single-crystal structure.

Single-crystal, pseudospherical Au seeds were also reported to evolve into more complex 20-fold twinned icosahedra in a stepwise manner (Figure 23B).[290] By irradiating the growth solution containing $AgNO_3$, sodium citrate, bis(p-sulfonatophenyl)-phenylphosphine dihydrate potassium salt, and plasmonic Au seeds with 550 nm light, Au@Ag tetrahedra were first formed, with a Au seed located at the center of each structure. As more Ag atoms were deposited, a twin plane started to appear on one of the triangular faces of the tetrahedron, transforming the shape into a bitetrahedron. As the particle grew larger, more twin planes and tetrahedral subunits were developed on each structure, and the shape changed to a truncated decahedron, decahedron, and eventually icosahedron in the final stage. In this case, the unique twinning mechanism and growth pathway could be ascribed to the plasmon mediation in lieu of lattice mismatch. It is worth pointing out that the exact formation pathways of these multiply-twinned structures are still elusive due to the difficulty in directly observing and monitoring the growth process. Further studies involving real-time and in situ characterization tools are expected to offer a better understanding of this matter.

4.1.2. Cubic Seeds. Cubic nanocrystals are usually obtained by selectively capping the {100} facets of the seeds with a proper capping agent to allow for growth primarily along the <111> directions. When serving as seeds, the capping agent can desorb partially or completely to expose the {100} facets for further growth along the <100> directions. Different from truncated octahedral or cuboctahedral seeds where the geometrical shape and side faces can be difficult to resolve under a transmission electron microscope, the surface of cubic seeds is mainly enclosed by {100} facets. As such, cubic seeds offer a much simpler system to investigate the mechanistic details of asymmetrical growth.

4.1.2.1. Formation of Nonconcentric Cubes and Bars. To break the symmetry of cubic seeds, a commonly used approach is based on kinetic control, by which the supply of precursor is regulated.[73,76] As illustrated in section 3.2.2, the heterogeneous

https://doi.org/10.1021/acs.chemrev.2c00468
Chem. Rev. 2023, 123, 3693−3760

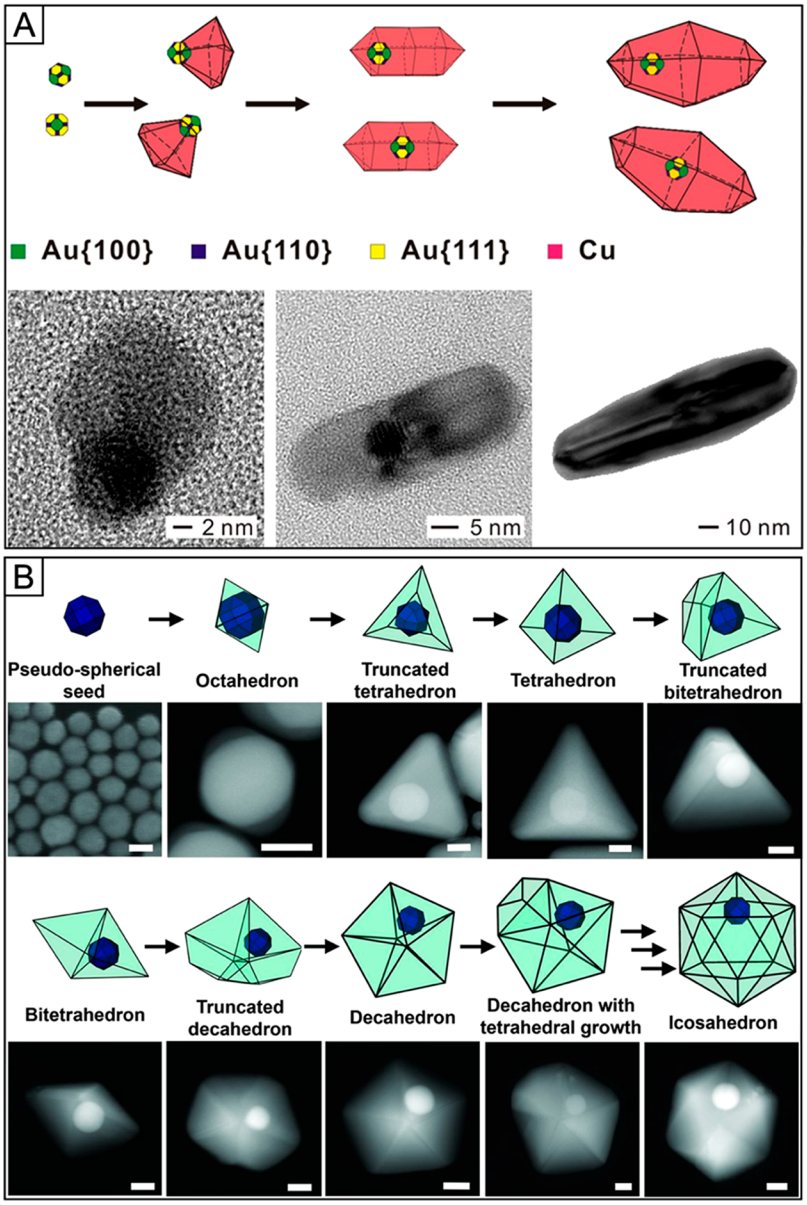

Figure 23. (A) Schematic showing the growth of Au@Cu nanorods and the corresponding TEM images of a Cu shell on a single-crystal Au seed at different stages of growth. (B) Models and representative STEM images depicting the proposed growth pathway of a Ag icosahedron from a single-crystal Au seed in a plasmon-mediated synthesis (scale bars: 25 nm). (A) Reproduced with permission from ref 286. Copyright 2015 American Chemical Society. (B) Adapted with permission from ref 290. Copyright 2012 American Association for the Advancement of Science.

nucleation and growth of a metal on cubic seeds can be limited to one or a few of the six equivalent {100} facets by simply controlling the rate at which the precursor is added and thus reducing the number of atoms available for deposition, provided that the growth on the side faces is not hindered by the surface capping agent. As a proof of concept, three different types of bimetallic nanocrystals, i.e., Pd−Ag hybrid dimers, Pd−Ag nonconcentric nanobars, and Pd@Ag core−shell nanocrystals were fabricated by confining the growth of Ag to one, three, and six side faces of the Pd cubic seeds at slow, moderate, and fast injection of the precursor, respectively.[73] A follow-up study further expanded the scope of kinetic control by involving the concentration of the capping agent (e.g., PVP), the reducing power of the reductant (L-ascorbic acid, AA, by adjusting the pH value), as well as the reaction temperature, to maneuver the deposition and surface diffusion rates of Ag atoms (Figure 24A).[296] It was found that at a higher concentration of capping agent, a slower titration rate, a lower temperature, coupled with a weaker reducing agent, Ag atoms would only be deposited on one of the side faces due to the restriction of both V_{dep} and V_{diff}, generating Pd−Ag Janus nanocrystals as the final product. On the other hand, if both deposition and diffusion were sufficiently fast, conformal growth would occur on all six facets, leading to the formation of concentric Pd@Ag core−shell nanocrystals. By carefully manipulating a set of kinetic knobs, six types of products corresponding to selective nucleation and growth of Ag on a specific number (ranging from one to six) of the side faces of cubic Pd seeds were all successfully demonstrated.

With knowledge of each parameter's role in kinetic control, a recent study further simplified the protocol for the synthesis of nonconcentric nanocubes (Figure 24B).[297] Instead of adding

https://doi.org/10.1021/acs.chemrev.2c00468
Chem. Rev. 2023, 123, 3693−3760

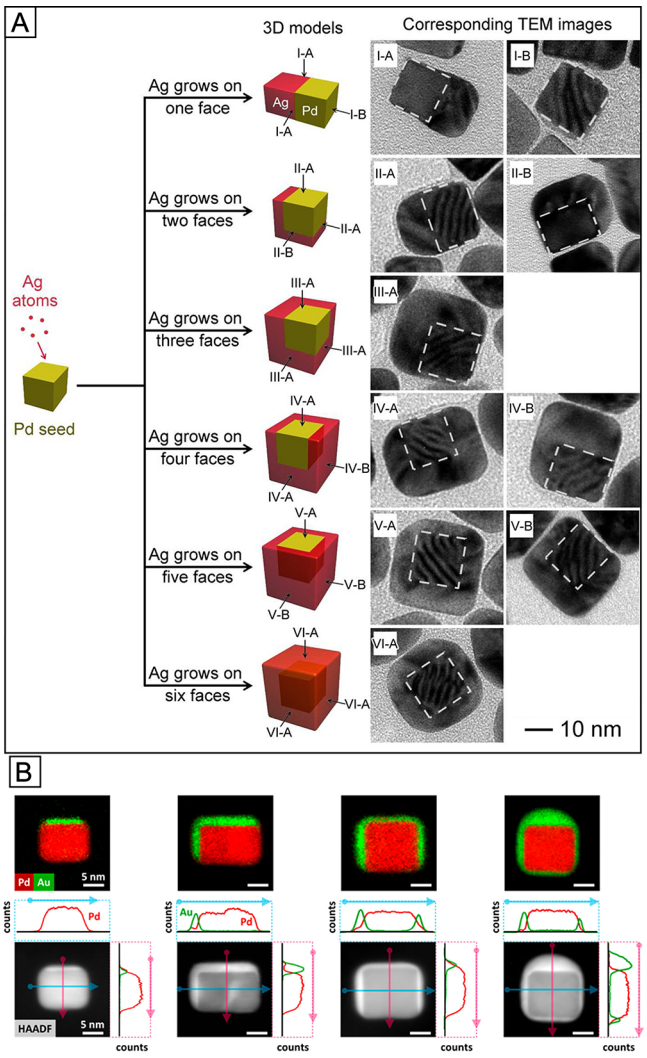

Figure 24. (A) Schematic showing the growth of Ag from different numbers of the side faces of a Pd cubic seed and the corresponding TEM images viewed along different directions. (B) STEM images of Pd−Au nonconcentric nanocrystals prepared through one-shot injection of different amounts of Au(III) precursor, together with the corresponding energy dispersive X-ray spectroscopy (EDS) mappings and line profiles. (A) Reproduced with permission from ref 296. Copyright 2012 American Chemical Society. (B) Adapted with permission from ref 297. Copyright 2021 American Association for the Advancement of Science.

the solution dropwise with the assistance of a syringe pump, the V_{dep} of Au atoms on cubic Pd seeds was controlled by simply varying the amount of Au precursor in the reaction mixture. A series of nonconcentric nanocubes with different numbers of Pd−Au interfaces were obtained even when the synthesis was conducted through one-shot injection of the precursor. It is worth noting that the seed-mediated growth was conducted directly in the original seed suspension containing a large amount of Br^- ions and the remaining AA. The Br^- ions are anticipated to coordinate with the Au(III) ions to help slow down their reduction kinetics. The authors claimed that the Br^- ions might also facilitate the formation of Au shells with smoother interfaces and better-defined {100} facets than in previous reports.

Beyond the limited supply of precursor, oxidative etching is another effective strategy for breaking the symmetry of cubic nanocrystals. Similar to the case of Pd truncated octahedral seeds, the asymmetrical growth of Br^--capped Pd cubes could be triggered on one of the six side faces due to localized surface activation through oxidative etching.[177] Further growth on this side face would result in the formation of Pd rectangular nanobars with aspect ratios of 2−4. A similar approach has also been extended to the successful synthesis of Pt rectangular nanobars.[177]

4.1.2.2. Formation of Semitruncated Octahedra. During seed-mediated growth, one factor that should not be neglected is the influence of thermodynamic control, especially when considering the effect of surface capping agents. For seeds with a cubic shape, their {100} facets have intrinsically higher surface energy and are less stable when compared to {111} facets, owing to a lower coordination number for atoms situated on {100} facets. Therefore, preferential deposition of atoms on all the {100} facets of a cubic seed would gradually transform the shape into an octahedron.[298] When combined with the limited supply of precursor, the same protocol can be used to create asymmetrical nanocrystals with diverse shapes. For instance, during the asymmetrical growth of monometallic Ag nanocrystals at a relatively low concentration of PVP, {111} facets were developed on different numbers of equivalent side faces of the cube since the initial stage of growth was dependent on the rate at which $AgNO_3$ was injected (Figure 25A).[76] After sufficient growth, the Ag nanocubes evolved into

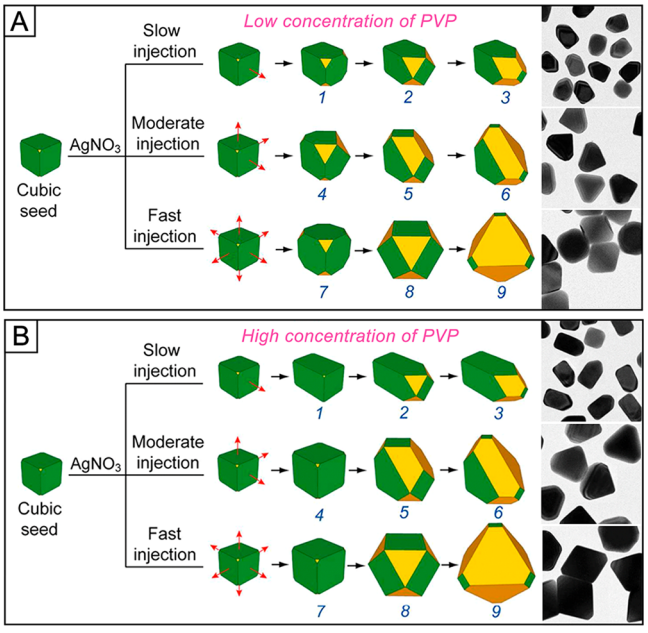

Figure 25. Growth patterns for Ag cubic seeds in the standard syntheses involving PVP at relatively low (panel A, 1 mg/mL) and high (panel B, 30 mg/mL) concentrations, respectively, with schematics showing the morphological changes to the Ag nanocrystals formed under three different injection rates for $AgNO_3$ solution. Adapted with permission from ref 76. Copyright 2012 American Chemical Society.

octahedra with different numbers of truncated faces, including semitruncated octahedra. On the contrary, at a relatively high concentration of PVP, the order of surface free energy would be reversed because the stronger binding of PVP to Ag(100) than Ag(111) stabilized the {100} facets (Figure 25B).[76] In this case, bars and enlarged cubes with no expression of {111}

https://doi.org/10.1021/acs.chemrev.2c00468
Chem. Rev. 2023, 123, 3693−3760

facets would be formed during the initial stage of growth. As the growth proceeded, more PVP would chemisorb onto the surface of the nanocrystals. As the concentration of PVP in the solution phase fell below a critical value, {111} facets would start to appear on the surface. Accordingly, truncated octahedra formed at a higher concentration of PVP possessed a higher aspect ratio, and all the products were of larger size.

4.1.2.3. Formation of Planar Tetrapods. In the aforementioned synthesis of bimetallic nonconcentric nanocrystals, one may notice that the shapes of some products deviated from a standard cube, especially those relatively large in size. This could be rationalized by the interfacial strain induced by the intrinsic lattice mismatch between the two metals. In fact, large lattice mismatch usually favors nonconformal asymmetrical growth, including the formation of branched arms as a manifestation of minimizing strain.[299,300] In another example, when Au(III) and Cu(II) precursors were reduced by a relatively weak reducing agent in the presence of 9 nm Pd cubic seeds and cetyltrimethylammonium chloride (CTAC), the lattice mismatch of 4.02% between the Pd core and the AuCu shell facilitated the formation of branched arms on the seeds (Figure 26A–D).[301] In particular, the slow reduction of the precursors, together with the selective capping of CTAC toward the side faces of Pd cubic seeds, confined the overgrowth to a set of four edges of each seed, leading to the formation of single-crystal, planar tetrapods.

4.1.2.4. Formation of Penta-Twinned Rods. The formation of branched arms is not the only way to release the strain energy at the interface between two metals during growth. In some cases, the formation of twin defects can be induced when the extent of lattice mismatch is large, offering another route to symmetry breaking. As an example, the overgrowth of Au on 10 nm Pt cubic seeds (4.08% mismatch) led to the formation of penta-twinned Au nanorods, with one Pt cube partially embedded in the perimeter of the rod (Figure 26E–H).[289] Even though the evolution pathway of such a highly asymmetrical structure is equivocal, it is not unreasonable to assume that, following the nucleation of Au on the Pt cube, penta-twinned defects were created to help minimize the total energy of the system. Further growth occurred bidirectionally along the axial directions, resulting in elongation of the penta-twinned Au nanorod, with the Pt cubic seed remaining at the middle point of the nanorod.

4.1.3. Octahedral Seeds. As another type of nanocrystal featuring the O_h symmetry, octahedral nanocrystals enclosed by {111} facets are formed when the {100} facets on truncated octahedral or cuboctahedral seeds are more favorable for growth.[298,302] Once the nanocrystals are fully covered by eight {111} facets, subsequently formed metal atoms can still be deposited on the {111} facets under certain conditions, resulting in size enlargement and well-maintained octahedral shape. In some cases, the O_h symmetry can be broken to generate nanocrystals with other shapes.

4.1.3.1. Formation of Tetrahedra. During the growth of octahedral seeds, if the supply of precursor is inadequate to support growth on all the eight faces, the shape would deviate from an octahedron, with the symmetry being reduced, similar to the case of cubic seeds. For example, when Pd(II) acetylacetonate ($acac^-$) with a fast reduction rate was used as the precursor for the seed-mediated growth in a mixture of PVP and EG, the 5 nm Pd truncated octahedral seeds grew into 7.1 nm octahedra in the first 5 min (Figure 27A,B).[252] Afterward, since over 77% of the precursor had been depleted,

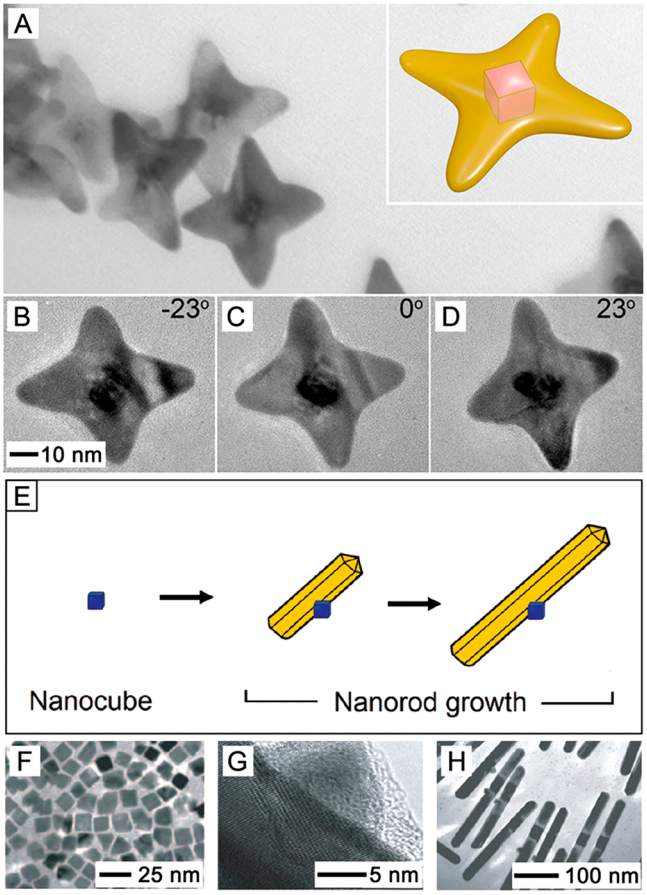

Figure 26. (A) TEM image of Pd@AuCu core–shell planar tetrapods, with a model of the planar tetrapod in the inset. (B–D) An individual Pd@AuCu planar tetrapod at different tilting angles. (E) Schematic showing the formation of a penta-twinned Au nanorod from a single-crystal Pt cubic seed. (F–H) STEM images of (F) the corresponding single-crystal Pt seeds, (G) a Pt seed partially embedded in the nanorod, and (H) Pt-seeded Au nanorods. (A–D) Reproduced with permission from ref 301. Copyright 2016 American Chemical Society. (E–H) Adapted with permission from ref 289. Copyright 2007 Nature Publishing Group.

the newly formed Pd atoms could only support growth (through direct deposition or surface migration) on four of the eight equivalent {111} facets of each octahedron. As the growth continued, tetrahedra terminated in {111} facets, together with an edge length of twice that of the octahedral intermediate, were formed as the final products (Figure 27C). In the case of Na_2PdCl_4 with slower reduction kinetics and thereby a more sustained supply of Pd atoms, the growth was switched to the highly symmetric pattern to give enlarged Pd octahedra as the final product (Figure 27D).

4.1.3.2. Formation of Hexapods. As a common feature of octahedral nanocrystals, their six corners are usually slightly truncated with the corresponding {100} facets exposed to lower the overall thermodynamic energy. Without the interference of surface capping agents, these {100} facets with higher surface energy are more favorable for atomic deposition in seed-mediated growth. However, since the activation energy barrier for adatoms to diffuse across {111} facets is much lower than that on {100} facets,[303] these adatoms can easily diffuse into the eight side faces of each octahedron, resulting in layer-by-layer growth of the octahedral seed without significant alternation to the shape. The selective

https://doi.org/10.1021/acs.chemrev.2c00468
Chem. Rev. 2023, 123, 3693–3760

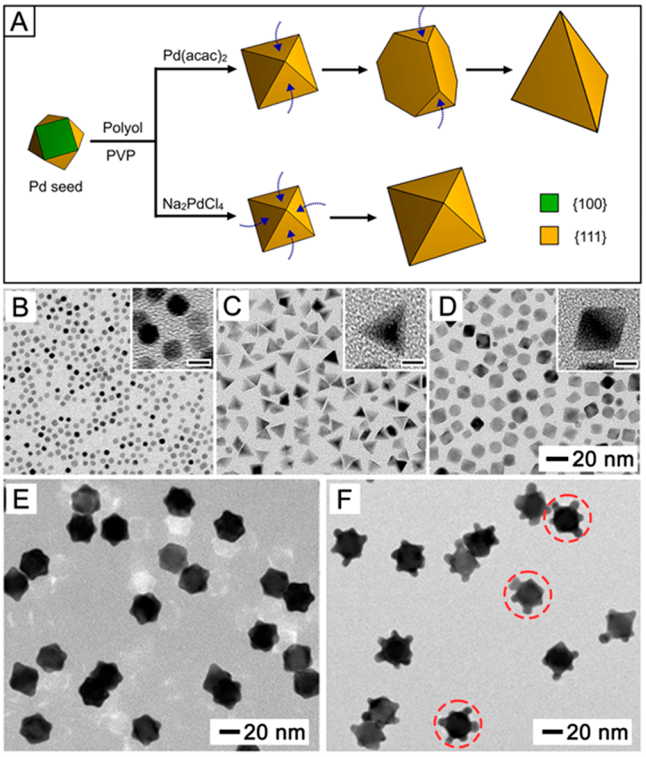

Figure 27. (A) Schematic showing the formation of Pd tetrahedra and octahedra, respectively, when using $Pd(acac)_2$ and Na_2PdCl_4 as the precursors for seed-mediated growth. (B–D) Typical TEM images of (B) Pd truncated octahedral seeds, (C) tetrahedral product, and (D) octahedral product. (E and F) TEM images of Au hexapods obtained with (E) 1 μL and (F) 5 μL of $HAuCl_4$ solution added, respectively. The dashed circles in panel F mark the nanocrystals with one or more arms missing. (A–D) Reproduced with permission from ref 252. Copyright 2013 American Chemical Society. (E, F) Adapted with permission from ref 304. Copyright 2011 Wiley-VCH.

growth on the corners can only be preserved when the synthesis is conducted at relatively low temperatures to suppress surface diffusion. For example, the slow dropwise addition of Pt(IV) precursor into a growth solution containing Pd octahedral seeds at 200 °C gave Pd@Pt conformal core–shell nanocrystals with truncated corners and a uniform Pt shell as the product.[303] On the contrary, with a one-shot injection of Pt(II) precursor and at a much lower reaction temperature of 95 °C, the preferential growth of Pt on the six corners of each octahedral seed resulted in a product possessing significantly enhanced corner sharpness and higher exposure of Pt{111} facets. In this case, the temperature was low enough to partially limit surface diffusion so that a large portion of the Pt atoms stayed on the corners and yet was high enough to provide sufficient energy for generating smooth {111} facets.

If a significantly lower temperature is used while more precursor is introduced into the reaction solution, the growth pattern can become very different. For instance, the deposition of Au atoms on octahedral Au seeds at room temperature resulted in complete island growth on the corners of each octahedron (Figure 27E,F).[304] The atoms in these quasi-spherical islands did not have enough energy to overcome the barrier to either surface rearrangement or surface diffusion. Therefore, hexapods with rough surfaces were observed as the main product. As proof of this mechanism, an elevated reaction temperature was shown to promote lateral growth on the octahedral seeds to produce hexapods with larger cores and shorter arms. Interestingly, some of the nanocrystals did not fully develop into hexapods but instead showed one or more arms missing (marked by dashed circles in Figure 27F), suggesting the occurrence of symmetry breaking. This process was most likely due to the insufficient supply of the Au atoms in this room-temperature reaction system, similar to the formation of nonconcentric cubes discussed in section 4.1.2.1.

4.1.4. Spherical Seeds. To avoid confusion with the truncated octahedral (pseudospherical) seeds, here we define spherical nanocrystals as those with a smooth surface and a circular cross-section when observed from different angles under a transmission electron microscope. Despite their origin from the same crystal structure as the aforementioned cubic and octahedral seeds, nanospheres are a unique class of nanostructures because their spherical shape endows them with even higher symmetry than their underlying unit cell (in fact, the highest symmetry possible!). Therefore, within the scope of our discussion, the transformation of a spherical seed into any other shape would involve symmetry breaking. Owing to their easily achieved uniformity in size, spherical nanocrystals, especially those made of Au, have been widely employed as seeds to investigate the mechanistic details involved in shape evolution.[305]

4.1.4.1. Formation of Cubes and Bars. The seed-mediated growth involving Au nanospheres offers a simple and general route to the generation of nanocubes made of various metals. In a recent report, well-defined Au nanocubes with precisely controlled size and corner sharpness were prepared by simply varying the concentration of the seeds and Br^- ions in the growth solution, respectively (Figure 28A).[306] Specifically, 10 nm Au spheres were first synthesized as seeds through the fast reduction of $HAuCl_4$ by $NaBH_4$, a strong reducing agent. For the subsequent growth, Br^- ions were employed as a surface capping agent toward the {100} facets to induce symmetrical growth along <111> directions. With increasing Br^- concentration (from 0 to 40 mM), the corner sharpness of the Au nanocubes gradually increased because the difference in growth rate between {100} and {111} facets was maximized. In the case of excessive Br^- concentration, however, the corner sharpness was reduced. The authors argued that this phenomenon could have two explanations. First, the Br^- ions would start to adsorb onto the {111} and {110} surfaces once the {100} facets had been saturated, narrowing the difference in growth rate among different facets. Second, the Br^- ions in the reaction solution could coordinate with Au(III) ions to form $AuBr_4^-$, which have higher stability and lower reduction potential than $AuCl_4^-$, and thus slower reduction kinetics. As a result, the newly deposited Au atoms, known to have a long self-diffusion distance, could diffuse from corners to edges and side faces to form more thermodynamically stable rounded cubes. This proposed mechanism for the non-monotonic dependence between the corner sharpness and Br^- concentration was supported by the UV–vis spectra. Among three selected Br^- concentrations (1, 40, and 200 mM), the intensity of the extinction peak associated with plasmon resonance increased most slowly in the case of 200 mM NaBr, suggesting that the increased Br^- concentration decelerated the reduction of the Au(III) precursor. It is worth pointing out that the etching effect of Br^- ions should not be neglected. At a high concentration of Br^- ions, the under-coordinated atoms on the corners and edges could be

https://doi.org/10.1021/acs.chemrev.2c00468
Chem. Rev. 2023, 123, 3693–3760

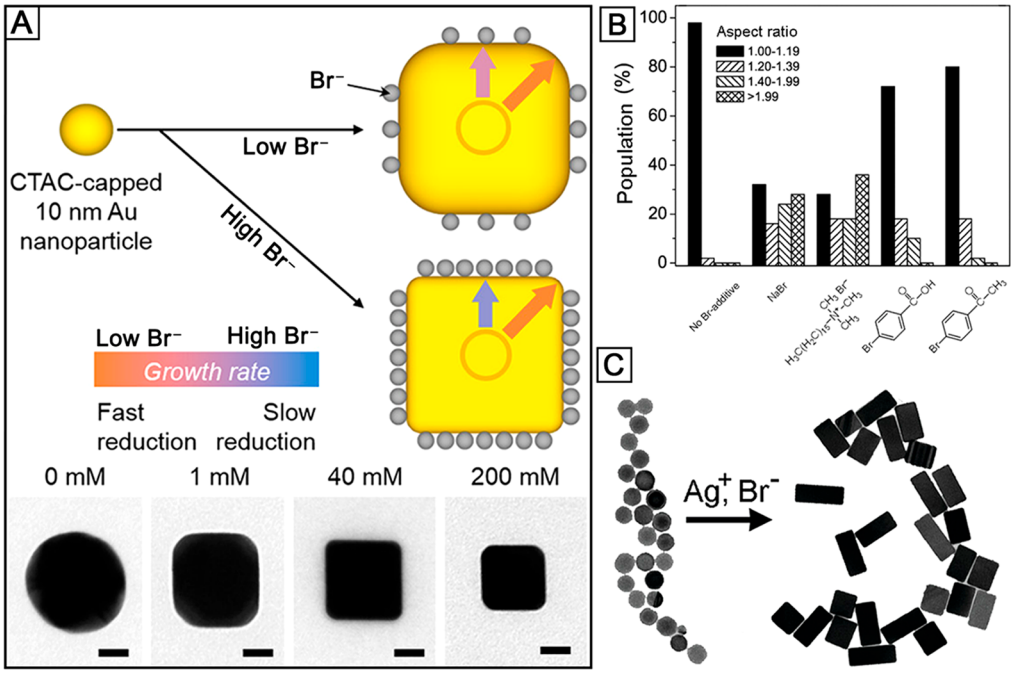

Figure 28. (A) Schematic showing the synthesis of Au nanocubes with different degrees of corner sharpness by varying the Br^- concentration and TEM images of the Au nanocubes obtained by adjusting the concentration of Br^- ions from 0−200 mM at the fixed amounts of seed and Au(III) precursor (scale bars: 20 nm). (B) Distributions of the aspect ratios of Ag nanobars grown from spherical seeds in the presence of different types of bromide compounds. (C) TEM images of the Ag spherical seeds and nanobars synthesized in the presence of NaBr. (A) Reproduced with permission from ref 306. Copyright 2018 American Chemical Society. (B, C) Reproduced with permission from ref 307. Copyright 2012 American Chemical Society.

selectively oxidized by O_2 in the presence of Br^-, generating cubes with more rounded corners. Based on the mechanistic insights, Au nanocubes with sizes down to 17 nm have been successfully synthesized by increasing the amounts of spherical seeds and NaBr.

More interestingly, when oxidative etching is involved in the growth process, the symmetry of spherical seeds can be reduced to generate nanobars with tunable aspect ratios, similar to the transformation from cubic seeds to bars as discussed in section 4.1.2.1. For seed-mediated growth with Ag nanospheres, another study demonstrated that the aspect ratio of the product was critically dependent on the chemical nature and concentration of the bromide compound added into the reaction system (Figure 28B).[307] Due to their smaller size, the Br^- ions from an ionic salt (e.g., NaBr and CTAB) could adsorb more easily and bind more strongly to the surface of Ag nanocrystals than the bromine in a covalent compound. Therefore, ionic salts were more effective in inducing and promoting the asymmetrical growth of Ag nanocrystals. Moreover, the use of Br^- ions at a higher concentration would result in the formation of complexes with more Ag^+ ions. As such, the reduction kinetics would be slowed down and the supply of atoms would become limited, favoring the growth along one direction and thus the formation of symmetry-broken nanobars (Figure 28C). It is worth noting that the products obtained from the synthesis involving NaBr contained two different types of nanobars, one with a square cross-section and the other with a rectangular cross-section. The formation of nanobars with two distinct cross-sections could be attributed to the difference in surface capping caused by a low concentration of Br^- ions.

Based on this study, the role of Br^- concentration was further explored to prepare square nanoplates. It was argued that when the concentration of Br^- was further reduced to a level to just inhibit the growth along one direction, growth along the other two orthogonal directions would lead to the formation of square plates instead of bars (Figure 29).[308] Interestingly, these symmetry-broken structures could be prepared in high uniformity, with a narrow distribution in terms of edge length and thickness. As the reaction proceeded and the nanocrystals grew larger, the aspect ratio became smaller (2.74 after one hour of growth vs 1.77 after five hours of growth), indicating that the shape gradually approached a cube. The optical properties of these Ag nanocrystals could be tuned by controlling the aspect ratio of edge length to thickness.

4.1.4.2. Formation of Nonconcentric Cubes. As discussed above in the case of cubic seeds, the seed-mediated growth of bimetallic nanocrystals with a large mismatch in lattice constant between the core and the shell can lead to atypical products. In principle, the trend should remain more or less the same for single-crystal seeds of other shapes. Indeed, the growth of a second metal on lattice-mismatched spherical seeds has also been reported to produce unique structures such as Au@Cu core−shell nanocubes with a nonconcentric structure (Figure 30).[309] Specifically, a spherical particle with different contrast could be observed on or near the surface of each cube under TEM, in stark contrast to the conventional core−shell structures with the core (seed) always located at the center. This observation indicated a nonuniform nucleation and growth pattern on the surface of a Au spherical seed. Tracing of the growth process revealed that, in the initial stage of Cu deposition onto 4.7 nm Au spheres (with 12% lattice mismatch), the Cu atoms nucleated and grew into several individual islands on the surface through a process known as localized epitaxial growth, which helped minimize the strain at

https://doi.org/10.1021/acs.chemrev.2c00468
Chem. Rev. 2023, 123, 3693−3760

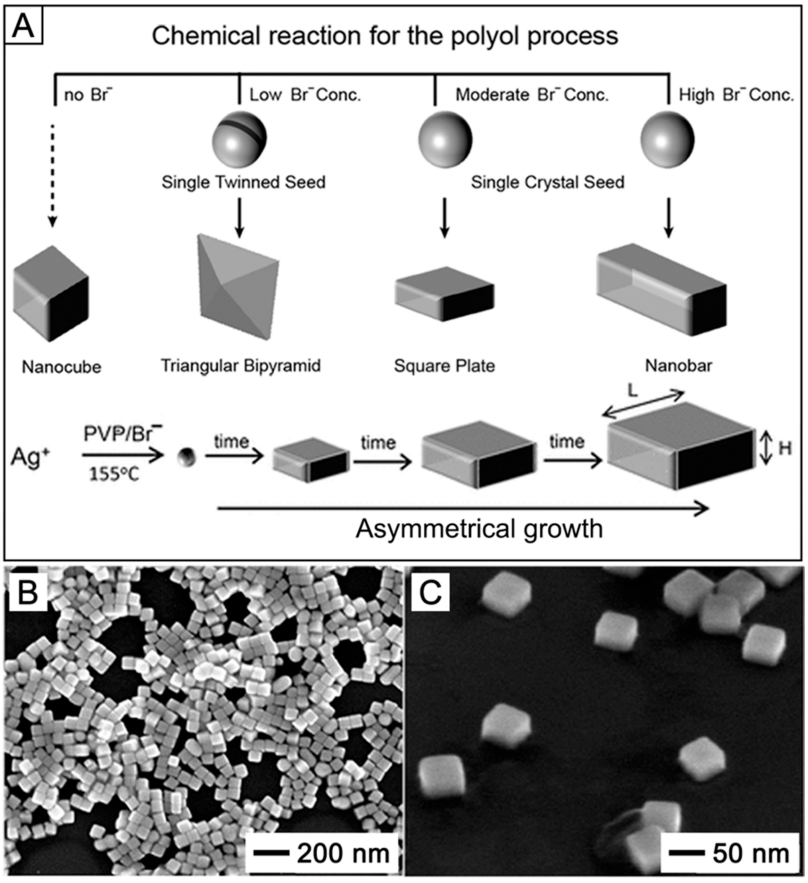

Figure 29. (A) Schematic showing the effect of bromide concentration on the internal structure of the seed and the shape of the nanocrystal in a Br^--mediated polyol synthesis, as well as the formation of square nanoplates. (B, C) Scanning electron microscopy (SEM) images at (B) top view and (C) 45° tilting angle, respectively. Reproduced with permission from ref 308. Copyright 2018 American Chemical Society.

the interface. As Cu deposition proceeded, these islands became large enough to merge together and completely encase the seed. With the capping effect from hexadecylamine (HDA) and Cl^- ions, the nanocrystals evolved into a cubic shape, together with different sizes. When the reaction solution was maintained at a high temperature for a long period of time, Ostwald ripening would occur, narrowing the size distribution to give uniform nanocubes of 27.1 ± 3.0 nm in edge length, together with a high purity greater than 85%.

4.1.4.3. Formation of Tetrahedra and Hexoctahedra. Like the transformation from octahedra to tetrahedra through kinetically controlled growth, tetrahedral nanocrystals with high purity and tunable sizes could be synthesized from Au spherical seeds using the same strategy. When a $HAuCl_4$ solution was slowly added into a reaction solution containing 10 nm Au spherical seeds with a single-crystal structure, AA, CTAC, and CTAB, only selected facets of each Au seed would participate in the heterogeneous nucleation and growth, breaking the symmetry and transforming the spheres into tetrahedra with sharp tips (Figure 31A).[310] In contrast, when the injection rate of precursor was increased, sufficient growth over the entire surface of the seeds would result in products with a truncated tetrahedral or quasi-spherical shape. Under more extreme conditions, that is, when the reduction was greatly accelerated, high-index facets were developed. For example, the reduction of Au(III) precursor on the spherical Au seeds by AA at a high concentration of 0.3 M and the boiling point of an aqueous reaction solution would result in hexoctahedral nanocrystals exclusively bounded by 48 triangular high-index {321} facets (Figure 31B).[311] The high V_{dep} arising from a plentiful supply of Au atoms ensured the formation of such thermodynamically unstable structures rich in energetic sites, including tips, edges, and intraparticle gaps.

4.1.4.4. Formation of Other Types of Asymmetrical Nanocrystals. In all aforementioned cases, the general strategy for symmetry breaking is to unevenly restrain the growth along certain directions of the nascent nanocrystals. For example, the growth of octahedral seeds along four of the eight symmetrical directions would result in tetrahedra, while the growth of truncated octahedral seeds along two opposite directions would give octagonal rods as the product. In addition, other asymmetrical shapes can emerge when growth only occurs in one direction, or more restrictedly, one specific site on the seed. As an intriguing example, site-specific growth was achieved for the multistep synthesis of Au−Ag−Ag triblock nanostructures (Figure 32A).[312] When a 2-mercapto-benzimidazole-5-carboxylic acid (MBIA) ligand containing a thiol group was used to strongly block the surface of Au spherical seeds, defects would be induced at one specific site on the seed during Ag deposition, which would trigger island growth of Ag from this site. Since the lateral expansion of Ag domain on the seed was restricted by the unfavorable interfacial energy, further deposition of Ag atoms was limited to only one specific direction. Under a limited supply of Ag atoms (controlled using a syringe pump), elongation of the Ag domain created a "fresh" Ag-solvent interface that was relatively ligand-deficient,

https://doi.org/10.1021/acs.chemrev.2c00468
Chem. Rev. 2023, 123, 3693−3760

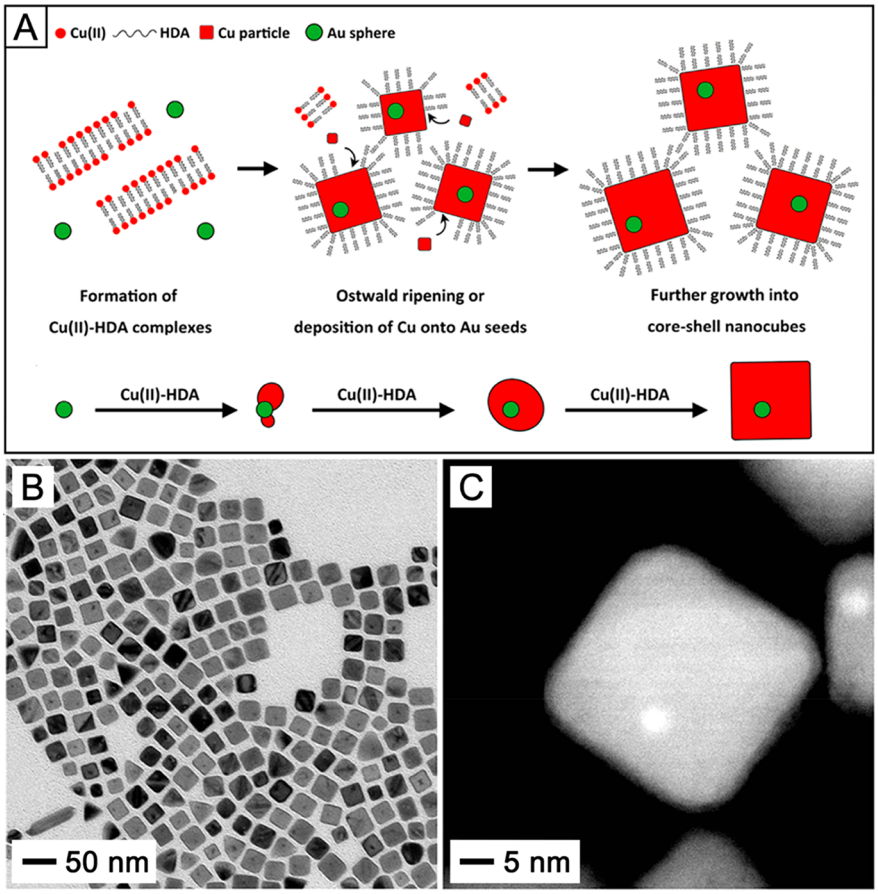

Figure 30. (A) Schematic showing the formation of Au@Cu core−shell nanocubes featuring a nonconcentric structure. (B) TEM and (C) HAADF-STEM images of the Au@Cu core−shell nanocubes obtained from 5 nm Au spherical seeds with a single-crystal structure. Reproduced with permission from ref 309. Copyright 2019 American Chemical Society.

serving as a new site for subsequent deposition. Once the "old" surface became more densely packed with MBIA ligands, the growth would be inhibited. This unique approach gave rise to the formation of a Ag nanowire featuring a Au sphere at one end. Furthermore, when excess amounts of sodium citrate, a reducing agent and a Ag(111)-selective capping agent, were added after a certain period of time of growth, the accelerated reduction of $AgNO_3$ diminished the difference between the "fresh" and "old" surfaces in terms of surface energy, promoting symmetrical growth of Ag on the unoccupied end of the nanowire. Assisted by the capping effect of citrate ions, a triangular or hexagonal plate-shaped block, with its surface dominated by {111} facets, was gradually formed (Figure 32B). Taken together, this work demonstrated an unexpected ability of colloidal synthesis to prepare sophisticated triblock structures with discrete shapes. It also emphasized the necessity to understand the multiple roles and fundamental mechanisms of each chemical species in controlling the growth of nanocrystals.

For Au nanospheres, another special feature of this symmetrical nanocrystal is that they are not stable when kept in an aqueous suspension involving CTAB or CTAC as the stabilizer. Upon dilution, the bilayer of ligand molecules on these nanostructures would start to desorb from the surface, changing the surface from hydrophilic to hydrophobic.[77] Driven by the hydrophobic interactions, these nanospheres would start to attach to each other, evolving into dimers, trimers, and larger aggregates with a necklace shape as more water was added into the suspension and the ligand concentration was further diluted (Figure 32C−F).[313] This attachment mechanism offers a unique route to symmetry breaking.

4.2. Asymmetrical Growth Involving Seeds with One or Multiple Twin Defects

In addition to single crystals with a continuous lattice across the entire particle, those with planar defects (e.g., twin planes and stacking faults) can also serve as seeds to obtain nanocrystals with the same internal structure as the seeds but in diverse symmetry. These nanocrystals can be further divided into three categories according to the type and number of planar defects present in the particle: singly-twinned, multiply-twinned, and stacking fault-lined. While the symmetry breaking of stacking fault-lined particles is rarely reported, seed-mediated growth of both singly- and multiply-twinned particles has contributed to many symmetry-broken nanostructures.

4.2.1. Singly-Twinned Seeds. Singly-twinned nanocrystals tend to exist as bipyramids or plates with triangular bases, which can be regarded as a base-to-base integration of two subunits, with the twin plane serving as the shared interface. In the bipyramidal system, there is a special case, namely right bipyramids, where all the side faces of both pyramidal subunits are right isosceles triangles terminated in {100} facets. As the formation pathway of these nanostructures remains elusive, it is still unclear when the twin plane is developed and how the 3-

https://doi.org/10.1021/acs.chemrev.2c00468
Chem. Rev. 2023, 123, 3693−3760

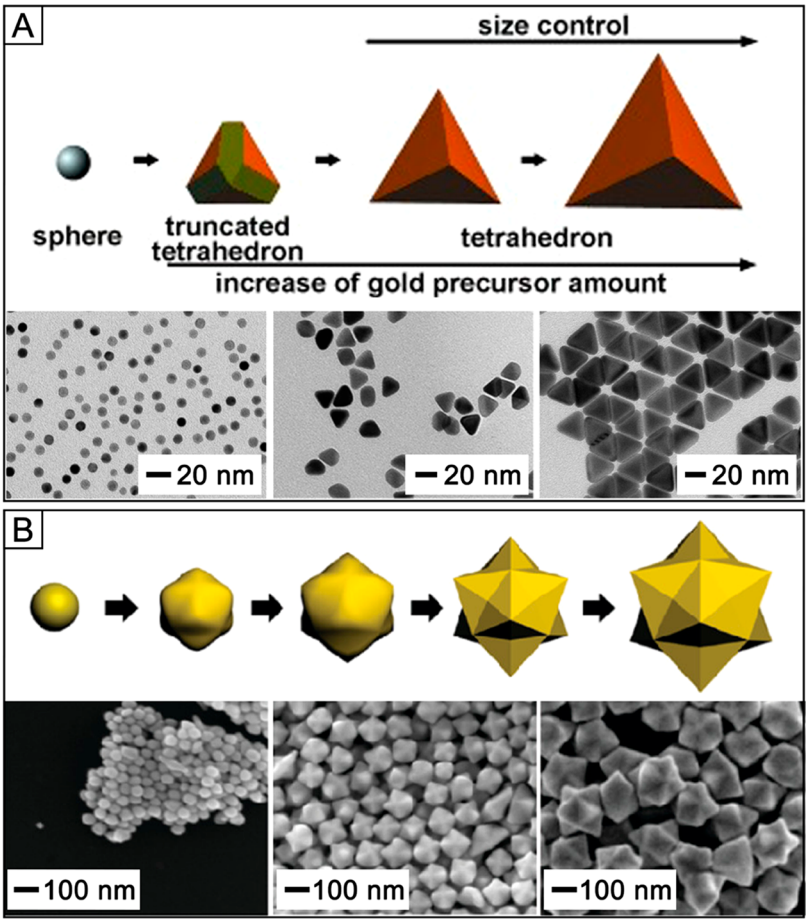

Figure 31. (A) Schematic showing the growth of Au tetrahedra from spherical seeds and typical TEM images of the products obtained at different stages of the synthesis. (B) Schematic showing the growth of hexoctahedra from spherical seeds and typical SEM images of the products obtained at different stages of the synthesis. (A) Reproduced with permission from ref 310. Copyright 2014 Wiley-VCH. (B) Reproduced with permission from ref 311. Copyright 2012 American Chemical Society.

fold rotational symmetry is evolved. When serving as a seed, asymmetrical growth can be initiated when atomic depositions on symmetry-related sites on the basal planes, equatorial or axial vertices, and side or basal edges of singly-twinned seeds occur at different rates (see Table 1). The products often exhibit different symmetry relative to the seeds, even though they all share the same twin plane.

4.2.1.1. Formation of Triangular Plates and Bipyramids. A mechanistic exploration of the symmetry breaking process was made by employing singly-twinned nanocrystals with a spherical shape as the seeds (Figure 33).[193] Specifically, Au triangular nanoplates prepared using an optimized protocol were etched in an aqueous solution containing CTAC and NaBr, with Au(III) serving as an oxidant. As the surface Au atoms were oxidated and dissolved away, the particle size was gradually reduced while the corners and edges became progressively rounded, turning the shape into a sphere. Singly-twinned nanospheres of 20 and 12 nm in size (51% and 29% purity, respectively) were produced after the etching process was repeated four and seven times, respectively. Similarly, Au single-crystal nanospheres of two similar sizes were obtained by etching octagonal nanorods and then used as the seeds. These spherical particles were introduced into aqueous solutions containing $HAuCl_4$, AA, CTAC, and different concentrations of NaI for seed-mediated growth of Au. Here I^- was argued to regulate the shape of the products and/or induce the formation of twin defects depending on its concentration. It was found that the shape of the final products remained pseudospherical in the absence of I^-, while symmetry-broken triangular plates, bipyramids, and octahedra would dominate the products and they are supposed to evolve from singly-twinned and single-crystal seeds, respectively, in the presence of 50 μM of I^-. Meanwhile, it was demonstrated that twin defects could be introduced into single-crystal seeds to create twinned products. However, the twin defects in singly-twinned seeds could not be removed during overgrowth, and such a trend of crystallinity change was more significant for the 12 nm seeds. This work presents a new approach to accessing seeds with different twin structures but relatively similar sizes and shapes. It holds potential for not only optimizing synthetic protocols of singly-twinned particles but also reaching a better understanding of the symmetry breaking phenomenon.

4.2.1.2. Formation of Beams. Another interesting example of asymmetrical growth involving singly-twinned seeds is the formation of nanobeams through the activation of uniaxial growth in a direction parallel to the twin plane. The nanobeams can be regarded as 1-D nanostructures with a single twin plane running along the longitudinal axis. In one study, Ag nanobeams were produced by slightly modifying the EG-based process developed for the synthesis of Ag right bipyramids (Figure 34).[314] As discussed in section 2.4, tuning

https://doi.org/10.1021/acs.chemrev.2c00468
Chem. Rev. 2023, 123, 3693−3760

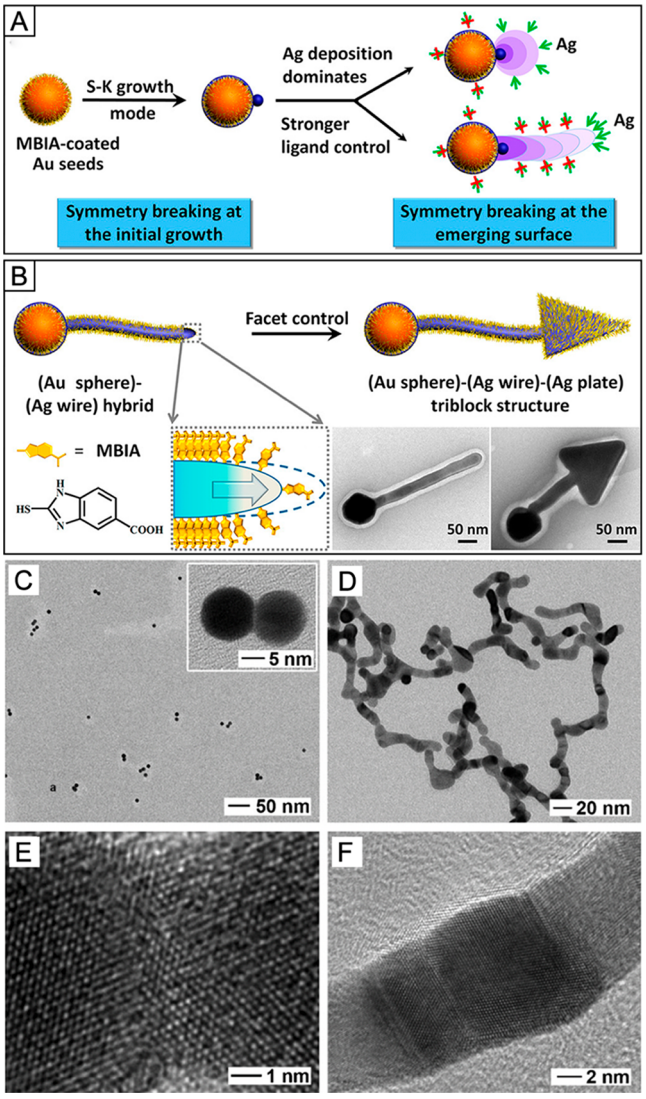

Figure 32. (A) Schematic showing the difference in symmetry breaking during the initiation of Ag domain and the subsequent growth. (B) Schematic showing the synthesis of a triblock structure with additional facet control and the corresponding (Au sphere)−(Ag wire) hybrid and (Au sphere)−(Ag wire)−(Ag plate) triblock nanostructure. (C−F) TEM images of Au nanostructures in the form of dimers and wavy nanowires, together with HRTEM images of the attached regions of a dimer and a wavy wire. (A, B) Reproduced with permission from ref 312. Copyright 2015 American Chemical Society. (C−F) Adapted with permission from ref 313. Copyright 2013 Wiley-VCH.

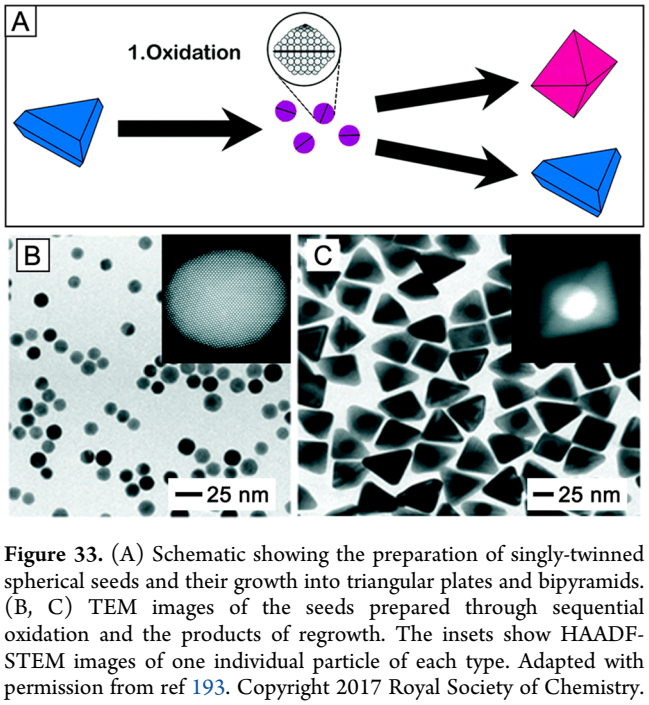

Figure 33. (A) Schematic showing the preparation of singly-twinned spherical seeds and their growth into triangular plates and bipyramids. (B, C) TEM images of the seeds prepared through sequential oxidation and the products of regrowth. The insets show HAADF-STEM images of one individual particle of each type. Adapted with permission from ref 193. Copyright 2017 Royal Society of Chemistry.

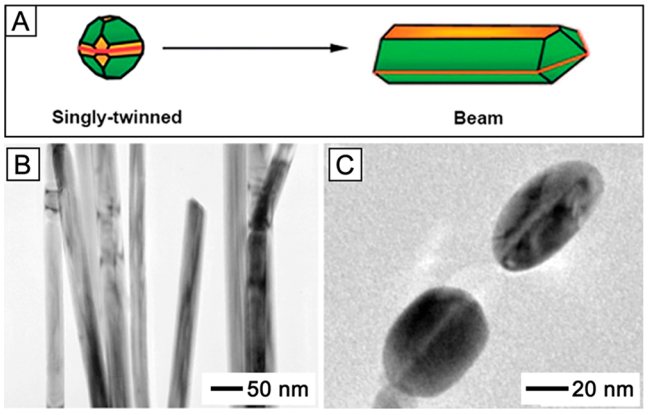

Figure 34. (A) Schematic showing the formation of a nanobeam from a singly-twinned seed. (B, C) TEM images of (B) Ag nanobeams and (C) their cross-section with a twin plane parallel to the basal plane. Reproduced with permission from ref 314. Copyright 2006 American Chemical Society.

the strength of the etchant involved in the oxidative etching process is a powerful method to regulate the number of twin defects in the seeds.[121,137,140] In this case, Br^-, a less corrosive etchant than Cl^-, induced moderate etching to only remove multiply-twinned seeds from the sample while keeping singly-twinned seeds in high yield. By doubling the concentrations of $AgNO_3$ and PVP while lowering the reaction temperature used for the polyol synthesis of Ag right bipyramids, the singly-twinned seeds would undergo asymmetrical growth under the slow reduction kinetics, generating products with a beam-like morphology instead of right bipyramids. The asymmetrical growth could be ascribed to the slow atomic addition and inadequate surface diffusion, coupled with the capping effect of Br^- toward Ag{100} facets. Specifically, atoms would mainly be deposited onto and accumulated at the high-energy defect zone on the triangular base of the singly-twinned seeds, resulting in a greater rate of atomic deposition along one direction and thus the induction of asymmetrical growth. The as-obtained Ag nanobeams could have lengths up to 300 nm, widths ranging from 17−70 nm, and a width-to-thickness ratio of about 1.4.

4.2.2. Penta-Twinned Decahedral Seeds. Multiply-twinned nanocrystals, including those with decahedral (D_{5h}) and icosahedral (I_h) shapes (section 4.2.3), are remarkable structures in terms of both geometric shape and atomic arrangement due to the unique assembly of different numbers of single-crystal apex- and facet-sharing tetrahedral subunits. These nanocrystals can be formed through at least two pathways: (i) direct nucleation into 5-fold and 20-fold twinned seeds and subsequent layer-by-layer growth, or (ii) stepwise formation of new twin boundaries on single-crystal seeds via atomic growth or attachment.[315] The latter case can be

https://doi.org/10.1021/acs.chemrev.2c00468
Chem. Rev. 2023, 123, 3693−3760

considered as a case of symmetry reduction for single-crystal seeds, which is discussed in section 4.1. Although the actual formation pathway of these nanocrystals is still under debate, their unique symmetry is widely used in seed-mediated growth to produce asymmetrical nanostructures hard to obtain through traditional means.

This subsection focuses on the nanocrystals emanating from symmetry breaking to decahedral seeds. Two types of edges exist on a decahedron, corresponding to the five edges along the pentagonal cross-section at the equatorial position and those located at the axial direction along the twin boundaries, respectively. Accordingly, there are two sets of vertices with coordination numbers of four and five, respectively. When decahedral seeds are employed as seeds to mediate nanocrystal growth, two different modes will be naturally developed, one along the 5-fold rotational axis and the other along the pentagonal cross-section; both can be manipulated to induce asymmetrical growth and symmetry breaking.

4.2.2.1. Formation of Janus Pentagonal Rods. Penta-twinned rods, also known as wires when the aspect ratio is relatively high, can be considered decahedra with the five equatorial edges vertically expanded to create the {100} side faces. In fact, they are usually synthesized through selective overgrowth along the <110> direction of decahedral seeds. It is worth pointing out that, while counterintuitive, a pentagonal rod and a decahedron display the same D_{5h} symmetry when the elemental composition is not taken into consideration. In order to observe symmetry breaking, one needs to ensure that (i) at least two metals are involved in the synthesis and (ii) the growth only occurs on one side of the pentagonal seed. The asymmetric distribution of the two metals leads to the formation of a bimetallic Janus nanorod. So far, examples of Au−Ag and Pd−Ag Janus nanorods have been reported.[253,316] In the former case, Ag(I) precursor was reduced by DEG in the presence of Au decahedral seeds, together with additives such as ammonia and poly(diallyldimethylammonium chloride) (PDDA) (Figure 35A).[253] It was argued that ammonia helped solubilize AgCl in the reaction solution by forming $Ag(NH_3)_2^+$ and facilitated the redox reaction by increasing the pH of the reaction solution. At a low concentration of ammonia, the slow reduction of Ag(I) precursor resulted in a limited supply of Ag atoms for growth along one of the axial directions. Such a growth pattern resulted in the formation of Ag−Au Janus nanorods (Figure 35B−D). As more ammonia was introduced into the growth solution, the reduction was accelerated due to the increase in pH and growth started to occur on both ends, giving symmetrical Ag−Au−Ag segmented nanorods as the final products. Meanwhile, the faster reduction of Ag(I) precursor increased the length from 64 to 87 nm as the amount of ammonia was increased from 15 to 45 μL. Such reduction-rate-dependent switch of growth pattern further emphasized the central role of kinetic control in dictating the outcome of a colloidal synthesis. Similarly, thinner Ag nanorods would be obtained when switching to 16 nm Pd decahedral seeds and PDDA as both Cl^- source and a capping agent for the Ag(100) surface (Figure 35E−G).[316]

4.2.2.2. Formation of Icosahedra. In section 4.1.1.2, we discussed the evolution of pseudospherical Au seeds into complex Au@Ag 20-fold twinned icosahedra in a stepwise manner, in which decahedron was observed as one of the intermediate states during the growth of Ag shell.[291] Presumably, if Au decahedra are directly used as seeds in the same synthesis, the overgrowth of Ag should follow the same

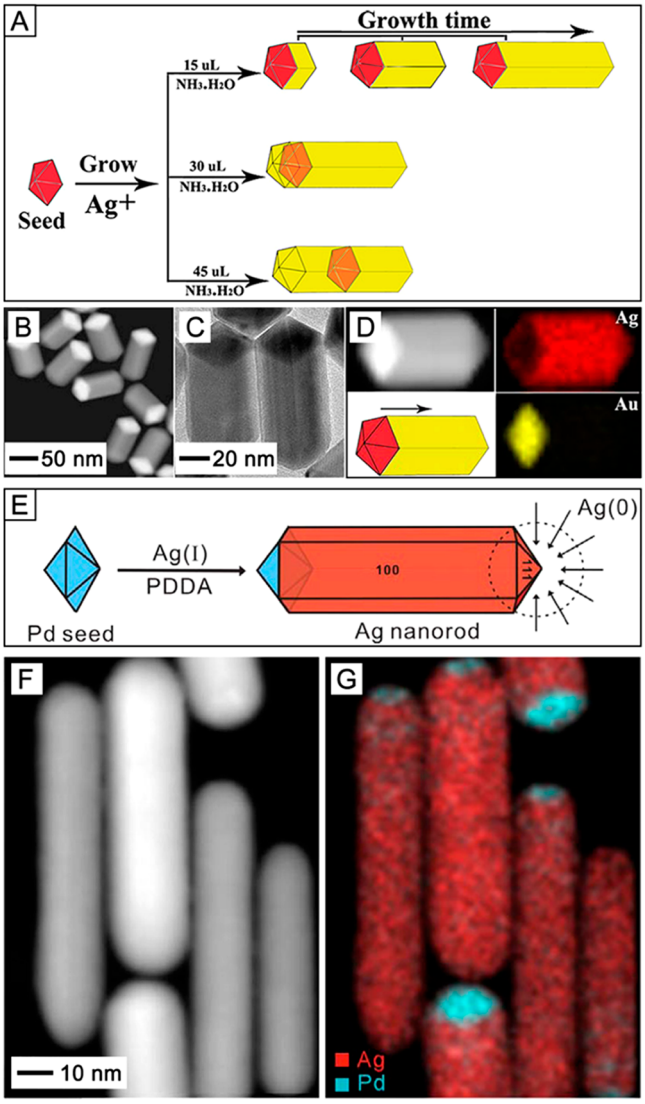

Figure 35. (A) Schematic showing the formation of different types of nanorods. (B−D) HAADF-STEM and TEM images of Au−Ag Janus nanorods, as well as the elemental mapping and schematic diagram. Au: red. Ag: yellow. The arrow in panel D indicates the growth direction. (E) Schematic showing the growth of a penta-twinned Ag nanorod from one side of a Pd decahedral seed. (F, G) HAADF-STEM image and EDS mapping of the Pd−Ag nanorods. (A−D) Adapted with permission from ref 253. Copyright 2012 American Chemical Society. (E−G) Adapted with permission from ref 316. Copyright 2015 American Chemical Society.

pattern and evolve into icosahedra. Indeed, Au−Ag heterometallic icosahedra have been obtained by slowly reducing Ag(I) with citrate ions in the presence of Au decahedral seeds and at a low concentration of OH^- (Figure 36).[288] In the initial stage, Ag was deposited symmetrically over the entire surface of the seed to form a core−shell decahedron. Once a twin plane was developed on one of the {111} faces of the decahedron, the formation of an icosahedron on the same side of the decahedron was initiated. The subsequent series of multiple twinning and growth events led to the outward expansion of more and more tetragonal subunits, gradually evolving into a decahedron-shaped indentation when 10 subunits were formed. Finally, filling of the indentation via Ag deposition completed the icosahedron morphology.

https://doi.org/10.1021/acs.chemrev.2c00468
Chem. Rev. 2023, 123, 3693−3760

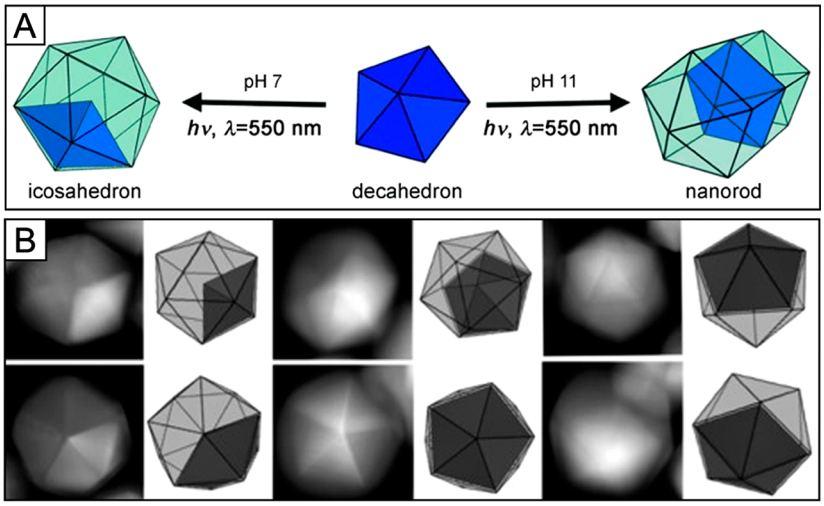

Figure 36. (A) Schematic showing the formation of penta-twinned nanorods through the photodeposition of Ag on plasmonic Au decahedral seeds. (B) HAADF-STEM images of individual heterometallic icosahedra in different orientations, next to their corresponding 3-D model in the identical orientation. Au: Dark gray. Ag: light gray. Reproduced with permission from ref 288. Copyright 2011 Wiley-VCH.

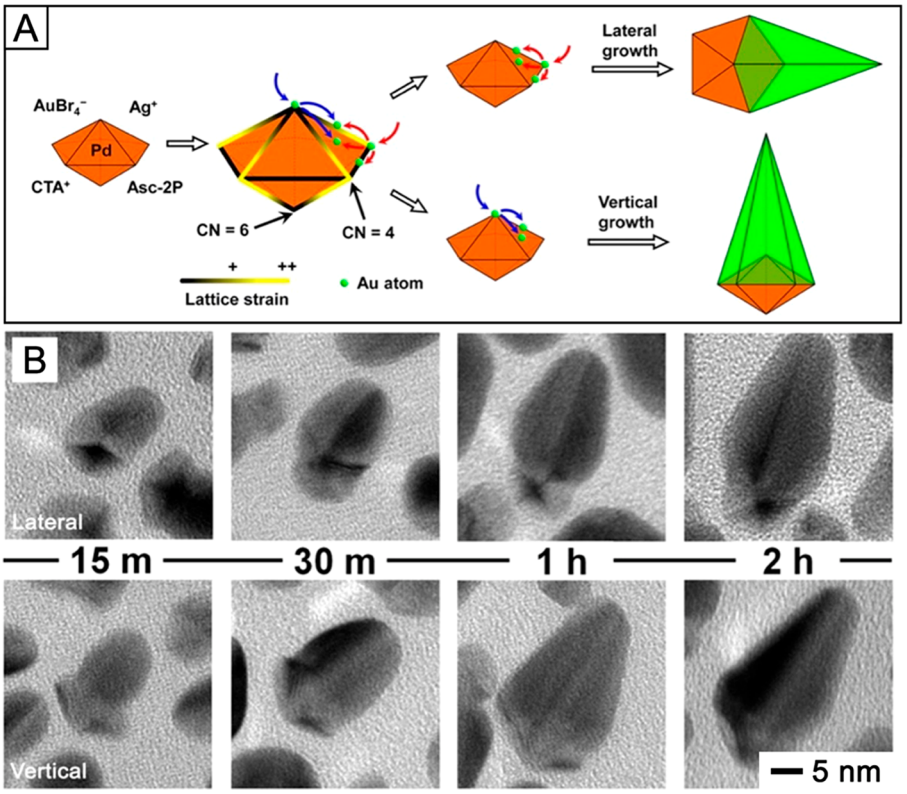

Figure 37. (A) Schematic showing the lateral and vertical modes involved in the growth of Au on Pd decahedral seeds. The site-selected and asymmetrical growth results in the formation of nanopyramids with a sharpened tip. (B) Typical morphologies of the Pd−Au nanopyramids obtained through lateral and vertical growth for different periods of time. Reproduced with permission from ref 317. Copyright 2021 American Chemical Society.

Interestingly, when NaOH was added into the solution to increase the pH from 7 to 11, a higher reduction rate would favor the heteroepitaxial growth on both ends of the decahedral seeds to form segmented nanorods. It should be pointed out that, although an icosahedron has a higher order of symmetry than a decahedron, which means an icosahedron should be considered a more symmetric shape, the evolution pathway from decahedral to icosahedral nanocrystals involves a series of observable intermediates that are highly asymmetrical. As such, this process should also be considered to involve symmetry breaking.

4.2.2.3. Formation of Asymmetrical Pyramids. Although longitudinal growth along the 5-fold axis is the most common pattern of site-selected growth for decahedral seeds, asymmetrical deposition has also been reported. For example, when $HAuCl_4$ was reduced by a weak reducing agent, L-ascorbic acid 2-phosphate trisodium salt (Asc-2P), in an aqueous solution containing Pd decahedral seeds, CTAB, and $AgNO_3$ held at 37

https://doi.org/10.1021/acs.chemrev.2c00468
Chem. Rev. 2023, 123, 3693−3760

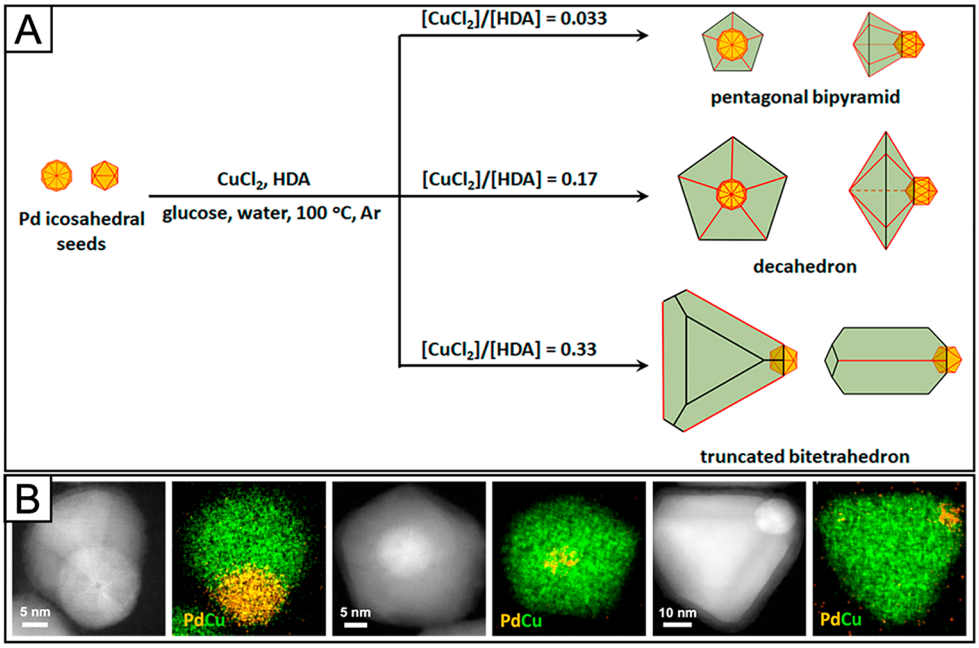

Figure 38. (A) Summary of the experimental conditions corresponding to the formation of Pd−Cu Janus nanocrystals with three distinctive shapes for the Cu component: pentagonal bipyramid, decahedron, and truncated bitetrahedron. Yellow: Pd. Green: Cu. The red lines indicate the twin boundaries on the nanocrystal. (B) HAADF-STEM images and the corresponding EDS mapping of the pentagonal bipyramids, decahedra and truncated bitetrahedra. Reproduced with permission from ref 318. Copyright 2021 American Chemical Society.

°C, the site-selected nucleation and growth of Au would lead to the formation of a pyramid at either longitudinal or lateral position relative to the Pd decahedron (Figure 37).[317] Specifically, the deposition was initiated from one of the vertices due to their higher energies caused by small coordination numbers and large lattice strains. From one of the five edge vertices, the surface reduction and deposition of Au onto the same site led to the formation of a pyramid with its rotational axis perpendicular to that of the decahedron. In comparison, when the growth site was switched to one of the two axial vertices, the growth became longitudinal, and the as-formed pyramid and the original decahedral seed were coaxial. It is worth noting that the formation of asymmetrical pyramids with well-defined features (e.g., smooth edges and sharp corners) should be attributed to the complex roles played by Ag^+ from $AgNO_3$. While the exact mechanism for the asymmetrical growth of Au on Pd decahedra is yet to be elucidated, the general requirements for a successful synthesis include the facet-selective capping effect of the $Ag−Br^−$ complex, the soft templating effect through shape conversion of CTAB micelles, and the UPD of Ag layers on certain facets. At a low concentration of Ag^+, the dominant morphology of the bimetallic nanocrystals would become nearly spherical.

4.2.3. Multiply-Twinned Icosahedral Seeds. A regular icosahedron is comprised of 20 tetrahedral subunits and 30 twin planes. It is one of the five Platonic solids and belongs to the I_h symmetry group with the highest symmetry order of 120. Compared to decahedral nanocrystals, icosahedral nanocrystals have more twin defects and strain in the bulk, making these particles increasingly unstable when their size is enlarged during seed-mediated growth. Moreover, there is only one type of edge and vertex on an icosahedron, limiting the variation in terms of asymmetrical growth pattern. However, owing to an improved understanding of the roles played by each factor in inducing asymmetrical growth, several recent reports have demonstrated the synthesis of complex nanostructures from icosahedral seeds.

4.2.3.1. Formation of Bipyramids, Decahedra, and Truncated Bitetrahedra. Covered by 12 equiv penta-twinned vertices, icosahedral nanocrystals hold promise in templating the growth of penta-twinned structures. On the other hand, it is a challenge to limit the deposition and growth to only one of the vertices instead of multiple vertices or even edges. Using the Pd−Cu Janus system as an example, it was recently demonstrated that a set of heteronanostructures could be obtained through kinetically controlled, seed-mediated growth (Figure 38).[318] Using a fixed amount of 12 nm Pd icosahedra as the seeds, glucose as a reducing agent, and HDA as a coordination ligand and colloidal stabilizer, the reduction rate of $CuCl_2$ precursor was controlled by varying its concentration in the growth solution. Specifically, at a relatively slow reduction rate, the Cu atoms nucleated from only one of the vertices on the seed for the formation of an elongated, pentagonal bipyramid. As the concentration of Cu(II) precursor was increased by five times and the reduction rate was increased, the as-formed Cu bipyramid became more symmetrical against the basal plane, evolving into a decahedron. If the reduction rate was further increased, however, the growth started to take a different pathway. With an abundant supply of Cu atoms to the icosahedral surface, nucleation could happen not only on the most energetic vertices but also on the edges. In the initial stage of growth, the deposition of Cu on one of the edges characterized by a single twin plane led to the formation of a singly-twinned rod-like shape with the icosahedral seed attached to one end of the rod. It is still unclear how such complex products with a completely different twin structure and symmetry could be obtained by solely changing the concentration of one reactant. This case study suggests the potential role of multiply-twinned nanocrystals in enriching the diversity and complexity of metal

https://doi.org/10.1021/acs.chemrev.2c00468
Chem. Rev. 2023, 123, 3693−3760

nanostructures. Meanwhile, it demonstrates the key role of reaction kinetic in manipulating the symmetry breaking process.

4.2.3.2. Formation of Pentagonal Pins. For each one of the 12 vertices on an icosahedron, there exists a set of five pentagonal twinned facets that is essentially the same as in a decahedron. It was argued that 1-D expansion of this set of facets along the <110> direction could also lead to the formation of penta-twinned structures, as discussed in section 4.2.2.1. Indeed, using a light-assisted synthetic protocol reported for the growth of penta-twinned rods from Ag decahedral seeds, Ag nanocrystals with an icosahedral structure were reported to grow into similar rod-like morphology.[287] With the icosahedral seed situated at one end of the rod, the overall shape displayed similarity to a sewing pin. Although the formation mechanism was not discussed in the report, it seems to be closely related to what was proposed for decahedra-seeded nanorod synthesis.[253,316]

5. PROPERTIES AND APPLICATIONS

Colloidal metal nanocrystals have found widespread use in an array of applications related to plasmonics, electronics, optoelectronics, magnetism, (electro)catalysis, and biomedicine. The shape of a nanocrystal has profound impacts on its properties and thus its performance in all these applications. Asymmetrical growth or symmetry breaking in a well-controlled manner allows for the creation of novel physical, chemical, and biological effects that would be difficult to achieve by simply adjusting the size or shape of symmetry-preserved systems. This section focuses on the unique properties and applications that benefit from the diversity and complexity introduced by symmetry breaking.

5.1. Optical Properties and Applications

The optical properties of noble-metal nanocrystals, such as LSPR and waveguiding, among others, have been extensively investigated. LSPR arises from the interaction between the electric field of light with the conduction electrons in a metal nanocrystal to induce the excitation of a collective oscillation of the electrons.[16,319] At specific wavelengths, the light can be strongly scattered or absorbed by metal nanocrystals as a result of LSPR. The spectral position and profile of LSPR depend on a number of parameters, including size, shape/morphology, and elemental composition/distribution of the nanocrystal.[16,320] Notably, the number of LSPR peaks in noble-metal nanocrystals correlates directly to the number of directions in which the electrons can be polarized. In other words, nanocrystals with lower symmetry tend to feature more plasmon modes than their more symmetrical counterparts due to the larger number of possible ways to polarize the electrons.[321] Thus, symmetry breaking phenomenon offers an effective means to maneuver the LSPR properties of nanocrystals.

A highly symmetrical, spherical nanocrystal made of plasmonic metals typically displays only one resonance mode since its optical excitation is equivalent along all directions. In the case of nanorods or nanowires lower in symmetry, two LSPR modes can be observed: the longitudinal mode resonant at longer wavelengths (where free electrons are polarized along the long axis) and the transverse mode resonant at shorter wavelengths (where electrons are polarized along the short axis).[321] For instance, dark-field scattering from a single Au nanorod led to the display of different colors when excited along either the transverse or longitudinal axis, while spherical nanoparticles did not show this effect.[322−324] In addition, the longitudinal mode can be fine-tuned to the desired wavelengths by adjusting the aspect ratio of the nanorods. In one report, the longitudinal LSPR of Au nanorods was shifted from 600 to >1300 nm by extending the nanorods only along the axial direction.[325] Such control over the aspect ratio would shift the wavelength of plasmonic resonators to the near-infrared region. Moreover, symmetry-broken nanocrystals of different sizes can be employed as plasmonic anticounterfeit tags. Taking Au nanorods as an example, when randomly deposited on a variety of surfaces, they could serve as unique tags with high security.[326] Considering the difficulty in manipulating the location and orientation of each Au nanorod individually, it is almost impossible to replicate the tags comprised of Au nanorods, creating a barrier to counterfeiting. Since Au nanorods could provide a wide range of color responses on account of different aspect ratios and light polarization sensitivity, the security tags were endowed with high encoding capability, which allowed for more information to be integrated into the tag in the form of optical response combinations. Such a feature was essential to the miniaturization and concealment of the tags.[326]

Besides geometric aspect, the symmetry associated with elemental distribution can affect the optical properties of nanocrystals. Since the dielectric function of each metal component in bimetallic nanocrystals contributes differently to the optical properties,[16] any variation to the ratio and/or the location of each plasmonic component would lead to LSPR shift. Taking the core−shell structure as an example, its optical response is sensitive to the location of the core metal. As shown in Figure 39A−C, Au@Ag nanorods with off-centered metal seeds displayed blue-shifted LSPR compared to the concentric Au@Ag nanorods.[327] In another example, the asymmetrical distribution of elements and the presence of heterogeneous phases gave heterodimers optical properties distinct from their monometallic counterparts.[86] The characteristic light absorption of heterodimers could be attributed to the plasmonic coupling at the interface of the two metals. The effect of heterogeneous interfaces was well demonstrated in the UV−vis extinction spectra of a series of Au−Ag Janus nanocrystals with different contact areas of 48 and 29 nm in diameter (Figure 39D).[272] While the extinction peaks around 420 and 531 nm could be assigned to the Ag and Au components, respectively, the other two peaks at 592 and 698 nm arose from the electromagnetic coupling between Au and Ag (Figure 39E). Both computational and experimental results demonstrated that the electromagnetic coupling and thus optical properties of Au−Ag Janus nanocrystals indeed depended on their geometric configuration or the spatial distribution of the individual element.[272] The unique optical properties of these symmetry-broken nanocrystals, such as higher refractive index sensitivity and tunable plasmon band, offer them great promise in applications as chemical or biological sensors for analytes such as heavy metal ions, DNA, and antibodies.[322,328−331]

Through the excitation of surface plasmons, the free-space light can be coupled into metal nanostructures and transformed into propagating plasmon modes confined to the metal surface. To this end, 1-D nanostructures (i.e., nanorods and nanowires) with low symmetry are well-suited for use as waveguides to direct the propagating plasmon modes.[332] The symmetry-broken morphology of metal nanowires and their

https://doi.org/10.1021/acs.chemrev.2c00468
Chem. Rev. 2023, 123, 3693−3760

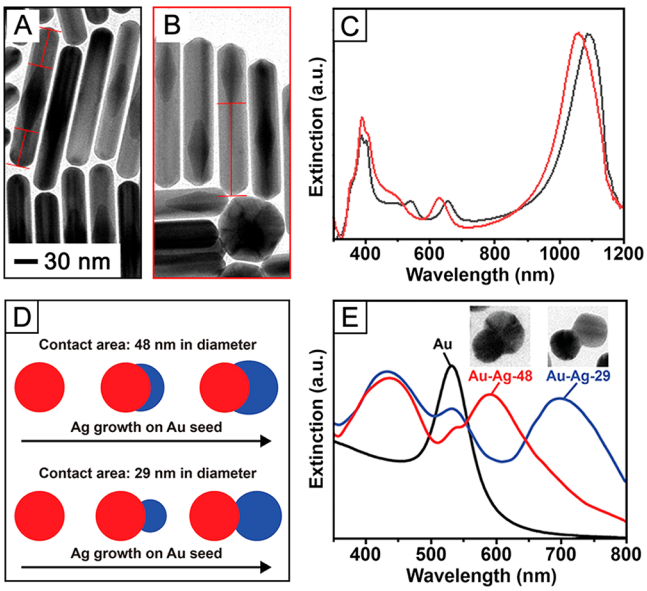

Figure 39. (A, B) TEM images of (A) symmetrical and (B) asymmetrical Au@Ag nanorods grown from Au bipyramidal seeds in the absence and presence of dimethyl sulfoxide, respectively. (C) UV−vis extinction spectra of symmetrical (black) and asymmetrical (red) Au@Ag nanorods. (D) Schematic showing the asymmetrical growth of Ag from Au nanoparticles to generate Au−Ag Janus nanoparticles with different contact areas. (E) UV−vis extinction spectra of the Au nanocrystals and the Au−Ag Janus nanoparticles with contact areas of 48 and 29 nm in diameter, respectively. (A−C) Reproduced with permission from ref 327. Copyright 2021 American Chemical Society. (D−E) Reproduced with permission from ref American Chemical Society. (D−E) Reproduced with permission from ref American Chemical Society. (D−E) Reproduced with permission from ref 272. Copyright 2019 American Chemical Society.

atomically smooth side faces allow for propagation of light over a long distance in one dimension with low scattering loss, while their small diameters facilitate the miniaturization of on-chip optical components.[71] Taking Ag nanowires as a typical example, the plasmon could propagate over a distance of more than 10 μm at a near-infrared wavelength (Figure 40A).[333] Since the momentum of free-space photons matches that of propagating plasmons at the tapered tips, the plasmon mode can be excited by incident radiation at one end, propagate in the axial direction, and finally re-emit as photons at the other end.[333−336] For effective and efficient light coupling to nanostructures, the plasmonic and photonic waveguides can be integrated to achieve nanoscale confinement. For example, the incident light could be guided and distributed into multiple Ag nanowires simultaneously with the help of a polymeric waveguide.[334] As shown in the dark-field microscopy images, Ag nanowires placed perpendicular to the polymeric waveguide were illuminated due to the plasmonic excitation, and the light was successfully guided from the center of the polymeric waveguide to the longitudinal direction of Ag nanowires (Figure 40B). This capability allowed the simultaneous supply of light to several nanoscale photonic devices in a highly integrated circuit. Similarly, Au nanorods embedded in polymer fibers have also been reported as nanoscale waveguides.[337] As shown in Figure 40C, Au nanorods were aligned in parallel along the axis of the fiber, and an intense polarization-dependent light scattering was observed. When the incident light matched the longitudinal resonance wavelength of the Au nanorods, the photon-to-plasmon conversion efficiency in the waveguiding fibers could reach 70%. Such highly efficient conversion could facilitate light-matter interactions and reduce power consumption. Since the LSPR of metal nanocrystals was sensitive to the surrounding environment, the embedded Au nanorods could also serve as optical sensors by displaying different responses to environ-

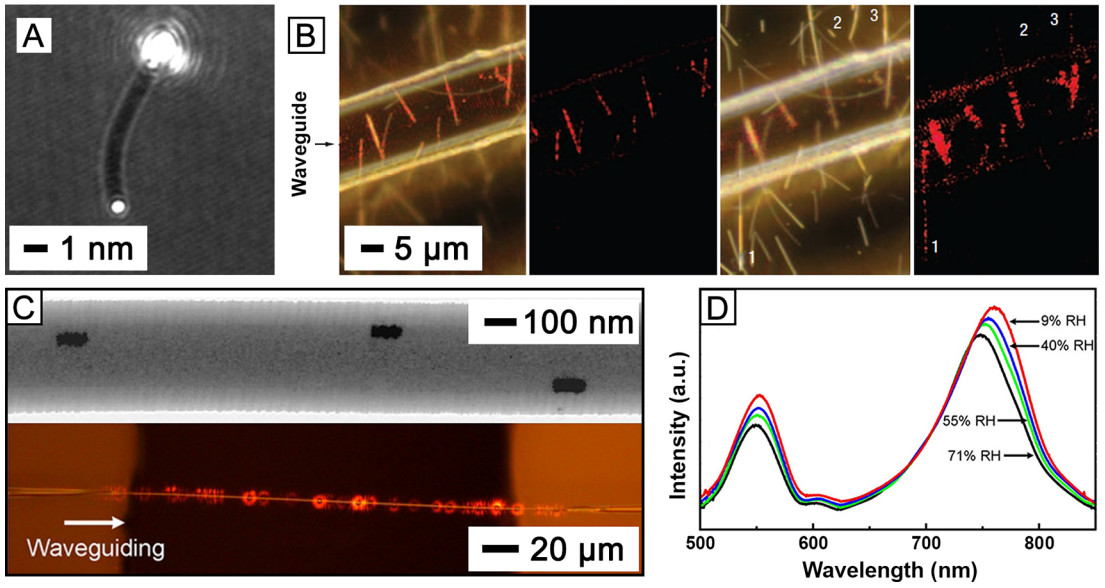

Figure 40. (A) Light waveguiding using silver nanowire with excitation at the upper end. (B) Optical microscopy images showing the coupling of light from a polymeric waveguide to multiple Ag nanowires. (C) TEM and optical micrograph of Au nanorods embedded in polymer nanofibers for waveguiding. The white arrow indicates the direction of light propagation. (D) Scattering spectra of Au nanorods embedded in nanofibers when exposed to ambient air with varying room humidity. (A) Reproduced with permission from ref 333. Copyright 2006 American Chemical Society. (B) Reproduced with permission from ref 334. Copyright 2008 Springer Nature. (C−D) Reproduced with permission from ref 337. Copyright 2012 American Chemical Society.

https://doi.org/10.1021/acs.chemrev.2c00468
Chem. Rev. 2023, 123, 3693−3760

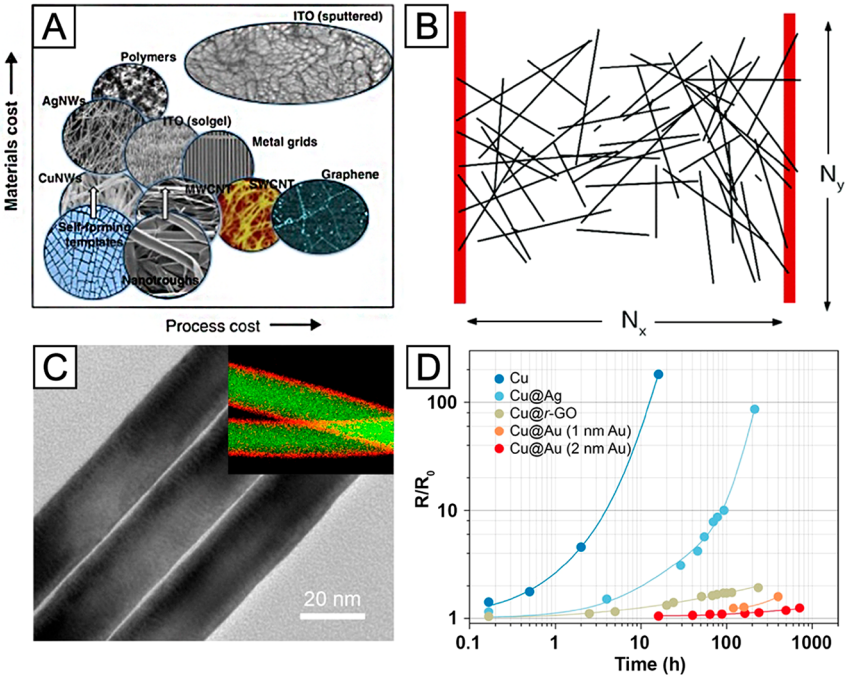

Figure 41. (A) Comparison plot of materials cost vs process cost for different transparent conductive materials. (B) Schematic illustration of the metal nanowire network between two electrodes. (C) TEM image of Cu@Au core−shell nanowires. The inset shows an EDS elemental mapping of Cu@Au core−shell nanowires, where red and green represent Au and Cu, respectively. (D) Stability test of conducting films made from bare Cu, Cu@Ag, Cu@reduced graphene oxide (r-GO), Cu@Au (1 nm Au), and Cu@Au (2 nm Au) in harsh environment (temperature: 80 °C, humidity: 80 ± 5%). (A) Reproduced with permission from ref 341. Copyright 2015 Elsevier. (B) Reproduced with permission from ref 342. Copyright 2016 Royal Society of Chemistry. (C−D) Reproduced with permission from ref 357. Copyright 2017 American Chemical Society.

mental changes. As room humidity was increased from 9 to 71%, the refractive index surrounding the embedded Au nanorods decreased, leading to the monotonic blue-shift of the LSPR peaks of Au nanorods (Figure 40D).[337] Moreover, the scattering intensity of Au nanorods was found to decrease with the increase in room humidity, enabling intensity-dependent humidity sensing. Compared to bare Au nanocrystals, the embedded Au nanorods exhibited 1 order of magnitude higher humidity sensitivity. As shown in Figure 40C, the LSPR response from each embedded Au nanorod could amplify in the output signal, leading to better overall sensitivity and resolution. Taken together, great versatility in developing compact plasmonic and photonic devices with miniaturized dimensions and high conversion efficiency can be achieved by integrating symmetry-broken nanocrystals with diverse photonic waveguides, presenting opportunities for shortening response time and lowering the energy consumption of the devices.

5.2. Electrical Properties and Applications

Materials with high electrical conductivity and optical transparency are crucial for modern optoelectronic devices, such as light-emitting diodes, solar cells, touchscreen panels, and transparent thin-film heaters.[338−340] In general, conductive materials are not transparent, while transparent materials are not conductive.[89] For this reason, ITO, a transparent semiconductor with a wide band gap, has dominated the field of transparent electrodes for many decades. However, the high cost of ITO and its poor stability to mechanical stress hinders its application, especially for those requiring flexibility or stretchability, such as wearable devices and electronic skins.[89]

High-aspect-ratio metal nanostructures such as nanowires have been widely explored as an alternative to ITO due to their excellent electrical conductivity and stretching capability. Compared to ITO, metal nanowires can be fabricated at a much faster rate and without the need for an expensive sputtering process. The cost comparison in Figure 41A highlights the significantly lower processing cost of metal nanowires than ITO.[341] More importantly, the unique morphology of metal nanowires allows them to construct interconnected networks at very low volume fractions. Since the conductive path can be easily formed among sparsely distributed high-aspect-ratio nanowires, the interconnected nanowire network would have high porosity and thus enhanced optical transparency to achieve high transmittance at low sheet resistances.[70] Such a combination of optical transparency and electrical conductivity in 2-D networks of nanowires enables them to be used as the key components in optoelectric devices.

In a typical nanowire network, a large number of metal nanowires with high aspect ratios are deposited on an insulating substrate and randomly dispersed between two metal electrodes (Figure 41B).[342] The resistance of the nanowire networks depends on various parameters, such as nanowire diameter, length, and distribution density, and all of them have been studied to guide the fabrication of highly conductive films. As the nanowire diameter or density was increased, the sheet resistance of the interconnected network decreased, thus enhancing their electrical performance at the expense of compromising optical performance. When switching to longer nanowires, the network's resistance was lowered due to the reduction of internanowire junctions while the transparency increased due to the decrease in nanowire density.[343] In practice, the electrical conductivity, optical

https://doi.org/10.1021/acs.chemrev.2c00468
Chem. Rev. 2023, 123, 3693−3760

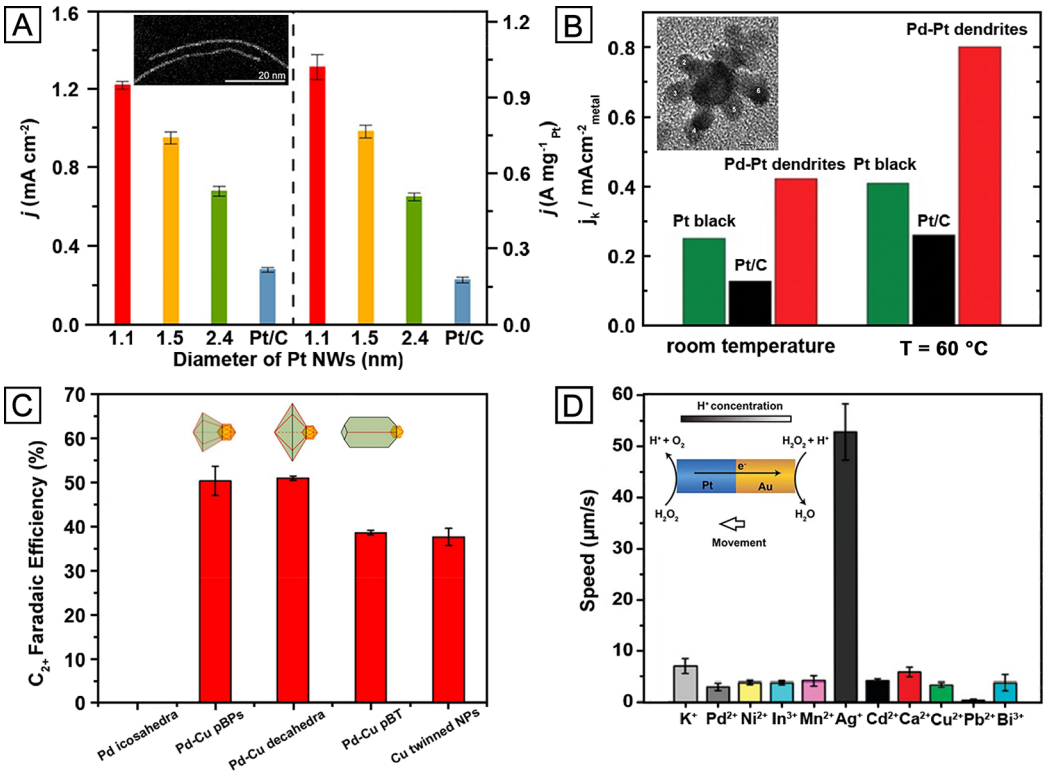

Figure 42. (A) Comparison of ORR performance for Pt nanowires with different diameters at 0.9 V. The left and right columns represent specific activity and mass activity, respectively. The inset is an HAADF-STEM image of Pt nanowires with a diameter of 1.1 nm. (B) Comparison of ORR performance for Pd−Pt nanodendrites, Pt/C catalyst (E-TEK) (20% by weight of 3.2 nm Pt nanoparticles on carbon support), and Pt black (Aldrich) (fuel cell grade) at 0.9 V. The inset is an HRTEM image of a single Pd−Pt nanodendrite. (C) Faradaic efficiency of electrochemical reduction of CO_2 to C_{2+} products in the presence of catalysts based on Pd−Cu nanoparticles with different shapes. (D) Comparison of the average speed of Au−Pt Janus nanorods as catalytic motors in a 5% H_2O_2 solution containing different metal cations. The inset is a schematic illustration of an Au−Pt catalytic nanomotor. The arrow indicates the direction of the nanomotor motion. (A) Reproduced with permission from ref 364. Copyright 2021 American Chemical Society. (B) Reproduced with permission from ref 367. Copyright 2009 American Association for the Advancement of Science. (C) Reproduced with permission from ref 318. Copyright 2021 American Chemical Society. (D) Reproduced with permission from ref 377. Copyright 2009 American Chemical Society. Inset in (D) Reproduced with permission from ref 88. Copyright 2013 American Chemical Society.

transmittance, material cost, and fabrication difficulties of metal nanowire networks all need to be optimized in order to achieve the desired performance in an effective and efficient way.

The optoelectronic properties of metal nanowires have been optimized while exploring their applications in the fabrication of transparent, conductive films for use in touchscreens,[344,345] solar cells,[346,347] organic light-emitting diodes,[348] and photovoltaics.[349] Among various materials, Ag nanowires have garnered the greatest attention as a candidate for transparent electrodes. They can be fabricated using low-cost solution-phase methods and coated onto various substrates to form interconnected networks. For instance, highly flexible networks of Ag nanowires with excellent transmittance (diffusive transmittance ≈ 95%) and high conductivity (sheet resistance ≈ 10 Ω sq^{-1}) have been employed as transparent electrodes in highly efficient and bendable electronic devices, such as organic solar cells.[350] Since the large-scale application of Ag nanowires for optoelectronic devices is potentially hindered by their high material cost, Cu with comparable conductivity to Ag (only 6% less conductive) but at a more than 100-times lower price may offer more benefits to various commercial applications.[90,351,352] Even though ultrathin Cu nanowires were found to exhibit an outstanding sheet resistance of 35 Ω sq^{-1} at 90% transparency,[353] they tend to suffer from oxidation in ambient conditions due to reactions with oxygen and sulfur in the air.[354] To this end, protecting Cu nanowires against such corrosion and avoiding the steep decline in their optoelectronic performance remain challenging. One possible solution involves coating Cu nanowires with a more inert metal to protect them from oxidation, while good electrical contact between the core and the shell still ensures excellent electric conductivity of the nanowires.[355] To this end, Cu@Ag nanowires have been demonstrated with oxidation resistance and optoelectrical properties similar to those of pure Ag nanowires.[356] The stability of Cu@Ag nanowires could be enhanced by increasing the shell thickness, but their optoelectronic properties would degrade accordingly. To find use as a transparent conductor under harsh conditions without compromising their electrical and optical properties, an inert metal shell that is more stable and thinner than Ag is needed. A recent study has demonstrated an epitaxial deposition method to coat the Cu nanowire with an ultrathin (a few atomic layers) and almost defect-free Au shell.[357] As shown in Figure 41C, the as-synthesized Cu@Au nanowires were free of surface pores or voids. Compared to unprotected Cu nanowires, the Cu@Au nanowires were able to retain the superior optoelectrical performance of the original nanowires under harsh conditions of 80% relative humidity at 80 °C for at least 700 h (Figure 41D). Taken together, metal nanowires with low

https://doi.org/10.1021/acs.chemrev.2c00468
Chem. Rev. 2023, 123, 3693−3760

symmetry can form highly conductive and transparent interconnected networks at low density. With appropriate protection strategies, the stability of the nanowire network can be significantly improved, moving them one step closer to industrial production and commercial application.

5.3. Catalytic Properties and Applications

Another field where symmetry-broken nanocrystals have found application is (electro)catalysis. Over the past few decades, numerous strategies have been developed to enhance the performance of a catalyst, including increasing the number of active sites by reducing the particle size and improving their area-specific activity by controlling the shape or elemental composition.[33] Increasing the anisotropy of nanocrystals through symmetry breaking can facilitate the selective exposure of specific facets or introduce surface strain, which in turn changes the electronic structure of active sites and affects their interactions with reaction intermediates, ultimately enhancing both the catalytic activity and selectivity.[18]

With the extremely small size and diversified morphology, metal nanoparticles supported on carbon are widely used as efficient electrocatalysts. The major issue of these catalysts with broad size and shape distribution is the degradation of catalytic performance as a result of Ostwald ripening, particle migration, and coalescence.[358] The gradual decrease in catalytic activity and durability of nanoparticles induced by these deactivation mechanisms can be mitigated by switching to symmetry-broken nanocrystals owing to their unique structural characteristics, including large specific surface areas, high stability, facile electron transfer, and/or preferential exposure of high-activity facets.[359−361] For instance, Pt nanotubes with high mass transport and atom utilization efficiency due to their 1-D morphology exhibited much higher activity, stability, and electrochemical surface area toward oxygen reduction reaction (ORR) than a commercial Pt/C catalyst.[362] The higher durability of Pt nanotubes could be attributed to the larger area in contact with the support, which could retard their movement and detachment under the harsh electrochemical conditions. In addition to enhanced catalytic performance, an anomalous size effect on catalytic activity toward ORR has also been observed in the symmetry-broken system. In general, as Pt nanoparticles decrease in size, the *d*-band center will shift toward the Fermi level, resulting in a stronger oxygen adsorption that suppresses ORR activity.[363] This effect would limit the effectiveness of the size reduction strategy in increasing the atom utilization efficiency. However, this limitation could be transcended by utilizing Pt nanowires. As the diameter of Pt nanowires was reduced from 2.4 to 1.1 nm, their specific activity toward ORR was boosted to 4.6 times that of commercial Pt/C catalyst (Figure 42A).[364] It was proposed that decreasing the diameter of nanowires would simultaneously increase the compressive surface strain and expose more low-coordinated sites.[364−366] The increased compressive surface strain would lead to a downward shift in the *d*-band center, weakening the absorption of oxygenated species while suppressing Pt dissolution. As a result, it would augment the catalytic activity and durability, in direct contrast to the increased exposure of low-coordinated sites. Since Pt nanowires had a much smaller proportion of low-coordinated sites compared to their highly symmetrical counterparts, the strain effect could outweigh the effect of low-coordinated sites on the catalytic activity of nanowires, unveiling the underlying reason for the anomalous size-dependent effect.

Beyond the monometallic systems, the improvement in catalytic performance benefiting from symmetry breaking can also be achieved in bi- or multimetallic nanocrystals. For example, it has been reported that Pd−Pt bimetallic nanodendrites exhibited a specific activity 3.1 times greater than that of a commercial Pt/C catalyst toward ORR (Figure 42B).[367] While the Pt branches were solely involved in the catalytic reaction, the truncated octahedral Pd seeds assisted the spatially separated Pt branches in increasing the surface area and stability of the catalyst. Since the poisoning effect and the adsorption of oxygen on Pt surface are facet-sensitive, the electrocatalytic kinetics of ORR heavily depends on the morphology of Pt catalysts.[368,369] Compared to truncated octahedral nanocrystals enclosed by a mix of {100} and {111} facets, the Pt branches preferentially exposed {111} facets, in addition to some {110} and high-index {311} facets with higher intrinsic activity toward ORR.[367] Thus, the superb activity of Pd−Pt bimetallic nanodendrites could be attributed to the asymmetrical morphology and exposure of particularly active facets on the surface.

Besides the geometrical configuration, the asymmetrical elemental distribution associated with symmetry breaking in bi- and multimetallic nanocrystals also greatly impacts their catalytic performance. Due to the electronic and chemical interactions between different metals, bi- or multimetallic nanocrystals can integrate the properties of each component to display superior catalytic activity. Moreover, the exposure of multiple phases on the surfaces of these symmetry-broken nanocrystals and the presence of an interface between different metal components can potentially provide unique interfacial reactivity and spillover effects, which may significantly change the catalytic activity and selectivity, especially in tandem catalysis.[189] For instance, to enhance the selective reduction of CO_2 to C_{2+} species by Cu-based catalysts, another metal (e.g., Pd, Ag, or Au) capable of reducing CO_2 to CO was incorporated into the Cu nanostructure to form bimetallic Janus nanocrystals.[318,370,371] The side-by-side elemental distribution in such symmetry-broken nanocrystals enabled the as-formed CO intermediate to migrate from the other metal to the Cu surface for subsequent coupling to generate C_{2+} products. A recent study has evaluated the catalytic capability of Pd−Cu nanocrystals with various shapes, including pentagonal bipyramids, decahedra, and truncated bitetrahedra.[318] Compared to twinned nanoparticles made of pure Cu, the reduction in symmetry from icosahedral seeds (I_h symmetry) to the resulting Pd−Cu pentagonal bipyramids and decahedra (approximately, C_{5v} symmetry) contributed to more efficient conversion of CO_2 to C_{2+} products (Figure 42C). The symmetry breaking in the formation of Pd−Cu Janus nanocrystals allowed for the simultaneous presence of Pd surface and twin boundaries of Cu in one particle, which could largely account for their superior performance in the electrochemical reduction of CO_2. Overall, nanocrystals with asymmetric elemental distribution can catalyze multistep, consecutive reactions that otherwise cannot be performed for the selective production of value-added products.

Owing to their unique elemental distribution, bimetallic nanocrystals with broken symmetry can simultaneously catalyze two or more reactions in different regions of the same particle. Such uneven occurrence of catalytic reactions can trigger changes in the surrounding ion concentration and electric field, thereby physically propelling the nanocrystals.[88,372,373] Under this circumstance, heterodimers integrating

https://doi.org/10.1021/acs.chemrev.2c00468
Chem. Rev. 2023, 123, 3693−3760

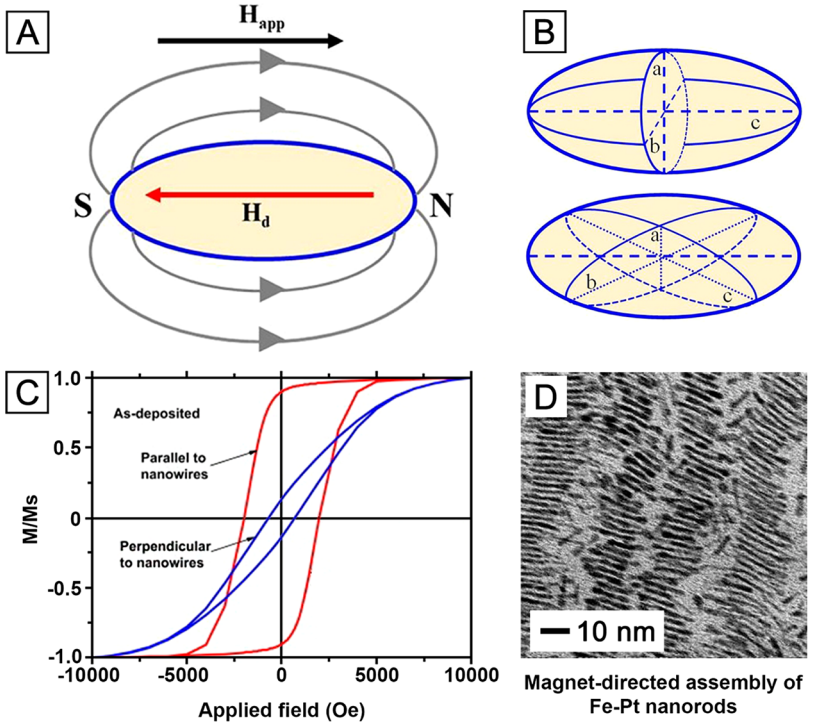

Figure 43. (A) Schematic illustration showing the demagnetization field lines of a magnetized elliptical particle. (B) Schematic illustration of nonspherical particles: a prolate spheroid (a = b < c) and an oblate spheroid (a < b = c). (C) Magnetic hysteresis loops of CuCo nanowire arrays with the applied magnetic field parallel and perpendicular to the nanowires, respectively. (D) Directed assembly of FePt nanorods guided by an external magnetic field. (A, B) Reproduced with permission from ref 380. Copyright 2022 American Chemical Society. (C) Reproduced with permission from ref 385. Copyright 2011 Elsevier. (D) Reproduced with permission from ref 392. Copyright 2007 American Chemical Society.

two distinct catalytic surfaces are ideal for use as nanomotors.[374,375] As shown in the inset of Figure 42D,[88] Pt−Au Janus nanorods could move directionally in an aqueous solution containing H_2O_2, where the nonuniformly distributed catalytic decomposition of H_2O_2 served as the driving force.[376] Since Pt and Au had different intrinsic catalytic activities, the oxidation and reduction of H_2O_2 occurred selectively on the Pt (anode) and Au (cathode) surfaces, respectively. During the catalytic process, the protons were generated at the Pt end and consumed at the Au end, leading to a graded distribution of protons along the nanorod. The resultant concentration gradient of protons would create a self-generated electric field around the nanorod, propelling it to move toward the Pt side.[88] The catalytic motors made of Pt−Au nanorods could be further employed as motion-based chemical sensors for the detection of a trace amount of Ag^+ ions.[377] In this case, Ag^+ ions were reduced and deposited on the surface of Pt−Au catalytic motors in the presence of H_2O_2. Interestingly, a significant acceleration in the speed of the nanomotors was observed in the presence of Ag^+ ions along with H_2O_2 (Figure 42D). This unusual increase in speed could be attributed to the deposition of Ag on Pt−Au nanorods, which might cause a greater potential difference between Pt and Au segments and more intense decomposition of H_2O_2, thereby accelerating the motion of the nanorods.[378]

5.4. Magnetic Properties and Applications

Magnetic nanocrystals have garnered significant interest due to their unique physicochemical properties for a wide variety of applications, such as data storage, drug release, and catalysis.[379] Besides the simple monometallic nanocrystals made of Fe, Ni, and Co, nanocrystals associated with ferromagnetism also encompass bi- and multimetallic systems, such as their alloys and intermetallic combinations (e.g., FePt, CoNi, and CuCo), metal oxides (e.g., Fe_3O_4, CoO, and NiO), and spinel-type ferromagnets (e.g., $MnFe_2O_4$ and $CoFe_2O_4$), as well as core−shell nanocrystals (e.g., $MnFe_2O_4$@$CoFe_2O_4$). In addition to size, the morphology, composition, and phase (crystal structure) of most magnetic nanocrystals can also provide orientation-dependent properties and thus affect their magnetization behaviors.[379] Generally, magnetocrystalline anisotropy is considered an intrinsic property of the material, while shape anisotropy is an extrinsic property that could be rationally tuned through shape-controlled synthesis.

In principle, the north (N) and south (S) poles at the two ends of a magnet not only create an external magnetic field (from N to S) but also generate a demagnetization field (H_d) inside the material in the opposite direction of the external magnetic field (Figure 43A).[380] The magnitude of H_d is linearly related to the magnetization (H_d=N_dM), where N_d represents the sum of the components of demagnetization factor N_a, N_b, and N_c along the a, b, and c axes, respectively. For a spherical nanoparticle, all components of the demagnetization factor are equal; therefore, the net contribution of shape anisotropy is zero. However, for nonspherical particles with low symmetry, a subtle change in aspect ratio can lead to a significant change to the demagnetization factor along different axes, and the demagnetizing field is no longer equal in all directions (Figure 43B).[380] In other words, the magnetic properties of nanocrystals are dependent on their symmetry. The difference in magnetic properties of nanospheres, nanocubes, nanorods, and nanostars was discovered to originate from the distinctive shape,[381] and such variation in magnetic properties would greatly impact their performance in

https://doi.org/10.1021/acs.chemrev.2c00468
Chem. Rev. 2023, 123, 3693−3760

magnetic resonance imaging. For instance, Fe_3O_4 nanorods would induce a stronger magnetic field perturbation over a larger volume compared to spherical counterparts.[382] Thus, Fe_3O_4 nanorods could potentially be used as efficient magnetic resonance imaging contrast agents due to their enhanced magnetic properties.

Other interesting magnetic properties arising from the symmetry-broken morphology of magnetic nanocrystals are high coercivity and magnetic anisotropy.[383,384] Taking symmetry-broken CuCo alloy nanowires as an example, the shape of their magnetic hysteresis loops and the magnitude of coercivity were strongly dependent on the direction of the applied magnetic field (Figure 43C).[385] When the applied magnetic field was parallel to the CuCo nanowire array, the loop was rectangular in shape, together with a coercivity of about 1976 Oe. In contrast, an approximately linear loop and a coercivity of only 691 Oe were observed when the magnetic field was applied perpendicular to the nanowire arrays. After annealing at 400 °C in vacuum, the coercivities of CuCo nanowires associated with the parallelly and perpendicularly applied magnetic fields were increased to 2245 and 758 Oe, respectively.[385] The remarkable improvement in coercivity after annealing could be attributed to the enhanced shape anisotropy in the local region, as well as the higher degree of crystallinity. A similar shape anisotropy, which has a profound impact on the coercivity and magnetic anisotropy, has also been reported for other metallic nanowires, including those based on Co,[386,387] Fe,[388] FePt,[389] CoPt,[390] and FePd.[391] These metal nanowires with high coercivity, high magnetization, and nanoscale sizes hold promise for application as high-density and low-noise magnetic recording media.

As mentioned above, many symmetry-broken nanocrystals have shown enhanced and/or anisotropic magnetic properties as a result of shape anisotropy. However, it remains challenging to establish uniform magnetic anisotropy among a population of symmetry-broken nanocrystals since they either have irregular, poorly defined shapes or suffer from aggregation. To solve this problem, an external magnetic field can be applied to guide the assembly of nanoparticles to form an ordered array, thus providing a unified anisotropic magnetic platform for magneto-electronic transmission and enhanced data storage, among others. For instance, when an external magnetic field was introduced during the formation of FePt nanorods, an ordered 2-D hexagonal array would be achieved (Figure 43D).[392] By adjusting the orientation and strength of the applied magnetic field, the assembled array of nanorods could be transformed from 1-D to 2-D and 3-D structures.

One of the most promising applications of magnetic nanocrystals is their use as efficient heaters to convert magnetic energy to thermal energy. When magnetic nanocrystals are in a magnetic field with constantly changing directions generated by an alternating current (AC), they have to continuously reverse their magnetization at the cost of magnetic energy loss, which is dissipated in the form of heat. Symmetry-broken magnetic nanostructures have been found to possess higher saturation magnetization and greater heating efficiency relative to their symmetrical counterparts due to the enhanced effective anisotropy.[393,394] The specific absorption rate (SAR) of iron oxide nanocrystals could be tuned by altering their symmetry. For instance, Fe_3O_4 nanorods exhibited superior inductive heating capability compared to nanospheres and nanocubes with similar volumes, especially in the high field region.[393] In the AC field of 800 Oe, the nanorods exhibited SAR values 6 times and 2.7 times higher than those of nanospheres and nanocubes, respectively. The symmetry and aspect ratio of magnetic nanocrystals played more critical roles than volume in tuning magnetic-induced heating efficiency. Increasing the aspect ratio from 6 to 11 could improve the SAR value by 1.5 times. Even higher heating efficiency could be achieved if high-aspect-ratio nanowires were employed due to the enhanced hysteresis loss corresponding to the high shape anisotropy.[395]

5.5. Biological Effects and Applications

Perhaps the most exciting frontier in metal nanocrystals research revolves around their potential applications in the biomedical field, especially for biosensing, bioimaging, cancer therapies, controlled release, and targeted drug delivery.[21,396,397] The intrinsic features of metal nanocrystals, such as physicochemical properties and LSPR, which directly impact their biomedical applications, can be enhanced by modulating the extrinsic characteristics of the particles, such as shape, size, and surrounding environment. Thus, the quest for a new generation of safer and more effective biosensors, biomedicines, and nanocarriers necessitates researchers to go beyond simple, symmetrical design.[398] The symmetry-broken structure and asymmetrical morphology promote more direct and effective interactions between the nanocrystals and biological systems at molecular, cellular, or tissue levels,[399,400] making them more competitive in diagnostic and therapeutic applications.

Due to the light absorption and scattering ability of biological tissues, optical imaging could be utilized to visualize cells, identify tissues, and distinguish pathological and nonpathological areas. However, the light-tissue interactions and the contrast from the tissue itself are often insufficient and not pathologically specific, thus requiring the use of contrast agents to optimize the visualization process. To this end, Au nanocrystals are strong candidates for imaging labels and contrast agents due to their excellent optical properties and bioinertness.[21,401,402] As discussed in section 5.1, different from highly symmetrical nanostructures (e.g., nanospheres), Au nanorods have transverse and longitudinal surface plasmon resonance modes. The unique longitudinal plasmon resonance of Au nanorods endows them with exceptional light absorption.[403] The light absorption efficiency of Au nanorods was found to be at least 20 times that of Au nanospheres of the same size,[404] with a scattering coefficient of one order magnitude higher.[403] Moreover, Au nanorods exhibit a high affinity toward the thiol group, making it versatile to efficiently attach numerous biomolecules to the surface.[405] As such, Au nanorods can be easily functionalized with ligands, antibodies, and other biomolecules to achieve targeted binding toward specific cells or tissues.[21,404,406] For instance, Au nanorods have been conjugated with antiepidermal growth factor receptor (anti-EGFR) monoclonal antibodies for the detection of tumor cells.[407] The bioconjugated Au nanorods were incubated with a normal skin cell line and a malignant oral epithelial cell line. Due to the overexpression of EGFR on the cytoplasmic membrane of many malignant cells, the modified Au nanorods were able to specifically bind to the surface of tumor cells with higher affinity. As shown in Figure 44A,B,[407] the malignant cells were brightly stained and distinctively visualized in the dark field as a result of the strong scattering of red light by the Au nanorods bound to their surface. This staining method could provide a new approach to differentiating cancer cells

https://doi.org/10.1021/acs.chemrev.2c00468
Chem. Rev. 2023, 123, 3693−3760

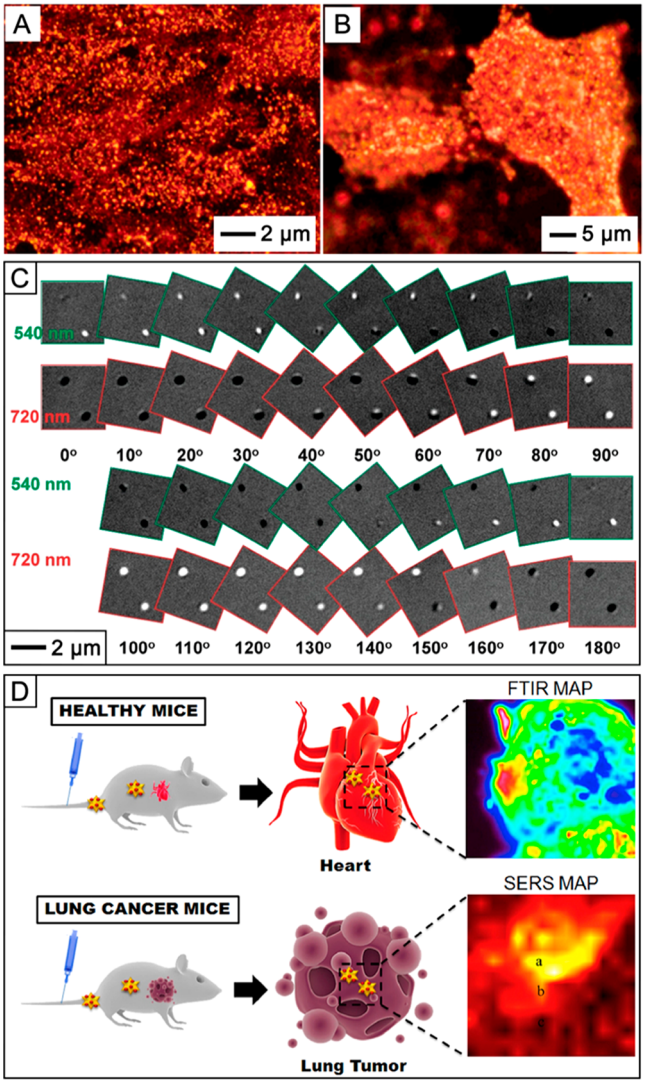

Figure 44. Dark-field images of (A) normal cells and (B) cancer cells labeled with anti-EGFR antibody conjugated Au nanorods. (C) DIC images of two Au nanorods at different orientations in 2-D space. The nanorods were illuminated at their transverse (540 nm) or longitudinal (720 nm) plasmonic resonance wavelength as indicated by the green and red frames for each image, respectively. The Au nanorods physically absorbed on a glass slide that was fixed to a rotating stage allowed for 360° rotation. (D) Gold nanostars for in vitro and in vivo real-time SERS detection of drug delivery using plasmon-dependent Raman or FTIR imaging. (A, B) Reproduced with permission from ref 407. Copyright 2006 American Chemical Society. (C) Reproduced with permission from ref 409. Copyright 2010 American Chemical Society. (D) Reproduced with permission from ref 412. Copyright 2016 Elsevier.

from normal cells. Notably, such Au nanorods could also find use in selective photothermal cancer therapy. After being exposed to a continuous near-infrared laser at 800 nm, the malignant cells targeted by anti-EGFR/Au nanorods could be killed photothermally.[408] The laser power energy required to destroy malignant cells was found to be about half of that needed to cause the destruction of normal cells. Thus, both diagnostics and photothermal therapy of cancer can be achieved simultaneously with the assistance of bioconjugated Au nanorods.

In addition, the anisotropic optical response of symmetry-broken nanocrystals can provide us with the capability to resolve the motion of nanomachines in both engineered environments and live cells. Although biological nanomachines, commonly in the form of protein complexes, perform various functions essential to life, their working mechanisms in a cellular environment, especially their rotational motions in live cells, remain elusive. The dynamic rotational motions of nanoscale cargos on both engineered surface and cytoskeleton track have recently been explored using a combination of Au nanorods and Nomarski-type differential interference contrast (DIC) microscopy.[409] In a DIC microscope, the sample was illuminated by two orthogonally polarized incident beams which were laterally shifted by ∼100 nm from each other. The interference pattern could be built by overlapping the two shifted intermediate images. There was no difference between the two intermediate images for spherical particles. In contrast, two different intermediate images were obtained for nanorods due to different extents of phase delay of two illumination beams. Because of the wavelength-dependent anisotropic refractive indexes arising from transverse and longitudinal LSPRs, different bright and dark intensities were observed depending on the orientation of the nanorod relative to the two polarization directions. As shown in Figure 44C, two single Au nanorods positioned at different orientations were illuminated at 540 and 720 nm, corresponding to the transverse and longitudinal LSPR peaks, respectively.[409] The rotational motions of nanorod-attached gliding microtubules and nanorod-containing vesicles on in vitro flat surfaces and in vivo cytoskeleton tracks have been revealed by monitoring the bright and dark DIC pattern of Au nanorods. This approach can also be extended to resolve the location and orientation of other macromolecules or microstructures by employing symmetry-broken nanocrystals with different compositions, structures, or surface modifications.

Besides diagnostics and bioimaging, symmetry-broken nanocrystals have been widely used as delivery vehicles to improve drug efficacy, reduce drug dosage, and minimize side effects.[410,411] To track the real-time drug delivery and release, a novel theranostic platform employing Raman spectroscopy has been designed for the monitoring of anticancer drug delivery and release in live cells and their biodistribution in vivo.[412] In this work, Mitoxantrone—an anticancer drug was conjugated to the surface of Au nanocrystals using thiolated and carboxylated poly(ethylene glycol). Interestingly, this drug had a red fluorescence emission as well as strong Raman scattering signals. To amplify the weak Raman signals in vivo, surface-enhanced Raman spectroscopy (SERS) was performed using symmetry-broken nanocrystals with sharp vertices (e.g., nanostars).[413] As the enhanced Raman signals varied with the distance between the drug molecule and the particle surface, the location of the anticancer drug could be tracked in real-time, while the drug accumulation in the hearts of healthy mice and in the tumors of mice bearing lung tumor could be monitored (Figure 44D).[412] This in vivo SERS method using symmetry-broken nanostructures enabled image-guided cancer chemotherapy and offered a promising nonspecific anti-inflammatory therapy for patients with heart disease. Similarly, Au nanostars on reduced graphene oxide could serve as an active SERS probe to monitor both the loading and release of anticancer drug doxorubicin.[414] The potential pH-dependent drug release has also been successfully demonstrated by this

https://doi.org/10.1021/acs.chemrev.2c00468
Chem. Rev. 2023, 123, 3693−3760

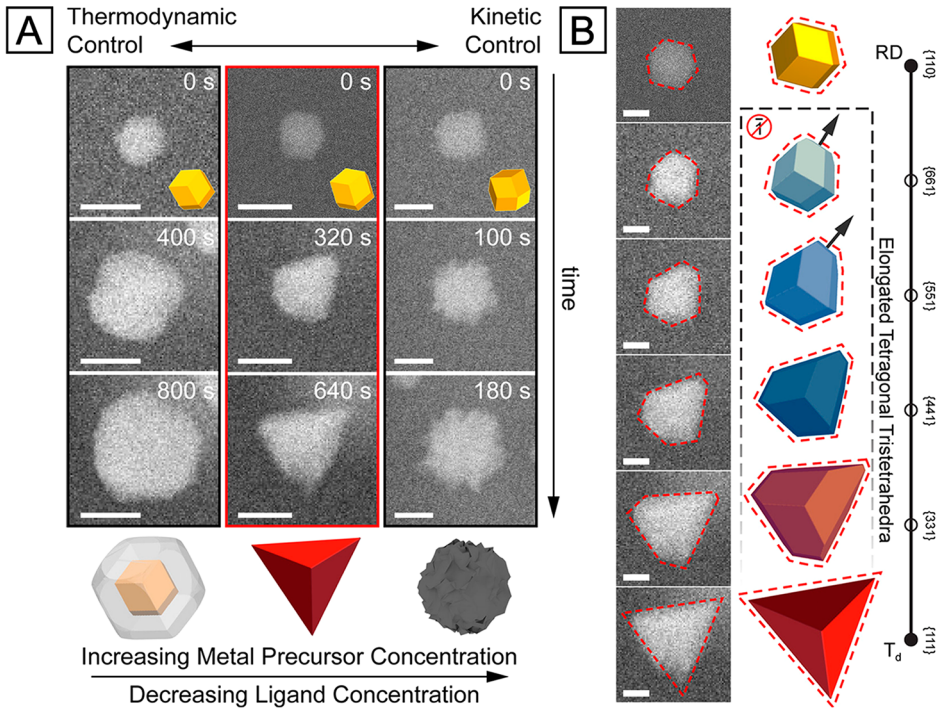

Figure 45. (A) In situ TEM observation of the three growth patterns (conformal growth, shape transformation to tetrahedron, and dendritic growth) of Au rhombic dodecahedra at different concentrations of ligands and metal precursor in a liquid cell (scale bars: 50 nm). (B) In situ TEM images and the corresponding geometrical models showing the transition from a rhombic dodecahedron to a tetrahedron (scale bars: 25 nm). Adapted with permission from ref 423. Copyright 2021 American Chemical Society.

method. Overall, using symmetry-broken nanocrystals as carriers or probes facilitates the efficiency of both photothermal therapy and chemotherapy while minimizing the side effects of drugs.

6. SUMMARY AND OUTLOOK

Over the past several decades, the explosion of nanomaterial research has been so dramatic that colloidal syntheses of nanocrystals have been reported for more than 15 metals in the periodic table, with thousands of follow-up studies to improve control of their size, shape, morphology, and structure, in addition to attempts to ensure reproducibility while achieving scale-up production at minimal cost and environmental impact. Among these studies, metal nanocrystals emanating from asymmetrical growth and symmetry breaking occupy a substantial fraction due to their complex morphologies, unique growth mechanisms, and remarkable performance in various applications. This Review represents our effort to recapitulate recent developments in the synthesis, mechanistic understanding, processing, and application of metal nanocrystals with symmetry deviated from the underlying unit cell. As a common theme in all synthetic protocols, kinetic and thermodynamic factors, which can be controlled by carefully manipulating the experimental conditions, are the deterministic switch to activate asymmetrical growth and thus symmetry breaking in a systematic manner. Understanding the roles of these parameters will provide the necessary rules for achieving rational synthesis of nanocrystals with the desired properties. In tandem with the exploration of different synthetic protocols, theoretical investigations have helped us rationalize the experimental results while providing additional insights into the role(s) played by each experimental parameter in initiating and continuing the asymmetrical growth pattern. Despite the major achievements, several challenges and opportunities still demand future attention before the full potential of these nanomaterials can be realized. Here we provide a brief discussion on some future directions that need further exploration, inspiring readers to initiate new research projects in this field.

6.1. Advanced Characterization Techniques

The mechanisms of symmetry breaking, as well as the growth pathways of various symmetry-broken nanostructures, have been the focus of discussion throughout this Review. Unfortunately, one must admit that many of the mechanisms presented in the above sections are deduced indirectly from empirical observations made using ex situ characterization techniques and may not necessarily be correct or accurate. This awkward and potentially problematic reality is deeply rooted in (i) the weak coupling between the shape of a nanocrystal and trackable physical properties (e.g., optical absorption, nuclear magnetic resonance spectroscopy, etc.), which makes the identification and monitoring of the intermediate products very challenging, especially for syntheses involving fast reactions; and (ii) the differences among particles in the same batch of sample due to either random or systematic influences. These challenges call for the development of techniques capable of directly observing the shape evolution of individual particles in situ and in real time.

In the last 10 years, direct and fast imaging of nanoscale objects in a liquid environment via TEM (namely, liquid-cell TEM) has emerged as a powerful and versatile tool to gather time-resolved information regarding intraparticle transformation and interparticle assembly.[415−417] Assisted with electron-transparent windows made of graphene or SiN_x on a sealed microcell, the behaviors of metal nanoparticles in a solution that resembles the actual reaction conditions can be captured

https://doi.org/10.1021/acs.chemrev.2c00468
Chem. Rev. 2023, 123, 3693−3760

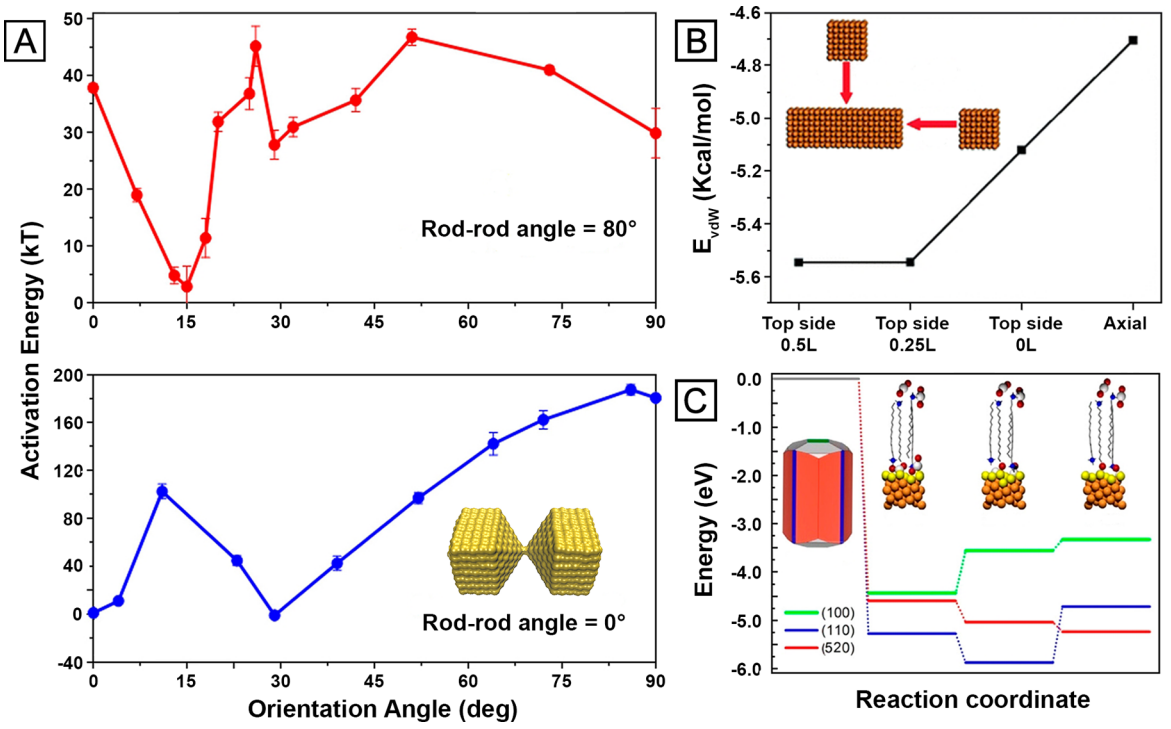

Figure 46. Computational simulations for the investigation of symmetry breaking mechanism. (A) Plot of coalescence activation energy vs orientation angle determined for different nanorod attachment approaches. Reactions with low activation energies (<29 kT) were found only at orientation angles <45°, so that the coalescence at the rod end is more favorable. (B) Plot of vdW interaction at zero separation between the nanoparticle and the nanorod vs different approaching directions: axial and top side (0, 0.25, and 0.5 L). L represents the length of the nanobar. (C) Energy changes during Au atomic addition onto pre-existing (100), (110), and (520) surfaces with the CTAB−AgBr complex adsorbed. (A) Reproduced with permission from ref 208. Copyright 2016 American Chemical Society. (B) Reproduced with permission from ref 429. Copyright 2015 Royal Society of Chemistry. (C) Reproduced with permission from ref 441. Copyright 2014 American Chemical Society.

with unprecedented spatial and temporal resolutions.[186,197,418,419] Thanks to the work of many research groups, fundamental processes regarding nanoparticle nucleation, growth, assembly, and oxidative etching have all been scrutinized at the single particle level.[313,420,421] With the use of in situ liquid-cell TEM, for example, the nucleation of Au or Ag nanocrystals from a supersaturated aqueous solution was found to involve three distinct steps: formation of a metal-rich liquid phase, nucleation of amorphous clusters, and crystallization of the amorphous clusters.[105] A nontraditional pathway was also found for the seed-mediated growth of Au@Ag nanocubes to involve the absorption and coalescence of Ag nuclei on the Au surface.[422] However, the mechanistic details involved in the symmetry breaking of nanocrystals have remained elusive and challenging to study for a long time due to its high sensitivity toward reaction conditions.

In a recent paper, a versatile method was reported for effectively screening more than one reaction parameters to capture and scrutinize specific symmetry breaking behaviors (Figure 45).[423] By flushing the metal precursor ($HAuCl_4$) solution into a liquid cell to create continuous and opposing concentration gradients of $HAuCl_4$ and ligands (cetylpyridinium chloride and CTAB), a variety of reaction conditions for the growth from Au rhombic dodecahedral seeds were probed in one experiment. It was found that at relatively high and low concentrations for the ligands and precursor, respectively, conformal growth of the seeds gave rise to pseudospherical nanocrystals (i.e., the thermodynamic product), whereas the opposite conditions resulted in a dendritic morphology (i.e., the kinetic product). Tetrahedral nanocrystals (a symmetry-broken product) would be developed only at intermediate concentrations for the ligands and precursor (Figure 45A). This phenomenon implied a complex interplay between the two factors. Further real-time monitoring and geometrical modeling of stepwise intermediates demonstrated that the shape transformation was achieved through simultaneous growth of all the {110} side faces of a rhombic dodecahedron into a series of high-index ({661}, {551}, {441}, and {331}) and finally {111} facets, accompanied by gradual elongation of the tetragonal tristetrahedral intermediates through the tip-selective growth (Figure 45B). Constant surface reconstruction and coalescence of four pairs of adjacent side faces reduced the symmetry order from 48 to 24 due to the rapid loss of inversion symmetry, marking the completion of the symmetry breaking event. The adoption of fluid flow during in situ imaging offers a powerful tool to screen multiple experimental parameters and thus determine if, when, and how the symmetry breaking event occurs. It is expected that the throughput of this screening process can be further improved by switching to multidimensional flow channels and even expanding to other physicochemical parameters such as temperature and light intensity.

6.2. Computational Studies

As discussed in section 6.1, a great deal of work has been done in the hope that the asymmetrical growth patterns of nanocrystals can be directly observed by experimental means. For instance, a very early study confirmed the dominant role of orientated attachment in asymmetrical growth by HRTEM imaging.[424] However, it remains unclear which orientation is preferred in terms of energy. While state-of-the-art techniques

https://doi.org/10.1021/acs.chemrev.2c00468
Chem. Rev. 2023, 123, 3693−3760

such as in situ TEM are increasingly applied to understand the essence of this asymmetrical growth process, computational simulations have also been increasingly conducted to shed light on the thermodynamic and kinetic aspects of this process, predicting the behaviors of the building blocks and testing the hypotheses that are challenging to substantiate experimentally. Specifically, computational studies have been extensively conducted to clarify the roles played by solvent, surface capping agent, and particle orientation in inducing and maintaining the asymmetrical growth pattern.

As a unique hallmark, oriented attachment involves "docking and matching" between two nanocrystals.[197,425,426] Preferred coalescence between the nanocrystals at certain positions and orientations will lead to the formation of specific structures. Great efforts have been made to uncover the mechanism of oriented attachment with the help of steered molecular dynamics. In one study involving the attachment of Au nanorods, the activation energy, mainly affected by the changes in metallic energy and solvation energy, was calculated by integrating all the relative physical interactions involved.[208] When plotting the activation energy as a function of the rod-to-rod angle (Figure 46A), the position of the minimum activation energy indicates that attachment between two nanorods is most favorable at a low orientation angle (<45°). In other words, the coalescence occurs much more likely at the ends of a rod. This finding provides a qualitative explanation for the rare observation of attachment involving large rod-to-rod angles.

The contributions from vdW interactions, Coulomb interactions, and dipolar interactions among nanocrystals, ligands, and solvent molecules to asymmetrical growth were also evaluated. For example, the role of solvent in the synthesis of symmetry-broken Ag nanocrystals has been explored using molecular dynamics simulations.[427] By characterizing the solvent layers around the nanocrystal surface, the initial contact of two particles was proposed to be most favorable at the smallest faces, which are the ends of the nanorods or the thin sides of the nanoplates due to the disruption of solvent ordering at these sites. In another study investigating the dependences of vdW and Coulomb interactions on the orientation between two nanocrystals, the vdW component was identified as the main driving force for two particles to coalesce in the solution.[206,428] Taking Ag as the model material, the magnitudes of the vdW interaction in different coalescence configurations were compared (Figure 46B).[429] When particles approached sideways and attached at the middle of nanorods (off-center from the side by 0.25−0.5 L, with L being the edge length of the square building block), the vdW interaction at zero separation reached the minimum value, suggesting that the sideway attachment was thermodynamically more favorable. The theoretical work not only deepens our understanding of attachment thermodynamics but also offers guidelines for designing experiments to achieve asymmetrical growth. Specifically, if selective axial growth is desired, appropriate ligands need to be introduced to passivate the lateral surface of the nanorods and thereby inhibit the thermodynamically favorable lateral growth.

In addition to attachment, atomic addition is another common route of nanocrystal growth. As discussed in section 3.1.2, the rate of atomic addition to a specific type of facet can be regulated using surface capping agent, resulting in the formation of nanocrystals enclosed by that facet.[119,226] To this end, experimental measurements such as electrochemical methods have been conducted to test which species are responsible for the facet-dependent growth.[430−435] However, it is still unclear why the actions of these species are facet selective. Many researchers have also endeavored to investigate the role of capping agent in the asymmetrical growth and symmetry breaking of Ag, Au, and Pd nanocrystals.[84,436−439] In the case of Au nanorods, different from the previously proposed bilayer model, molecular dynamics simulations suggested that CTAB was distributed as cylindrical micelles on the Au surface.[440] Water−ion channels between two cylindrical, adsorbed micelles were observed at the interface, which allowed for the diffusion of Au(III) cations to the seed surface for their subsequent surface reduction. It was found that different facets had different areas available for the diffusion of Au(III) precursor, and the lower stacking density of CTAB on a specific facet would promote atomic addition. In a similar study, density functional theory simulations have been performed to model the synergistic role of CTAB and Ag^+ ions in breaking the symmetry of Au nanorods.[441] To better understand the energetics during atomic addition, the growth was divided into three steps: (i) absorption of the CTAB-AgBr complex on the Au surface, (ii) separation of one Br atom from the complex, and (iii) addition of incoming Au atoms to the surface for the formation of new facets. As shown in Figure 46C, the addition of Au atoms was more favorable on {520} facets than {100} and {110} facets. Based on these calculations, a modified Wulff structure was adopted to account for the formation of Au nanorods mainly enclosed by {520} facets. Such computational predictions qualitatively rationalize the experimental observations and provide the foundation for more precise control over the outcome of a synthesis.

6.3. Prediction and Deterministic Control of Symmetry Breaking

The symmetry breaking in a colloidal synthesis involving seed-mediated growth is almost exclusively controlled by kinetic parameters.[72,73,100] To develop mechanistic insights into this process from a kinetic point of view, as well as to control the outcome of the synthesis in a predictable and deterministic manner, it is necessary to regulate the key kinetic parameters throughout a synthesis. Unfortunately, the concentrations of the reactants (including precursor, reducing agent, and even capping agent) in a synthesis constantly decrease and so as the overall reaction kinetics. This variation can be attributed to the typical one-shot injection of the precursor into the reaction mixture in a conventional colloidal synthesis. The instantaneous number of precursor molecules in the reaction mixture will drastically increase to a high level upon injection and then exponentially decay during nanocrystal growth. Accordingly, the number of atoms derived from the precursor is expected to undergo significant changes as a function of reaction time. Although an analytical model can be established via theoretical approximation of the redox reaction (e.g., pseudo-first-order reaction when the reducing agent is in large excess relative to the precursor) and experimental measurement of kinetic parameters (e.g., activation energy and reaction rate constant) to track the instantaneous concentrations during a synthesis, their nonlinear dependence on time and temperature makes it difficult to precisely adjust the overall reaction rate.

A recently emerged method that features dropwise addition of the precursor provides a robust and transformative approach to quantitatively control the reaction rate responsible for

https://doi.org/10.1021/acs.chemrev.2c00468
Chem. Rev. 2023, 123, 3693−3760

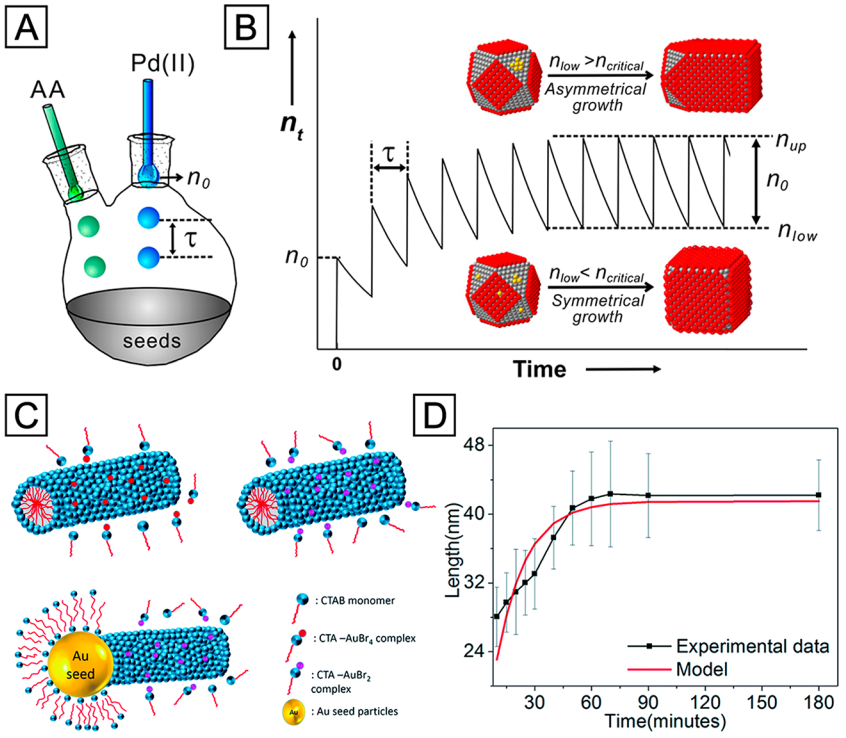

Figure 47. (A) Schematic illustration of the experimental setup used for seed-mediated growth with the dropwise addition of a precursor solution. (B) Plot showing the instantaneous number of Pd(II) ions (the precursor) in the growth solution. The inset is a schematic showing how the reaction kinetics and surface diffusion affect the growth pattern (symmetrical vs asymmetrical) when Pd truncated octahedral seeds are used. (C) Schematic illustration of the proposed mechanism involving the diffusion of $HAuCl_4$ and complex formation with CTAB micelle, the reduction of Au(III) to Au(I) in the complex by AA, with the seed positioned at one end of the cylindrical micelle. (D) Comparison of the model-predicted lengths with the experimentally measured lengths of Au nanorods. (A, B) Adapted with permission from ref 181. Copyright 2015 American Chemical Society. (C, D) Adapted with permission from ref 443. Copyright 2016 Royal Society of Chemistry.

switching between symmetrical and asymmetrical growth (Figure 47A,B).[181] In this approach, the precursor solution is titrated dropwise into a reaction mixture at a programmable injection rate through the use of a syringe pump. Taking the seed-mediated growth of Pd nanobars as an example, the instantaneous concentration of the precursor in the reaction solution and thus the reaction rate can be maintained in a predefined steady state throughout the synthesis by controlling the initial concentrations of the precursor (Na_2PdCl_4) in the droplets and the pace at which the droplets are titrated. Powered by this dropwise approach, the growth pattern (e.g., symmetrical vs asymmetrical) of a Pd seed could be regulated by judiciously tuning parameters such as the interval between two adjacent droplets of the precursor and its initial concentration to manipulate the reaction kinetics quantitatively. This study revealed that the symmetry breaking of nanocubes could be initiated and retained by maintaining a reduction rate slow enough to limit the number of nucleation sites on the surface of a cubic seed but fast enough to surpass surface diffusion. This approach is expected to find extensive use in understanding and controlling the symmetry breaking process.

Besides experimental control, mathematical modeling is also helpful in explaining the growth mechanism and validating key empirical conclusions.[442] For example, based on the insights from a series of control experiments, a mechanism was proposed to account for the seed-mediated growth of Au nanorods (Figure 47C). In this mechanism, Au(III) ions in the surfactant–Au(III) cylindrical micelles were reduced to Au(I) ions, followed by their diffusion to one end of each cylindrical micelle for the formation of a nanorod through autocatalytic reduction and template-guided growth.[443] Based on this mechanism and some observed or predetermined reaction parameters such as reaction rate constants and reactant concentrations, a mathematic model was developed to predict the time-dependent shape evolution of Au nanorods during a synthesis. As shown in Figure 47D, the time evolution of the nanorod's length obtained from experimental measurements and the mathematical model showed satisfactory agreement, supporting the rationality of the proposed mechanism. However, it should be pointed out that for more complex systems (which are common in nanocrystal synthesis), mathematical models tend to fail to predict the outcome of a synthesis. Direct in situ observations of the growth process, in combination with control experiments, are often more straightforward and reliable in validating the growth mechanism.

6.4. Extension of the Concept to Hollow Seeds

The focus of this Review is primarily placed on simple solid nanocrystals. However, there are many examples in literature where core–shell nanocrystals have been generated by conformably depositing a second metal on nanocrystal templates.[24,444] By selectively etching away the template from the core, hollow nanocrystals such as nanocages with well-defined surface structures can be readily obtained.[445−451] More significantly, both the outer and inner surfaces of the nanocage will be available for further modifications to suit applications such as catalysis or biomedicine in the context of encapsulation, controlled release, and drug delivery.[448,452,453]

https://doi.org/10.1021/acs.chemrev.2c00468
Chem. Rev. 2023, 123, 3693−3760

Most studies on hollow nanocrystals center on symmetry-preserved structures such as cubic or octahedral nanocages. Interestingly, such nanocages can also be used to form nanocages with asymmetrical walls through the deposition of a second metal onto the outer surface only (Figure 48A). In one example, Au nanocages were used as a template for the deposition of Pd atoms, with the reduction kinetics serving as an experimental knob to control the morphology of the final products.[454] When $PdCl_4^{2-}$ was used to provide fast reduction, deposition occurred mainly on the outer surface of the nanocage, giving rise to a Pd−Au asymmetrical wall structure (Figure 48B,C). When switching to $PdBr_4^{-}$ to slow down the reduction, deposition took place on both sides of the Au nanocage, resulting in the formation of a Pd−Au−Pd trilayered symmetrical structure for the wall (Figure 48D,E).[163,454,455] In this case, the slow reduction allowed the precursor to diffuse into the void space, activating symmetrical growth on both surfaces of the nanocage.[163] Under fast reduction, in contrast, asymmetrical growth (with deposition mainly on the outer surface) was initiated owing to the inadequate diffusion of the Pd atoms into the void space. While the overall shape and symmetry of the nanocrystal was preserved in both cases, the change in elemental distribution could still result in symmetry breaking for the wall of the nanocages.

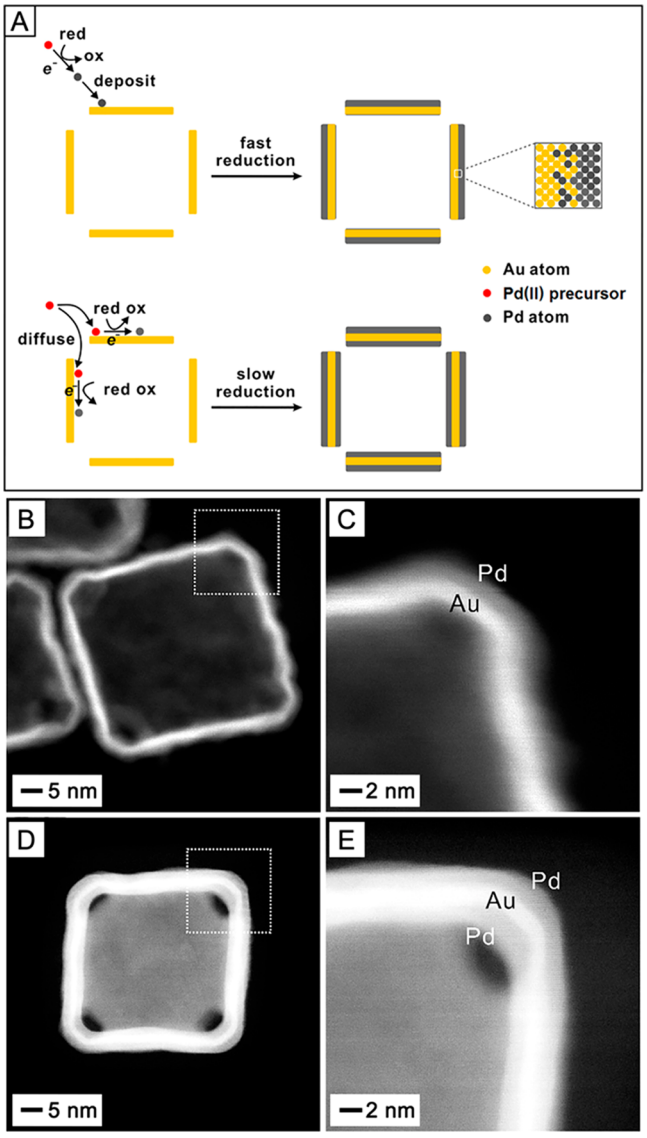

Figure 48. Symmetry reduction in terms of the composition of a nanocage. (A) Schematic illustration of two different scenarios for the deposition of Pd on the surfaces of Au nanocages with openings at the corners. Top panel: Pd was mainly deposited on the outer surface. Bottom panel: Pd was deposited on both the outer and inner surfaces. The deposition pattern could be controlled by varying the reduction kinetics of the precursor. (B) HAADF-STEM image of a Au−Pd nanocage prepared using 0.75 mL of aqueous $PdCl_4^{2-}$ solution to give a fast reduction rate. (C) HAADF-STEM image taken from the corner marked by a box in panel B, showing a Au−Pd bilayer structure. (D) HAADF-STEM image of a Pd−Au−Pd nanocage prepared using 0.75 mL of $PdBr_4^{2-}$ solution to give a slow reduction rate. (E) HAADF-STEM image taken from the corner marked by a box in panel D, showing a Pd−Au−Pd trilayer structure. Reproduced with permission from ref 454. Copyright 2017 American Chemical Society.

In principle, a similar pattern of deposition can occur on a wide variety of hollow nanocrystals. Since the reaction kinetics affect the growth patterns of both solid and hollow seeds, the synthetic methods discussed in section 3 for symmetry breaking should be applicable to hollow particles too. As such, a vast collection of symmetry-broken hollow nanocrystals can be created by controlling the pattern of deposition on hollow seeds. For instance, deposition might only occur on one portion of the nanocage's surface if the hollow particle is confined to an interface.[262,454] Similarly, when the deposited metal has a large lattice mismatch with the metal in the hollow template, it should also be possible to access complex nanocrystals with asymmetrical growth on either surface of the nanocage.[286,454] There is no doubt that symmetry breaking could be extended to hollow particles in unexpected and novel ways by creatively combining and applying various synthetic techniques. In turn, the novel morphologies could be used to further fine-tune the applicability of these hollow structures to specific applications.

6.5. Extension to Different Metals and Other Solid Materials

Although the focus of this Review is on nanocrystals composed of noble metals, it should be pointed out that similar strategies have achieved the same success when extended to systems involving other types of materials such as inorganic semiconductors, metal/semiconductor hybrids, and even multicomponent structures containing different materials.[456−459] For example, CdS semiconductor nanocrystals have been synthesized in the form of monopods or multipods with different symmetries by controlling the V_{dep} of Cd precursor using a syringe pump (Figure 49A).[457] When cadmium acetate was added into an oleylamine solution containing sulfur, thermodynamically stable CdS tetrahedral particles enclosed by {111} facets were crystallized in the zinc blende (zb) phase in the initial stage. In the subsequent growth process, the limited number of the CdS monomers formed through slow injection could only activate one of the four {111} facets of each nascent tetrahedral seed, generating a protrusion in Wurtzite phase on each seed. At a high injection rate of 30 mL/h, the limited supply and surface diffusion of monomers led to the formation of asymmetrical shapes in the form of monopods (Figure 49B). As the injection rate was gradually reduced to 2.0 and 0.5 mL/h, however, the atoms on the initially formed protrusion started to diffuse onto and activate other adjacent {111} facets, producing bipods and tripods/

https://doi.org/10.1021/acs.chemrev.2c00468
Chem. Rev. 2023, 123, 3693−3760

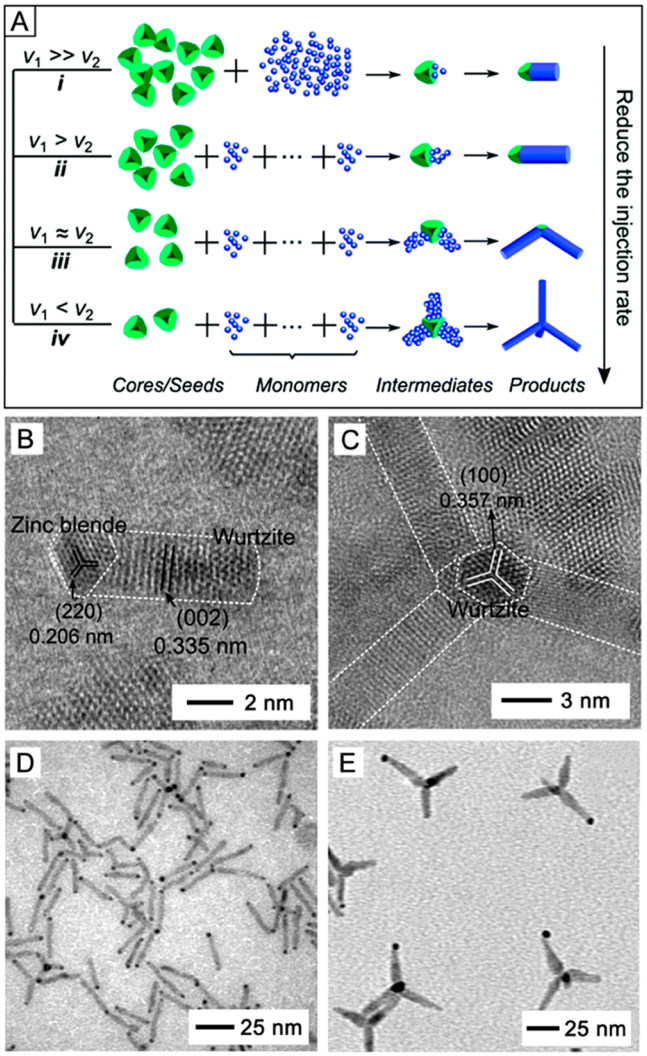

Figure 49. (A) Schematic illustration showing the formation of CdS nanostructures with different morphologies. (B and C) HRTEM images of CdS nanostructures in the form of monopod and tetrapod, respectively. (D) TEM image of metal/semiconductor heterostructures where CdSe nanorods served as seeds for the deposition of Au tips. (E) TEM image of multicomponent heterostructures obtained through overgrowth of CdS from CdSe seeds into tetrapods, followed by selective deposition of Au on one of the four tips. (A–C) Reproduced with permission from ref 457. Copyright 2016 Royal Society of Chemistry. (D) Reproduced with permission from ref 460. Copyright 2004 American Association for the Advancement of Science. (E) Reproduced with permission from ref 461. Copyright 2012 American Chemical Society.

tetrapods as the main products (Figure 49C). Similarly, controlled deposition of Au on CdSe nanorods could lead to the growth of a Au tip on only one end of each nanorod to generate a matchstick-like structure (Figure 49D).[460]

However, one should also admit that some of the strategies discussed in section 3 rely on the specific properties of metals and may not be suitable for other materials. In the meantime, these materials can have their own unique features that may promote symmetry breaking and thus production of complex architectures that are not accessible with metals, such as hybrid structures comprised of different materials.[458,459] For example, when Au was deposited on zb-CdSe/CdS tapered tetrapods, the deposition site could be precisely controlled to be only one of the four tips of each tetrapod due to the enhanced electrochemical Ostwald ripening process in this unique metal/semiconductor configuration (Figure 49E).[461] While Au atoms could be deposited on all the four tips during the initial growth stage, smaller Au particles at most tips would be dissolved and transferred to the largest ones during the subsequent aging process, reducing the symmetry of this hybrid structure. Furthermore, the remaining three unoccupied tips could be decorated with Ag_2S through cation exchange between Ag^+ and Cd^{2+}, creating a complex multicomponent structure.

6.6. Emerging Niche Applications

Emerging as purely trial-and-errors from scientific curiosities, metal nanocrystals derived from asymmetrical growth and symmetry breaking have continuously shown transformative impacts in a plethora of areas, as illustrated in section 5. However, current optical and electrical applications of symmetry-broken nanocrystals primarily center on nanorods and nanowires due to the extensive and robust protocols available for producing these 1-D nanostructures, coupled with the flexibility to tune their aspect ratios in favor of long-range, directed propagation of photons or electrons. As such, this subsection mainly focuses on future directions in terms of applications for symmetry-broken nanocrystals beyond nanorods and nanowires and highlights how symmetry breaking makes them stand out.

Symmetry breaking in structure or composition confers distinct properties on nanocrystals at different locations, which may make symmetry-broken nanocrystals inherently suitable for multifunctional tasks. Considering drug carriers as a potential example, traditional drug carriers possessing symmetrical geometry with single storage space can only accommodate one drug or several drugs with similar properties, while symmetry-broken nanoparticles can be loaded with multiple drugs with relatively different surface chemistry (e.g., hydrophilicity/hydrophobicity and acidity/basicity, among others) in distinct domains.[462,463] In addition, the multidrug carriers based on symmetry-broken nanoparticles will allow the release of each drug to be controlled independently. Functionally distinctive surfaces of symmetry-broken nanoparticles can selectively bind to specific triggers to achieve individual responsive release under different circumstances.[464] Similarly, symmetry breaking makes it possible to integrate very distinct catalytic properties into a single structure, which is the prerequisite for nanoparticles to be used as nanomotors. Currently, most existing nanomotors can only be driven in high concentration of hydrogen peroxide, limiting their practical applications in complex and dynamic environments.[465] As methods for producing symmetry-broken nanocrystals continue to develop, a higher degree of versatility in composition and surface features can eventually be achieved in one structure. Such symmetry-broken nanomotors are expected to harvest energy from various reactions and even magnetic fields.[466−468] To this end, multifuel-driven nanomotors based on Janus structure have been fabricated to exhibit high adaptability to harsh industrial environments with an autonomous fuel switching process.[469] Undoubtedly, symmetry breaking is expected to not only broaden the application scenarios of nanocrystals but also make them superior in terms of selective response and suitability to different environments.

Beyond the individual use, self-assembly of symmetry-broken nanocrystals into superstructures in a controllable

https://doi.org/10.1021/acs.chemrev.2c00468
Chem. Rev. 2023, 123, 3693−3760

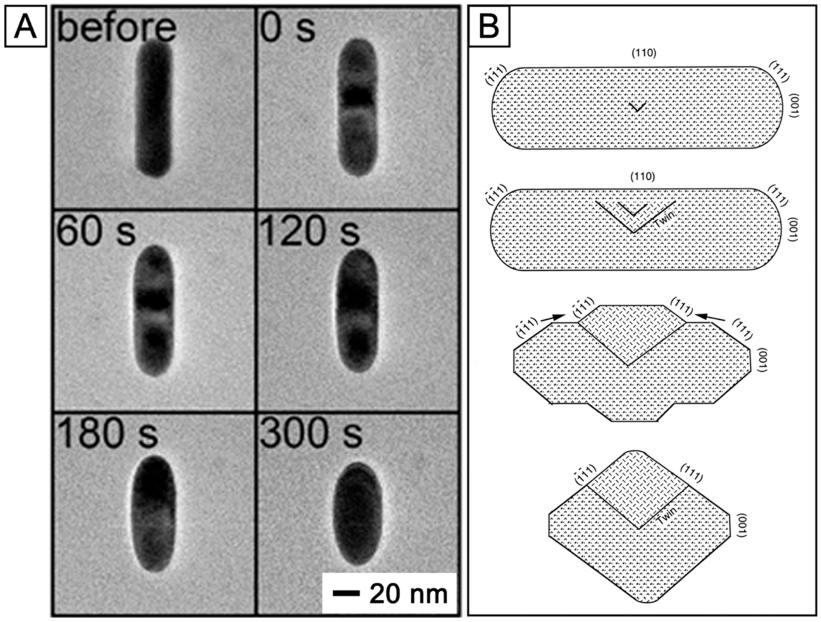

Figure 50. (A) TEM images of Au nanorods when heated at 300 °C for up to 300 s. (B) Schematic illustration showing the transformation of Au nanorods upon laser heating through the formation of planar defects and the associated surface reconstruction. (A) Reproduced from ref 482. Copyright 2020 American Chemical Society. (B) Reproduced from ref 483. Copyright 2000 American Chemical Society.

manner provides another promising way to manipulate these particles and thus make full use of their collective properties.[470,471] Compared to nanocrystals with spherical geometry, symmetry-broken nanocrystals bear inequivalent particle orientations and show great potential in forming more intriguing hierarchical structures and packing symmetries. Considering that symmetry breaking in nanocrystals also gives rise to numerous directional physical properties (e.g., optical, electrical, and magnetic), an ordered ensemble of symmetry-broken nanocrystals likely amplifies these properties, leading to hierarchical materials with enhanced and even unprecedented performance for their intended application.[472−474] At the moment, one of the frontiers in nanomaterials research includes regulating the intricate interparticle forces for self-assembly by modifying the surface chemistry of nanoparticles or applying an external field.[475] With the development of tools for in situ characterization, how symmetry-broken nanocrystals behave differently from symmetry-preserved nanocrystals during the self-assembly process and how the symmetry breaking in each particle affects the emerging collective properties will be better understood and utilized in the future.

6.7. Thermal Stability of Metal Nanocrystals

As discussed previously, the thermodynamically stable shape of a metal nanocrystal is defined by the Wulff construction.[1] Any deviation from this shape indicates that the particle is in a metastable state.[119] In other words, shapes other than those obtained through Wulff construction are kinetic rather than thermodynamic products. Consequently, the asymmetrical shapes usually adopted by symmetry-broken nanocrystals are even less stable. Such intrinsic instability means that at elevated temperatures, the nanocrystals can overcome the energy barriers that keep them at the local minima of the energy curve and start to lose their distinct shapes as they move toward the thermodynamic product.[476] If such nanocrystals are intended for use in catalysis, they should be equipped with good thermal stability, as many catalytic processes are carried out at elevated temperatures over extended periods of time.[26,477] Since shape is intrinsically tied to catalytic performance, any thermally induced changes to the shape and structure will drastically alter the activity and/or selectivity of a catalyst.[18] For this reason, there is a pressing need to understand and enhance the thermal stability of asymmetrical nanocrystals.

At the moment, there are only limited reports on the thermal stability of metal nanocrystals. While it is commonly known that nanocrystals melt below the melting point of the bulk material, systematic studies on their thermal stability remain sparse.[478] Most studies regarding the thermal stability of metal nanocrystals focus on octahedra, icosahedra, and other symmetrical shapes, with few of them on the thermal stability of nanorods and nanowires.[476−481] In one report, Au nanorods were shown to deform into ellipsoidal nanocrystals after heating at 300 °C for 5 min (Figure 50A).[482] When heated to 180 °C, the thiolate molecules desorbed from the Au surface, allowing the surface atoms to migrate and reshape the Au nanorods into ellipsoids, and eventually spheres after 15 min. Since the applied temperatures were significantly lower than the melting point of bulk Au, the shape transformation was ascribed to surface melting.[478,482] Alternatively, when the Au nanorods were heated using laser pulses, they could retain their shape up to 750 °C, likely because the laser pulses were too short to allow for sufficient thermal activation to induce surface melting.[478,483] Instead, the laser pulses induced the formation of point and line defects in the nanorod, which could ultimately turn into planar defects that raise the energy of the system (Figure 50B).[483] As a result, surface reconstruction and diffusion caused the transformation from rods to spheroidal particles as higher energy {110} facets were converted into more stable {100} and {111} faces to minimize the overall energy of the nanorods. Besides Au nanorods, Pt nanorods were heated at temperatures ranging from 250 to 1100 °C.[484] The nanorods were relatively stable upon heating up to 800 °C. However, they started to lose their morphology

https://doi.org/10.1021/acs.chemrev.2c00468
Chem. Rev. 2023, 123, 3693−3760

at higher temperatures as the rods began to split into two spherical domains, one being single crystal and the other containing defects. Such morphological changes are typically observed in thermal stability studies. At first, extensions or protrusions start to disappear from the nanostructure, followed by rounding to the corners and edges, and finally, the formation of a spheroidal nanoparticle.[485] As expected, when altering both the surface area and faceting of the nanostructures, the thermal behaviors of the nanocrystals will be changed entirely.

Due to the importance of thermal stability, several methods have been developed to improve it for a number of systems. The thermal stability of nanostructures could be enhanced by applying polymer coatings, but at the expense of altering their surface and thus compromising their applicability.[486,487] Silica coatings have also been shown to greatly boost the thermal stability of metal nanocrystals, albeit with similar drawbacks.[480,488] Another approach involves the synthesis of alloy nanocrystals made of two metals with different melting points in an effort to obtain an alloy with a higher melting point than one of the constituents.[489,490] While this method leaves an unimpeded surface, alloy particles have distinct properties from their monometallic counterparts and may not be the best choice for all applications. Additionally, the elemental distribution of the metals in an alloy can shift upon heating, once again affecting their catalytic performance.[489,491] Other attempts to improve the thermal stability of nanocrystals include changing the atmosphere for heating, attaching the nanocrystals to a proper substrate, and controlling the internal structure of the nanocrystals.[476,485,492,493] As illustrated in all these studies, the issue of thermal stability cannot be ignored when designing nanoparticle catalysts. It would be impractical to design catalysts that work perfectly in a lab environment but instantly deactivate in real-world conditions. For this reason, further research into nanocrystal stability is urgently needed.

In conclusion, we will encounter inexhaustible possibilities to improve the synthetic protocols and utilizations of metal nanocrystals with symmetry-broken shapes or morphologies. As we continuously venture into the realm of understanding asymmetrical growth and symmetry breaking, we will be able to overcome the current roadblock by progressing from empirical studies to "real-world" applications with the use of less expensive and more sustainable materials to benefit the fields of plasmonics, photonics, electronics, sensing, catalysis, and medicine. Before then, we hope that readers can use this Review as a roadmap to continue extending the complexity and functionality of the nanomaterials to the larger, macroscopic world, which is also one of the ultimate goals of nanoscience and nanotechnology.

AUTHOR INFORMATION

Corresponding Author

Younan Xia − *School of Chemistry and Biochemistry, Georgia Institute of Technology, Atlanta, Georgia 30332, United States; The Wallace H. Coulter Department of Biomedical Engineering, Georgia Institute of Technology and Emory University, Atlanta, Georgia 30332, United States;* orcid.org/0000-0003-2431-7048; Email: younan.xia@bme.gatech.edu

Authors

Quynh N. Nguyen − *School of Chemistry and Biochemistry, Georgia Institute of Technology, Atlanta, Georgia 30332, United States;* orcid.org/0000-0003-1544-6139

Chenxiao Wang − *School of Chemistry and Biochemistry, Georgia Institute of Technology, Atlanta, Georgia 30332, United States*

Yuxin Shang − *School of Chemistry and Biochemistry, Georgia Institute of Technology, Atlanta, Georgia 30332, United States;* orcid.org/0000-0003-1667-3544

Annemieke Janssen − *School of Chemistry and Biochemistry, Georgia Institute of Technology, Atlanta, Georgia 30332, United States;* orcid.org/0000-0002-7721-597X

Complete contact information is available at: https://pubs.acs.org/10.1021/acs.chemrev.2c00468

Author Contributions

[§]Q.N.N., C.W., Y.S., and A.J. contributed equally to the preparation of this review article. Q.N.N., C.W., Y.S., and A.J. wrote the manuscript. Y.X. defined the scope and structure of this review article and was involved in the editing process.

Notes

The authors declare no competing financial interest.

Biographies

Quynh N. Nguyen received her B.S. in chemistry from Agnes Scott College in 2020. As a National Science Foundation Graduate Research Fellow, she is pursuing her Ph.D. in the School of Chemistry and Biochemistry at the Georgia Institute of Technology under the supervision of Prof. Xia. Her research interest includes the phase- and shape-controlled synthesis of metal nanocrystals for catalysis and energy-related applications.

Chenxiao Wang received his B.S. in chemistry in 2018 from Wuhan University, China. He is pursuing his Ph.D. degree in the School of Chemistry and Biochemistry at the Georgia Institute of Technology in the Xia group. His research interest includes the synthesis of bi- and multimetallic nanocrystals and study of their thermal and catalytic properties.

Yuxin Shang received her B.S. in chemistry from Nankai University in 2020. She is pursuing her Ph.D. in the School of Chemistry and Biochemistry at the Georgia Institute of Technology under the supervision of Prof. Xia. Her current research interest includes the design and rational synthesis of nanostructured materials for catalytic and biomedical applications.

Annemieke Janssen received her B.S. in chemistry from University College Utrecht in 2016, and her M.S. in materials science from Imperial College, London in 2017. She joined the Xia group in 2018 and completed her Ph.D. dissertation in June 2022. Her research centered on noble-metal nanocrystals in metastable phases and their structure−property relationship. She is working as a research scientist at Intel (Hillsboro, Oregon).

Younan Xia studied at the University of Science and Technology of China (B.S., 1987) and University of Pennsylvania (M.S., 1993) before receiving his Ph.D. from Harvard University in 1996 (with George M. Whitesides). He started as an assistant professor of chemistry at the University of Washington (Seattle) in 1997 and was promoted to associate professor and professor in 2002 and 2004, respectively. He joined the Department of Biomedical Engineering at Washington University in St. Louis in 2007 as the James M. McKelvey Professor. Since 2012, he holds the position of Brock Family Chair

https://doi.org/10.1021/acs.chemrev.2c00468
Chem. Rev. 2023, 123, 3693−3760

and Georgia Research Alliance (GRA) Eminent Scholar in Nanomedicine at the Georgia Institute of Technology.

ACKNOWLEDGMENTS

This work has been supported in part by the National Science Foundation (CHE-2105602, CHE-1804970, CHE-1505441, and DMR-1506018) and startup funds from the Georgia Institute of Technology. Q.N.N. acknowledges the support from the National Science Foundation Graduate Research Fellowship under Grant No. DGE-2039655 for the preparation of this manuscript.

ABBREVIATIONS

1-D = one-dimensional
2-D = two-dimensional
3-D = three-dimensional
AA = L-ascorbic acid
$acac^-$ = acetylacetonate
AC = alternating current
Anti-EGFR = antiepidermal growth factor receptor
Asc-2P = L-ascorbic acid 2-phosphate trisodium salt
CTAB = cetyltrimethylammonium bromide
CTAC = cetyltrimethylammonium chloride
d = atomic diameter
DEG = diethylene glycol
DIC = differential interference contrast
EDS = energy dispersive X-ray spectroscopy
EG = ethylene glycol
fcc = face-centered cubic
FTIR = Fourier-transform infrared spectroscopy
HAADF-STEM = high-angle annular dark-field scanning transmission electron microscopy
H_d = demagnetization field
HDA = hexadecylamine
HRTEM = high-resolution transmission electron microscopy
ICP-MS = inductively coupled plasma mass spectrometry
ITO = indium−tin oxide
LSPR = localized surface plasmon resonance
MBIA = 2-mercapto-benzimidazole-5-carboxylic acid
ORR = oxygen reduction reaction
PDDA = poly(diallyldimethylammonium chloride)
PVP = poly(vinyl pyrrolidone)
SAR = specific absorption rate
SEM = scanning electron microscopy
SERS = surface-enhanced Raman scattering
TEM = transmission electron microscopy
UPD = underpotential deposition
UV−vis = ultraviolet−visible
V_{dep} = deposition rate
V_{diff} = diffusion rate
vdW = van der Waals
zb = zinc blende

REFERENCES

(1) Xia, Y.; Xiong, Y.; Lim, B.; Skrabalak, S. E. Shape-Controlled Synthesis of Metal Nanocrystals: Simple Chemistry Meets Complex Physics? *Angew. Chem., Int. Ed.* **2009**, *48*, 60−103.
(2) Verita, M.; Santopadre, P. Analysis of Gold-Colored Ruby Glass Tesserae in Roman Church Mosaics of the Fourth to 12th Centuries. *J. Glass Stud.* **2010**, *52*, 11−24.
(3) Barber, D. J.; Freestone, I. C. An Investigation of the Origin of the Color of the Lycurgus Cup by Analytical Transmission Electron Microscopy. *Archaeometry* **1990**, *32*, 33−45.
(4) Freestone, I.; Meeks, N.; Sax, M.; Higgitt, C. The Lycurgus Cup—A Roman Nanotechnology. *Gold Bull.* **2007**, *40*, 270−277.
(5) Faraday, M. Experimental Relations of Gold (and Other Metals) to Light. *Philos. Trans.* **1857**, *14*, 145−181.
(6) Feynman, R. P. There's Plenty of Room at the Bottom. *Eng. Sci.* **1960**, *23*, 22−36.
(7) Rycenga, M.; Cobley, C. M.; Zeng, J.; Li, W.; Moran, C. H.; Zhang, Q.; Qin, D.; Xia, Y. Controlling the Synthesis and Assembly of Silver Nanostructures for Plasmonic Applications. *Chem. Rev.* **2011**, *111*, 3669−3712.
(8) Kauranen, M.; Zayats, A. V. Nonlinear Plasmonics. *Nat. Photonics* **2012**, *6*, 737−748.
(9) Jones, M. R.; Osberg, K. D.; Macfarlane, R. J.; Langille, M. R.; Mirkin, C. A. Templated Techniques for the Synthesis and Assembly of Plasmonic Nanostructures. *Chem. Rev.* **2011**, *111*, 3736−3827.
(10) Lal, S.; Link, S.; Halas, N. J. Nano-Optics from Sensing to Waveguiding. *Nat. Photonics* **2007**, *1*, 641−648.
(11) Koenderink, A. F.; Alù, A.; Polman, A. Nanophotonics: Shrinking Light-Based Technology. *Science* **2015**, *348*, 516−521.
(12) Quan, L. N.; Kang, J.; Ning, C.-Z.; Yang, P. Nanowires for Photonics. *Chem. Rev.* **2019**, *119*, 9153−9169.
(13) Zhu, B.; Gong, S.; Cheng, W. Softening Gold for Elastronics. *Chem. Soc. Rev.* **2019**, *48*, 1668−1711.
(14) Kamyshny, A.; Magdassi, S. Conductive Nanomaterials for Printed Electronics. *Small* **2014**, *10*, 3515−3535.
(15) Talapin, D. V.; Lee, J.-S.; Kovalenko, M. V.; Shevchenko, E. V. Prospects of Colloidal Nanocrystals for Electronic and Optoelectronic Applications. *Chem. Rev.* **2010**, *110*, 389−458.
(16) Mayer, K. M.; Hafner, J. H. Localized Surface Plasmon Resonance Sensors. *Chem. Rev.* **2011**, *111*, 3828−3857.
(17) Konstantatos, G.; Sargent, E. H. Nanostructured Materials for Photon Detection. *Nat. Nanotechnol.* **2010**, *5*, 391−400.
(18) Shi, Y.; Lyu, Z.; Zhao, M.; Chen, R.; Nguyen, Q. N.; Xia, Y. Noble-Metal Nanocrystals with Controlled Shapes for Catalytic and Electrocatalytic Applications. *Chem. Rev.* **2021**, *121*, 649−735.
(19) Wu, Y.; Wang, D.; Li, Y. Nanocrystals from Solutions: Catalysts. *Chem. Soc. Rev.* **2014**, *43*, 2112−2124.
(20) Zhao, Z.; Chen, C.; Liu, Z.; Huang, J.; Wu, M.; Liu, H.; Li, Y.; Huang, Y. Pt-Based Nanocrystal for Electrocatalytic Oxygen Reduction. *Adv. Mater.* **2019**, *31*, 1808115.
(21) Yang, X.; Yang, M.; Pang, B.; Vara, M.; Xia, Y. Gold Nanomaterials at Work in Biomedicine. *Chem. Rev.* **2015**, *115*, 10410−10488.
(22) Dreaden, E. C.; Alkilany, A. M.; Huang, X.; Murphy, C. J.; El-Sayed, M. A. The Golden Age: Gold Nanoparticles for Biomedicine. *Chem. Soc. Rev.* **2012**, *41*, 2740−2779.
(23) Alivisatos, P. The Use of Nanocrystals in Biological Detection. *Nat. Biotechnol.* **2004**, *22*, 47−52.
(24) Gilroy, K. D.; Ruditskiy, A.; Peng, H.-C.; Qin, D.; Xia, Y. Bimetallic Nanocrystals: Syntheses, Properties, and Applications. *Chem. Rev.* **2016**, *116*, 10414−10472.
(25) Liu, X.; Wang, D.; Li, Y. Synthesis and Catalytic Properties of Bimetallic Nanomaterials with Various Architectures. *Nano Today* **2012**, *7*, 448−466.
(26) An, K.; Somorjai, G. A. Size and Shape Control of Metal Nanoparticles for Reaction Selectivity in Catalysis. *ChemCatChem.* **2012**, *4*, 1512−1524.
(27) Cao, S.; Tao, F. F.; Tang, Y.; Li, Y.; Yu, J. Size- and Shape-Dependent Catalytic Performances of Oxidation and Reduction Reactions on Nanocatalysts. *Chem. Soc. Rev.* **2016**, *45*, 4747−4765.
(28) Ringe, E.; McMahon, J. M.; Sohn, K.; Cobley, C.; Xia, Y.; Huang, J.; Schatz, G. C.; Marks, L. D.; Van Duyne, R. P. Unraveling the Effects of Size, Composition, and Substrate on the Localized Surface Plasmon Resonance Frequencies of Gold and Silver Nanocubes: A Systematic Single-Particle Approach. *J. Phys. Chem. C* **2010**, *114*, 12511−12516.

https://doi.org/10.1021/acs.chemrev.2c00468
Chem. Rev. 2023, 123, 3693−3760

(29) Xie, S.; Choi, S.-I.; Xia, X.; Xia, Y. Catalysis on Faceted Noble-Metal Nanocrystals: Both Shape and Size Matter. *Curr. Opin. Chem. Eng.* **2013**, *2*, 142−150.
(30) Burda, C.; Chen, X.; Narayanan, R.; El-Sayed, M. A. Chemistry and Properties of Nanocrystals of Different Shapes. *Chem. Rev.* **2005**, *105*, 1025−1102.
(31) Quan, Z.; Wang, Y.; Fang, J. High-Index Faceted Noble Metal Nanocrystals. *Acc. Chem. Res.* **2013**, *46*, 191−202.
(32) Yang, H. Platinum-Based Electrocatalysts with Core−Shell Nanostructures. *Angew. Chem., Int. Ed.* **2011**, *50*, 2674−2676.
(33) Xia, Y.; Yang, X. Toward Cost-Effective and Sustainable Use of Precious Metals in Heterogeneous Catalysts. *Acc. Chem. Res.* **2017**, *50*, 450−454.
(34) Chen, Y.; Fan, Z.; Zhang, Z.; Niu, W.; Li, C.; Yang, N.; Chen, B.; Zhang, H. Two-Dimensional Metal Nanomaterials: Synthesis, Properties, and Applications. *Chem. Rev.* **2018**, *118*, 6409−6455.
(35) Li, J.; Sun, S. Intermetallic Nanoparticles: Synthetic Control and Their Enhanced Electrocatalysis. *Acc. Chem. Res.* **2019**, *52*, 2015−2025.
(36) Xie, C.; Niu, Z.; Kim, D.; Li, M.; Yang, P. Surface and Interface Control in Nanoparticle Catalysis. *Chem. Rev.* **2020**, *120*, 1184−1249.
(37) Stewart, M. E.; Anderton, C. R.; Thompson, L. B.; Maria, J.; Gray, S. K.; Rogers, J. A.; Nuzzo, R. G. Nanostructured Plasmonic Sensors. *Chem. Rev.* **2008**, *108*, 494−521.
(38) Kelly, K. L.; Coronado, E.; Zhao, L. L.; Schatz, G. C. The Optical Properties of Metal Nanoparticles: The Influence of Size, Shape, and Dielectric Environment. *J. Phys. Chem. B* **2003**, *107*, 668−677.
(39) Jeong, U.; Teng, X.; Wang, Y.; Yang, H.; Xia, Y. Superparamagnetic Colloids: Controlled Synthesis and Niche Applications. *Adv. Mater.* **2007**, *19*, 33−60.
(40) Zhou, K.; Li, Y. Catalysis Based on Nanocrystals with Well-Defined Facets. *Angew. Chem., Int. Ed.* **2012**, *51*, 602−613.
(41) Ruditskiy, A.; Peng, H.-C.; Xia, Y. Shape-Controlled Metal Nanocrystals for Heterogeneous Catalysis. *Annu. Rev. Chem. Biomol. Eng.* **2016**, *7*, 327−348.
(42) Ruban, A.; Hammer, B.; Stoltze, P.; Skriver, H. L.; Norskov, J. K. Surface Electronic Structure and Reactivity of Transition and Noble Metals. *J. Mol. Catal. A: Chem.* **1997**, *115*, 421−429.
(43) Guo, S.; Zhang, S.; Sun, S. Tuning Nanoparticle Catalysis for the Oxygen Reduction Reaction. *Angew. Chem., Int. Ed.* **2013**, *52*, 8526−8544.
(44) Xia, Y.; Halas, N. J. Shape-Controlled Synthesis and Surface Plasmonic Properties of Metallic Nanostructures. *MRS Bull.* **2005**, *30*, 338−344.
(45) Eustis, S.; El-Sayed, M. A. Why Gold Nanoparticles Are More Precious Than Pretty Gold: Noble Metal Surface Plasmon Resonance and Its Enhancement of the Radiative and Nonradiative Properties of Nanocrystals of Different Shapes. *Chem. Soc. Rev.* **2006**, *35*, 209−217.
(46) Wiley, B. J.; Im, S. H.; Li, Z.-Y.; McLellan, J.; Siekkinen, A.; Xia, Y. Maneuvering the Surface Plasmon Resonance of Silver Nanostructures through Shape-Controlled Synthesis. *J. Phys. Chem. B* **2006**, *110*, 15666−15675.
(47) Evanoff, D. D., Jr.; Chumanov, G. Synthesis and Optical Properties of Silver Nanoparticles and Arrays. *ChemPhysChem* **2005**, *6*, 1221−1231.
(48) Zhang, Q.; Li, W.; Moran, C.; Zeng, J.; Chen, J.; Wen, L.-P.; Xia, Y. Seed-Mediated Synthesis of Ag Nanocubes with Controllable Edge Lengths in the Range of 30−200 nm and Comparison of Their Optical Properties. *J. Am. Chem. Soc.* **2010**, *132*, 11372−11378.
(49) Christopher, P.; Linic, S. Engineering Selectivity in Heterogeneous Catalysis: Ag Nanowires as Selective Ethylene Epoxidation Catalysts. *J. Am. Chem. Soc.* **2008**, *130*, 11264−11265.
(50) Christopher, P.; Linic, S. Shape- and Size-Specific Chemistry of Ag Nanostructures in Catalytic Ethylene Epoxidation. *ChemCatChem.* **2010**, *2*, 78−83.
(51) Zheng, Y.; Tao, J.; Liu, H.; Zeng, J.; Yu, T.; Ma, Y.; Moran, C.; Wu, L.; Zhu, Y.; Liu, J.; et al. Facile Synthesis of Gold Nanorice Enclosed by High-Index Facets and Its Application for CO Oxidation. *Small* **2011**, *7*, 2307−2312.
(52) Wang, C.; Daimon, H.; Lee, Y.; Kim, J.; Sun, S. Synthesis of Monodisperse Pt Nanocubes and Their Enhanced Catalysis for Oxygen Reduction. *J. Am. Chem. Soc.* **2007**, *129*, 6974−6975.
(53) Bratlie, K. M.; Lee, H.; Komvopoulos, K.; Yang, P.; Somorjai, G. A. Platinum Nanoparticle Shape Effects on Benzene Hydrogenation Selectivity. *Nano Lett.* **2007**, *7*, 3097−3101.
(54) Choi, S.-I.; Herron, J. A.; Scaranto, J.; Huang, H.; Wang, Y.; Xia, X.; Lv, T.; Park, J.; Peng, H.-C.; Mavrikakis, M.; et al. A Comprehensive Study of Formic Acid Oxidation on Palladium Nanocrystals with Different Types of Facets and Twin Defects. *ChemCatChem.* **2015**, *7*, 2077−2084.
(55) Park, K. H.; Jang, K.; Kim, H. J.; Son, S. U. Near-Monodisperse Tetrahedral Rhodium Nanoparticles on Charcoal: The Shape-Dependent Catalytic Hydrogenation of Arenes. *Angew. Chem.* **2007**, *119*, 1170−1173.
(56) Zhang, N.; Shao, Q.; Pi, Y.; Guo, J.; Huang, X. Solvent-Mediated Shape Tuning of Well-Defined Rhodium Nanocrystals for Efficient Electrochemical Water Splitting. *Chem. Mater.* **2017**, *29*, 5009−5015.
(57) Sánchez-Iglesias, A.; Pastoriza-Santos, I.; Pérez-Juste, J.; Rodríguez-González, B.; García de Abajo, F. J.; Liz-Marzán, L. M. Synthesis and Optical Properties of Gold Nanodecahedra with Size Control. *Adv. Mater.* **2006**, *18*, 2529−2534.
(58) Rodrigues, T. S.; Zhao, M.; Yang, T.-H.; Gilroy, K. D.; da Silva, A. G. M.; Camargo, P. H. C.; Xia, Y. Synthesis of Colloidal Metal Nanocrystals: A Comprehensive Review on the Reductants. *Chem. Eur. J.* **2018**, *24*, 16944−16963.
(59) Baletto, F.; Rapallo, A.; Rossi, G.; Ferrando, R. Dynamical Effects in the Formation of Magic Cluster Structures. *Phys. Rev. B* **2004**, *69*, 235421.
(60) Song, M.; Zhou, G.; Lu, N.; Lee, J.; Nakouzi, E.; Wang, H.; Li, D. Oriented Attachment Induces Fivefold Twins by Forming and Decomposing High-Energy Grain Boundaries. *Science* **2020**, *367*, 40−45.
(61) De Yoreo, J. J.; Gilbert, P. U. P. A.; Sommerdijk, N. A. J. M.; Penn, R. L.; Whitelam, S.; Joester, D.; Zhang, H.; Rimer, J. D.; Navrotsky, A.; Banfield, J. F.; et al. Crystallization by Particle Attachment in Synthetic, Biogenic, and Geologic Environments. *Science* **2015**, *349*, aaa6760.
(62) Thanh, N. T. K.; Maclean, N.; Mahiddine, S. Mechanisms of Nucleation and Growth of Nanoparticles in Solution. *Chem. Rev.* **2014**, *114*, 7610−7630.
(63) Zhang, Q.; Liu, S.-J.; Yu, S.-H. Recent Advances in Oriented Attachment Growth and Synthesis of Functional Materials: Concept, Evidence, Mechanism, and Future. *J. Mater. Chem.* **2009**, *19*, 191−207.
(64) Zhang, H.; De Yoreo, J. J.; Banfield, J. F. A Unified Description of Attachment-Based Crystal Growth. *ACS Nano* **2014**, *8*, 6526−6530.
(65) Xia, Y.; Gilroy, K. D.; Peng, H.-C.; Xia, X. Seed-Mediated Growth of Colloidal Metal Nanocrystals. *Angew. Chem., Int. Ed.* **2017**, *56*, 60−95.
(66) Gilroy, K. D.; Yang, X.; Xie, S.; Zhao, M.; Qin, D.; Xia, Y. Shape-Controlled Synthesis of Colloidal Metal Nanocrystals by Replicating the Surface Atomic Structure on the Seed. *Adv. Mater.* **2018**, *30*, 1706312.
(67) Walsh, M. J.; Tong, W.; Katz-Boon, H.; Mulvaney, P.; Etheridge, J.; Funston, A. M. A Mechanism for Symmetry Breaking and Shape Control in Single-Crystal Gold Nanorods. *Acc. Chem. Res.* **2017**, *50*, 2925−2935.
(68) Gilroy, K. D.; Peng, H.-C.; Yang, X.; Ruditskiy, A.; Xia, Y. Symmetry Breaking During Nanocrystal Growth. *Chem. Commun.* **2017**, *53*, 4530−4541.
(69) Skrabalak, S. E. Symmetry in Seeded Metal Nanocrystal Growth. *Acc. Mater. Res.* **2021**, *2*, 621−629.

https://doi.org/10.1021/acs.chemrev.2c00468
Chem. Rev. 2023, 123, 3693−3760

(70) Huo, D.; Kim, M. J.; Lyu, Z.; Shi, Y.; Wiley, B. J.; Xia, Y. One-Dimensional Metal Nanostructures: From Colloidal Syntheses to Applications. *Chem. Rev.* **2019**, *119*, 8972−9073.
(71) Tao, A. R.; Habas, S.; Yang, P. Shape Control of Colloidal Metal Nanocrystals. *Small* **2008**, *4*, 310−325.
(72) Xia, Y.; Xia, X.; Peng, H.-C. Shape-Controlled Synthesis of Colloidal Metal Nanocrystals: Thermodynamic versus Kinetic Products. *J. Am. Chem. Soc.* **2015**, *137*, 7947−7966.
(73) Zeng, J.; Zhu, C.; Tao, J.; Jin, M.; Zhang, H.; Li, Z.-Y.; Zhu, Y.; Xia, Y. Controlling the Nucleation and Growth of Silver on Palladium Nanocubes by Manipulating the Reaction Kinetics. *Angew. Chem., Int. Ed.* **2012**, *51*, 2354−2358.
(74) DeSantis, C. J.; Skrabalak, S. E. Core Values: Elucidating the Role of Seed Structure in the Synthesis of Symmetrically Branched Nanocrystals. *J. Am. Chem. Soc.* **2013**, *135*, 10−13.
(75) Chen, J.; Wiley, B. J.; Xia, Y. One-Dimensional Nanostructures of Metals: Large-Scale Synthesis and Some Potential Applications. *Langmuir* **2007**, *23*, 4120−4129.
(76) Xia, X.; Xia, Y. Symmetry Breaking During Seeded Growth of Nanocrystals. *Nano Lett.* **2012**, *12*, 6038−6042.
(77) Zhu, C.; Peng, H.-C.; Zeng, J.; Liu, J.; Gu, Z.; Xia, Y. Facile Synthesis of Gold Wavy Nanowires and Investigation of Their Growth Mechanism. *J. Am. Chem. Soc.* **2012**, *134*, 20234−20237.
(78) Zhang, Z.-P.; Wang, X.-Y.; Yuan, K.; Zhu, W.; Zhang, T.; Wang, Y.-H.; Ke, J.; Zheng, X.-Y.; Yan, C.-H.; Zhang, Y.-W. Free-Standing Iridium and Rhodium-Based Hierarchically-Coiled Ultrathin Nanosheets for Highly Selective Reduction of Nitrobenzene to Azoxybenzene under Ambient Conditions. *Nanoscale* **2016**, *8*, 15744−15752.
(79) Chen, R.; Nguyen, Q. N.; Xia, Y. Oriented Attachment: A Unique Mechanism for the Colloidal Synthesis of Metal Nanostructures. *ChemNanoMat* **2022**, *8*, e20210047.
(80) Wang, Y.; Choi, S.-I.; Zhao, X.; Xie, S.; Peng, H.-C.; Chi, M.; Huang, C. Z.; Xia, Y. Polyol Synthesis of Ultrathin Pd Nanowires via Attachment-Based Growth and Their Enhanced Activity Towards Formic Acid Oxidation. *Adv. Funct. Mater.* **2014**, *24*, 131−139.
(81) Yu, X.; Wang, D.; Peng, Q.; Li, Y. Pt−M (M = Cu, Co, Ni, Fe) Nanocrystals: From Small Nanoparticles to Wormlike Nanowires by Oriented Attachment. *Chem. Eur. J.* **2013**, *19*, 233−239.
(82) Lim, B.; Kobayashi, H.; Camargo, P. H. C.; Allard, L. F.; Liu, J.; Xia, Y. New Insights into the Growth Mechanism and Surface Structure of Palladium Nanocrystals. *Nano Res.* **2010**, *3*, 180−188.
(83) Xiao, D.; Wu, Z.; Song, M.; Chun, J.; Schenter, G. K.; Li, D. Silver Nanocube and Nanobar Growth via Anisotropic Monomer Addition and Particle Attachment Processes. *Langmuir* **2018**, *34*, 1466−1472.
(84) Wiley, B. J.; Chen, Y.; McLellan, J. M.; Xiong, Y.; Li, Z.-Y.; Ginger, D.; Xia, Y. Synthesis and Optical Properties of Silver Nanobars and Nanorice. *Nano Lett.* **2007**, *7*, 1032−1036.
(85) Song, Y.; Liu, K.; Chen, S. AgAu Bimetallic Janus Nanoparticles and Their Electrocatalytic Activity for Oxygen Reduction in Alkaline Media. *Langmuir* **2012**, *28*, 17143−17152.
(86) Qiu, J.; Nguyen, Q. N.; Lyu, Z.; Wang, Q.; Xia, Y. Bimetallic Janus Nanocrystals: Syntheses and Applications. *Adv. Mater.* **2022**, *34*, 2102591.
(87) Zheng, Z. K.; Tachikawa, T.; Majima, T. Single-Particle Study of Pt-Modified Au Nanorods for Plasmon-Enhanced Hydrogen Generation in Visible to Near-Infrared Region. *J. Am. Chem. Soc.* **2014**, *136*, 6870−6873.
(88) Wang, W.; Chiang, T.-Y.; Velegol, D.; Mallouk, T. E. Understanding the Efficiency of Autonomous Nano- and Microscale Motors. *J. Am. Chem. Soc.* **2013**, *135*, 10557−10565.
(89) Guo, C. F.; Ren, Z. Flexible Transparent Conductors Based on Metal Nanowire Networks. *Mater. Today* **2015**, *18*, 143−154.
(90) Tang, Y.; Gong, S.; Chen, Y.; Yap, L. W.; Cheng, W. Manufacturable Conducting Rubber Ambers and Stretchable Conductors from Copper Nanowire Aerogel Monoliths. *ACS Nano* **2014**, *8*, 5707−5714.
(91) Ye, S.; Rathmell, A. R.; Chen, Z.; Stewart, I. E.; Wiley, B. J. Metal Nanowire Networks: The Next Generation of Transparent Conductors. *Adv. Mater.* **2014**, *26*, 6670−6687.
(92) De, S.; Higgins, T. M.; Lyons, P. E.; Doherty, E. M.; Nirmalraj, P. N.; Blau, W. J.; Boland, J. J.; Coleman, J. N. Silver Nanowire Networks as Flexible, Transparent, Conducting Films: Extremely High DC to Optical Conductivity Ratios. *ACS Nano* **2009**, *3*, 1767−1774.
(93) Ji, X.; Song, X.; Li, J.; Bai, Y.; Yang, W.; Peng, X. Size Control of Gold Nanocrystals in Citrate Reduction: The Third Role of Citrate. *J. Am. Chem. Soc.* **2007**, *129*, 13939−13948.
(94) Yin, Y.; Li, Z.-Y.; Zhong, Z.; Gates, B.; Xia, Y.; Venkateswaran, S. Synthesis and Characterization of Stable Aqueous Dispersions of Silver Nanoparticles through the Tollens Process. *J. Mater. Chem.* **2002**, *12*, 522−527.
(95) Xiong, Y.; Xia, Y. Shape-Controlled Synthesis of Metal Nanostructures: The Case of Palladium. *Adv. Mater.* **2007**, *19*, 3385−3391.
(96) Liz-Marzán, L. M. Nanometals: Formation and Color. *Mater. Today* **2004**, *7*, 26−31.
(97) Storhoff, J. J.; Elghanian, R.; Mirkin, C. A.; Letsinger, R. L. Sequence-Dependent Stability of DNA-Modified Gold Nanoparticles. *Langmuir* **2002**, *18*, 6666−6670.
(98) Kim, F.; Connor, S.; Song, H.; Kuykendall, T.; Yang, P. Platonic Gold Nanocrystals. *Angew. Chem., Int. Ed.* **2004**, *43*, 3673−3677.
(99) Sun, Y.; Xia, Y. Shape-Controlled Synthesis of Gold and Silver Nanoparticles. *Science* **2002**, *298*, 2176−2179.
(100) Nguyen, Q. N.; Chen, R.; Lyu, Z.; Xia, Y. Using Reduction Kinetics to Control and Predict the Outcome of a Colloidal Synthesis of Noble-Metal Nanocrystals. *Inorg. Chem.* **2021**, *60*, 4182−4197.
(101) Tro, N. J.Solids and Modern Materials. In *Chemistry: A Molecular Approach*, 4th ed.; Pearson, 2017; pp 537−548.
(102) Atkins, P.; Overton, T.; Rourke, J.; Weller, M.; Armstrong, F.The Structures of Simple Solids. In *Shriver and Atkins' Inorganic Chemistry*, 5th ed.; W. H. Freeman, 2009; pp 65−110.
(103) Quinson, J.; Jensen, K. M. Ø. From Platinum Atoms in Molecules to Colloidal Nanoparticles: A Review on Reduction, Nucleation and Growth Mechanisms. *Adv. Colloid Interface Sci.* **2020**, *286*, 102300.
(104) Yao, T.; Sun, Z.; Li, Y.; Pan, Z.; Wei, H.; Xie, Y.; Nomura, M.; Niwa, Y.; Yan, W.; Wu, Z.; et al. Insights into Initial Kinetic Nucleation of Gold Nanocrystals. *J. Am. Chem. Soc.* **2010**, *132*, 7696−7701.
(105) Loh, N. D.; Sen, S.; Bosman, M.; Tan, S. F.; Zhong, J.; Nijhuis, C. A.; Král, P.; Matsudaira, P.; Mirsaidov, U. Multistep Nucleation of Nanocrystals in Aqueous Solution. *Nat. Chem.* **2017**, *9*, 77−82.
(106) Jin, B.; Wang, Y.; Liu, Z.; France-Lanord, A.; Grossman, J. C.; Jin, C.; Tang, R. Revealing the Cluster-Cloud and Its Role in Nanocrystallization. *Adv. Mater.* **2019**, *31*, 1808225.
(107) Janssen, A.; Nguyen, Q. N.; Xia, Y. Colloidal Metal Nanocrystals with Metastable Crystal Structures. *Angew. Chem., Int. Ed.* **2021**, *60*, 12192−12203.
(108) Kibey, S.; Liu, J. B.; Johnson, D. D.; Sehitoglu, H. Predicting Twinning Stress in fcc Metals: Linking Twin-Energy Pathways to Twin Nucleation. *Acta Mater.* **2007**, *55*, 6843−6851.
(109) Germain, V.; Li, J.; Ingert, D.; Wang, Z. L.; Pileni, M. P. Stacking Faults in Formation of Silver Nanodisks. *J. Phys. Chem. B* **2003**, *107*, 8717−8720.
(110) Kirkland, A. I.; Jefferson, D. A.; Duff, D. G.; Edwards, P. P.; Gameson, I.; Johnson, B. F. G.; Smith, D. J. Structural Studies of Trigonal Lamellar Particles of Gold and Silver. *Proc. R. Soc. London, Ser. A* **1993**, *440*, 589−609.
(111) Huang, X.; Li, S.; Huang, Y.; Wu, S.; Zhou, X.; Li, S.; Gan, C. L.; Boey, F.; Mirkin, C. A.; Zhang, H. Synthesis of Hexagonal Close-Packed Gold Nanostructures. *Nat. Commun.* **2011**, *2*, 292.
(112) Colombi Ciacchi, L.; Pompe, W.; De Vita, A. Initial Nucleation of Platinum Clusters after Reduction of K_2PtCl_4 in

https://doi.org/10.1021/acs.chemrev.2c00468
Chem. Rev. 2023, 123, 3693−3760

Aqueous Solution: A First Principles Study. *J. Am. Chem. Soc.* **2001**, *123*, 7371−7380.
(113) Colombi Ciacchi, L.; Mertig, M.; Pompe, W.; Meriani, S.; De Vita, A. Nucleation and Growth of Platinum Clusters in Solution and on Biopolymers. *Platinum Met. Rev.* **2003**, *47*, 98−107.
(114) Colombi Ciacchi, L.; Pompe, W.; De Vita, A. Growth of Platinum Clusters via Addition of Pt(II) Complexes: A First Principles Investigation. *J. Phys. Chem. B* **2003**, *107*, 1755−1764.
(115) Widegren, J. A.; Bennett, M. A.; Finke, R. G. Is It Homogeneous or Heterogeneous Catalysis? Identification of Bulk Ruthenium Metal as the True Catalyst in Benzene Hydrogenations Starting with the Monometallic Precursor, Ru(II)(η^6-C_6Me_6)$(OAc)_2$, Plus Kinetic Characterization of the Heterogeneous Nucleation, Then Autocatalytic Surface-Growth Mechanism of Metal Film Formation. *J. Am. Chem. Soc.* **2003**, *125*, 10301−10310.
(116) Finney, E. E.; Finke, R. G. Nanocluster Nucleation and Growth Kinetic and Mechanistic Studies: A Review Emphasizing Transition-Metal Nanoclusters. *J. Colloid Interface Sci.* **2008**, *317*, 351−374.
(117) Besson, C.; Finney, E. E.; Finke, R. G. Nanocluster Nucleation, Growth, and Then Agglomeration Kinetic and Mechanistic Studies: A More General, Four-Step Mechanism Involving Double Autocatalysis. *Chem. Mater.* **2005**, *17*, 4925−4938.
(118) Watzky, M. A.; Finke, R. G. Transition Metal Nanocluster Formation Kinetic and Mechanistic Studies. A New Mechanism When Hydrogen Is the Reductant: Slow, Continuous Nucleation and Fast Autocatalytic Surface Growth. *J. Am. Chem. Soc.* **1997**, *119*, 10382−10400.
(119) Yang, T.-H.; Shi, Y.; Janssen, A.; Xia, Y. Surface Capping Agents and Their Roles in Shape-Controlled Synthesis of Colloidal Metal Nanocrystals. *Angew. Chem., Int. Ed.* **2020**, *59*, 15378−15401.
(120) Lamer, V. K.; Dinegar, R. H. Theory, Production and Mechanism of Formation of Monodispersed Hydrosols. *J. Am. Chem. Soc.* **1950**, *72*, 4847−4854.
(121) Zheng, Y.; Zeng, J.; Ruditskiy, A.; Liu, M.; Xia, Y. Oxidative Etching and Its Role in Manipulating the Nucleation and Growth of Noble-Metal Nanocrystals. *Chem. Mater.* **2014**, *26*, 22−33.
(122) Long, R.; Zhou, S.; Wiley, B. J.; Xiong, Y. Oxidative Etching for Controlled Synthesis of Metal Nanocrystals: Atomic Addition and Subtraction. *Chem. Soc. Rev.* **2014**, *43*, 6288−6310.
(123) Aiken, J. D., III; Finke, R. G. A Review of Modern Transition-Metal Nanoclusters: Their Synthesis, Characterization, and Applications in Catalysis. *J. Mol. Catal. A: Chem.* **1999**, *145*, 1−44.
(124) Li, J.; Li, X.; Zhai, H.-J.; Wang, L.-S. Au_{20}: A Tetrahedral Cluster. *Science* **2003**, *299*, 864−867.
(125) Baletto, F.; Ferrando, R.; Fortunelli, A.; Montalenti, F.; Mottet, C. Crossover among Structural Motifs in Transition and Noble-Metal Clusters. *J. Chem. Phys.* **2002**, *116*, 3856−3863.
(126) Schmid, G. Large Clusters and Colloids. Metals in the Embryonic State. *Chem. Rev.* **1992**, *92*, 1709−1727.
(127) Zhang, H. J.; Schmid, G.; Hartmann, U. Reduced Metallic Properties of Ligand-Stabilized Small Metal Clusters. *Nano Lett.* **2003**, *3*, 305−307.
(128) Zhang, H.-F.; Stender, M.; Zhang, R.; Wang, C.; Li, J.; Wang, L.-S. Toward the Solution Synthesis of the Tetrahedral Au_{20} Cluster. *J. Phys. Chem. B* **2004**, *108*, 12259−12263.
(129) Barmparis, G. D.; Lodziana, Z.; Lopez, N.; Remediakis, I. N. Nanoparticle Shapes by Using Wulff Constructions and First-Principles Calculations. *Beilstein J. Nanotechnol.* **2015**, *6*, 361−368.
(130) Wulff, G. Zur Frage der Geschwindigkeit des Wachsthums und der Auflösung der Krystallflächen. *Z. Kristallogr. - Cryst. Mater.* **1901**, *34*, 449−530.
(131) Markov, I. V.Crystal-Ambient Phase Equilibrium. In *Crystal Growth for Beginners: Fundamentals of Nucleation, Crystal Growth and Epitaxy*; World Scientific: Singapore, 1995; pp 1−62.
(132) Vitos, L.; Ruban, A. V.; Skriver, H. L.; Kollár, J. The Surface Energy of Metals. *Surf. Sci.* **1998**, *411*, 186−202.
(133) Wang, Y.; Peng, H.-C.; Liu, J.; Huang, C. Z.; Xia, Y. Use of Reduction Rate as a Quantitative Knob for Controlling the Twin Structure and Shape of Palladium Nanocrystals. *Nano Lett.* **2015**, *15*, 1445−1450.
(134) Froseth, A. G.; Derlet, P. M.; Van Swygenhoven, H. Twinning in Nanocrystalline fcc Metals. *Adv. Eng. Mater.* **2005**, *7*, 16−20.
(135) Ding, J.; Yu, Q.; Asta, M.; Ritchie, R. O. Tunable Stacking Fault Energies by Tailoring Local Chemical Order in CrCoNi Medium-Entropy Alloys. *Proc. Natl. Acad. Sci. U.S.A.* **2018**, *115*, 8919−8924.
(136) Rosengaard, N. M.; Skriver, H. L. Calculated Stacking-Fault Energies of Elemental Metals. *Phys. Rev. B: Condens. Matter Mater. Phys.* **1993**, *47*, 12865−12873.
(137) Xia, X.; Choi, S.-I.; Herron, J. A.; Lu, N.; Scaranto, J.; Peng, H.-C.; Wang, J.; Mavrikakis, M.; Kim, M. J.; Xia, Y. Facile Synthesis of Palladium Right Bipyramids and Their Use as Seeds for Overgrowth and as Catalysts for Formic Acid Oxidation. *J. Am. Chem. Soc.* **2013**, *135*, 15706−15709.
(138) Chen, R.; Shi, Y.; Xie, M.; Xia, Y. Facile Synthesis of Platinum Right Bipyramids by Separating and Controlling the Nucleation Step in a Continuous Flow System. *Chem. Eur. J.* **2021**, *27*, 13855−13863.
(139) Lyu, Z.; Xie, M.; Gilroy, K. D.; Hood, Z. D.; Zhao, M.; Zhou, S.; Liu, J.; Xia, Y. A Rationally Designed Route to the One-Pot Synthesis of Right Bipyramidal Nanocrystals of Copper. *Chem. Mater.* **2018**, *30*, 6469−6477.
(140) Wiley, B. J.; Xiong, Y.; Li, Z.-Y.; Yin, Y.; Xia, Y. Right Bipyramids of Silver: A New Shape Derived from Single Twinned Seeds. *Nano Lett.* **2006**, *6*, 765−768.
(141) Ruan, L.; Chiu, C.-Y.; Li, Y.; Huang, Y. Synthesis of Platinum Single-Twinned Right Bipyramid and {111}-Bipyramid through Targeted Control over Both Nucleation and Growth Using Specific Peptides. *Nano Lett.* **2011**, *11*, 3040−3046.
(142) Wu, D.; Cao, M.; Cao, R. Ru-Assisted Synthesis of {111}-Faceted Pd Truncated Bipyramids: A Highly Reactive, Stable and Restorable Catalyst for Formic Acid Oxidation. *Chem. Commun.* **2014**, *50*, 12970−12972.
(143) Personick, M. L.; Langille, M. R.; Zhang, J.; Harris, N.; Schatz, G. C.; Mirkin, C. A. Synthesis and Isolation of {110}-Faceted Gold Bipyramids and Rhombic Dodecahedra. *J. Am. Chem. Soc.* **2011**, *133*, 6170−6173.
(144) Zhou, S.; Zhao, M.; Yang, T.-H.; Xia, Y. Decahedral Nanocrystals of Noble Metals: Synthesis, Characterization, and Applications. *Mater. Today* **2019**, *22*, 108−131.
(145) Wang, H.; Zhou, S.; Gilroy, K. D.; Cai, Z.; Xia, Y. Icosahedral Nanocrystals of Noble Metals: Synthesis and Applications. *Nano Today* **2017**, *15*, 121−144.
(146) Casillas, G.; Velázquez-Salazar, J. J.; Jose-Yacaman, M. A New Mechanism of Stabilization of Large Decahedral Nanoparticles. *J. Phys. Chem. C* **2012**, *116*, 8844−8848.
(147) Johnson, C. L.; Snoeck, E.; Ezcurdia, M.; Rodríguez-González, B.; Pastoriza-Santos, I.; Liz-Marzán, L. M.; Hÿtch, M. J. Effects of Elastic Anisotropy on Strain Distributions in Decahedral Gold Nanoparticles. *Nat. Mater.* **2008**, *7*, 120−124.
(148) Huang, L.; Shan, A.; Li, Z.; Chen, C.; Wang, R. Phase Formation, Magnetic and Optical Properties of Epitaxially Grown Icosahedral Au@Ni Nanoparticles with Ultrathin Shells. *CrystEngComm* **2013**, *15*, 2527−2531.
(149) Haji-Akbari, A.; Engel, M.; Keys, A. S.; Zheng, X.; Petschek, R. G.; Palffy-Muhoray, P.; Glotzer, S. C. Disordered, Quasicrystalline and Crystalline Phases of Densely Packed Tetrahedra. *Nature* **2009**, *462*, 773−777.
(150) Sneed, B. T.; Young, A. P.; Tsung, C.-K. Building up Strain in Colloidal Metal Nanoparticle Catalysts. *Nanoscale* **2015**, *7*, 12248−12265.
(151) Lofton, C.; Sigmund, W. Mechanisms Controlling Crystal Habits of Gold and Silver Colloids. *Adv. Funct. Mater.* **2005**, *15*, 1197−1208.
(152) Barnard, A. S.; Young, N. P.; Kirkland, A. I.; van Huis, M. A.; Xu, H. Nanogold: A Quantitative Phase Map. *ACS Nano* **2009**, *3*, 1431−1436.

https://doi.org/10.1021/acs.chemrev.2c00468
Chem. Rev. 2023, 123, 3693−3760

(153) Xiong, Y.; McLellan, J. M.; Chen, J.; Yin, Y.; Li, Z.-Y.; Xia, Y. Kinetically Controlled Synthesis of Triangular and Hexagonal Nanoplates of Palladium and Their SPR/SERS Properties. *J. Am. Chem. Soc.* **2005**, *127*, 17118−17127.
(154) Xiong, Y.; Washio, I.; Chen, J.; Cai, H.; Li, Z.-Y.; Xia, Y. Poly(vinyl pyrrolidone): A Dual Functional Reductant and Stabilizer for the Facile Synthesis of Noble Metal Nanoplates in Aqueous Solutions. *Langmuir* **2006**, *22*, 8563−8570.
(155) Washio, I.; Xiong, Y.; Yin, Y.; Xia, Y. Reduction by the End Groups of Poly(vinyl pyrrolidone): A New and Versatile Route to the Kinetically Controlled Synthesis of Ag Triangular Nanoplates. *Adv. Mater.* **2006**, *18*, 1745−1749.
(156) Deivaraj, T. C.; Lala, N. L.; Lee, J. Y. Solvent-Induced Shape Evolution of PVP Protected Spherical Silver Nanoparticles into Triangular Nanoplates and Nanorods. *J. Colloid Interface Sci.* **2005**, *289*, 402−409.
(157) Chen, L.; Ji, F.; Xu, Y.; He, L.; Mi, Y.; Bao, F.; Sun, B.; Zhang, X.; Zhang, Q. High-Yield Seedless Synthesis of Triangular Gold Nanoplates through Oxidative Etching. *Nano Lett.* **2014**, *14*, 7201−7206.
(158) Yang, T.-H.; Gilroy, K. D.; Xia, Y. Reduction Rate as a Quantitative Knob for Achieving Deterministic Synthesis of Colloidal Metal Nanocrystals. *Chem. Sci.* **2017**, *8*, 6730−6749.
(159) Wang, Y.; He, J.; Liu, C.; Chong, W. H.; Chen, H. Thermodynamics versus Kinetics in Nanosynthesis. *Angew. Chem., Int. Ed.* **2015**, *54*, 2022−2051.
(160) Baletto, F.; Ferrando, R. Structural Properties of Nanoclusters: Energetic, Thermodynamic, and Kinetic Effects. *Rev. Mod. Phys.* **2005**, *77*, 371−423.
(161) Yin, X.; Shi, M.; Wu, J.; Pan, Y.-T.; Gray, D. L.; Bertke, J. A.; Yang, H. Quantitative Analysis of Different Formation Modes of Platinum Nanocrystals Controlled by Ligand Chemistry. *Nano Lett.* **2017**, *17*, 6146−6150.
(162) Yang, T.-H.; Zhou, S.; Gilroy, K. D.; Figueroa-Cosme, L.; Lee, Y.-H.; Wu, J.-M.; Xia, Y. Autocatalytic Surface Reduction and Its Role in Controlling Seed-Mediated Growth of Colloidal Metal Nanocrystals. *Proc. Natl. Acad. Sci. U.S.A.* **2017**, *114*, 13619−13624.
(163) Yang, T.-H.; Peng, H.-C.; Zhou, S.; Lee, C.-T.; Bao, S.; Lee, Y.-H.; Wu, J.-M.; Xia, Y. Toward a Quantitative Understanding of the Reduction Pathways of a Salt Precursor in the Synthesis of Metal Nanocrystals. *Nano Lett.* **2017**, *17*, 334−340.
(164) Vara, M.; Xia, Y. Facile Synthesis of Pd Concave Nanocubes: From Kinetics to Mechanistic Understanding and Rationally Designed Protocol. *Nano Res.* **2018**, *11*, 3122−3131.
(165) Xie, M.; Zhou, S.; Zhu, J.; Lyu, Z.; Chen, R.; Xia, Y. A Quantitative Analysis of the Reduction Kinetics Involved in the Synthesis of Au@Pd Concave Nanocubes. *Chem. Eur. J.* **2019**, *25*, 16397−16404.
(166) Zhou, S.; Yang, T.-H.; Zhao, M.; Xia, Y. Quantitative Analysis of the Reduction Kinetics of a Pt(II) Precursor in the Context of Pt Nanocrystal Synthesis. *Chin. J. Chem. Phys.* **2018**, *31*, 370−374.
(167) Luty-Błocho, M.; Pacławski, K.; Wojnicki, M.; Fitzner, K. The Kinetics of Redox Reaction of Gold(III) Chloride Complex Ions with L-Ascorbic Acid. *Inorg. Chim. Acta* **2013**, *395*, 189−196.
(168) Figueroa-Cosme, L.; Hood, Z. D.; Gilroy, K. D.; Xia, Y. A Facile, Robust and Scalable Method for the Synthesis of Pd Nanoplates with Hydroxylamine as a Reducing Agent and Mechanistic Insights from Kinetic Analysis. *J. Mater. Chem. C* **2018**, *6*, 4677−4682.
(169) Huang, H.; Wang, Y.; Ruditskiy, A.; Peng, H.-C.; Zhao, X.; Zhang, L.; Liu, J.; Ye, Z.; Xia, Y. Polyol Syntheses of Palladium Decahedra and Icosahedra as Pure Samples by Maneuvering the Reaction Kinetics with Additives. *ACS Nano* **2014**, *8*, 7041−7050.
(170) Ruditskiy, A.; Zhao, M.; Gilroy, K. D.; Vara, M.; Xia, Y. Toward a Quantitative Understanding of the Sulfate-Mediated Synthesis of Pd Decahedral Nanocrystals with High Conversion and Morphology Yields. *Chem. Mater.* **2016**, *28*, 8800−8806.
(171) Lee, C.-T.; Wang, H.; Zhao, M.; Yang, T.-H.; Vara, M.; Xia, Y. One-Pot Synthesis of Pd@Pt_{nL} Core−Shell Icosahedral Nanocrystals in High Throughput through a Quantitative Analysis of the Reduction Kinetics. *Chem. Eur. J.* **2019**, *25*, 5322−5329.
(172) Zhou, M.; Wang, H.; Vara, M.; Hood, Z. D.; Luo, M.; Yang, T.-H.; Bao, S.; Chi, M.; Xiao, P.; Zhang, Y.; et al. Quantitative Analysis of the Reduction Kinetics Responsible for the One-Pot Synthesis of Pd−Pt Bimetallic Nanocrystals with Different Structures. *J. Am. Chem. Soc.* **2016**, *138*, 12263−12270.
(173) Biacchi, A. J.; Schaak, R. E. The Solvent Matters: Kinetic versus Thermodynamic Shape Control in the Polyol Synthesis of Rhodium Nanoparticles. *ACS Nano* **2011**, *5*, 8089−8099.
(174) Qian, J.; Shen, M.; Zhou, S.; Lee, C.-T.; Zhao, M.; Lyu, Z.; Hood, Z. D.; Vara, M.; Gilroy, K. D.; Wang, K.; et al. Synthesis of Pt Nanocrystals with Different Shapes Using the Same Protocol to Optimize Their Catalytic Activity toward Oxygen Reduction. *Mater. Today* **2018**, *21*, 834−844.
(175) Wiley, B.; Herricks, T.; Sun, Y.; Xia, Y. Polyol Synthesis of Silver Nanoparticles: Use of Chloride and Oxygen to Promote the Formation of Single-Crystal, Truncated Cubes and Tetrahedrons. *Nano Lett.* **2004**, *4*, 1733−1739.
(176) Chen, R.; Nguyen, Q. N.; Zhao, M.; Chen, Z.; Chi, M.; Xia, Y. A Simple Route to the Synthesis of Pt Nanobars and the Mechanistic Understanding of Symmetry Reduction. *Chem. Eur. J.* **2021**, *27*, 2760−2766.
(177) Xiong, Y.; Cai, H.; Wiley, B. J.; Wang, J.; Kim, M. J.; Xia, Y. Synthesis and Mechanistic Study of Palladium Nanobars and Nanorods. *J. Am. Chem. Soc.* **2007**, *129*, 3665−3675.
(178) Xiong, Y.; McLellan, J. M.; Yin, Y.; Xia, Y. Synthesis of Palladium Icosahedra with Twinned Structure by Blocking Oxidative Etching with Citric Acid or Citrate Ions. *Angew. Chem., Int. Ed.* **2007**, *46*, 790−794.
(179) Xu, J.; Li, S.; Weng, J.; Wang, X.; Zhou, Z.; Yang, K.; Liu, M.; Chen, X.; Cui, Q.; Cao, M.; et al. Hydrothermal Syntheses of Gold Nanocrystals: From Icosahedral to Its Truncated Form. *Adv. Funct. Mater.* **2008**, *18*, 277−284.
(180) Yang, T.-H.; Zhou, S.; Zhao, M.; Xia, Y. Quantitative Analysis of the Multiple Roles Played by Halide Ions in Controlling the Growth Patterns of Palladium Nanocrystals. *ChemNanoMat* **2020**, *6*, 576−588.
(181) Peng, H.-C.; Park, J.; Zhang, L.; Xia, Y. Toward a Quantitative Understanding of Symmetry Reduction Involved in the Seed-Mediated Growth of Pd Nanocrystals. *J. Am. Chem. Soc.* **2015**, *137*, 6643−6652.
(182) Tong, W. M.; Walsh, M. J.; Mulvaney, P.; Etheridge, J.; Funston, A. M. Control of Symmetry Breaking Size and Aspect Ratio in Gold Nanorods: Underlying Role of Silver Nitrate. *J. Phys. Chem. C* **2017**, *121*, 3549−3559.
(183) Walsh, M. J.; Barrow, S. J.; Tong, W. M.; Funston, A. M.; Etheridge, J. Symmetry Breaking and Silver in Gold Nanorod Growth. *ACS Nano* **2015**, *9*, 715−724.
(184) González-Rubio, G.; Scarabelli, L.; Guerrero-Martínez, A.; Liz-Marzán, L. M. Surfactant-Assisted Symmetry Breaking in Colloidal Gold Nanocrystal Growth. *ChemNanoMat* **2020**, *6*, 698−707.
(185) Zhang, J.; Li, H.; Jiang, Z.; Xie, Z. Size and Shape Controlled Synthesis of Pd Nanocrystals. *Phys. Sci. Rev.* **2018**, *3*, 20170101.
(186) Zheng, H.; Smith, R. K.; Jun, Y.-W.; Kisielowski, C.; Dahmen, U.; Alivisatos, A. P. Observation of Single Colloidal Platinum Nanocrystal Growth Trajectories. *Science* **2009**, *324*, 1309−1312.
(187) Ma, Y.; Gao, W.; Shan, H.; Chen, W.; Shang, W.; Tao, P.; Song, C.; Addiego, C.; Deng, T.; Pan, X.; et al. Platinum-Based Nanowires as Active Catalysts toward Oxygen Reduction Reaction: in situ Observation of Surface-Diffusion-Assisted, Solid-State Oriented Attachment. *Adv. Mater.* **2017**, *29*, 1703460.
(188) Hong, X.; Wang, D.; Yu, R.; Yan, H.; Sun, Y.; He, L.; Niu, Z.; Peng, Q.; Li, Y. Ultrathin Au−Ag Bimetallic Nanowires with Coulomb Blockade Effects. *Chem. Commun.* **2011**, *47*, 5160−5162.
(189) Woessner, Z. J.; Skrabalak, S. E. Symmetry-Reduced Metal Nanostructures Offer New Opportunities in Plasmonics and Catalysis. *J. Phys. Chem. C* **2021**, *125*, 23587−23596.

https://doi.org/10.1021/acs.chemrev.2c00468
Chem. Rev. 2023, 123, 3693−3760

(190) Li, Y.; Lin, H.; Zhou, W.; Sun, L.; Samanta, D.; Mirkin, C. A. Corner-, Edge-, and Facet-Controlled Growth of Nanocrystals. *Sci. Adv.* **2021**, *7*, eabf1410.
(191) Lohse, S. E.; Burrows, N. D.; Scarabelli, L.; Liz-Marzán, L. M.; Murphy, C. J. Anisotropic Noble Metal Nanocrystal Growth: The Role of Halides. *Chem. Mater.* **2014**, *26*, 34−43.
(192) Cobley, C. M.; Rycenga, M.; Zhou, F.; Li, Z.-Y.; Xia, Y. Etching and Growth: An Intertwined Pathway to Silver Nanocrystals with Exotic Shapes. *Angew. Chem., Int. Ed.* **2009**, *48*, 4824−4827.
(193) González-Rubio, G.; de Oliveira, T. M.; Altantzis, T.; La Porta, A.; Guerrero-Martínez, A.; Bals, S.; Scarabelli, L.; Liz-Marzán, L. M. Disentangling the Effect of Seed Size and Crystal Habit on Gold Nanoparticle Seeded Growth. *Chem. Commun.* **2017**, *53*, 11360−11363.
(194) Jin, B.; Sushko, M. L.; Liu, Z.; Cao, X.; Jin, C.; Tang, R. Understanding Anisotropic Growth of Au Penta-Twinned Nanorods by Liquid Cell Transmission Electron Microscopy. *J. Phys. Chem. Lett.* **2019**, *10*, 1443−1449.
(195) Kim, M. J.; Cruz, M. A.; Chen, Z.; Xu, H.; Brown, M.; Fichthorn, K. A.; Wiley, B. J. Isotropic Iodide Adsorption Causes Anisotropic Growth of Copper Microplates. *Chem. Mater.* **2021**, *33*, 881−891.
(196) Xu, H.; Wiley, B. J. The Roles of Citrate and Defects in the Anisotropic Growth of Ag Nanostructures. *Chem. Mater.* **2021**, *33*, 8301−8311.
(197) Lv, W.; He, W.; Wang, X.; Niu, Y.; Cao, H.; Dickerson, J. H.; Wang, Z. Understanding the Oriented-Attachment Growth of Nanocrystals from an Energy Point of View: A Review. *Nanoscale* **2014**, *6*, 2531−2547.
(198) Salzmann, B. B. V.; van der Sluijs, M. M.; Soligno, G.; Vanmaekelbergh, D. Oriented Attachment: From Natural Crystal Growth to a Materials Engineering Tool. *Acc. Chem. Res.* **2021**, *54*, 787−797.
(199) Niederberger, M.; Cölfen, H. Oriented Attachment and Mesocrystals: Non-Classical Crystallization Mechanisms Based on Nanoparticle Assembly. *Phys. Chem. Chem. Phys.* **2006**, *8*, 3271−3287.
(200) Jing, S.; Guo, X.; Tan, Y. Branched Pd and Pd-Based Trimetallic Nanocrystals with Highly Open Structures for Methanol Electrooxidation. *J. Mater. Chem. A* **2016**, *4*, 7950−7961.
(201) Lu, S.; Eid, K.; Deng, Y.; Guo, J.; Wang, L.; Wang, H.; Gu, H. One-Pot Synthesis of PtIr Tripods with a Dendritic Surface as an Efficient Catalyst for the Oxygen Reduction Reaction. *J. Mater. Chem. A* **2017**, *5*, 9107−9112.
(202) Liang, H.; Yang, H.; Wang, W.; Li, J.; Xu, H. High-Yield Uniform Synthesis and Microstructure-Determination of Rice-Shaped Silver Nanocrystals. *J. Am. Chem. Soc.* **2009**, *131*, 6068−6069.
(203) Huang, W.; Kang, X.; Xu, C.; Zhou, J.; Deng, J.; Li, Y.; Cheng, S. 2D PdAg Alloy Nanodendrites for Enhanced Ethanol Electrooxidation. *Adv. Mater.* **2018**, *30*, 1706962.
(204) Lu, S.; Eid, K.; Ge, D.; Guo, J.; Wang, L.; Wang, H.; Gu, H. One-Pot Synthesis of PtRu Nanodendrites as Efficient Catalysts for Methanol Oxidation Reaction. *Nanoscale* **2017**, *9*, 1033−1039.
(205) Liang, H.; Zhao, H.; Rossouw, D.; Wang, W.; Xu, H.; Botton, G. A.; Ma, D. Silver Nanorice Structures: Oriented Attachment-Dominated Growth, High Environmental Sensitivity, and Real-Space Visualization of Multipolar Resonances. *Chem. Mater.* **2012**, *24*, 2339−2346.
(206) Zhang, H.; Banfield, J. F. Energy Calculations Predict Nanoparticle Attachment Orientations and Asymmetric Crystal Formation. *J. Phys. Chem. Lett.* **2012**, *3*, 2882−2886.
(207) Balankura, T.; Yan, T. Y.; Jahanmahin, O.; Narukatpichai, J.; Ng, A.; Fichthorn, K. A. Oriented Attachment Mechanism of Triangular Ag Nanoplates: A Molecular Dynamics Study. *Nanoscale Adv.* **2020**, *2*, 2265−2270.
(208) Welch, D. A.; Woehl, T. J.; Park, C.; Faller, R.; Evans, J. E.; Browning, N. D. Understanding the Role of Solvation Forces on the Preferential Attachment of Nanoparticles in Liquid. *ACS Nano* **2016**, *10*, 181−187.
(209) Aabdin, Z.; Lu, J.; Zhu, X.; Anand, U.; Loh, N. D.; Su, H.; Mirsaidov, U. Bonding Pathways of Gold Nanocrystals in Solution. *Nano Lett.* **2014**, *14*, 6639−6643.
(210) Zhang, Y.; He, W.; Wen, K.; Wang, X.; Lu, H.; Lin, X.; Dickerson, J. H. Quantitative Evaluation of Coulombic Interactions in the Oriented-Attachment Growth of Nanotubes. *Analyst* **2014**, *139*, 371−374.
(211) Halder, A.; Ravishankar, N. Ultrafine Single-Crystalline Gold Nanowire Arrays by Oriented Attachment. *Adv. Mater.* **2007**, *19*, 1854−1858.
(212) Zhu, C.; Liang, S.; Song, E.; Zhou, Y.; Wang, W.; Shan, F.; Shi, Y.; Hao, C.; Yin, K.; Zhang, T.; et al. In-situ Liquid Cell Transmission Electron Microscopy Investigation on Oriented Attachment of Gold Nanoparticles. *Nat. Commun.* **2018**, *9*, 1−7.
(213) Sun, Y. Silver Nanowires − Unique Templates for Functional Nanostructures. *Nanoscale* **2010**, *2*, 1626−1642.
(214) Sannicolo, T.; Lagrange, M.; Cabos, A.; Celle, C.; Simonato, J.-P.; Bellet, D. Metallic Nanowire-Based Transparent Electrodes for Next Generation Flexible Devices: A Review. *Small* **2016**, *12*, 6052−6075.
(215) Shen, Y.; Gong, B.; Xiao, K.; Wang, L. In situ Assembly of Ultrathin PtRh Nanowires to Graphene Nanosheets as Highly Efficient Electrocatalysts for the Oxidation of Ethanol. *ACS Appl. Mater. Interfaces* **2017**, *9*, 3535−3543.
(216) Li, B.; Wen, X.; Li, R.; Wang, Z.; Clem, P. G.; Fan, H. Stress-Induced Phase Transformation and Optical Coupling of Silver Nanoparticle Superlattices into Mechanically Stable Nanowires. *Nat. Commun.* **2014**, *5*, 4179.
(217) Jiang, X.; Fu, G.; Wu, X.; Liu, Y.; Zhang, M.; Sun, D.; Xu, L.; Tang, Y. Ultrathin AgPt Alloy Nanowires as a High-Performance Electrocatalyst for Formic Acid Oxidation. *Nano Res.* **2018**, *11*, 499−510.
(218) Cao, Y.; Yang, Y.; Shan, Y.; Fu, C.; Long, N. V.; Huang, Z.; Guo, X.; Nogami, M. Large-Scale Template-Free Synthesis of Ordered Mesoporous Platinum Nanocubes and Their Electrocatalytic Properties. *Nanoscale* **2015**, *7*, 19461−19467.
(219) Zhang, H.; Li, W.; Jin, M.; Zeng, J.; Yu, T.; Yang, D.; Xia, Y. Controlling the Morphology of Rhodium Nanocrystals by Manipulating the Growth Kinetics with a Syringe Pump. *Nano Lett.* **2011**, *11*, 898−903.
(220) Janssen, A.; Shi, Y.; Xia, Y. Separating Growth from Nucleation for Facile Control over the Size and Shape of Palladium Nanocrystals. *Chem. Eur. J.* **2020**, *26*, 13890−13895.
(221) Newnham, R. E.Chemical Anisotropy. In *Properties of Materials: Anisotropy, Symmetry, Structure*; Oxford University Press: Oxford, 2004; pp 354−368.
(222) Wu, H.-L.; Kuo, C.-H.; Huang, M. H. Seed-Mediated Synthesis of Gold Nanocrystals with Systematic Shape Evolution from Cubic to Trisoctahedral and Rhombic Dodecahedral Structures. *Langmuir* **2010**, *26*, 12307−12313.
(223) Zhou, S.; Mesina, D. S.; Organt, M. A.; Yang, T.-H.; Yang, X.; Huo, D.; Zhao, M.; Xia, Y. Site-Selective Growth of Ag Nanocubes for Sharpening Their Corners and Edges, Followed by Elongation into Nanobars through Symmetry Reduction. *J. Mater. Chem. C* **2018**, *6*, 1384−1392.
(224) Chen, A. N.; Scanlan, M. M.; Skrabalak, S. E. Surface Passivation and Supersaturation: Strategies for Regioselective Deposition in Seeded Syntheses. *ACS Nano* **2017**, *11*, 12624−12631.
(225) Inose, T.; Toyouchi, S.; Lu, G.; Umemoto, K.; Tezuka, Y.; Lyu, B.; Masuhara, A.; Fron, E.; Fujita, Y.; Hirai, K.; et al. Water-Mediated Polyol Synthesis of Pencil-Like Sharp Silver Nanowires Suitable for Nonlinear Plasmonics. *Chem. Commun.* **2019**, *55*, 11630−11633.
(226) Xia, X.; Xie, S.; Liu, M.; Peng, H.-C.; Lu, N.; Wang, J.; Kim, M. J.; Xia, Y. On the Role of Surface Diffusion in Determining the Shape or Morphology of Noble-Metal Nanocrystals. *Proc. Natl. Acad. Sci. U.S.A.* **2013**, *110*, 6669−6673.
(227) Wu, S.; Li, M.; Sun, Y. In situ Synchrotron X-Ray Characterization Shining Light on the Nucleation and Growth

https://doi.org/10.1021/acs.chemrev.2c00468
Chem. Rev. 2023, 123, 3693−3760

Kinetics of Colloidal Nanoparticles. *Angew. Chem., Int. Ed.* **2019**, *58*, 8987−8995.
(228) Lee, J.; Yang, J.; Kwon, S. G.; Hyeon, T. Nonclassical Nucleation and Growth of Inorganic Nanoparticles. *Nat. Rev. Mater.* **2016**, *1*, 16034.
(229) Wang, M.; Park, C.; Woehl, T. J. Quantifying the Nucleation and Growth Kinetics of Electron Beam Nanochemistry with Liquid Cell Scanning Transmission Electron Microscopy. *Chem. Mater.* **2018**, *30*, 7727−7736.
(230) Tan, T.; Zhang, S.; Wang, J.; Zheng, Y.; Lai, H.; Liu, J.; Qin, F.; Wang, C. Resolving the Stacking Fault Structure of Silver Nanoplates. *Nanoscale* **2021**, *13*, 195−205.
(231) Ge, Y.; Huang, Z.; Ling, C.; Chen, B.; Liu, G.; Zhou, M.; Liu, J.; Zhang, X.; Cheng, H.; Liu, G.; et al. Phase-Selective Epitaxial Growth of Heterophase Nanostructures on Unconventional 2H-Pd Nanoparticles. *J. Am. Chem. Soc.* **2020**, *142*, 18971−18980.
(232) Zhao, M.; Figueroa-Cosme, L.; Elnabawy, A. O.; Vara, M.; Yang, X.; Roling, L. T.; Chi, M.; Mavrikakis, M.; Xia, Y. Synthesis and Characterization of Ru Cubic Nanocages with a Face-Centered Cubic Structure by Templating with Pd Nanocubes. *Nano Lett.* **2016**, *16*, 5310−5317.
(233) Huang, Z.; Gong, J.; Nie, Z. Symmetry-Breaking Synthesis of Multicomponent Nanoparticles. *Acc. Chem. Res.* **2019**, *52*, 1125−1133.
(234) Johnson, C. J.; Dujardin, E.; Davis, S. A.; Murphy, C. J.; Mann, S. Growth and Form of Gold Nanorods Prepared by Seed-Mediated, Surfactant-Directed Synthesis. *J. Mater. Chem.* **2002**, *12*, 1765−1770.
(235) Zeng, J.; Zheng, Y.; Rycenga, M.; Tao, J.; Li, Z.-Y.; Zhang, Q.; Zhu, Y.; Xia, Y. Controlling the Shapes of Silver Nanocrystals with Different Capping Agents. *J. Am. Chem. Soc.* **2010**, *132*, 8552−8553.
(236) Chiu, C.-Y.; Ruan, L.; Huang, Y. Biomolecular Specificity Controlled Nanomaterial Synthesis. *Chem. Soc. Rev.* **2013**, *42*, 2512−2527.
(237) Ortiz, N.; Skrabalak, S. E. On the Dual Roles of Ligands in the Synthesis of Colloidal Metal Nanostructures. *Langmuir* **2014**, *30*, 6649−6659.
(238) Niu, Z.; Li, Y. Removal and Utilization of Capping Agents in Nanocatalysis. *Chem. Mater.* **2014**, *26*, 72−83.
(239) Liu, M.; Gilroy, K. D.; Peng, H.-C.; Chi, M.; Guo, L.; Xia, Y. The Effect of Surface Capping on the Diffusion of Adatoms in the Synthesis of Pd@Au Core−Shell Nanocrystals. *Chem. Commun.* **2016**, *52*, 13159−13162.
(240) Jin, M.; Liu, H.; Zhang, H.; Xie, Z.; Liu, J.; Xia, Y. Synthesis of Pd Nanocrystals Enclosed by {100} Facets and with Sizes < 10 nm for Application in CO Oxidation. *Nano Res.* **2011**, *4*, 83−91.
(241) Lim, B.; Xiong, Y.; Xia, Y. A Water-Based Synthesis of Octahedral, Decahedral, and Icosahedral Pd Nanocrystals. *Angew. Chem., Int. Ed.* **2007**, *46*, 9279−9282.
(242) Heinz, H.; Ramezani-Dakhel, H. Simulations of Inorganic−Bioorganic Interfaces to Discover New Materials: Insights, Comparisons to Experiment, Challenges, and Opportunities. *Chem. Soc. Rev.* **2016**, *45*, 412−448.
(243) Al-Saidi, W.; Feng, H.; Fichthorn, K. A. Adsorption of Polyvinylpyrrolidone on Ag Surfaces: Insight into a Structure-Directing Agent. *Nano Lett.* **2012**, *12*, 997−1001.
(244) Ye, X.; Jin, L.; Caglayan, H.; Chen, J.; Xing, G.; Zheng, C.; Doan-Nguyen, V.; Kang, Y.; Engheta, N.; Kagan, C. R.; et al. Improved Size-Tunable Synthesis of Monodisperse Gold Nanorods through the Use of Aromatic Additives. *ACS Nano* **2012**, *6*, 2804−2817.
(245) Orendorff, C. J.; Murphy, C. J. Quantitation of Metal Content in the Silver-Assisted Growth of Gold Nanorods. *J. Phys. Chem. B* **2006**, *110*, 3990−3994.
(246) Feng, Y.; He, J.; Wang, H.; Tay, Y. Y.; Sun, H.; Zhu, L.; Chen, H. An Unconventional Role of Ligand in Continuously Tuning of Metal−Metal Interfacial Strain. *J. Am. Chem. Soc.* **2012**, *134*, 2004−2007.
(247) Lee, S.-U.; Hong, J. W.; Choi, S.-I.; Han, S. W. Universal Sulfide-Assisted Synthesis of M−Ag Heterodimers (M = Pd, Au, Pt) as Efficient Platforms for Fabricating Metal−Semiconductor Heteronanostructures. *J. Am. Chem. Soc.* **2014**, *136*, 5221−5224.
(248) Cathcart, N.; Kitaev, V. Symmetry Breaking by Surface Blocking: Synthesis of Bimorphic Silver Nanoparticles, Nanoscale Fishes and Apples. *Sci. Rep.* **2016**, *6*, 32561.
(249) Jeong, E.; Kim, K.; Choi, I.; Jeong, S.; Park, Y.; Lee, H.; Kim, S. H.; Lee, L. P.; Choi, Y.; Kang, T. Three-Dimensional Reduced-Symmetry of Colloidal Plasmonic Nanoparticles. *Nano Lett.* **2012**, *12*, 2436−2440.
(250) Crane, C. C.; Tao, J.; Wang, F.; Zhu, Y.; Chen, J. Mask-Assisted Seeded Growth of Segmented Metallic Heteronanostructures. *J. Phys. Chem. C* **2014**, *118*, 28134−28142.
(251) Chen, T.; Chen, G.; Xing, S.; Wu, T.; Chen, H. Scalable Routes to Janus Au−SiO_2 and Ternary Ag−Au−SiO_2 Nanoparticles. *Chem. Mater.* **2010**, *22*, 3826−3828.
(252) Wang, Y.; Xie, S.; Liu, J. Y.; Park, J.; Huang, C. Z.; Xia, Y. Shape-Controlled Synthesis of Palladium Nanocrystals: A Mechanistic Understanding of the Evolution from Octahedrons to Tetrahedrons. *Nano Lett.* **2013**, *13*, 2276−2281.
(253) Yang, Y.; Wang, W.; Li, X.; Chen, W.; Fan, N.; Zou, C.; Chen, X.; Xu, X.; Zhang, L.; Huang, S. Controlled Growth of Ag/Au Bimetallic Nanorods through Kinetics Control. *Chem. Mater.* **2013**, *25*, 34−41.
(254) Gilroy, K. D.; Hughes, R. A.; Neretina, S. Kinetically Controlled Nucleation of Silver on Surfactant-Free Gold Seeds. *J. Am. Chem. Soc.* **2014**, *136*, 15337−15345.
(255) Ye, H.; Wang, Q.; Catalano, M.; Lu, N.; Vermeylen, J.; Kim, M. J.; Liu, Y.; Sun, Y.; Xia, X. Ru Nanoframes with an fcc Structure and Enhanced Catalytic Properties. *Nano Lett.* **2016**, *16*, 2812−2817.
(256) Butt, H.-J.; Graf, K.; Kappl, M.Introduction. In *Physics and Chemistry of Interfaces*; Wiley-VCH: Weinheim, 2003; pp 1−3.
(257) Neretina, S.; Hughes, R. A.; Gilroy, K. D.; Hajfathalian, M. Noble Metal Nanostructure Synthesis at the Liquid−Substrate Interface: New Structures, New Insights, and New Possibilities. *Acc. Chem. Res.* **2016**, *49*, 2243−2250.
(258) Wang, Y.; Schmidt, V.; Senz, S.; Gösele, U. Epitaxial Growth of Silicon Nanowires Using an Aluminium Catalyst. *Nat. Nanotechnol.* **2006**, *1*, 186−189.
(259) Wagner, R. S.; Ellis, W. C. Vapor-Liquid-Solid Mechanism of Single Crystal Growth. *Appl. Phys. Lett.* **1964**, *4*, 89−90.
(260) Gu, H.; Yang, Z.; Gao, J.; Chang, C. K.; Xu, B. Heterodimers of Nanoparticles: Formation at a Liquid−Liquid Interface and Particle-Specific Surface Modification by Functional Molecules. *J. Am. Chem. Soc.* **2005**, *127*, 34−35.
(261) Agrawal, V. V.; Kulkarni, G. U.; Rao, C. N. R. Nature and Properties of Ultrathin Nanocrystalline Gold Films Formed at the Organic−Aqueous Interface. *J. Phys. Chem. B* **2005**, *109*, 7300−7305.
(262) Zhang, L.; Wang, Y.; Tong, L.; Xia, Y. Synthesis of Colloidal Metal Nanocrystals in Droplet Reactors: The Pros and Cons of Interfacial Adsorption. *Nano Lett.* **2014**, *14*, 4189−4194.
(263) Ghosh Chaudhuri, R.; Paria, S. Core/Shell Nanoparticles: Classes, Properties, Synthesis Mechanisms, Characterization, and Applications. *Chem. Rev.* **2012**, *112*, 2373−2433.
(264) Merg, A. D.; Zhou, Y. C.; Smith, A. M.; Millstone, J. E.; Rosi, N. L. Ligand Exchange for Controlling the Surface Chemistry and Properties of Nanoparticle Superstructures. *ChemNanoMat* **2017**, *3*, 745−749.
(265) Song, Y.; Garcia, R. M.; Dorin, R. M.; Wang, H.; Qiu, Y.; Coker, E. N.; Steen, W. A.; Miller, J. E.; Shelnutt, J. A. Synthesis of Platinum Nanowire Networks Using a Soft Template. *Nano Lett.* **2007**, *7*, 3650−3655.
(266) Shin, H. J.; Ryoo, R.; Liu, Z.; Terasaki, O. Template Synthesis of Asymmetrically Mesostructured Platinum Networks. *J. Am. Chem. Soc.* **2001**, *123*, 1246−1247.
(267) Smith, D. K.; Korgel, B. A. The Importance of the CTAB Surfactant on the Colloidal Seed-Mediated Synthesis of Gold Nanorods. *Langmuir* **2008**, *24*, 644−649.

https://doi.org/10.1021/acs.chemrev.2c00468
Chem. Rev. 2023, 123, 3693−3760

(268) Ezrahi, S.; Tuval, E.; Aserin, A. Properties, Main Applications and Perspectives of Worm Micelles. *Adv. Colloid Interface Sci.* **2006**, *128*, 77−102.
(269) Murphy, C. J.; Jana, N. R. Controlling the Aspect Ratio of Inorganic Nanorods and Nanowires. *Adv. Mater.* **2002**, *14*, 80−82.
(270) Das, N. C.; Cao, H.; Kaiser, H.; Warren, G. T.; Gladden, J. R.; Sokol, P. E. Shape and Size of Highly Concentrated Micelles in CTAB/NaSal Solutions by Small Angle Neutron Scattering (SANS). *Langmuir* **2012**, *28*, 11962−11968.
(271) Jana, N. R. Gram-Scale Synthesis of Soluble, Near-Monodisperse Gold Nanorods and Other Anisotropic Nanoparticles. *Small* **2005**, *1*, 875−882.
(272) Qiu, J.; Xie, M.; Lyu, Z.; Gilroy, K. D.; Liu, H.; Xia, Y. General Approach to the Synthesis of Heterodimers of Metal Nanoparticles through Site-Selected Protection and Growth. *Nano Lett.* **2019**, *19*, 6703−6708.
(273) Hu, Y.; Sun, Y. A Generic Approach for the Synthesis of Dimer Nanoclusters and Asymmetric Nanoassemblies. *J. Am. Chem. Soc.* **2013**, *135*, 2213−2221.
(274) Jiang, S.; Chen, Q.; Tripathy, M.; Luijten, E.; Schweizer, K. S.; Granick, S. Janus Particle Synthesis and Assembly. *Adv. Mater.* **2010**, *22*, 1060−1071.
(275) Ding, Y.; Fan, F.; Tian, Z.; Wang, Z. L. Atomic Structure of Au−Pd Bimetallic Alloyed Nanoparticles. *J. Am. Chem. Soc.* **2010**, *132*, 12480−12486.
(276) Fan, F.-R.; Liu, D.-Y.; Wu, Y.-F.; Duan, S.; Xie, Z.-X.; Jiang, Z.-Y.; Tian, Z.-Q. Epitaxial Growth of Heterogeneous Metal Nanocrystals: From Gold Nano-Octahedra to Palladium and Silver Nanocubes. *J. Am. Chem. Soc.* **2008**, *130*, 6949−6951.
(277) Zhang, Z.; Lagally, M. G. Atomistic Processes in the Early Stages of Thin-Film Growth. *Science* **1997**, *276*, 377−383.
(278) Sun, Y. Interfaced Heterogeneous Nanodimers. *Natl. Sci. Rev.* **2015**, *2*, 329−348.
(279) Mo, Y.-W.; Savage, D. E.; Swartzentruber, B. S.; Lagally, M. G. Kinetic Pathway in Stranski-Krastanov Growth of Ge on Si(001). *Phys. Rev. Lett.* **1990**, *65*, 1020−1023.
(280) Venables, J. A.; Spiller, G. D. T.Nucleation and Growth of Thin Films. In *Surface Mobilities on Solid Materials*; Springer, 1983; pp 341−404.
(281) Rein, G.; Mehrer, H. Effect of Hydrostatic Pressure and Temperature on the Self-Diffusion Rate in Single Crystals of Silver and Gold. *Philos. Mag. A* **1982**, *45*, 467−492.
(282) Lang, C.; Schmitz, G. Microstructure-Controlled Interdiffusion of Cu/Co/Au Thin Films Investigated by Three-Dimensional Atom Probe. *Mater. Sci. Eng., A* **2003**, *353*, 119−125.
(283) Jin, M.; Zhang, H.; Wang, J.; Zhong, X.; Lu, N.; Li, Z.; Xie, Z.; Kim, M. J.; Xia, Y. Copper Can Still Be Epitaxially Deposited on Palladium Nanocrystals to Generate Core-Shell Nanocubes Despite Their Large Lattice Mismatch. *ACS Nano* **2012**, *6*, 2566−2573.
(284) Tringides, M. C.Surface Diffusion and Epitaxy. In *Surface Diffusion: Atomistic and Collective Processes*; Plenum Press, 1997; pp 83−160.
(285) Zhang, L.; Chen, Q.; Wang, X.; Jiang, Z. Nucleation-Mediated Synthesis and Enhanced Catalytic Properties of Au−Pd Bimetallic Tripods and Bipyramids with Twinned Structures and High-Energy Facets. *Nanoscale* **2016**, *8*, 2819−2825.
(286) Wang, Z.; Chen, Z.; Zhang, H.; Zhang, Z.; Wu, H.; Jin, M.; Wu, C.; Yang, D.; Yin, Y. Lattice-Mismatch-Induced Twinning for Seeded Growth of Anisotropic Nano Structures. *ACS Nano* **2015**, *9*, 3307−3313.
(287) Keunen, R.; Cathcart, N.; Kitaev, V. Plasmon Mediated Shape and Size Selective Synthesis of Icosahedral Silver Nanoparticles via Oxidative Etching and Their 1-D Transformation to Pentagonal Pins. *Nanoscale* **2014**, *6*, 8045−8051.
(288) Langille, M. R.; Zhang, J.; Mirkin, C. A. Plasmon-Mediated Synthesis of Heterometallic Nanorods and Icosahedra. *Angew. Chem., Int. Ed.* **2011**, *50*, 3543−3547.
(289) Habas, S. E.; Lee, H.; Radmilovic, V.; Somorjai, G. A.; Yang, P. Shaping Binary Metal Nanocrystals through Epitaxial Seeded Growth. *Nat. Mater.* **2007**, *6*, 692−697.
(290) Langille, M. R.; Zhang, J.; Personick, M. L.; Li, S.; Mirkin, C. A. Stepwise Evolution of Spherical Seeds into 20-Fold Twinned Icosahedra. *Science* **2012**, *337*, 954−957.
(291) Huang, X.; Neretina, S.; El-Sayed, M. A. Gold Nanorods: From Synthesis and Properties to Biological and Biomedical Applications. *Adv. Mater.* **2009**, *21*, 4880−4910.
(292) Zheng, J.; Cheng, X.; Zhang, H.; Bai, X.; Ai, R.; Shao, L.; Wang, J. Gold Nanorods: The Most Versatile Plasmonic Nanoparticles. *Chem. Rev.* **2021**, *121*, 13342−13453.
(293) de Aberasturi, D. J.; Serrano-Montes, A. B.; Liz-Marzán, L. M. Modern Applications of Plasmonic Nanoparticles: From Energy to Health. *Adv. Opt. Mater.* **2015**, *3*, 602−617.
(294) Boisselier, E.; Astruc, D. Gold Nanoparticles in Nanomedicine: Preparations, Imaging, Diagnostics, Therapies and Toxicity. *Chem. Soc. Rev.* **2009**, *38*, 1759−1782.
(295) Grzelczak, M.; Pérez-Juste, J.; Mulvaney, P.; Liz-Marzán, L. M. Shape Control in Gold Nanoparticle Synthesis. *Chem. Soc. Rev.* **2008**, *37*, 1783−1791.
(296) Zhu, C.; Zeng, J.; Tao, J.; Johnson, M. C.; Schmidt-Krey, I.; Blubaugh, L.; Zhu, Y.; Gu, Z.; Xia, Y. Kinetically Controlled Overgrowth of Ag or Au on Pd Nanocrystal Seeds: From Hybrid Dimers to Nonconcentric and Concentric Bimetallic Nanocrystals. *J. Am. Chem. Soc.* **2012**, *134*, 15822−15831.
(297) Lee, H. W.; Jung, E.; Han, G.-H.; Kim, M.-C.; Kim, D.; Lee, K.-Y.; Han, S. S.; Yu, T. Three-in-One Strategy to Improve Both Catalytic Activity and Selectivity: Nonconcentric Pd−Au Nanoparticles. *J. Phys. Chem. Lett.* **2021**, *12*, 11098−11105.
(298) Jin, M.; Zhang, H.; Xie, Z.; Xia, Y. Palladium Nanocrystals Enclosed by {100} and {111} Facets in Controlled Proportions and Their Catalytic Activities for Formic Acid Oxidation. *Energy Environ. Sci.* **2012**, *5*, 6352−6357.
(299) Smith, J. D.; Bladt, E.; Burkhart, J. A. C.; Winckelmans, N.; Koczkur, K. M.; Ashberry, H. M.; Bals, S.; Skrabalak, S. E. Defect-Directed Growth of Symmetrically Branched Metal Nanocrystals. *Angew. Chem., Int. Ed.* **2020**, *59*, 943−950.
(300) Poerwoprajitno, A. R.; Cheong, S.; Gloag, L.; Gooding, J. J.; Tilley, R. D. Synthetic Strategies to Enhance the Electrocatalytic Properties of Branched Metal Nanoparticles. *Acc. Chem. Res.* **2022**, *55*, 12760−12764.
(301) Meng, M.; Fang, Z.; Zhang, C.; Su, H.; He, R.; Zhang, R.; Li, H.; Li, Z.-Y.; Wu, X.; Ma, C.; et al. Integration of Kinetic Control and Lattice Mismatch to Synthesize Pd@AuCu Core−Shell Planar Tetrapods with Size-Dependent Optical Properties. *Nano Lett.* **2016**, *16*, 3036−3041.
(302) Zhao, M.; Chen, Z.; Shi, Y.; Hood, Z. D.; Lyu, Z.; Xie, M.; Chi, M.; Xia, Y. Kinetically Controlled Synthesis of Rhodium Nanocrystals with Different Shapes and a Comparison Study of Their Thermal and Catalytic Properties. *J. Am. Chem. Soc.* **2021**, *143*, 6293−6302.
(303) Park, J.; Zhang, L.; Choi, S.-I.; Roling, L. T.; Lu, N.; Herron, J. A.; Xie, S.; Wang, J.; Kim, M. J.; Mavrikakis, M.; et al. Atomic Layer-by-Layer Deposition of Platinum on Palladium Octahedra for Enhanced Catalysts toward the Oxygen Reduction Reaction. *ACS Nano* **2015**, *9*, 2635−2647.
(304) Kim, D. Y.; Yu, T.; Cho, E. C.; Ma, Y.; Park, O. O.; Xia, Y. Synthesis of Gold Nano-Hexapods with Controllable Arm Lengths and Their Tunable Optical Properties. *Angew. Chem.* **2011**, *123*, 6452−6455.
(305) Park, J.; Joo, J.; Kwon, S. G.; Jang, Y.; Hyeon, T. Synthesis of Monodisperse Spherical Nanocrystals. *Angew. Chem., Int. Ed.* **2007**, *46*, 4630−4660.
(306) Park, J.-E.; Lee, Y.; Nam, J.-M. Precisely Shaped, Uniformly Formed Gold Nanocubes with Ultrahigh Reproducibility in Single-Particle Scattering and Surface-Enhanced Raman Scattering. *Nano Lett.* **2018**, *18*, 6475−6482.

https://doi.org/10.1021/acs.chemrev.2c00468
Chem. Rev. 2023, 123, 3693−3760

(307) Zhang, Q.; Moran, C. H.; Xia, X.; Rycenga, M.; Li, N.; Xia, Y. Synthesis of Ag Nanobars in the Presence of Single-Crystal Seeds and a Bromide Compound, and Their Surface-Enhanced Raman Scattering (SERS) Properties. *Langmuir* **2012**, *28*, 9047−9054.
(308) Hsu, S.-W.; Tao, A. R. Halide-Directed Synthesis of Square Prismatic Ag Nanocrystals by the Polyol Method. *Chem. Mater.* **2018**, *30*, 4617−4623.
(309) Lyu, Z.; Xie, M.; Aldama, E.; Zhao, M.; Qiu, J.; Zhou, S.; Xia, Y. Au@Cu Core−Shell Nanocubes with Controllable Sizes in the Range of 20−30 nm for Applications in Catalysis and Plasmonics. *ACS Appl. Nano Mater.* **2019**, *2*, 1533−1540.
(310) Zheng, Y.; Liu, W.; Lv, T.; Luo, M.; Hu, H.; Lu, P.; Choi, S.-I.; Zhang, C.; Tao, J.; Zhu, Y.; et al. Seed-Mediated Synthesis of Gold Tetrahedra in High Purity and with Tunable, Well-Controlled Sizes. *Chem. Asian J.* **2014**, *9*, 2635−2640.
(311) Hong, J. W.; Lee, S.-U.; Lee, Y. W.; Han, S. W. Hexoctahedral Au Nanocrystals with High-Index Facets and Their Optical and Surface-Enhanced Raman Scattering Properties. *J. Am. Chem. Soc.* **2012**, *134*, 4565−4568.
(312) Feng, Y.; Wang, Y.; He, J.; Song, X.; Tay, Y. Y.; Hng, H. H.; Ling, X. Y.; Chen, H. Achieving Site-Specificity in Multistep Colloidal Synthesis. *J. Am. Chem. Soc.* **2015**, *137*, 7624−7627.
(313) Zheng, Y.; Ma, Y.; Zeng, J.; Zhong, X.; Jin, M.; Li, Z.-Y.; Xia, Y. Seed-Mediated Synthesis of Single-Crystal Gold Nanospheres with Controlled Diameters in the Range 5−30 nm and Their Self-Assembly Upon Dilution. *Chem. Asian J.* **2013**, *8*, 792−799.
(314) Wiley, B. J.; Wang, Z.; Wei, J.; Yin, Y.; Cobden, D. H.; Xia, Y. Synthesis and Electrical Characterization of Silver Nanobeams. *Nano Lett.* **2006**, *6*, 2273−2278.
(315) Du, J. S.; Zhou, W.; Rupich, S. M.; Mirkin, C. A. Twin Pathways: Discerning the Origins of Multiply Twinned Colloidal Nanoparticles. *Angew. Chem.* **2021**, *133*, 6934−6939.
(316) Luo, M.; Huang, H.; Choi, S.-I.; Zhang, C.; da Silva, R. R.; Peng, H.-C.; Li, Z.-Y.; Liu, J.; He, Z.; Xia, Y. Facile Synthesis of Ag Nanorods with No Plasmon Resonance Peak in the Visible Region by Using Pd Decahedra of 16 nm in Size as Seeds. *ACS Nano* **2015**, *9*, 10523−10532.
(317) Zhou, L.; Qiu, X.; Lyu, Z.; Zhao, M.; Xia, Y. Pd−Au Asymmetric Nanopyramids: Lateral vs Vertical Growth of Au on Pd Decahedral Seeds. *Chem. Mater.* **2021**, *33*, 5391−5400.
(318) Lyu, Z.; Zhu, S.; Xu, L.; Chen, Z.; Zhang, Y.; Xie, M.; Li, T.; Zhou, S.; Liu, J.; Chi, M.; et al. Kinetically Controlled Synthesis of Pd−Cu Janus Nanocrystals with Enriched Surface Structures and Enhanced Catalytic Activities toward CO_2 Reduction. *J. Am. Chem. Soc.* **2021**, *143*, 149−162.
(319) Myroshnychenko, V.; Rodríguez-Fernández, J.; Pastoriza-Santos, I.; Funston, A. M.; Novo, C.; Mulvaney, P.; Liz-Marzán, L. M.; De Abajo, F. J. G. Modelling the Optical Response of Gold Nanoparticles. *Chem. Soc. Rev.* **2008**, *37*, 1792−1805.
(320) Willets, K. A.; Van Duyne, R. P. Localized Surface Plasmon Resonance Spectroscopy and Sensing. *Annu. Rev. Phys. Chem.* **2007**, *58*, 267−297.
(321) Liu, S.-Y.; Huang, L.; Li, J.-F.; Wang, C.; Li, Q.; Xu, H.-X.; Guo, H.-L.; Meng, Z.-M.; Shi, Z.; Li, Z.-Y. Simultaneous Excitation and Emission Enhancement of Fluorescence Assisted by Double Plasmon Modes of Gold Nanorods. *J. Phys. Chem. C* **2013**, *117*, 10636−10642.
(322) Murphy, C. J.; Sau, T. K.; Gole, A. M.; Orendorff, C. J.; Gao, J.; Gou, L.; Hunyadi, S. E.; Li, T. Anisotropic Metal Nanoparticles: Synthesis, Assembly, and Optical Applications. *J. Phys. Chem. B* **2005**, *109*, 13857−13870.
(323) Ye, X.; Zheng, C.; Chen, J.; Gao, Y.; Murray, C. B. Using Binary Surfactant Mixtures to Simultaneously Improve the Dimensional Tunability and Monodispersity in the Seeded Growth of Gold Nanorods. *Nano Lett.* **2013**, *13*, 765−771.
(324) Sau, T. K.; Murphy, C. J. Room Temperature, High-Yield Synthesis of Multiple Shapes of Gold Nanoparticles in Aqueous Solution. *J. Am. Chem. Soc.* **2004**, *126*, 8648−8649.
(325) Chang, H.-H.; Murphy, C. J. Mini Gold Nanorods with Tunable Plasmonic Peaks Beyond 1000 nm. *Chem. Mater.* **2018**, *30*, 1427−1435.
(326) Smith, J. D.; Reza, M. A.; Smith, N. L.; Gu, J.; Ibrar, M.; Crandall, D. J.; Skrabalak, S. E. Plasmonic Anticounterfeit Tags with High Encoding Capacity Rapidly Authenticated with Deep Machine Learning. *ACS Nano* **2021**, *15*, 2901−2910.
(327) Goldmann, C.; De Frutos, M.; Hill, E. H.; Constantin, D.; Hamon, C. Symmetry Breaking in Seed-Mediated Silver Nanorod Growth Induced by Dimethyl Sulfoxide. *Chem. Mater.* **2021**, *33*, 2948−2956.
(328) Cao, J.; Sun, T.; Grattan, K. T. V. Gold Nanorod-Based Localized Surface Plasmon Resonance Biosensors: A Review. *Sens. Actuators B Chem.* **2014**, *195*, 332−351.
(329) Storhoff, J. J.; Elghanian, R.; Mucic, R. C.; Mirkin, C. A.; Letsinger, R. L. One-Pot Colorimetric Differentiation of Polynucleotides with Single Base Imperfections Using Gold Nanoparticle Probes. *J. Am. Chem. Soc.* **1998**, *120*, 1959−1964.
(330) Lin, S.-Y.; Liu, S.-W.; Lin, C.-M.; Chen, C.-H. Recognition of Potassium Ion in Water by 15-Crown-5 Functionalized Gold Nanoparticles. *Anal. Chem.* **2002**, *74*, 330−335.
(331) Liu, J.; Lu, Y. Adenosine-Dependent Assembly of Aptazyme-Functionalized Gold Nanoparticles and Its Application as a Colorimetric Biosensor. *Anal. Chem.* **2004**, *76*, 1627−1632.
(332) Wei, H.; Pan, D.; Zhang, S.; Li, Z.; Li, Q.; Liu, N.; Wang, W.; Xu, H. Plasmon Waveguiding in Nanowires. *Chem. Rev.* **2018**, *118*, 2882−2926.
(333) Sanders, A. W.; Routenberg, D. A.; Wiley, B. J.; Xia, Y.; Dufresne, E. R.; Reed, M. A. Observation of Plasmon Propagation, Redirection, and Fan-Out in Silver Nanowires. *Nano Lett.* **2006**, *6*, 1822−1826.
(334) Pyayt, A. L.; Wiley, B.; Xia, Y.; Chen, A.; Dalton, L. Integration of Photonic and Silver Nanowire Plasmonic Waveguides. *Nat. Nanotechnol.* **2008**, *3*, 660−665.
(335) Guo, X.; Qiu, M.; Bao, J.; Wiley, B. J.; Yang, Q.; Zhang, X.; Ma, Y.; Yu, H.; Tong, L. Direct Coupling of Plasmonic and Photonic Nanowires for Hybrid Nanophotonic Components and Circuits. *Nano Lett.* **2009**, *9*, 4515−4519.
(336) Yan, R.; Pausauskie, P.; Huang, J.; Yang, P. Direct Photonic−Plasmonic Coupling and Routing in Single Nanowires. *Proc. Natl. Acad. Sci. U.S.A.* **2009**, *106*, 21045−21050.
(337) Wang, P.; Zhang, L.; Xia, Y.; Tong, L.; Xu, X.; Ying, Y. Polymer Nanofibers Embedded with Aligned Gold Nanorods: A New Platform for Plasmonic Studies and Optical Sensing. *Nano Lett.* **2012**, *12*, 3145−3150.
(338) Hecht, D. S.; Hu, L.; Irvin, G. Emerging Transparent Electrodes Based on Thin Films of Carbon Nanotubes, Graphene, and Metallic Nanostructures. *Adv. Mater.* **2011**, *23*, 1482−1513.
(339) McCoul, D.; Hu, W.; Gao, M.; Mehta, V.; Pei, Q. Recent Advances in Stretchable and Transparent Electronic Materials. *Adv. Electron. Mater.* **2016**, *2*, 1500407.
(340) Layani, M.; Kamyshny, A.; Magdassi, S. Transparent Conductors Composed of Nanomaterials. *Nanoscale* **2014**, *6*, 5581−5591.
(341) Kulkarni, G. U.; Kiruthika, S.; Gupta, R.; Rao, K. D. M. Towards Low Cost Materials and Methods for Transparent Electrodes. *Curr. Opin. Chem. Eng.* **2015**, *8*, 60−68.
(342) O'Callaghan, C.; da Rocha, C. G.; Manning, H. G.; Boland, J. J.; Ferreira, M. S. Effective Medium Theory for the Conductivity of Disordered Metallic Nanowire Networks. *Phys. Chem. Chem. Phys.* **2016**, *18*, 27564−27571.
(343) Lee, J.; Lee, P.; Lee, H.; Lee, D.; Lee, S. S.; Ko, S. H. Very Long Ag Nanowire Synthesis and Its Application in a Highly Transparent, Conductive and Flexible Metal Electrode Touch Panel. *Nanoscale* **2012**, *4*, 6408−6414.
(344) Cui, Z.; Poblete, F. R.; Cheng, G.; Yao, S.; Jiang, X.; Zhu, Y. Design and Operation of Silver Nanowire Based Flexible and Stretchable Touch Sensors. *J. Mater. Res.* **2015**, *30*, 79−85.

https://doi.org/10.1021/acs.chemrev.2c00468
Chem. Rev. 2023, 123, 3693−3760

(345) Madaria, A. R.; Kumar, A.; Zhou, C. Large Scale, Highly Conductive and Patterned Transparent Films of Silver Nanowires on Arbitrary Substrates and Their Application in Touch Screens. *Nanotechnology* **2011**, *22*, 245201.
(346) Morgenstern, F. S. F.; Kabra, D.; Massip, S.; Brenner, T. J. K.; Lyons, P. E.; Coleman, J. N.; Friend, R. H. Ag-Nanowire Films Coated with ZnO Nanoparticles as a Transparent Electrode for Solar Cells. *Appl. Phys. Lett.* **2011**, *99*, 183307.
(347) Langley, D. P.; Giusti, G.; Lagrange, M.; Collins, R.; Jiménez, C.; Bréchet, Y.; Bellet, D. Silver Nanowire Networks: Physical Properties and Potential Integration in Solar Cells. *Sol. Energy Mater. Sol. Cells* **2014**, *125*, 318−324.
(348) Coskun, S.; Ates, E. S.; Unalan, H. E. Optimization of Silver Nanowire Networks for Polymer Light Emitting Diode Electrodes. *Nanotechnology* **2013**, *24*, 125202.
(349) Liu, J.; Jia, D.; Gardner, J. M.; Johansson, E. M.; Zhang, X. Metal Nanowire Networks: Recent Advances and Challenges for New Generation Photovoltaics. *Mater. Today Energy* **2019**, *13*, 152−185.
(350) Song, M.; You, D. S.; Lim, K.; Park, S.; Jung, S.; Kim, C. S.; Kim, D.-H.; Kim, D.-G.; Kim, J.-K.; Park, J.; et al. Highly Efficient and Bendable Organic Solar Cells with Solution-Processed Silver Nanowire Electrodes. *Adv. Funct. Mater.* **2013**, *23*, 4177−4184.
(351) Giancoli, D. C.Electric Currents. In *Physics: Principles with Applications*; Prentice Hall: London, 2004; pp 493−519.
(352) Rathmell, A. R.; Bergin, S. M.; Hua, Y.-L.; Li, Z.-Y.; Wiley, B. J. The Growth Mechanism of Copper Nanowires and Their Properties in Flexible, Transparent Conducting Films. *Adv. Mater.* **2010**, *22*, 3558−3563.
(353) Cui, F.; Yu, Y.; Dou, L.; Sun, J.; Yang, Q.; Schildknecht, C.; Schierle-Arndt, K.; Yang, P. Synthesis of Ultrathin Copper Nanowires Using Tris(trimethylsilyl)silane for High-Performance and Low-Haze Transparent Conductors. *Nano Lett.* **2015**, *15*, 7610−7615.
(354) Scott, D. A.Corrosion and Environment. In *Copper and Bronze in Art: Corrosion, Colorants, Conservation*; The Getty Conservation Institute: Los Angeles, 2002; pp 10−80.
(355) Dou, L.; Cui, F.; Yu, Y.; Khanarian, G.; Eaton, S. W.; Yang, Q.; Resasco, J.; Schildknecht, C.; Schierle-Arndt, K.; Yang, P. Solution-Processed Copper/Reduced-Graphene-Oxide Core/Shell Nanowire Transparent Conductors. *ACS Nano* **2016**, *10*, 2600−2606.
(356) Stewart, I. E.; Ye, S.; Chen, Z.; Flowers, P. F.; Wiley, B. J. Synthesis of Cu−Ag, Cu−Au, and Cu−Pt Core−Shell Nanowires and Their Use in Transparent Conducting Films. *Chem. Mater.* **2015**, *27*, 7788−7794.
(357) Niu, Z.; Cui, F.; Yu, Y.; Becknell, N.; Sun, Y.; Khanarian, G.; Kim, D.; Dou, L.; Dehestani, A.; Schierle-Arndt, K.; et al. Ultrathin Epitaxial Cu@Au Core−Shell Nanowires for Stable Transparent Conductors. *J. Am. Chem. Soc.* **2017**, *139*, 7348−7354.
(358) Hansen, T. W.; DeLaRiva, A. T.; Challa, S. R.; Datye, A. K. Sintering of Catalytic Nanoparticles: Particle Migration or Ostwald Ripening? *Acc. Chem. Res.* **2013**, *46*, 1720−1730.
(359) Sun, S.; Jaouen, F.; Dodelet, J.-P. Controlled Growth of Pt Nanowires on Carbon Nanospheres and Their Enhanced Performance as Electrocatalysts in PEM Fuel Cells. *Adv. Mater.* **2008**, *20*, 3900−3904.
(360) Zhang, H.; Zhou, W.; Du, Y.; Yang, P.; Wang, C. One-Step Electrodeposition of Platinum Nanoflowers and Their High Efficient Catalytic Activity for Methanol Electro-Oxidation. *Electrochem. Commun.* **2010**, *12*, 882−885.
(361) Zhou, H.; Zhou, W.-P.; Adzic, R. R.; Wong, S. S. Enhanced Electrocatalytic Performance of One-Dimensional Metal Nanowires and Arrays Generated via an Ambient, Surfactantless Synthesis. *J. Phys. Chem. C* **2009**, *113*, 5460−5466.
(362) Chen, Z.; Waje, M.; Li, W.; Yan, Y. Supportless Pt and PtPd Nanotubes as Electrocatalysts for Oxygen-Reduction Reactions. *Angew. Chem., Int. Ed.* **2007**, *46*, 4060−4063.
(363) Toyoda, E.; Jinnouchi, R.; Hatanaka, T.; Morimoto, Y.; Mitsuhara, K.; Visikovskiy, A.; Kido, Y. The d-Band Structure of Pt Nanoclusters Correlated with the Catalytic Activity for an Oxygen Reduction Reaction. *J. Phys. Chem. C* **2011**, *115*, 21236−21240.
(364) Yao, Z.; Yuan, Y.; Cheng, T.; Gao, L.; Sun, T.; Lu, Y.; Zhou, Y.-G.; Galindo, P. L.; Yang, Z.; Xu, L.; et al. Anomalous Size Effect of Pt Ultrathin Nanowires on Oxygen Reduction Reaction. *Nano Lett.* **2021**, *21*, 9354−9360.
(365) Wang, L.; Zeng, Z.; Gao, W.; Maxson, T.; Raciti, D.; Giroux, M.; Pan, X.; Wang, C.; Greeley, J. Tunable Intrinsic Strain in Two-Dimensional Transition Metal Electrocatalysts. *Science* **2019**, *363*, 870−874.
(366) Huang, X.; Li, G.; Kong, L. B.; Huang, Y. Z.; Wu, T. Anisotropic Surface Strain in Single Crystalline Cobalt Nanowires and Its Impact on the Diameter-Dependent Young's Modulus. *Nanoscale* **2013**, *5*, 11643−11648.
(367) Lim, B.; Jiang, M.; Camargo, P. H. C.; Cho, E. C.; Tao, J.; Lu, X.; Zhu, Y.; Xia, Y. Pd-Pt Bimetallic Nanodendrites with High Activity for Oxygen Reduction. *Science* **2009**, *324*, 1302−1305.
(368) Kuzume, A.; Herrero, E.; Feliu, J. M. Oxygen Reduction on Stepped Platinum Surfaces in Acidic Media. *J. Electroanal. Chem.* **2007**, *599*, 333−343.
(369) Marković, N. M.; Adžić, R. R.; Cahan, B. D.; Yeager, E. B. Structural Effects in Electrocatalysis: Oxygen Reduction on Platinum Low Index Single-Crystal Surfaces in Perchloric Acid Solutions. *J. Electroanal. Chem.* **1994**, *377*, 249−259.
(370) Huang, J.; Mensi, M.; Oveisi, E.; Mantella, V.; Buonsanti, R. Structural Sensitivities in Bimetallic Catalysts for Electrochemical CO_2 Reduction Revealed by Ag−Cu Nanodimers. *J. Am. Chem. Soc.* **2019**, *141*, 2490−2499.
(371) Jia, H.; Yang, Y.; Chow, T. H.; Zhang, H.; Liu, X.; Wang, J.; Zhang, C.-Y. Symmetry-Broken Au−Cu Heterostructures and Their Tandem Catalysis Process in Electrochemical CO_2 Reduction. *Adv. Funct. Mater.* **2021**, *31*, 2101255.
(372) Dhar, P.; Fischer, T. M.; Wang, Y.; Mallouk, T. E.; Paxton, W. F.; Sen, A. Autonomously Moving Nanorods at a Viscous Interface. *Nano Lett.* **2006**, *6*, 66−72.
(373) Sattayasamitsathit, S.; Gao, W.; Calvo-Marzal, P.; Manesh, K. M.; Wang, J. Simplified Cost-Effective Preparation of High-Performance Ag−Pt Nanowire Motors. *ChemPhysChem* **2010**, *11*, 2802−2805.
(374) Paxton, W. F.; Sen, A.; Mallouk, T. E. Motility of Catalytic Nanoparticles through Self-Generated Forces. *Chem. Eur. J.* **2005**, *11*, 6462−6470.
(375) Paxton, W. F.; Baker, P. T.; Kline, T. R.; Wang, Y.; Mallouk, T. E.; Sen, A. Catalytically Induced Electrokinetics for Motors and Micropumps. *J. Am. Chem. Soc.* **2006**, *128*, 14881−14888.
(376) Wang, Y.; Hernandez, R. M.; Bartlett, D. J.; Bingham, J. M.; Kline, T. R.; Sen, A.; Mallouk, T. E. Bipolar Electrochemical Mechanism for the Propulsion of Catalytic Nanomotors in Hydrogen Peroxide Solutions. *Langmuir* **2006**, *22*, 10451−10456.
(377) Kagan, D.; Calvo-Marzal, P.; Balasubramanian, S.; Sattayasamitsathit, S.; Manesh, K. M.; Flechsig, G.-U.; Wang, J. Chemical Sensing Based on Catalytic Nanomotors: Motion-Based Detection of Trace Silver. *J. Am. Chem. Soc.* **2009**, *131*, 12082−12083.
(378) Howse, J. R.; Jones, R. A. L.; Ryan, A. J.; Gough, T.; Vafabakhsh, R.; Golestanian, R. Self-Motile Colloidal Particles: From Directed Propulsion to Random Walk. *Phys. Rev. Lett.* **2007**, *99*, No. 048102.
(379) Spaldin, N. A.Device Applications and Novel Materials. In *Magnetic Materials: Fundamentals and Applications*; Cambridge University Press, 2010; pp 175−228.
(380) Ma, Z.; Mohapatra, J.; Wei, K.; Liu, J. P.; Sun, S. Magnetic Nanoparticles: Synthesis, Anisotropy, and Applications. *Chem. Rev.* **2021**, DOI: 10.1021/acs.chemrev.1c00860.
(381) Şimşek, T.; Özcan, Ş. Effective Magnetic Anisotropy Enhancement of FePt Nanocrystals through Shape Control. *J. Magn. Magn. Mater.* **2014**, *351*, 47−51.
(382) Mohapatra, J.; Mitra, A.; Tyagi, H.; Bahadur, D.; Aslam, M. Iron Oxide Nanorods as High-Performance Magnetic Resonance Imaging Contrast Agents. *Nanoscale* **2015**, *7*, 9174−9184.
(383) Paulus, P. M.; Luis, F.; Kröll, M.; Schmid, G.; De Jongh, L. J. Low-Temperature Study of the Magnetization Reversal and Magnetic

Anisotropy of Fe, Ni, and Co Nanowires. *J. Magn. Magn. Mater.* **2001**, *224*, 180−196.
(384) Zhang, Z.; Wu, Q.; Zhong, K.; Yang, S.; Lin, X.; Huang, Z. The Size and Space Arrangement Roles on Coercivity of Electrodeposited $Co_{1-x}Cu_x$ Nanowires. *J. Magn. Magn. Mater.* **2006**, *303*, e304−e307.
(385) Yang, Z. H.; Li, Z. W.; Liu, L.; Kong, L. B. Microstructure and Magnetic Properties of Co−Cu Nanowire Arrays Fabricated by Galvanic Displacement Deposition. *J. Magn. Magn. Mater.* **2011**, *323*, 2674−2677.
(386) Pousthomis, M.; Anagnostopoulou, E.; Panagiotopoulos, I.; Boubekri, R.; Fang, W.; Ott, F.; Atmane, K. A.; Piquemal, J. Y.; Lacroix, L. M.; Viau, G. Localized Magnetization Reversal Processes in Cobalt Nanorods with Different Aspect Ratios. *Nano Res.* **2015**, *8*, 2231−2241.
(387) Anagnostopoulou, E.; Grindi, B.; Lacroix, L.-M.; Ott, F.; Panagiotopoulos, I.; Viau, G. Dense Arrays of Cobalt Nanorods as Rare-Earth Free Permanent Magnets. *Nanoscale* **2016**, *8*, 4020−4029.
(388) Lin, W.-S.; Jian, Z.-J.; Lin, H.-M.; Lai, L.-C.; Chiou, W.-A.; Hwu, Y.-K.; Wu, S.-H.; Chen, W.-C.; Yao, Y. D. Synthesis and Characterization of Iron Nanowires. *J. Chin. Chem. Soc.* **2013**, *60*, 85−91.
(389) Wang, C.; Hou, Y.; Kim, J.; Sun, S. A General Strategy for Synthesizing FePt Nanowires and Nanorods. *Angew. Chem.* **2007**, *119*, 6449−6451.
(390) Dahmane, Y.; Cagnon, L.; Voiron, J.; Pairis, S.; Bacia, M.; Ortega, L.; Benbrahim, N.; Kadri, A. Magnetic and Structural Properties of Electrodeposited CoPt and FePt Nanowires in Nanoporous Alumina Templates. *J. Phys. D: Appl. Phys.* **2006**, *39*, 4523−4528.
(391) Fei, X. L.; Tang, S. L.; Wang, R. L.; Su, H. L.; Du, Y. W. Fabrication and Magnetic Properties of Fe−Pd Nanowire Arrays. *Solid State Commun.* **2007**, *141*, 25−28.
(392) Chen, M.; Pica, T.; Jiang, Y.-B.; Li, P.; Yano, K.; Liu, J. P.; Datye, A. K.; Fan, H. Synthesis and Self-Assembly of fcc Phase FePt Nanorods. *J. Am. Chem. Soc.* **2007**, *129*, 6348−6349.
(393) Das, R.; Alonso, J.; Nemati Porshokouh, Z.; Kalappattil, V.; Torres, D.; Phan, M. H.; Garaio, E.; García, J. A.; Sanchez Llamazares, J. L.; Srikanth, H. Tunable High Aspect Ratio Iron Oxide Nanorods for Enhanced Hyperthermia. *J. Phys. Chem. C* **2016**, *120*, 10086−10093.
(394) Valdés, D. P.; Lima, E.; Zysler, R. D.; Goya, G. F.; De Biasi, E. Role of Anisotropy, Frequency, and Interactions in Magnetic Hyperthermia Applications: Noninteracting Nanoparticles and Linear Chain Arrangements. *Phys. Rev. Appl.* **2021**, *15*, No. 044005.
(395) Mohapatra, J.; Xing, M.; Beatty, J.; Elkins, J.; Seda, T.; Mishra, S. R.; Liu, J. P. Enhancing the Magnetic and Inductive Heating Properties of Fe_3O_4 Nanoparticles via Morphology Control. *Nanotechnology* **2020**, *31*, 275706.
(396) Azharuddin, M.; Zhu, G. H.; Das, D.; Ozgur, E.; Uzun, L.; Turner, A. P. F.; Patra, H. K. A Repertoire of Biomedical Applications of Noble Metal Nanoparticles. *Chem. Commun.* **2019**, *55*, 6964−6996.
(397) Cobley, C. M.; Chen, J.; Cho, E. C.; Wang, L. V.; Xia, Y. Gold Nanostructures: A Class of Multifunctional Materials for Biomedical Applications. *Chem. Soc. Rev.* **2011**, *40*, 44−56.
(398) Pearce, A. K.; Wilks, T. R.; Arno, M. C.; O'Reilly, R. K. Synthesis and Applications of Anisotropic Nanoparticles with Precisely Defined Dimensions. *Nat. Rev. Chem.* **2021**, *5*, 21−45.
(399) Gratton, S. E. A.; Ropp, P. A.; Pohlhaus, P. D.; Luft, J. C.; Madden, V. J.; Napier, M. E.; DeSimone, J. M. The Effect of Particle Design on Cellular Internalization Pathways. *Proc. Natl. Acad. Sci. U.S.A.* **2008**, *105*, 11613−11618.
(400) Kolhar, P.; Anselmo, A. C.; Gupta, V.; Pant, K.; Prabhakarpandian, B.; Ruoslahti, E.; Mitragotri, S. Using Shape Effects to Target Antibody-Coated Nanoparticles to Lung and Brain Endothelium. *Proc. Natl. Acad. Sci. U.S.A.* **2013**, *110*, 10753−10758.
(401) Jin, Y.; Jia, C.; Huang, S.-W.; O'donnell, M.; Gao, X. Multifunctional Nanoparticles as Coupled Contrast Agents. *Nat. Commun.* **2010**, *1*, 1−8.
(402) Richards-Kortum, R.; Sevick-Muraca, E. Quantitative Optical Spectroscopy for Tissue Diagnosis. *Annu. Rev. Phys. Chem.* **1996**, *47*, 555−606.
(403) Jain, P. K.; Lee, K. S.; El-Sayed, I. H.; El-Sayed, M. A. Calculated Absorption and Scattering Properties of Gold Nanoparticles of Different Size, Shape, and Composition: Applications in Biological Imaging and Biomedicine. *J. Phys. Chem. B* **2006**, *110*, 7238−7248.
(404) Copland, J. A.; Eghtedari, M.; Popov, V. L.; Kotov, N.; Mamedova, N.; Motamedi, M.; Oraevsky, A. A. Bioconjugated Gold Nanoparticles as a Molecular Based Contrast Agent: Implications for Imaging of Deep Tumors Using Optoacoustic Tomography. *Mol. Imag. Biol.* **2004**, *6*, 341−349.
(405) Liao, H.; Hafner, J. H. Gold Nanorod Bioconjugates. *Chem. Mater.* **2005**, *17*, 4636−4641.
(406) Pissuwan, D.; Valenzuela, S. M.; Miller, C. M.; Cortie, M. B. A Golden Bullet? Selective Targeting of Toxoplasma Gondii Tachyzoites Using Antibody-Functionalized Gold Nanorods. *Nano Lett.* **2007**, *7*, 3808−3812.
(407) Huang, X.; El-Sayed, I. H.; Qian, W.; El-Sayed, M. A. Cancer Cells Assemble and Align Gold Nanorods Conjugated to Antibodies to Produce Highly Enhanced, Sharp, and Polarized Surface Raman Spectra: A Potential Cancer Diagnostic Marker. *Nano Lett.* **2007**, *7*, 1591−1597.
(408) Huang, X. H.; El-Sayed, I. H.; Qian, W.; El-Sayed, M. A. Cancer Cell Imaging and Photothermal Therapy in the Near-Infrared Region by Using Gold Nanorods. *J. Am. Chem. Soc.* **2006**, *128*, 2115−2120.
(409) Wang, G.; Sun, W.; Luo, Y.; Fang, N. Resolving Rotational Motions of Nano-Objects in Engineered Environments and Live Cells with Gold Nanorods and Differential Interference Contrast Microscopy. *J. Am. Chem. Soc.* **2010**, *132*, 16417−16422.
(410) Tong, S.; Fine, E. J.; Lin, Y.; Cradick, T. J.; Bao, G. Nanomedicine: Tiny Particles and Machines Give Huge Gains. *Ann. Biomed. Eng.* **2014**, *42*, 243−259.
(411) Mitchell, M. J.; Billingsley, M. M.; Haley, R. M.; Wechsler, M. E.; Peppas, N. A.; Langer, R. Engineering Precision Nanoparticles for Drug Delivery. *Nat. Rev. Drug Discovery* **2021**, *20*, 101−124.
(412) Tian, F.; Conde, J.; Bao, C.; Chen, Y.; Curtin, J.; Cui, D. Gold Nanostars for Efficient in vitro and in vivo Real-Time SERS Detection and Drug Delivery via Plasmonic-Tunable Raman/FTIR Imaging. *Biomaterials* **2016**, *106*, 87−97.
(413) Bao, C.; Conde, J.; Polo, E.; Del Pino, P.; Moros, M.; Baptista, P. V.; Grazu, V.; Cui, D.; De La Fuente, J. M. A Promising Road with Challenges: Where Are Gold Nanoparticles in Translational Research? *Nanomedicine* **2014**, *9*, 2353−2370.
(414) Wang, Y.; Polavarapu, L.; Liz-Marzán, L. M. Reduced Graphene Oxide-Supported Gold Nanostars for Improved Sers Sensing and Drug Delivery. *ACS Appl. Mater. Interfaces* **2014**, *6*, 21798−21805.
(415) Liao, H.-G.; Zheng, H. Liquid Cell Transmission Electron Microscopy. *Annu. Rev. Phys. Chem.* **2016**, *67*, 719−747.
(416) Shi, F.; Li, F.; Ma, Y.; Zheng, F.; Feng, R.; Song, C.; Tao, P.; Shang, W.; Deng, T.; Wu, J. In situ Transmission Electron Microscopy Study of Nanocrystal Formation for Electrocatalysis. *ChemNanoMat* **2019**, *5*, 1439−1455.
(417) Chee, S. W.; Pratt, S. H.; Hattar, K.; Duquette, D.; Ross, F. M.; Hull, R. Studying Localized Corrosion Using Liquid Cell Transmission Electron Microscopy. *Chem. Commun.* **2015**, *51*, 168−171.
(418) Murray, C. B. Watching Nanocrystals Grow. *Science* **2009**, *324*, 1276−1277.
(419) Yuk, J. M.; Park, J.; Ercius, P.; Kim, K.; Hellebusch, D. J.; Crommie, M. F.; Lee, J. Y.; Zettl, A.; Alivisatos, A. P. High-Resolution EM of Colloidal Nanocrystal Growth Using Graphene Liquid Cells. *Science* **2012**, *336*, 61−64.
(420) Ye, X.; Jones, M. R.; Frechette, L. B.; Chen, Q.; Powers, A. S.; Ercius, P.; Dunn, G.; Rotskoff, G. M.; Nguyen, S. C.; Adiga, V. P.;

https://doi.org/10.1021/acs.chemrev.2c00468
Chem. Rev. 2023, 123, 3693−3760

et al. Single-Particle Mapping of Nonequilibrium Nanocrystal Transformations. *Science* **2016**, *354*, 874−877.
(421) Hauwiller, M. R.; Frechette, L. B.; Jones, M. R.; Ondry, J. C.; Rotskoff, G. M.; Geissler, P.; Alivisatos, A. P. Unraveling Kinetically-Driven Mechanisms of Gold Nanocrystal Shape Transformations Using Graphene Liquid Cell Electron Microscopy. *Nano Lett.* **2018**, *18*, 5731−5737.
(422) Tan, S. F.; Chee, S. W.; Lin, G.; Bosman, M.; Lin, M.; Mirsaidov, U.; Nijhuis, C. A. Real-Time Imaging of the Formation of Au−Ag Core−Shell Nanoparticles. *J. Am. Chem. Soc.* **2016**, *138*, 5190−5193.
(423) Sun, M.; Cheng, Z.; Chen, W.; Jones, M. Understanding Symmetry Breaking at the Single-Particle Level via the Growth of Tetrahedron-Shaped Nanocrystals from Higher-Symmetry Precursors. *ACS Nano* **2021**, *15*, 15953−15961.
(424) Penn, R. L.; Banfield, J. F. Imperfect Oriented Attachment: Dislocation Generation in Defect-Free Nanocrystals. *Science* **1998**, *281*, 969−971.
(425) Burrows, N. D.; Yuwono, V. M.; Penn, R. L. Quantifying the Kinetics of Crystal Growth by Oriented Aggregation. *MRS Bull.* **2010**, *35*, 133−137.
(426) Zhang, J.; Huang, F.; Lin, Z. Progress of Nanocrystalline Growth Kinetics Based on Oriented Attachment. *Nanoscale* **2010**, *2*, 18−34.
(427) Sathiyanarayanan, R.; Alimohammadi, M.; Zhou, Y.; Fichthorn, K. A. Role of Solvent in the Shape-Controlled Synthesis of Anisotropic Colloidal Nanostructures. *J. Phys. Chem. C* **2011**, *115*, 18983−18990.
(428) Zhang, H.; Banfield, J. F. Interatomic Coulombic Interactions as the Driving Force for Oriented Attachment. *CrystEngComm* **2014**, *16*, 1568−1578.
(429) Lv, W.; Huo, W.; Niu, Y.; Zhu, Y.; Xie, Y.; Guo, X.; He, W. Oriented-Attachment Dimensionality Build-up via van der Waals Interaction. *CrystEngComm* **2015**, *17*, 729−733.
(430) Vivek, J. P.; Burgess, I. J. Quaternary Ammonium Bromide Surfactant Adsorption on Low-Index Surfaces of Gold. 2. Au(100) and the Role of Crystallographic-Dependent Adsorption in the Formation of Anisotropic Nanoparticles. *Langmuir* **2012**, *28*, 5040−5047.
(431) Vivek, J. P.; Burgess, I. J. Quaternary Ammonium Bromide Surfactant Adsorption on Low-Index Surfaces of Gold. 1. Au(111). *Langmuir* **2012**, *28*, 5031−5039.
(432) Vivek, J. P.; Monsur, A.; Burgess, I. J. Differential Capacity and Chronocoulometry Studies of a Quaternary Ammonium Surfactant Adsorbed on Au(111). *Surf. Interface Anal.* **2013**, *45*, 1402−1409.
(433) Kim, M. J.; Flowers, P. F.; Stewart, I. E.; Ye, S.; Baek, S.; Kim, J. J.; Wiley, B. J. Ethylenediamine Promotes Cu Nanowire Growth by Inhibiting Oxidation of Cu(111). *J. Am. Chem. Soc.* **2017**, *139*, 277−284.
(434) Fisher, E. A.; Leung, K. K.; Casanova-Moreno, J.; Masuda, T.; Young, J.; Bizzotto, D. Quantifying the Selective Modification of Au(111) Facets via Electrochemical and Electroless Treatments for Manipulating Gold Nanorod Surface Composition. *Langmuir* **2017**, *33*, 12887−12896.
(435) Danger, B. R.; Fan, D.; Vivek, J. P.; Burgess, I. J. Electrochemical Studies of Capping Agent Adsorption Provide Insight into the Formation of Anisotropic Gold Nanocrystals. *ACS Nano* **2012**, *6*, 11018−11026.
(436) Sun, Y.; Gates, B.; Mayers, B.; Xia, Y. Crystalline Silver Nanowires by Soft Solution Processing. *Nano Lett.* **2002**, *2*, 165−168.
(437) Au, L.; Lim, B.; Colletti, P.; Jun, Y. S.; Xia, Y. Synthesis of Gold Microplates Using Bovine Serum Albumin as a Reductant and a Stabilizer. *Chem. Asian J.* **2010**, *5*, 123−129.
(438) Zhang, Y.-L.; Sui, X.-L.; Zhao, L.; Gu, D.-M.; Huang, G.-S.; Wang, Z.-B. Controlling the Surface Roughness of Chain-Like Pd Nanowires by Ph Values as Excellent Catalysts for Oxygen Reduction Reaction. *Int. J. Hydrogen Energy* **2019**, *44*, 6551−6559.
(439) Lim, B.; Jiang, M.; Tao, J.; Camargo, P. H. C.; Zhu, Y.; Xia, Y. Shape-Controlled Synthesis of Pd Nanocrystals in Aqueous Solutions. *Adv. Funct. Mater.* **2009**, *19*, 189−200.
(440) Meena, S. K.; Sulpizi, M. Understanding the Microscopic Origin of Gold Nanoparticle Anisotropic Growth from Molecular Dynamics Simulations. *Langmuir* **2013**, *29*, 14954−14961.
(441) Almora-Barrios, N.; Novell-Leruth, G.; Whiting, P.; Liz-Marzán, L. M.; López, N. Theoretical Description of the Role of Halides, Silver, and Surfactants on the Structure of Gold Nanorods. *Nano Lett.* **2014**, *14*, 871−875.
(442) Ni, B.; González-Rubio, G.; Kirner, F.; Zhang, S.; Cölfen, H. A Symmetry-Based Kinematic Theory for Nanocrystal Morphology Design. *Angew. Chem., Int. Ed.* **2022**, *61*, e202200753.
(443) Thomas, N.; Mani, E. An Analytical Solution to the Kinetics of Growth of Gold Nanorods. *RSC Adv.* **2016**, *6*, 30028−30036.
(444) Zhao, M.; Wang, X.; Yang, X.; Gilroy, K. D.; Qin, D.; Xia, Y. Hollow Metal Nanocrystals with Ultrathin, Porous Walls and Well-Controlled Surface Structures. *Adv. Mater.* **2018**, *30*, 1801956.
(445) Skrabalak, S. E.; Chen, J.; Sun, Y.; Lu, X.; Au, L.; Cobley, C. M.; Xia, Y. Gold Nanocages: Synthesis, Properties, and Applications. *Acc. Chem. Res.* **2008**, *41*, 1587−1595.
(446) Skrabalak, S. E.; Au, L.; Li, X.; Xia, Y. Facile Synthesis of Ag Nanocubes and Au Nanocages. *Nature protocols* **2007**, *2*, 2182−2190.
(447) Zhu, J.; Chen, Z.; Xie, M.; Lyu, Z.; Chi, M.; Mavrikakis, M.; Jin, W.; Xia, Y. Iridium-Based Cubic Nanocages with 1.1-nm-Thick Walls: A Highly Efficient and Durable Electrocatalyst for Water Oxidation in an Acidic Medium. *Angew. Chem.* **2019**, *131*, 7322−7326.
(448) Zhang, L.; Roling, L. T.; Wang, X.; Vara, M.; Chi, M.; Liu, J.; Choi, S.-I.; Park, J.; Herron, J. A.; Xie, Z.; et al. Platinum-Based Nanocages with Subnanometer-Thick Walls and Well-Defined, Controllable Facets. *Science* **2015**, *349*, 412−416.
(449) Wang, X.; Figueroa-Cosme, L.; Yang, X.; Luo, M.; Liu, J.; Xie, Z.; Xia, Y. Pt-Based Icosahedral Nanocages: Using a Combination of {111} Facets, Twin Defects, and Ultrathin Walls to Greatly Enhance Their Activity toward Oxygen Reduction. *Nano Lett.* **2016**, *16*, 1467−1471.
(450) Zhao, M.; Xu, L.; Vara, M.; Elnabawy, A. O.; Gilroy, K. D.; Hood, Z. D.; Zhou, S.; Figueroa-Cosme, L.; Chi, M.; Mavrikakis, M.; et al. Synthesis of Ru Icosahedral Nanocages with a Face-Centered-Cubic Structure and Evaluation of Their Catalytic Properties. *ACS Catal.* **2018**, *8*, 6948−6960.
(451) Zhu, J.; Xu, L.; Lyu, Z.; Xie, M.; Chen, R.; Jin, W.; Mavrikakis, M.; Xia, Y. Janus Nanocages of Platinum-Group Metals and Their Use as Effective Dual-Electrocatalysts. *Angew. Chem., Int. Ed.* **2021**, *60*, 10384−10392.
(452) Zeng, J.; Zhang, Q.; Chen, J.; Xia, Y. A Comparison Study of the Catalytic Properties of Au-Based Nanocages, Nanoboxes, and Nanoparticles. *Nano Lett.* **2010**, *10*, 30−35.
(453) Yavuz, M. S.; Cheng, Y.; Chen, J.; Cobley, C. M.; Zhang, Q.; Rycenga, M.; Xie, J.; Kim, C.; Song, K. H.; Schwartz, A. G.; et al. Gold Nanocages Covered by Smart Polymers for Controlled Release with near-Infrared Light. *Nat. Mater.* **2009**, *8*, 935−939.
(454) Yang, M.; Wang, W.; Gilroy, K. D.; Xia, Y. Controlling the Deposition of Pd on Au Nanocages: Outer Surface Only versus Both Outer and Inner Surfaces. *Nano Lett.* **2017**, *17*, 5682−5687.
(455) Timoshkin, A. Y.; Kudrev, A. G. Calculations of Micro-constants and Equilibrium Formation Constants for Platinum(II) and Palladium(II) Halide Complexes in Solution. *Russ. J. Inorg. Chem.* **2012**, *57*, 1362−1370.
(456) Talapin, D. V.; Koeppe, R.; Götzinger, S.; Kornowski, A.; Lupton, J. M.; Rogach, A. L.; Benson, O.; Feldmann, J.; Weller, H. Highly Emissive Colloidal CdSe/CdS Heterostructures of Mixed Dimensionality. *Nano Lett.* **2003**, *3*, 1677−1681.
(457) Wang, X.; Liu, M.; Chen, Y.; Fu, W.; Wang, B.; Guo, L. Symmetry Breaking in Semiconductor Nanocrystals via Kinetic-Controlled Surface Diffusion: A Strategy for Manipulating the Junction Structure. *Nanoscale* **2016**, *8*, 15970−15977.

https://doi.org/10.1021/acs.chemrev.2c00468
Chem. Rev. 2023, 123, 3693−3760

(458) Xiong, S.; Xi, B.; Zhang, K.; Chen, Y.; Jiang, J.; Hu, J.; Zeng, H. C. Ag Nanoprisms with Ag_2S Attachment. *Sci. Rep.* **2013**, *3*, 1−9.
(459) Scarfiello, R.; Nobile, C.; Cozzoli, P. D. Colloidal Magnetic Heterostructured Nanocrystals with Asymmetric Topologies: Seeded-Growth Synthetic Routes and Formation Mechanisms. *Front. Mater.* **2016**, *3*, 56.
(460) Mokari, T.; Rothenberg, E.; Popov, I.; Costi, R.; Banin, U. Selective Growth of Metal Tips onto Semiconductor Quantum Rods and Tetrapods. *Science* **2004**, *304*, 1787−1790.
(461) Mishra, N.; Lian, J.; Chakrabortty, S.; Lin, M.; Chan, Y. Unusual Selectivity of Metal Deposition on Tapered Semiconductor Nanostructures. *Chem. Mater.* **2012**, *24*, 2040−2046.
(462) Wang, Z.; Shao, D.; Chang, Z.; Lu, M.; Wang, Y.; Yue, J.; Yang, D.; Li, M.; Xu, Q.; Dong, W.-f. Janus Gold Nanoplatform for Synergetic Chemoradiotherapy and Computed Tomography Imaging of Hepatocellular Carcinoma. *ACS Nano* **2017**, *11*, 12732−12741.
(463) Zhang, L.; Chen, Y.; Li, Z.; Li, L.; Saint-Cricq, P.; Li, C.; Lin, J.; Wang, C.; Su, Z.; Zink, J. I. Tailored Synthesis of Octopus-Type Janus Nanoparticles for Synergistic Actively-Targeted and Chemo-Photothermal Therapy. *Angew. Chem., Int. Ed.* **2016**, *55*, 2118−2121.
(464) Li, X.; Zhou, L.; Wei, Y.; El-Toni, A. M.; Zhang, F.; Zhao, D. Anisotropic Growth-Induced Synthesis of Dual-Compartment Janus Mesoporous Silica Nanoparticles for Bimodal Triggered Drugs Delivery. *J. Am. Chem. Soc.* **2014**, *136*, 15086−15092.
(465) Wang, J.; Gao, W. Nano/Microscale Motors: Biomedical Opportunities and Challenges. *ACS Nano* **2012**, *6*, 5745−5751.
(466) Liu, R.; Sen, A. Autonomous Nanomotor Based on Copper−Platinum Segmented Nanobattery. *J. Am. Chem. Soc.* **2011**, *133*, 20064−20067.
(467) Gao, W.; Uygun, A.; Wang, J. Hydrogen-Bubble-Propelled Zinc-Based Microrockets in Strongly Acidic Media. *J. Am. Chem. Soc.* **2012**, *134*, 897−900.
(468) Gao, W.; Pei, A.; Wang, J. Water-Driven Micromotors. *ACS Nano* **2012**, *6*, 8432−8438.
(469) Gao, W.; D'Agostino, M.; Garcia-Gradilla, V.; Orozco, J.; Wang, J. Multi-Fuel Driven Janus Micromotors. *Small* **2013**, *9*, 467−471.
(470) Deng, K.; Luo, Z.; Tan, L.; Quan, Z. Self-Assembly of Anisotropic Nanoparticles into Functional Superstructures. *Chem. Soc. Rev.* **2020**, *49*, 6002−6038.
(471) Gong, J.; Li, G.; Tang, Z. Self-Assembly of Noble Metal Nanocrystals: Fabrication, Optical Property, and Application. *Nano Today* **2012**, *7*, 564−585.
(472) Boles, M. A.; Engel, M.; Talapin, D. V. Self-Assembly of Colloidal Nanocrystals: From Intricate Structures to Functional Materials. *Chem. Rev.* **2016**, *116*, 11220−11289.
(473) Nie, Z.; Petukhova, A.; Kumacheva, E. Properties and Emerging Applications of Self-Assembled Structures Made from Inorganic Nanoparticles. *Nat. Nanotechnol.* **2010**, *5*, 15−25.
(474) Yan, C.; Wang, T. A New View for Nanoparticle Assemblies: From Crystalline to Binary Cooperative Complementarity. *Chem. Soc. Rev.* **2017**, *46*, 1483−1509.
(475) Singh, G.; Chan, H.; Baskin, A.; Gelman, E.; Repnin, N.; Král, P.; Klajn, R. Self-Assembly of Magnetite Nanocubes into Helical Superstructures. *Science* **2014**, *345*, 1149−1153.
(476) Gilroy, K. D.; Elnabawy, A. O.; Yang, T.-H.; Roling, L. T.; Howe, J.; Mavrikakis, M.; Xia, Y. Thermal Stability of Metal Nanocrystals: An Investigation of the Surface and Bulk Reconstructions of Pd Concave Icosahedra. *Nano Lett.* **2017**, *17*, 3655−3661.
(477) Young, N. P.; van Huis, M. A.; Zandbergen, H. W.; Xu, H.; Kirkland, A. I. Transformations of Gold Nanoparticles Investigated Using Variable Temperature High-Resolution Transmission Electron Microscopy. *Ultramicroscopy* **2010**, *110*, 506−516.
(478) Petrova, H.; Juste, J. P.; Pastoriza-Santos, I.; Hartland, G. V.; Liz-Marzán, L. M.; Mulvaney, P. On the Temperature Stability of Gold Nanorods: Comparison between Thermal and Ultrafast Laser-Induced Heating. *Phys. Chem. Chem. Phys.* **2006**, *8*, 814−821.
(479) Taylor, A. B.; Siddiquee, A. M.; Chon, J. W. M. Below Melting Point Photothermal Reshaping of Single Gold Nanorods Driven by Surface Diffusion. *ACS Nano* **2014**, *8*, 12071−12079.
(480) Chen, Y.-S.; Frey, W.; Kim, S.; Homan, K.; Kruizinga, P.; Sokolov, K.; Emelianov, S. Enhanced Thermal Stability of Silica-Coated Gold Nanorods for Photoacoustic Imaging and Image-Guided Therapy. *Opt. Express* **2010**, *18*, 8867−8877.
(481) Zhao, M.; Chen, Z.; Lyu, Z.; Hood, Z. D.; Xie, M.; Vara, M.; Chi, M.; Xia, Y. Ru Octahedral Nanocrystals with a Face-Centered Cubic Structure, {111} Facets, Thermal Stability up to 400 °C, and Enhanced Catalytic Activity. *J. Am. Chem. Soc.* **2019**, *141*, 7028−7036.
(482) Cho, H.; Shin, J. W.; Ryoo, R. Atomic Scale Mechanisms Underlying Thermal Reshaping of Anisotropic Gold Nanocrystals Revealed by in situ Electron Microscopy. *J. Phys. Chem. C* **2020**, *124*, 12855−12863.
(483) Link, S.; Wang, Z. L.; El-Sayed, M. A. How Does a Gold Nanorod Melt? *J. Phys. Chem. B* **2000**, *104*, 7867−7870.
(484) Walbert, T.; Muench, F.; Yang, Y.; Kunz, U.; Xu, B.-X.; Ensinger, W.; Molina-Luna, L. In situ Transmission Electron Microscopy Analysis of Thermally Decaying Polycrystalline Platinum Nanowires. *ACS Nano* **2020**, *14*, 11309−11318.
(485) Albrecht, W.; Bladt, E.; Vanrompay, H.; Smith, J. D.; Skrabalak, S. E.; Bals, S. Thermal Stability of Gold/Palladium Octopods Studied in situ in 3D: Understanding Design Rules for Thermally Stable Metal Nanoparticles. *ACS Nano* **2019**, *13*, 6522−6530.
(486) Antonello, A.; Della Gaspera, E.; Baldauf, J.; Mattei, G.; Martucci, A. Improved Thermal Stability of Au Nanorods by Use of Photosensitive Layered Titanates for Gas Sensing Applications. *J. Mater. Chem.* **2011**, *21*, 13074−13078.
(487) Danielsen, S. P. O.; Choi, J.; Composto, R. J. Retardation of Shape Change of Au Nanorods Using Photo-Cross-Linkable Ligands. *J. Polym. Sci., Part B: Polym. Phys.* **2016**, *54*, 301−307.
(488) Albrecht, W.; Deng, T.-S.; Goris, B.; van Huis, M. A.; Bals, S.; van Blaaderen, A. Single Particle Deformation and Analysis of Silica-Coated Gold Nanorods before and after Femtosecond Laser Pulse Excitation. *Nano Lett.* **2016**, *16*, 1818−1825.
(489) Cao, A.; Veser, G. Exceptional High-Temperature Stability through Distillation-Like Self-Stabilization in Bimetallic Nanoparticles. *Nat. Mater.* **2010**, *9*, 75−81.
(490) Mejía-Rosales, S. J.; Fernández-Navarro, C.; Pérez-Tijerina, E.; Montejano-Carrizales, J. M.; José-Yacamán, M. Two-Stage Melting of Au−Pd Nanoparticles. *J. Phys. Chem. B* **2006**, *110*, 12884−12889.
(491) van der Hoeven, J. E. S.; Welling, T. A. J.; Silva, T. A. G.; van den Reijen, J. E.; La Fontaine, C.; Carrier, X.; Louis, C.; van Blaaderen, A.; de Jongh, P. E. In situ Observation of Atomic Redistribution in Alloying Gold−Silver Nanorods. *ACS Nano* **2018**, *12*, 8467−8476.
(492) Gilroy, K. D.; Puibasset, J.; Vara, M.; Xia, Y. On the Thermodynamics and Experimental Control of Twinning in Metal Nanocrystals. *Angew. Chem., Int. Ed.* **2017**, *56*, 8647−8651.
(493) Albrecht, W.; van de Glind, A.; Yoshida, H.; Isozaki, Y.; Imhof, A.; van Blaaderen, A.; de Jongh, P. E.; de Jong, K. P.; Zečević, J.; Takeda, S. Impact of the Electron Beam on the Thermal Stability of Gold Nanorods Studied by Environmental Transmission Electron Microscopy. *Ultramicroscopy* **2018**, *193*, 97−103.

https://doi.org/10.1021/acs.chemrev.2c00468
Chem. Rev. 2023, 123, 3693−3760